NON-EQUILIBRIUM THERMODYNAMIC APPROACH BASED ON STEEPEST-ENTROPY-ASCENT QUANTUM THERMODYNAMICS APPLICABLE ACROSS ALL TEMPORAL AND SPATIAL SCALES

Guanchen Li

Dissertation submitted to the Faculty of the
Virginia Polytechnic Institute and State University
In partial fulfillment of the requirements for the degree of

DOCTOR OF PHILOSOPHY
in
Mechanical Engineering

Michael R. von Spakovsky, Chair
Gian Paolo Beretta
Céline Hin
Peizhen Lu
Mark Paul
Leigh Winfrey

December 8, 2015, Blacksburg, Virginia, USA

Keywords: non-equilibrium thermodynamics, multiscale modeling, quantum thermodynamics, steepest-entropy-ascent quantum thermodynamics

NON-EQUILIBRIUM THERMODYNAMIC APPROACH BASED ON STEEPEST-ENTROPY-ASCENT QUANTUM THERMODYNAMICS APPLICABLE ACROSS ALL TEMPORAL AND SPATIAL SCALES

Guanchen Li

Abstract

In this research, a first-principles, non-equilibrium thermodynamic-ensemble approach applicable across all temporal and spatial scales is developed based on steepest-entropy-ascent quantum thermodynamics (SEAQT). The SEAQT framework provides an equation of motion consisting of both reversible mechanical dynamics and irreversible relaxation dynamics, which is able to describe the evolution of any state of any system, equilibrium or non-equilibrium. Its key feature is that the irreversible dynamics is based on a gradient dynamics in system state space instead of the microscopic mechanics of more traditional approaches. System energy eigenstructure and density operator (or ensemble probability distribution) describe the system and system thermodynamic state, respectively. Extensive properties (i.e., energy, entropy, and particle number) play a key role in formulating the equation of motion and in describing non-equilibrium state evolutions. All the concepts involved in this framework (i.e., eigentstructure, density operator, and extensive properties) are well defined at all temporal and spatial scales leading to the extremely broad applicability of SEAQT.

The focus of the present research is that of developing non-equilibrium thermodynamic models based specifically on the irreversible part of the equation of motion of SEAQT and applying these to the study of pure relaxation processes of systems in non-equilibrium states undergoing chemical reactions and heat and mass diffusion. As part of the theoretical investigation, the new concept of hypo-equilibrium state is introduced and developed. It is able to describe any non-equilibrium state going through a pure relaxation process and is a generalization of the concept of stable equilibrium of equilibrium thermodynamics to the non-equilibrium realm. Using the concept of hypo-equilibrium state, it is shown that non-equilibrium intensive properties can be fundamentally defined throughout the relaxation process. The definition of non-equilibrium intensive properties also relies on various ensemble descriptions of system state. In this research, three SEAQT ensemble descriptions, i.e., the canonical, grand canonical, and isothermal-isobaric,

are derived corresponding, respectively, to the definition of temperature, chemical potential, and pressure. To computationally and not just theoretically permit the application of the SEAQT framework across all scales, a density of states method is developed, which is applicable to solving the SEAQT equation of motion for all types of non-equilibrium relaxation processes. In addition, a heterogeneous multiscale method (HMM) algorithm is also applied to extend the application of the SEAQT framework to multiscale modeling. Applications of this framework are given for systems involving chemical kinetics, the heat and mass diffusion of indistinguishable particles, power cycles, and the complex, coupled reaction-diffusion pathways of a solid oxide fuel cell (SOFC) cathode.

To

My parents, Jing Yu and Xiaojiu Li,

The teachers who inspired me

Acknowledgments

It has been a great adventure to work on this attractive topic, and I have experienced four years of fun and challenge. I would like to thank my advisor, Dr. Michael R. von Spakovsky, for his guidance to my life, my research, and my career. His personality, intelligence, and leadership have taught me how to become a good man, a creative researcher, and a reliable leader.

I would like to thank Dr. Gian Paolo Beretta for his pioneering work in development of the SEAQT framework and for his guidance and essential suggestions all through my research. Special thanks go to Dr. Kathy Lu and Kris in collaborating on the Solid Oxide Fuel Cell research. My thanks also go to Dr. Céline Hin for her helpful discussions and valuable suggestions in my research and to my committee members: Dr. Leigh Winfrey, and Dr. Mark Paul for their advice and help during the development of this dissertation. My gratitude also extends to Dr. Alireza Haghighat for his great course and his support to my career.

I am also grateful to the U.S. Office of Naval Research (ONR) under grant N00014-11-1-0266 and to the Virginia Tech Hord Fellowship for financial support of my doctoral studies. My gratitude also goes to Dr. Mehdi Setareh for his helpful advice and financial support in my first semester at Virginia Tech.

I feel very lucky to have worked with such a great research group: Alejandro, Omar, Aimen, Charles, Sergio and Scott. Although our backgrounds are quite different, there are no borders to our friendships. Thank you for your support and companionship. It has been of great interest to get to know about all kinds of interesting cultures.

Last but not least, I would like to thank all my friends in Blacksburg for their friendship and all our wonderful times together. Also, I send my thanks to my best friends spread throughout the world. It is your companionship, which has made my journey not a lonely one.

Contents

List of Figures

List of Tables

Chapter 1

Introduction

1.1 Non-equilibrium modeling

Conventional approaches [1–8] to studying non-equilibrium phenomena are of two types. The first is based on the mechanics of individual particles or quantum states. The mechanics is acquired from first-principles (i.e. Newton's law or quantum mechanics) using, for example, molecular dynamics (MD) [6] and kinetic theory (KT) [4] or from stochastic dynamics using, for example, Monte Carlo (MC) simulations [5, 7]. These approaches contain all the details of the mechanical features of the system (e.g., particle position and velocity at any instant of time, particle collisions, etc.) to arrive at a set of macroscopic properties, resulting in huge computational burden. The second type is based on an ensemble view with the laws of thermodynamics acting as first principles. Onsager's theory, linear response theory, and fluctuation theory are the examples of this type of approach. However, the applicability of these methods is the limited in the non-equilibrium realm. Local-equilibrium or near-equilibrium assumptions are needed, and limitations to steady state or the use of an environmental reservoir are also necessary in many applications.

In contrast to these conventional approaches, the SEAQT framework attempts to explain non-equilibrium phenomena from a first-principle, thermodynamic-ensemble viewpoint. Irreversibility is captured via intrinsic entropy generation using the steepest entropy ascent principle rather than from collisions or some scattering process, which means system state evolution is entropy-driven and the laws of thermodynamics act as first principles. The equation of motion is developed on the basis of a gradient dynamics in system state space instead of the microscopic mechanics of more traditional approaches and can be regarded as resulting from a pattern of the more micro-

scopic mechanical model. In a manner similar to the way at stable equilibrium one can view the "Maxwellian distribution" as an invariant pattern even though the mechanical details of the individual particle states constantly change, steepest entropy ascent can also be viewed as a changing global pattern or effect of the details of the mechanics in relaxation. Thus, without including all of the details of the more microscopic model (i.e., of the mechanics), the pattern of this model serves as a modification of the more macroscopic model (i.e., of the non-equilibrium thermodynamics). This, of course, greatly simplifies the computational complexity, while the clear physical meaning and geometrical description of the SEA landscape facilitates the discovery of general but unique patterns of relaxation in the non-equilibrium realm at any scale. As an example of computational time, to model a transient multiphase, multicomponent, multiscale system (i.e., a solid oxide fuel cell (SOFC) cathode) with heat conduction, an externally applied field, diffusion, and multiple coupled electrochemical reaction pathways requires only a few hours on a PC workstation [9, 10].

1.2 Multiscale modeling

A number of approaches are used to model non-equilibrium phenomena at different time and length scales [11–13]. However, a particular limitation of all of these approaches is that they are restricted to an effective time and length scale even though in many cases microscopic and mesoscopic level properties may have a strong influence on macroscopic performance. For example, chemical reactions and species transport are greatly affected by microstructure parameters [11]. The traditional solution to this dilemma is to define macroscopic phenomenological parameters (e.g., tortuosity, porosity, diffusivity, viscosity, thermal conductivity, etc.), which average atomistic-level dynamics and microscopic geometrical features, and incorporate them into the macroscopic-level model in order to capture microscopic and mesoscopic influences. At times, the microscopic and/or mesoscopic model can be incorporated into the macroscopic one to form a multiphysics, multiscale model in which the phenomenological parameters of the macroscopic description can be updated in real-time. Of course, in doing so, the issue of dealing with huge differences in both the description of the system and the equations of motion at different scales must be dealt with. For example, a macroscopic continuum model may use concentration and temperature as state variables and balance equations resulting from the laws of thermodynamics as stand-ins for an equation of motion. In contrast, microscopic MD lacks any thermodynamic information at all and uses particle position

and momentum as state variables and the dynamics resulting from Newton's laws as its equation of motion. As a result, there is no shared form for the microscopic and macroscopic variables or properties, and, thus, a need exists for some sort of link between scales to transform property information at one scale into that at another, which usually is very computationally expensive. [10] This is an important feature of any multiphysics, multiscale model.

SEAQT framework addresses these issues of time and length scales and the influence of microscopic and mesoscopic parameters. A SEAQT model can in a single coherent description deal with a much wider range of scales than that of previous models since the model consists of a set of local systems with length scales in the mesoscopic range, while each local system is characterized by particle energy eigenstate properties, which provide information about atomistic or microscopic features. Energy eigenstates are calculated from atomistic-level information, and microscopic parameters such as the mean free path of a particle or a microscopic potential well influence performance via the energy eigenstates. In the SEAQT framework, the basic system state variables are energy and entropy, which are well defined at the microscopic and mesoscopic levels as well as at the macroscopic level. Using the same state variables at all scales of description permits the transfer of information between scales by simple scaling, which naturally extends the range of scales to which the SEAQT model can be applied. Furthermore, since the SEAQT framework uses the principle of steepest entropy ascent as the basis for its dynamics, its equation of motion is applicable from the atomistic to the macroscopic level, exhibiting the same basic features across different time and length scales. Thus, a consistent description and dynamics across scales makes this novel approach a good choice for studying microscopic parameter influences on mesoscopic and macroscopic system performance. It is also a good choice since it can predict system behavior in the presence of transport-reaction coupling both in the steady state and transient regimes, even those far from equilibrium where non-linearities and entropy generation play a significant role.

1.3 Dissertation objectives and originality for SEAQT

The SEAQT framework is a significant theoretical advance over existing approaches to non-equilibrium modeling and facilitates multiscale modeling because of its single kinematic and dynamic description applicable across all scales. For this reason, it is desirable to develop the theory and methodology of this modeling framework so that it is not just theoretically but practically applicable across

all scales and to apply it to the study of various non-equilibrium phenomena and systems of interest. To achieve this, the overall objectives of this doctoral research are as follow:

- Develop the methodology of modeling non-equilibrium phenomena using the SEAQT framework, especially for systems with high-dimensional state spaces and for complex meso-/macroscopic systems. The purpose of this objective is, thus, to move SEAQT from a framework computationally limited to modeling quantum systems with low-dimensional state spaces to one applicable to non-equilibrium phenomena at all temporal and spatial scales.
- Study the general features or patterns of the non-equilibrium relaxation process using the modeling methodology developed. The purpose of this objective is to explore a general and more comprehensive way of describing the non-equilibrium relaxation process.
- Apply the developed methodology to the modeling and analysis of fundamental non-equilibrium phenomena (i.e., chemical reactions and heat and mass diffusion), power cycles, and a complex network of local systems (i.e., to the modeling of SOFC cathode oxygen reduction and chromium oxide poisoning pathways). The purpose of this objective is to provide a complete set of paradigms for the application of SEAQT to single phenomena, multiple processes, and multiscale systems.

In order to achieve these three overall objectives, the following set of original contributions are made in this research. Theoretical and methodological developments include

- Development of a density of states method to solve the pure relaxation process for an infinite dimensional state space starting with any initial probability distribution using the SEAQT equation of motion.
- Introduction of the concept of hypo-equilibrium state, which is a generalization of the concept of stable equilibrium to the non-equilibrium realm, and derivation of its mathematical form. This concept and its mathematical features allow a simple yet general description of the relaxation process of any non-equilibrium state.
- Introduction of the concept of non-equilibrium intensive properties, which is a generalization of the concept of equilibrium intensive properties, and derivation of its mathematical form. Non-equilibrium intensive properties together with extensive properties offer a complete physical description of the relaxation process.

- Introduction of a fundamental definition for non-equilibrium temperature using the concept of hypo-equilibrium state and the mathematical form of the SEAQT equation of motion based on the canonical ensemble.
- Introduction of a fundamental definition for non-equilibrium chemical potential using the concept of hypo-equilibrium state and the mathematical form of the SEAQT equation of motion based on the grand canonical ensemble.
- Introduction of a fundamental definition for non-equilibrium pressure using the concept of hypo-equilibrium state and the mathematical form of the SEAQT equation of motion based on the isothermal-isobaric ensemble.
- Application of a heterogeneous multiscale method (HMM) to the SEAQT equation of motion and development of a flowchart for modeling a multiscale/multiphysics system network with multiple coupled interactions.

Original contributions associated with applications of the theoretical and methodological developments include application of the SEAQT framework to the study of

- Chemical kinetics.
- Heat and mass diffusion in a simple system.
- Heat and mass diffusion of a many particle system with indistinguishability.
- Power cycles.
- SOFC cathode oxygen reduction and chromium oxide poisoning pathways under transient and steady state conditions and their effect on microstructure degradation and chromium oxide poisoning.

1.4 Outline of the dissertation

In this dissertation, seven general topics are discussed with each chapter forming an independent paper, which has either already been published, submitted for publication, or will be submitted for publication. The outline for each chapter is as follows:

Chapter 2:

This chapter presents a study of the non-equilibrium relaxation process of chemically reactive systems using SEAQT. The trajectory of the chemical reaction, i.e., the accessible intermediate

states, is predicted and discussed. The concept of density of states is introduced to simplify the application of the relaxation model, which in effect extends the application of the SEAQT framework even to infinite energy eigenlevel systems. The energy eigenstructure of the reactive system considered here consists of an extremely large number of such levels (on the order of 10130) and yields to the quasi-continuous assumption. The principle of SEA results in a unique trajectory of system thermodynamic state evolution in Hilbert space in the non-equilibrium realm, even far from equilibrium. To describe this trajectory, the concepts of subsystem hypo-equilibrium state and temperature are introduced and used to characterize each system-level, non-equilibrium state. This definition of temperature is fundamental rather than phenomenological and is a generalization of the temperature defined at stable equilibrium. In addition, to deal with the large number of energy eigenlevels, the equation of motion is formulated on the basis of the density of states and a set of associated degeneracies. Their significance for the non-equilibrium evolution of system state is discussed. For the application presented, the numerical method used is described and is based on the density of states, which is specifically developed to solve the SEAQT equation of motion. Results for different kinds of initial non-equilibrium conditions, i.e., those for gamma and Maxwellian distributions, are studied. The advantage of the concept of hypo-equilibrium state in studying non-equilibrium trajectories is discussed. This study has been accepted and will be published in *Physical Review E* [14].

Chapter 3:

This chapter outlines an application of SEAQT to the study of the chemical kinetics of the reaction mechanism $H_2 + F \leftrightarrow FH + H$. The SEAQT non-equilibrium model is able to provide detailed information during the reaction process, providing a picture of the changes occurring in key thermodynamic properties (e.g., the instantaneous species concentrations, entropy and entropy generation rate, reaction coordinate, chemical affinities, reaction rate, etc.). As a comparison, results using the density of states method are compared with previous work by Dr. von Spakovsky's group. This study has been published in *Journal of Physics: Conference Series* [15].

Chapter 4:

This chapter presents a thermodynamic model on the relaxation process of a local, isolated system in non-equilibrium. This model uses the SEAQT equation of motion for the canonical ensemble and applies it to a simple system. The model is able to arrive at the Onsager relations for a local, isolated system in non-equilibrium. Since no local equilibrium assumption is made,

the conjugate fluxes and forces are intrinsic to the subspaces of state space and defined through the concepts of hypo-equilibrium state and non-equilibrium intensive properties, which describe the non-mutual equilibrium status between subspaces of thermodynamic state space. The Onsager relations are shown to be thermodynamic kinematic features of the system and are found without knowledge of the detailed mechanics of the dynamic process. Two kinds of relaxation processes are studied with different constraints (conservation laws) corresponding to heat diffusion and to mass diffusion. Linear behavior in near equilibrium region as well as non-linear behavior in far-from-equilibrium region are discussed. Thermodynamic relations from the equilibrium and near-equilibrium realms, including the Gibbs relation, the 2^{nd} law of thermodynamics, and the Onsager relations, are generalized to non-equilibrium realm. The variational principle in the space spanned by the intrinsic conjugate fluxes and forces is given via the quadratic dissipation potential. As an application, the model is applied to the study of the heat and mass diffusion of a system represented by single particle ensemble, which can also be applied to a simple system of many particles. Phenomenological transport coefficient are also derived in near equilibrium realm. This study is in preparation for journal publication [16].

Chapter 5:

This chapter presents a thermodynamic model the relaxation process of interacting non-equilibrium systems. This model uses the SEAQT equation of motion for the grand canonical ensemble and applies it to a many particle system of classical or indistinguishable particles. Two kinds of interactions are discussed, including pure heat diffusion and heat and mass diffusion together. The Onsager relations are shown to be a thermodynamic kinematic feature of the system using conjugate fluxes and forces defined as intrinsic to the subspaces of the state space of one system and/or of the state space of two interacting systems. The thermodynamic explanation of the measurement of the intensive properties of a system in a non-equilibrium state is given. The thermodynamic definition of reservoir is also discussed. Finally, the equation of motion for a system undergoing multiple interactions is provided, which permits the modeling of a network of local systems in non-equilibrium. This study is in preparation for journal publication [17].

Chapter 6:

This chapter applies the grand canonical formulation of SEAQT to the study of the mass and heat diffusion of indistinguishable particle systems. SEAQT is a non-equilibrium framework applicable across all spatial scales and makes possible the general study of the thermodynamic fea-

tures of heat and mass diffusion (i.e., entropy generation) across spatial scales. Specifically, the study focuses on the thermodynamic features of far-from-equilibrium state evolution, which can be accomplished independent of the specific mechanics of individual particle interactions. The thermodynamic trajectory of indistinguishable particles as well as its limit to classical particles is discussed. Two kinds of size effects on the evolution trajectory, i.e., those of concentration and volume, are also discussed. This study has been published in the *Proceedings of ASME 2015 International Mechanical Engineering Congress* and Exposition [18], and is in preparation for journal publication.

Chapter 7:

This chapter outlines the SEAQT formulation based on the isothermal-isobaric ensemble and its application to the modeling of a non-quasi-equilibrium cycle using a system with variable volume. This formulation is given for a classical system in phase space as well as thermodynamic state space using macroscopic properties. The derivation of the equation of motion needs a complete definition of volume for any microscopic state in configuration space and the concept of the isothermal-isobaric partition function. The cycle consists of two isothermal and two isobaric processes. Using the concept of hypo-equilibrium state and non-equilibrium intensive properties, SEAQT provides a complete description of the non-equilibrium evolution of the cycle. How the non-equilibrium effects influence the performance of the cycle is discussed via a parametric study of the characteristic times of the system and reservoir. This study has been presented in the *13th Joint European Thermodynamics Conference*, and is in preparation for journal publication [19].

Chapter 8:

This chapter discusses the use of the SEAQT framework in modeling multiscale problems and applies it to the modeling of the cathode of a solid oxide fuel cell (SOFC). The oxygen reduction process at the cathode is important for SOFC performance and is influenced by both mesoscopic as well as atomistic-level phenomena. Of particular importance for long-term operation are, microstructure degradation and chromium oxide poisoning both of which degrade cathode performance. To capture the influence of these two phenomena, an oxygen and chromium oxide reduction model is introduced in this chapter using SEAQT. The model efficiently calculates the transient process of system particle number and temperature evolution even for coupled chemical kinetic-diffusion pathways and permits the study of the detailed state evolution of the SOFC cathode system. In this study, the multiscale phenomena of oxygen reduction are revealed including

the influence of microstructure degradation on performance. A qualitative comparison with experimental results is made. Results are also included for the effects of chromium oxide concentrations on cathode output as is a parametric study of the effects of interconnect-three-phase-boundary (TPB) length, oxygen mean-free path, and adsorption site effectiveness. Based on this parametric study and the experimental results presented, the influence of microstructure degradation and chromium oxide poisoning are revealed. This study has been published in the *Proceedings of ASME 2015 International Mechanical Engineering Congress and Exposition* [9], and has been submitted for journal publication.

List of my publication:

- G. Li and M. R. von Spakovsky, “Steepest-entropy-ascent quantum thermodynamic modeling of the relaxation process of isolated chemically reactive systems using density of states and the concept of hypo-equilibrium state," *Phys. Rev. E*, 2015. (in publication). [14]
- G. Li, O. Al-Abbasi, and M. R. von Spakovsky, “Atomistic-level non-equilibrium model for chemically reactive systems based on steepest-entropy-ascent quantum thermodynamics," *Journal of Physics: Conference Series*, vol. 538, no. 1, p. 012013, 2014. [15]
- G. Li and M. R. von Spakovsky, “Steepest-entropy-ascent quantum thermodynamic modeling of heat and mass diffusion in a far-from-equilibrium system based on a single particle ensemble." (unpublished). [16]
- G. Li and M. R. von Spakovsky, “Steepest-entropy-ascent quantum thermodynamic modeling of the far-from-equilibrium interactions between non-equilibrium systems of indistinguishable particle ensembles." (unpublished). [17]
- G. Li and M. R. von Spakovsky, “Application of steepest-entropy-ascent quantum thermodynamics to predicting heat and mass diffusion from the atomistic up to the macroscopic level," in *ASME 2015 International Mechanical Engineering Congress and Exposition*, American Society of Mechanical Engineers, 2015. No. IMECE2015-53581. [18]
- G. Li and M. R. von Spakovsky, “Steepest-entropy-ascent model of reservoir and engine cycle in non-equilibrium using hypo-equilibrium state and an isothermal-isobaric ensemble." (unpublished). [19]
- G. Li and M. R. von Spakovsky, “Study of the transient behavior and microstructure degradation of a SOFC cathode using an oxygen reduction model based on steepest-entropy-ascent quantum thermodynamics," in *ASME 2015 International Mechanical Engineering Congress*

and Exposition, American Society of Mechanical Engineers, 2015. No. IMECE2015-53726. [9]

- G. Li, M. R. von Spakovsky, F. Shen, K. Lu, “Multiscale transient and steady state study of the influence of microstructure degradation and chromium oxide poisoning on SOFC cathode performance." (submitted for publication). [10]

Chapter 2

Steepest-Entropy-Ascent Quantum Thermodynamic Modeling of the Relaxation Process of Isolated Chemically Reactive Systems Using Density of States and the Concept of Hypo-equilibrium State

2.1 Introduction

There are many modeling approaches in non-equilibrium thermodynamics. From a practical standpoint, models developed from any one of these is typically applicable to a given set of spatial and temporal scales so that in the vein of Grmela and Öttinger [20, 21], each model can be classified as being either more macroscopic or less microscopic (or vice versa). Thus, when the non-equilibrium phenomena studied cross different spatial and temporal scales, some form of multi-scale model must be employed. This is typically done via multi-scale computational techniques, which are able to pass system properties from one scale to another [11, 22, 23]. For example, parameters or phenomenological coefficients used in a more macroscopic model are calculated via a more microscopic model, and feedback is used to update them after a time (or distance) interval that is between the characteristic time (or distance) length of the two different models. Such multi-scale

approaches, nonetheless, present a number of significant drawbacks, not the least of which are computational.

Of course, a general rigorous theoretical framework that permits the study of irreversible phenomena across spatial and temporal scales is of great significance. Two such frameworks exist. The first developed by Grmela and Öttinger [20, 21] provides a general equation for non-equilibrium reversible-irreversible coupling (GENERIC) able to couple models from two different scales or levels, i.e., one more microscopic (a level 1 model) and the other more macroscopic (a level 2 model). In general, level 2 models are simpler and rely more on observation and phenomenological descriptions, while those at level 1 are more fundamental and require a significantly higher level of complexity. Grmela and Öttinger suggest that a specific GENERIC equation of motion, which is based on models from two different levels of description, should take the form that satisfies the compatibility of the two models. The analysis of this compatibility, i.e., the passing from a more to a less detailed level, involves a pattern recognition process [20, 21], which corresponds to a kind of coarse graining [24, 25] that results in what looks like dissipation even if the level 1 dynamics is reversible as in fact they are in mechanics. In this way, the two models and levels are linked via a single equation of motion. Clearly, this approach is more rigorous and fundamental than the multiscale computational technique described earlier. It allows the study of the far-from-equilibrium realm where near-equilibrium parameters no longer hold and the link between two different scale models ensures the compatibility of the two levels in a way that simple parameter delivery cannot.

The second general, rigorous theoretical framework is that developed by Beretta [24, 26–29], which provides a general non-equilibrium dynamics for relaxation crossing different scales. Unlike GENERIC, which bases its approach on the linking of models across scales into a single equation of motion, Beretta explains irreversible phenomena at different scales using a single thermodynamic model and a single equation of motion, doing so on the basis of the general principle of steepest entropy ascent (SEA) [26, 27, 30] or equivalently maximum entropy production (e.g., [31]). In this framework, the irreversible part of the equation of motion is built on a geometrical explanation of relaxation, which results in a gradient dynamics of entropy in state space constrained by the energy, particle number, etc. Since thermodynamic rules and the properties used (specifically, extensive thermodynamic properties such as the energy and the entropy) are applicable across all spatial and temporal scales [32, 33], the equation of motion of SEA is well defined and rigorous at all scales. In addition, in [24], Beretta demonstrates that all of the well-known classical and

quantum non-equilibrium frameworks can be formulated within his more general non-equilibrium thermodynamic SEA framework, which is applicable even far from equilibrium.

Although the GENERIC and SEA frameworks approach non-equilibrium thermodynamics from different viewpoint, Montefusco, Consonni, and Beretta [34] show that the dissipative components of the two theories are closely related and in some cases essentially mathematically equivalent, provided that the choice of kinematics is the same, i.e., that both have a common starting point. Furthermore, both provide a geometrical foundation for their dynamics [24, 35]. However, differences exist since the SEA framework is a local theory, which starts from local balance equations and implements the principle of maximum local entropy generation compatible with the local conservation constraints, while the GENERIC framework is global, implementing an entropy gradient dynamics compatible with the global conservation constraints.

To date, the SEA framework, which extends a first principle thermodynamic and ensemble representation into the non-equilibrium realm, even that far from equilibrium, has successfully been applied to very microscopic systems such as the state evolution of quantum systems (e.g., [15, 36–40]) as well as to a single-particle classical system [41] whose available microstates are uniformly distributed in phase space. However, its application to high-dimensional state spaces and, thus, to infinite energy eigenlevel (i.e., more macroscopic) systems has necessarily been limited.

To address this limitation, the GENERIC concept of patterns is used here. To begin with, one may view the irreversible term in the SEA framework as resulting from a pattern in a more microscopic model. In a manner similar to the way at stable equilibrium one can view the “Maxwellian distribution" as an invariant pattern even though the mechanical details of the individual particle states constantly change, steepest entropy ascent can also be viewed as a changing global pattern or effect of the details of the mechanics in relaxation. Thus, without including all of the details of the more microscopic model (i.e., of the mechanics), the pattern of this model serves as a modification of the more macroscopic model (i.e., of the non-equilibrium thermodynamics). This, of course, greatly simplifies the computational complexity, while the clear physical meaning and geometrical description of the SEA landscape facilitates the discovery of general but unique patterns of relaxation in the non-equilibrium realm at any scale.

In view of this, two non-equilibrium relaxation patterns present themselves, which offer two methods for practically (i.e., computationally) extending the application of the SEAQT framework to infinite-dimensional state spaces, even those in the macroscopic continuous spectrum, and

for extending an equilibrium-type description to non-equilibrium states. This extension focuses on the irreversible process of thermodynamic mixture states in which the Hamiltonian dynamics vanishes and the state evolution is due only to thermodynamic irreversibilities. Both methods originate from physical concepts. The discussion begins in Section 2.2 with a brief description of the SEAQT framework and focuses on the trajectory of system thermodynamic state evolution and not its time evolution, since it is the trajectory, which reveals the geometric features of interest. The concept of hypo-equilibrium state is then introduced, which permits temperature to be defined for all non-equilibrium states and implies that the energy eigenlevels in mutual equilibrium evolve as a group. This is followed in Section 2.3 by a description of our density of state method, which allows the macroscopic-level SEAQT equation of motion to be solved. It is based on the idea that similar eigenlevels with similar initial conditions evolve similarly. Finally, in Section 2.4, the novel thermodynamic-ensemble based approach developed and presented in the previous sections is applied within the SEAQT framework to the study of an isolated, chemically reactive, macroscopic system undergoing a non-equilibrium evolution in state. This approach, in fact, represents a computationally simpler, alternative global method for predicting the chemical kinetics of systems, even those far from equilibrium, and does so without the need for the detailed particle mechanics (e.g., that of particle collisions) of conventional approaches or for such limiting assumptions as local or global equilibrium. Topics illustrated and discussed include the features of the non-equilibrium trajectories predicted, the density of states of the chemical reaction process, and the influence of the initial non-equilibrium states on the trajectories. Two generalizations to the non-equilibrium realm of stable equilibrium concepts are also physically illustrated and discussed, i.e., that of hypo-equilibrium state and that of non-equilibrium temperature. The former leads to the definition of the latter and to the possibility of representing a very large class of non-equilibrium states and of approximating an even larger class of other non-equilibrium states in the study of non-equilibrium trajectories.

2.2 Theory: Steepest-entropy-ascent equation of motion

2.2.1 Non-equilirbium evolution framework

Based on the discussion by Grmela [20, 21, 35] and Beretta [24, 34] the general form of a non-equilibrium framework is a combination of both irreversible relaxation and reversible symplectic dynamics. If written in a generalized form of the Ginzburg-Landau equation [20, 34], the equation of motion takes the following form:

$$\frac{d}{dt}\phi(t) = X^H_{\phi(t)} + Y^H_{\phi(t)} \tag{2.1}$$

where $\phi(t)$ represents the state evolution trajectory, $X^H_{\phi(t)}$ and $Y^H_{\phi(t)}$ are functions of the system state $\phi(t)$ and represent the reversible symplectic dynamics and irreversible relaxation process, respectively. In the SEAQT framework, the system state is represented by the density operator $\hat{\rho}$, $X^H_{\phi(t)}$ follows the Schrödinger equation, and $Y^H_{\phi(t)}$ is derived from the SEA principle. Thus,

$$\frac{d\hat{\rho}}{dt} = \frac{1}{i\hbar}[\hat{\rho}, \hat{H}] + \frac{1}{\tau(\hat{\rho})}\hat{D}(\hat{\rho}) \tag{2.2}$$

$\hat{D}$ is the dissipation operator determined via a constrained gradient in Hilbert space. A metric tensor must be specified in the derivation of this dissipation term, since it describes the geometric features of the Hilbert space [24]. τ is the relaxation time, which represents the speed of system evolution in Hilbert space. A general discussion of the SEA formulation of dissipation, using other forms of metric and symplectic terms, is given in [24] with examples of five non-equilibrium thermodynamic frameworks. Furthermore, a version of Eq. (2.2) for a general quantum system is used in [38] to predict and compare with experimental results the decorrelation and decoherence of a system in which the Schrödinger dynamics and relaxation process are coupled. In this paper, the version of Eq. (2.2) considered is for the case when the symplectic part vanishes and only the relaxation part remains. For this case, the SEA equation of motion exhibits useful mathematical features (e.g., hypo-equilibrium states) that enable a clear physical representation of non-equilibrium state evolution and lead to a fast and accurate computational solution.

An example of such an evolution, i.e., that of a pure relaxation process, is the application here of the SEAQT framework to the modeling of an isolated chemically reactive system. The system

is restricted to the class of dilute-Boltzmann-gas states in which the particles are independently distributed [28]. Such states can be represented by a single-particle density operator that is diagonal in the basis of the single-particle eigenstates. In addition, the Hilbert space metric chosen is the Fisher-Rao metric, which is uniform in different dimensions of Hilbert space. Under these conditions, the symplectic Schrödinger term in the equation of motion vanishes, and the study is able to focus on the irreversible relaxation process only.

2.2.2 System and state

Sections 2.2 and 2.3 provide a brief introduction to the SEA equation of motion for dilute-Boltzmann-gases. More details can be found in [28, 42]. The system studied has the Hamiltonian H, and the eigenvalues and eigenvectors of the corresponding operator $\hat{H}$ take the form

$$\hat{H}|\phi_k\rangle = \epsilon_k|\phi_k\rangle \quad k = 1, 2, ... \tag{2.3}$$

where k is the index for the energy eigenlevels. Degeneracy in which an energy eigenlevel can have the same eigenvalue with different eigenvectors is allowed. Equivalently, the system can also be defined by a group of energy eigenlevels and eigenvectors such that

$$\hat{H} = \sum_k \epsilon_k|\phi_k\rangle\langle\phi_k| \tag{2.4}$$

The thermodynamic state of the system can be defined via a probability distribution $\{p_k\}$ among the energy eigenlevels $\{\epsilon_k\}$, which accounts for the diagonal term of the density operator. An element of $\{\epsilon_k\}$ can share the same value in case of degeneracy. As an example, the stable equilibrium state of the system has the following canonical distribution, which provides the maximum entropy:

$$p_k = \frac{1}{Z} e^{-\frac{\epsilon_k}{k_b T}} \tag{2.5}$$

where Z is the partition function $Z = \sum e^{-\frac{\epsilon_k}{k_b T}}$ and the equilibrium temperature is T. Any other state, represented by a probability distribution other than the canonical distribution, is a non-equilibrium state, since the entropy is not a maximum.

The probability space $\{p_k\}$ is the state space for the system. The statistical distance dl between

$p_k(\theta)$ and $p_k(\theta + d\theta)$ can be defined by the Fisher-Rao metric such that

$$dl = \frac{1}{2}\sqrt{\sum_k p_k(\frac{d\ln p_k}{d\theta})^2 d\theta} \tag{2.6}$$

More discussion on choosing a metric can be found in [24]. The parameter θ is continuous and can be chosen as the time t. Now, in order to simplify the representation of the development of the equation of motion in the next two sections (*Section* 2.2.2 and 2.2.3), the square root of the probability $x_i = \sqrt{p_i}$ is defined so that the probability space can be represented by $\boldsymbol{x} = \{x_i\}$. The statistical distance then takes the form

$$dl = \frac{1}{2}\sqrt{\sum_k \frac{1}{p_k}(\frac{dp_k}{d\theta})^2 d\theta} = \sqrt{\sum_k (dx_k)^2} \tag{2.7}$$

where the distance between any two distributions $\boldsymbol{x^a}$ and $\boldsymbol{x^b}$ is the angle:

$$d(\boldsymbol{x^a}, \boldsymbol{x^b}) = \cos^{-1}(\sum_k x_k^a x_k^b) = \cos^{-1}(\boldsymbol{x^a} \cdot \boldsymbol{x^b}) \tag{2.8}$$

According to the discussion in [43], this statistical distance is equivalent to an angle in Hilbert space and has a precise physical meaning in quantum mechanics. Thus, the state of the system as well as the distance in state space can be represented by $\boldsymbol{x}$ and $dl^2 = \sum_k (dx_k)^2 = d\boldsymbol{x} \cdot d\boldsymbol{x}$.

Now, if time t is chosen as the parameter, from Eq. (2.7) one can arrive at

$$\frac{dl}{dt} = \sqrt{\sum_k (\frac{dx_k}{dt})^2} \tag{2.9}$$

which is the speed of the motion in probability or state space.

2.2.3 Property and the equation of motion

A property of the system can be defined as a function of state $\{x_k\}$ such that:

$$I = \sum_k x_k^2 \tag{2.10}$$

$$E = \langle e \rangle = \sum_k \epsilon_k x_k^2 \tag{2.11}$$

$$S = \langle s \rangle = \sum_k -x_k^2 \ln(x_k^2) \tag{2.12}$$

where $\langle \cdot \rangle$ means the ensemble average. The von Neumann formula for entropy is used, because as shown in [32], it has all the characteristics required by thermodynamics.

The gradient of a given property in state space is then expressed by

$$\boldsymbol{g_I} = \sum_k \frac{\partial I}{\partial x_k} \hat{e_k} = \sum_k 2x_k \hat{e_k} \tag{2.13}$$

$$\boldsymbol{g_E} = \sum_k \frac{\partial E}{\partial x_k} \hat{e_k} = \sum_k 2\epsilon_k x_k \hat{e_k} \tag{2.14}$$

$$\boldsymbol{g_S} = \sum_k \frac{\partial S}{\partial x_k} \hat{e_k} = \sum_k [-2x_k - 2x_k \ln(x_k^2)] \hat{e_k} \tag{2.15}$$

where $\hat{e_k}$ is the unit vector for each dimension. Furthermore, for an isolated system, the system satisfies the conservation laws for probability and energy, i.e.,

$$I = \sum_k x_k^2 = 1 \tag{2.16}$$

$$E = \sum_k \epsilon_k x_k^2 = \text{constant} \tag{2.17}$$

and the principle of SEA upon which the equation of motion is based is defined as the system state evolving along the direction that at any instant of time has the largest entropy gradient consistent with the conservation constraints. Since the reversible term vanishes for dilute-Boltzmann-gases in an isolated system, the equation of motion for the irreversible relaxation process is given by

$$\frac{d\boldsymbol{x}}{dt} = \frac{1}{4\tau(\boldsymbol{x})} \boldsymbol{g_S}_{\perp L(\boldsymbol{g_I}, \boldsymbol{g_E})} \tag{2.18}$$

where τ, which is a function of system state, is the relaxation time that describes the speed at which the state evolves in state space in the direction of steepest entropy ascent. $L(\boldsymbol{g_I}, \boldsymbol{g_E})$ is the manifold spanned by $\boldsymbol{g_I}$ and $\boldsymbol{g_E}$, and $\boldsymbol{g_{S\perp L(g_I,g_E)}}$, which lies parallel to the hyper-surface that conserves the probability and the energy, is the perpendicular component of the gradient of the entropy to the manifold $L(\boldsymbol{g_I}, \boldsymbol{g_E})$. It takes the form of a ratio of Gram determinants such that

$$\boldsymbol{g_{S\perp L(g_I,g_E)}} = \frac{\begin{vmatrix} \boldsymbol{g_S} & \boldsymbol{g_I} & \boldsymbol{g_E} \\ (\boldsymbol{g_S},\boldsymbol{g_I}) & (\boldsymbol{g_I},\boldsymbol{g_I}) & (\boldsymbol{g_E},\boldsymbol{g_I}) \\ (\boldsymbol{g_S},\boldsymbol{g_E}) & (\boldsymbol{g_I},\boldsymbol{g_E}) & (\boldsymbol{g_E},\boldsymbol{g_E}) \end{vmatrix}}{\begin{vmatrix} (\boldsymbol{g_I},\boldsymbol{g_I}) & (\boldsymbol{g_E},\boldsymbol{g_I}) \\ (\boldsymbol{g_I},\boldsymbol{g_E}) & (\boldsymbol{g_E},\boldsymbol{g_E}) \end{vmatrix}} \tag{2.19}$$

where $(,)$ denotes the scalar product of two vectors in state space. The explicit form of Eq. (2.18) for $\{x_k\}$ is, thus,

$$\frac{dx_k^2}{dt} = \frac{1}{\tau}\frac{\begin{vmatrix} -x_k^2 \ln x_k^2 & x_k^2 & \epsilon_k x_k^2 \\ \langle s\rangle & 1 & \langle e\rangle \\ \langle es\rangle & \langle e\rangle & \langle e^2\rangle \end{vmatrix}}{\begin{vmatrix} 1 & \langle e\rangle \\ \langle e\rangle & \langle e^2\rangle \end{vmatrix}} \tag{2.20}$$

and for $\{p_k\}$ [28]

$$\frac{dp_k}{dt} = \frac{1}{\tau}\frac{\begin{vmatrix} -p_k \ln p_k & p_k & \epsilon_k p_k \\ \langle s\rangle & 1 & \langle e\rangle \\ \langle es\rangle & \langle e\rangle & \langle e^2\rangle \end{vmatrix}}{\begin{vmatrix} 1 & \langle e\rangle \\ \langle e\rangle & \langle e^2\rangle \end{vmatrix}} \tag{2.21}$$

2.2.4 Equation of motion with degeneracy

The energy eigenlevels $\{\epsilon_k,\ k = 1, 2, ...\}$ and $\{|\phi_k\rangle,\ k = 1, 2, ...\}$ can be reordered and grouped into $\{\epsilon_{ij}, i = 1, 2, ...,\ j = 1, ..., n_i\}$ and $\{|\phi_{ij}\rangle,\ i = 1, 2, ...,\ j = 1, ..., n_i\}$, where $\{\epsilon_{ij} = \epsilon_i,\ j = 1, ..., n_i\}$ are degenerate energy eigenlevels with degeneracy n_i. For the equation of motion (21), the degenerate eigenstates for a given eigenvalue with the same initial probability are equivalent,

and have the same occupation probabilities at all times, which means $p_{ij} = p_{ik}$ for any j, k. For example, the initial distribution among these eigenlevels is proportional to the canonical distribution that gives equal initial probabilities for each degenerate eigenstate. This is the case when these eigenlevels come from the same subsystem of a system in a hypo-equilibrium state (see *Section* 2.2.6). Thus, without loss of generality, the degenerate energy eigenlevels with the same initial probabilities can be combined, and the energy eigenlevels represented by the monotonically non-decreasing energy eigenvalue series $\{\tilde{\epsilon}_i\}$ with degeneracy $\{n_i\}$. The probability $\{\tilde{p}_i\}$ at energy eigenlevel $\{\tilde{\epsilon}_i\}$ is given by

$$\tilde{p}_i = \tilde{x}_i^2 = \sum_{j=1}^{n_i} x_{ij}^2 \tag{2.22}$$

$$x_{ij}^2 = \frac{1}{n_i}\tilde{p}_i = \frac{1}{n_i}\tilde{x}_i^2 \tag{2.23}$$

The system state can, therefore, be represented by a new vector $\{\tilde{x}_i\}$ or $\{\tilde{p}_i\}$ in a new probability space formed by the probability distribution among the energy eigenlevels $\{\tilde{\epsilon}_i\}$. The equality of statistical distance in the original probability space with that in the new probability space is shown by the following development:

$$dl^2 = \sum_i \sum_{j=1}^{n_i} (dx_{ij})^2 = \sum_i \sum_{j=1}^{n_i} (\frac{1}{\sqrt{n_i}} d\tilde{x}_i)^2 = \sum_i (d\tilde{x}_i)^2 \tag{2.24}$$

$$\begin{aligned} d(\boldsymbol{x^a}, \boldsymbol{x^b}) &= \cos^{-1}(\sum_i \sum_{j=1}^{n_i} x_{ij}^a x_{ij}^b) = \cos^{-1}(\sum_i \sum_{j=1}^{n_i} \frac{1}{\sqrt{n_i}}\tilde{x}_i^a \frac{1}{\sqrt{n_i}}\tilde{x}_i^b) \\ &= \cos^{-1}(\sum_i \tilde{x}_i^a \tilde{x}_i^b) = d(\tilde{\boldsymbol{x}}^{\boldsymbol{a}}, \tilde{\boldsymbol{x}}^{\boldsymbol{b}}) \end{aligned} \tag{2.25}$$

In this new vector space, system properties such as I, E, and S are expressed as

$$I = \sum_i \tilde{x}_i^2 \tag{2.26}$$

$$E = \langle e \rangle = \sum_i \tilde{\epsilon}_i \tilde{x}_i^2 \tag{2.27}$$

$$S = \langle s \rangle = \sum_i -\tilde{x}_i^2 \ln(\frac{\tilde{x}_i^2}{n_i}) \tag{2.28}$$

while the equation of motion changes to the following forms for $\{\tilde{x}_j\}$ and $\{\tilde{p}_j\}$:

$$\frac{d\tilde{x}_j^2}{dt} = \frac{1}{\tau}\frac{\begin{vmatrix} -\tilde{x}_j^2 \ln \frac{\tilde{x}_j^2}{n_j} & \tilde{p}_j & \epsilon_j \tilde{x}_j^2 \\ \langle s \rangle & 1 & \langle e \rangle \\ \langle es \rangle & \langle e \rangle & \langle e^2 \rangle \end{vmatrix}}{\begin{vmatrix} 1 & \langle e \rangle \\ \langle e \rangle & \langle e^2 \rangle \end{vmatrix}} \tag{2.29}$$

$$\frac{d\tilde{p}_j}{dt} = \frac{1}{\tau}\frac{\begin{vmatrix} -\tilde{p}_j \ln \frac{\tilde{p}}{n_j} & \tilde{p}_j & \epsilon_j \tilde{p}_j \\ \langle s \rangle & 1 & \langle e \rangle \\ \langle es \rangle & \langle e \rangle & \langle e^2 \rangle \end{vmatrix}}{\begin{vmatrix} 1 & \langle e \rangle \\ \langle e \rangle & \langle e^2 \rangle \end{vmatrix}} \tag{2.30}$$

This new equation of motion for degenerate energy eigenlevels is a simplification of the equation of motion of *Section* 2.2.3 for the assumption that $p_{ij} = p_{ik}$ for any j, k. Equations (2.24) to (2.30) are acquired by substituting Eq. (2.22) into Eqs. (2.7), (2.8), (2.10) to (2.12), (2.20), and (2.21). Since the discussions in the next sections are based on Eq. (2.30), the tilde used to designate the probabilities of the new probability space are dropped for simplicity.

2.2.5 Non-equilibrium evolution trajectory: kinetics versus dynamics

In this section, the kinetics and dynamics of non-equilibrium state evolution are introduced. The result of this section applies to a system with a relaxation process only (i.e., without a symplectic term in the equation of motion) but is not limited to a Fisher-Rao metric system. The equation of motion for a degenerate system, Eq. (2.30), is first simplified by defining A_1, A_2, and A_3 such that

$$A_1 = \begin{vmatrix} 1 & \langle e \rangle \\ \langle e \rangle & \langle e^2 \rangle \end{vmatrix}, A_2 = \begin{vmatrix} \langle s \rangle & \langle e \rangle \\ \langle es \rangle & \langle e^2 \rangle \end{vmatrix}, A_3 = \begin{vmatrix} \langle s \rangle & 1 \\ \langle es \rangle & \langle e \rangle \end{vmatrix} \tag{2.31}$$

The equation of motion then becomes

$$\frac{dp_j}{dt} = \frac{1}{\tau}(-p_j \ln \frac{p_j}{n_j} - p_j \frac{A_2}{A_1} + \epsilon_j p_j \frac{A_3}{A_1}) \tag{2.32}$$

The solution of this equation is

$$p_j = p_j(t) \tag{2.33}$$

where the time evolution of the probability can be regarded as a parametric equation with parameter t. If t is the real time, the solution of Eq. (2.32) provides both the trajectory in state space and the system state at any instant of time.

In general, the relaxation time τ can be a function of system state such that

$$\tau = \tau(\boldsymbol{p}(t)) \tag{2.34}$$

since for a given initial state of the system, the non-equilibrium path of state evolution is uniquely obtained from the equation of motion, Eq. (2.32). This path can be used to define a new parameter $\tilde{\tau}$ given by

$$d\tilde{\tau} = \frac{1}{\tau(\boldsymbol{p}(t))}dt, \quad \text{or} \quad \tilde{\tau} = \int_{path} \frac{1}{\tau(\boldsymbol{p}(t'))}dt' = \tilde{\tau}(t) \tag{2.35}$$

where $\tilde{\tau}$ is called the dimensionless time. With this time, the independent variable for the equation of motion can be changed so that

$$\frac{dp_j}{d\tilde{\tau}} = -p_j \ln \frac{p_j}{n_j} - p_j \frac{A_2}{A_1} + \epsilon_j p_j \frac{A_3}{A_1} \tag{2.36}$$

The solution for this equation is written as

$$p_j = p_j(\tilde{\tau}) \tag{2.37}$$

No matter how the relaxation time τ depends on the real time t and the state, the equation of motion can always be transformed into Eq. (2.36) with the parameter change defined by Eq. (2.35). Furthermore, the evolution of system state follows the same function (Eq. (2.37)) in $\tilde{\tau}$. Physically, this means that the system follows the same trajectory in state space, while τ decides the speed with which the system's state moves along the trajectory. If the relaxation time is chosen to be a constant, Eq. (2.33) gives the same parametric equation, Eq. (2.37), with a parametric scaling in the relaxation time τ. Thus, the kinetics and dynamics of the system are separated. The former are found via Eq. (2.36) and Eq. (2.37) and result in the trajectory in state space based on the parameter $\tilde{\tau}$ or a constant relaxation time τ. The dynamics is found via Eq. (2.32)

and the functional dependence $\tau = \tau(\boldsymbol{p})$ (Eq. (2.34)) and result in the trajectory in state space based on the real time t. Recent numerical results show that a uniform (Fisher-Rao) metric may for some systems provide poor performance relative to the time evolution [41] at least in the near-equilibrium limit. In such cases, the time evolution needs more information on the dynamics or the function τ. For this reason, the results presented here are restricted to the kinetic evolution trajectory and the intermediate states of the relaxation process, and, thus, to the purely geometrical features of the relaxation process.

2.2.6 Description of the trajectory: Subsystem hypo-equilibrium state and temperature

In this section, the concepts of subsystem hypo-equilibrium state and temperature for a system in a non-equilibrium state are defined. These two concepts support the physical description of the evolution trajectory in state space rather than just its mathematical description. However, this description is restricted to systems with irreversible relaxations only. These concepts originate from a generalization of the canonical distribution to a non-equilibrium distribution in Hilbert space with a uniform metric (Fisher-Rao metric). However, such a generalization under any metric is an open question. Furthermore, to be general, the relaxation time τ in this section can be constant or a function of system state, which means that the conclusions drawn apply to both the kinetic and dynamic characteristics of the state space trajectory.

For a given system represented by an energy eigenlevel set $\Omega = \{\epsilon_k\}$, the system can be divided into M subsystems (i.e., subspaces in state space) $\Omega_i = \{\epsilon_{ik}\}$, $\Omega = \bigcup \Omega_i$ and $\Omega_i \cap \Omega_j = \emptyset$ for any $i, j = 1, \cdots, M$. If the probability distribution in each subsystem yields to a canonical distribution, the system is designated as being in an M^{th}-order hypo-equilibrium state. Based on this definition, any state of the system (strictly speaking, a diagonal density operator in an eigenstate basis) is a hypo-equilibrium state with order M, where M is less than or equal to the number of system eigenlevels. A hypo-equilibrium state of order 1 corresponds to a state in stable equilibrium. The probability distribution of the M^{th}-order hypo-equilibrium state takes the form

$$\forall i = 1, 2, ..., M,\ p_{ik} = \alpha_i n_{ik} e^{-\beta_i \epsilon_{ik}},\ k = 1, 2, ..., w_i \tag{2.38}$$

where α_i and β_i are parameters, and n_{ik} is the degeneracy of ϵ_{ik}. To be complete, $\beta_i = 0$ if $w_i = 1$,

and w_i can be infinite.

$\alpha_i Z_i(\beta_i)$ has the physical meaning of particle number where Z_i is the partition function of the subsystem. The inverse of the temperature of each subsystem Ω_i is β_i with a scale of the Boltzmann constant. This temperature is defined for each subsystem when the system is in a state of non-equilibrium. It is proven below that if a system begins in an M^{th}-order hypo-equilibrium state, it will remain in an M^{th}-order hypo-equilibrium state throughout the time evolution as will the subsystem division. To show this, Eq. (2.32) is reformulated such that

$$\frac{d}{dt}\ln\frac{p_j}{n_j} = \frac{1}{\tau}(-\ln\frac{p_j}{n_j} - \frac{A_2}{A_1} + \epsilon_j\frac{A_3}{A_1}) \tag{2.39}$$

where it is noted that $d(\ln n_j)/dt$ is zero and that A_1, A_2, and A_3 are the same for all chosen energy eigenlevels p_j and only a function of the entire probability distribution at a given instant of time. Subtracting the equations of motion for the i^{th} and k^{th} energy eigenlevels results in

$$\frac{d}{dt}(\ln\frac{p_j}{n_j} - \ln\frac{p_k}{n_k}) = -\frac{1}{\tau}(\ln\frac{p_j}{n_j} - \ln\frac{p_k}{n_k}) + \frac{1}{\tau}\frac{A_3}{A_1}(\epsilon_j - \epsilon_k) \tag{2.40}$$

Defining a new variable

$$W_{jk} = \frac{1}{\epsilon_j - \epsilon_k}(\ln\frac{p_j}{n_j} - \ln\frac{p_k}{n_k}) \tag{2.41}$$

the time evolution of W_{jk} yields to the ordinary differential equation

$$\frac{dx}{dt} = -\frac{1}{\tau}x + \frac{1}{\tau}\frac{A_3}{A_1} \tag{2.42}$$

If p_j and p_k are in the same subsystem for which the initial probability distribution is a canonical one, i.e., if

$$p_j(t=0) = \alpha_p n_j e^{-\epsilon_j\beta_p}, \quad p_k(t=0) = \alpha_p n_k e^{-\epsilon_k\beta_p} \tag{2.43}$$

then

$$W_{jk}(t=0) = \frac{1}{\epsilon_j - \epsilon_k}(\ln\frac{p_j}{n_j} - \ln\frac{p_k}{n_k}) = -\beta_p \tag{2.44}$$

For $\forall p_j, p_k$ in the same subsystem Ω_p, the time evolution of W_{jk} yields to the same ordinary differential equation (ODE) with the same initial value, namely,

$$\frac{dx}{dt} = -\frac{1}{\tau}x + \frac{1}{\tau}\frac{A_3}{A_1},\ x = W_{jk}(t=0) = -\beta_p \tag{2.45}$$

so that the solution of W_{jk} is the same $W_{jk}(t) = \beta_p(t)$. Therefore, the probability distribution in this subsystem maintains the canonical distribution with the parameter $\beta_p(t)$ given by

$$p_j(t) = \alpha_p(t) n_j e^{-\epsilon_j \beta_p(t)} \tag{2.46}$$

In addition, the temperature of the subsystem at time t is defined by

$$T_p(t) = \frac{1}{k_b \beta_p(t)} \tag{2.47}$$

Thus, for a system in a non-equilibrium state, the hypo-equilibrium temperature for each subsystem is defined. This temperature can be the same or different from that of any other subsystem. If a system is in an M^{th}-order hypo-equilibrium state, it remains at least of order M throughout as well as after the evolution, and the probability distribution of each subsystem remains canonical. More discussion on the evolution of temperature is given in *Section* 2.5. In addition, the ODE for β_p (Eq. (2.45)) is independent of α_p so that different subsystems with the same initial β_p also keep the same $\beta_p(t)$ in the evolution. This phenomenon is consistent with the idea that energy via a heat interaction cannot transfer between systems with the same temperature to produce a temperature difference. Equal temperature subsystems maintain equal temperatures.

Moreover, if two subsystems A and B are in mutual equilibrium at time t_{me} ($\alpha_p(t_{me})^A = \alpha_p(t_{me})^B$, $\beta_p(t_{me})^A = \beta_p(t_{me})^B$), the combination of these two subsystems yields a subsystem with a canonical distribution. This new subsystem maintains a canonical distribution throughout its state evolution, which means that the two original subsystems maintain their hypo-equilibrium states as well as a state of mutual equilibrium with each other.

The results just demonstrated are summarized as follows: i) the manner of subdividing the system is invariant with respect to the irreversible relaxation trajectory; ii) the probability distribution in each subsystem remains canonical along the trajectory so that temperature can be defined based on a parameter of the canonical distribution; and iii) equal temperature subsystems maintain equal temperatures, and subsystems in mutual equilibrium remain in mutual equilibrium. With the concept of subsystem hypo-equilibrium state, the trajectory for system state evolution in state space is described by two functions $\alpha_p(t)$ and $\beta_p(t)$. Physically each instantaneous value of $\alpha_p(t) Z_p(\beta_p(t))$ is the total probability (particle number) of a given subsystem, while each instantaneous value of $\beta_p(t)$ is the parameter of the canonical distribution and the inverse of the subsystem temperature.

$Z_p(\beta(t))$ is the partition function, which is a function of β. Thus, $\alpha_p(t)$ describes the probability transfer between subsystems, while $\beta_p(t)$ describes the temperature evolution and heat diffusion between subsystems. No longer is the canonical distribution simply a characteristic of stable equilibrium but instead a characteristic of subsystem hypo-equilibrium and maximum entropy generation as well. This feature provides a convenient pattern for studying the evolution of a system's state distribution during an irreversible relaxation process.

For a complete discussion on subspace temperature and a set of general non-equilibrium intensive properties, the reader is referred to [16–18]. Some conclusions from these references are given in *Appendix* A.2, including a clear physical picture, based on the concepts of hypo-equilibrium state and non-equilibrium intensive property, of the generalization of the Onsager relations and the dissipation potential to the non-equilibrium realm. In addition, for a discussion of the relationship of the general Onsager framework of non-equilibrium thermodynamics [44] to SEAQT and GENERIC, the reader is referred to [24, 42] for the SEAQT framework and to [45] for the GENERIC.

2.3 Model: Density of state method

In this section, the numerical method for solving the SEAQT equation of motion is introduced. Called the density of state method, its purpose is to solve this equation for an extremely large number of energy eigenlevels, a number, in fact, so large that even the state evolution of macroscopic systems can be determined. This numerical method follows the same idea as the derivation of the equation of motion for a degenerate system, namely, that similar eigenlevels with similar initial states evolve similarly. An example of a system with a very large number of levels is that of an ideal gas at a temperature higher than the characteristic temperature for translation. A practical illustration is given in *Section* 2.4.

2.3.1 Probability cut

For an isolated system with unbounded energy, the probability distribution is assumed to be limited to a bounded range of energy eigenlevels. This means that in the $\lim_{K\to\infty} p(\epsilon > \epsilon_K) = 0$, and the energy eigenlevels in the bounded range can be used to approximate the unbounded range of the system. For a given system $\{\epsilon_i,\ i = 1, 2, ...\}$ and initial state $\{p_i, i = 1, 2, ...\}$, K is chosen

such that $\sum_{i>K} p_K < \delta$ resulting in $\epsilon_{cut} = \epsilon_K$ and the set of system bounded energy eigenvalues $\epsilon_i < \epsilon_{cut}$.

2.3.2 Evolution of probability in energy intervals

For a system with bounded energy eigenvalues, a subset of the energy eigenlevels can be chosen to be a subsystem or an entire system. The range of energy eigenlevels of this subset are then separated into finite intervals such that

$$e_i = \epsilon_{ground} + \frac{i}{R}(\epsilon_{cut} - \epsilon_{ground}) \tag{2.48}$$

$$\text{Interval: } [e_{i-1}, e_i], \quad i = 1, ..., R$$

$$\text{Interval length: } \Delta E = e_i - e_{i-1}, \quad i = 1, ..., R$$

where R is the number of intervals. Integrating the equation of motion Eq. (2.32) over the i^{th} interval $[e_{i-1}, e_i]$ yields the equation of motion for the probability in the i^{th} interval, namely,

$$\frac{dP_i}{dt} = \frac{1}{\tau}(\langle s \rangle_i - P_i \frac{A_2}{A_1} + \langle e \rangle_i \frac{A_3}{A_1}) \tag{2.49}$$

where $P_i = \sum_{\epsilon_k \in [e_{i-1}, e_i]} p_k$ is the probability distributed over the energy levels in the interval $[e_i, e_{i-1}]$, $\langle s \rangle_i = -\sum_{\epsilon_k \in [e_{i-1}, e_i]} p_k \ln(p_k/n_k)$ is the contribution of this energy interval to the total entropy, and $\langle e \rangle_i = \sum_{\epsilon_k \in [e_{i-1}, e_i]} \epsilon_k p_k$ is the contribution of this energy interval to the total energy. By summing the property of every energy interval, the property of the whole system (e.g., the total entropy and total energy) can be determined.

2.3.3 Energy spectrum agglomeration

For a given initial state, the energy eigenlevels of the system can be separated into M groups. Each group forms a subsystem, and the probability distribution of each subsystem is assumed to be a gamma distribution or its linear combination, which can cover quite a large range of initial conditions. A subsystem K is chosen, and its range of energy eigenvalues divided into R intervals. It is assumed that there are m_i energy eigenvalues $\{\epsilon_j^i, j = 1, ...m_i\}$ with degeneracies $\{n_j^i, j = 1, ...m_i\}$ in the interval $[e_{i-1}, e_i]$ of subsystem K where m_i can be infinity.

A pseudo subsystem with energy eigenvalues $\{E_i,\ i = 1, ..., R\}$ and degeneracies $\{N_i,\ i = 1, ..., R\}$ is then constructed such that

$$N_i = \sum_{j=1}^{m_i} n_j^i \tag{2.50}$$

$$E_i = \frac{1}{N_i} \sum_{j=1}^{m_i} n_j^i \epsilon_j^i \tag{2.51}$$

For any distribution, P_i is the distribution of the i^{th} interval of the K^{th} subsystem expressed by

$$P_i = \sum_{j=1}^{m_i} p_j^i \tag{2.52}$$

If the subsystem is has a distribution given by

$$p_j^i = C n_j^i (\epsilon_j^i)^\theta e^{-\epsilon_j^i \beta} \tag{2.53}$$

where C is a constant, n_j^i is the degeneracy of energy eigenlevel ϵ_j^i. The pseudo subsystem distribution at the same temperature is expressed as

$$\hat{P}_i = C N_i (E_i)^\theta e^{-E_i \beta} \tag{2.54}$$

where C is the same as in Eq. (2.53). In *Appendix* A.1, $\hat{P}_i$ is proven to be equal to P_i for most energy intervals under the quasi-continuous condition expressed as

$$\frac{1}{\beta} \gg |E_{i+1} - E_i| > |\epsilon_j^i - E_i| \tag{2.55}$$

Note that $\hat{P}_i$ becomes a probability distribution with normalization condition when the system as a whole is considered. It is assumed that the quasi-continuous condition holds both for the pseudo

as well as the original subsystem. Now, for the original subsystem,

$$\langle e\rangle_i = \sum_j p_j^i \epsilon_j^i \tag{2.56}$$

$$\langle s\rangle_i = -\sum_j p_j^i \ln \frac{p_j^i}{n_j^i} \tag{2.57}$$

$$\langle e\rangle_K = \sum_i \sum_j p_j^i \epsilon_j^i \tag{2.58}$$

$$\langle s\rangle_K = -\sum_i \sum_j p_j^i \ln \frac{p_j^i}{n_j^i} \tag{2.59}$$

$$\langle es\rangle_K = -\sum_i \sum_j p_j^i \epsilon_j^i \ln \frac{p_j^i}{n_j^i} \tag{2.60}$$

$$\langle e^2\rangle_K = \sum_i \sum_j p_j^i (\epsilon_j^i)^2 \tag{2.61}$$

while for the pseudo subsystem,

$$\langle \hat{e}\rangle_i = E_i \hat{P}_i \tag{2.62}$$

$$\langle \hat{s}\rangle_i = -\hat{P}_i \ln \frac{\hat{P}_i}{N_i} \tag{2.63}$$

$$\langle \hat{e}\rangle_K = \sum_i \hat{P}_i E_i \tag{2.64}$$

$$\langle \hat{s}\rangle_K = -\sum_i \hat{P}_i \ln \frac{\hat{P}_i}{N_i} \tag{2.65}$$

$$\langle \hat{es}\rangle_K = -\sum_i \hat{P}_i E_i \ln \frac{\hat{P}_i}{N_i} \tag{2.66}$$

$$\langle \hat{e^2}\rangle_K = \sum_i \hat{P}_i E_i^2 \tag{2.67}$$

Here $\langle\cdot\rangle_i$ stands for the contribution of the i^{th} interval of the pseudo or original subsystem to the system property, while $\langle\cdot\rangle_K$ stands for the contribution of the entire K^{th} subsystem to the system property. The system properties are then found as is done in *Appendix* A.1 by summing the subsystem properties over the index K. In *Appendix* A.1, it is proven that under the quasi-continuous condition, a pseudo subsystem property in a given energy interval is in most cases equal to that of the original subsystem, and the associated subsystem and system property as well as A_1, A_2, A_3, $\hat{A}_1$, $\hat{A}_2$, and $\hat{A}_3$ are equal to those of the original subsystem. The latter are written

as

$$A_1 = \begin{vmatrix} 1 & \langle e \rangle \\ \langle e \rangle & \langle e^2 \rangle \end{vmatrix}, A_2 = \begin{vmatrix} \langle s \rangle & \langle e \rangle \\ \langle es \rangle & \langle e^2 \rangle \end{vmatrix}, A_3 = \begin{vmatrix} \langle s \rangle & 1 \\ \langle es \rangle & \langle e \rangle \end{vmatrix} \tag{2.68}$$

$$\hat{A}_1 = \begin{vmatrix} 1 & \langle \hat{e} \rangle \\ \langle \hat{e} \rangle & \langle \hat{e^2} \rangle \end{vmatrix}, \hat{A}_2 = \begin{vmatrix} \langle \hat{s} \rangle & \langle \hat{e} \rangle \\ \langle \hat{es} \rangle & \langle \hat{e^2} \rangle \end{vmatrix}, \hat{A}_3 = \begin{vmatrix} \langle \hat{s} \rangle & 1 \\ \langle \hat{es} \rangle & \langle \hat{e} \rangle \end{vmatrix} \tag{2.69}$$

The combination of M pseudo subsystems can then be used as a numerical approximation of the original system for each energy interval (Eq. (2.49)), i.e.,

$$\text{Original system: } \frac{dP_i}{dt} = \frac{1}{\tau}(\langle s \rangle_i - P_i \frac{A_2}{A_1} + \langle e \rangle_i \frac{A_3}{A_1}), \quad P_i(t=0) = C \sum_j n_j^i e^{-\epsilon_j^i \beta} \tag{2.70}$$

$$\text{Pseudo system: } \frac{d\hat{P}_i}{dt} = \frac{1}{\tau}(\langle \hat{s} \rangle_i - \hat{P}_i \frac{\hat{A}_2}{\hat{A}_1} + \langle \hat{e} \rangle_i \frac{\hat{A}_3}{\hat{A}_1}), \quad \hat{P}_i(t=0) = C N_i e^{-E_i \beta} \tag{2.71}$$

Using the time evolution of the pseudo system, the property evolution of the system, such as that for temperature and entropy, can be determined.

2.4 Application to an isolated chemically reactive ideal gas mixture

2.4.1 System definition and state representation

2.4.1.1 Microstate

The state space of a chemically reactive system is composed of two subspaces, reactant and product. The energy eigenlevels of the reactants and those of the products together form the energy eigenlevels for the system as a whole. Denoting the state space of the reactants by $\mathcal{H}^{reactant}$ and that of the products by $\mathcal{H}^{product}$, the system state space $\mathcal{H}$ takes the form

$$\mathcal{H} = \mathcal{H}^{reactant} \oplus \mathcal{H}^{product} \tag{2.72}$$

The simple yet well-studied chemical reaction mechanism considered here is

$$F + H_2 \Leftrightarrow FH + H \tag{2.73}$$

since it is well-adapted to illustrating our general approach. Reaction mechanisms in the vein of the general Guldberg-Waage chemical relaxation equation are considered in [46] where the SEAQT framework is used to model coupled reaction mechanisms while in [9, 10] complex, coupled reaction-diffusion pathways are used to predict the effects of micro-structural degradation and chromium oxide poisoning on the performance of a solid oxide fuel cell cathode. Predictions made are compared with experimental data. A study of chemical reaction rate is also given in [15]. In addition, Grmela provides a study using GENERIC [47] of the entropy production that occurs in chemically reactive systems represented by the general Guldberg-Waage chemical relaxation equation.

Now, the available energy eigenvalues for one subspace (reactant or product) are constructed from the energy eigenvalues of each degree of freedom, i.e.,

$$\epsilon^{reactant} = \epsilon_{t,H_2} + \epsilon_{r,H_2} + \epsilon_{v,H_2} + \epsilon_{t,F} \tag{2.74}$$

$$\epsilon^{product} = \epsilon_{t,FH} + \epsilon_{r,FH} + \epsilon_{v,FH} + \epsilon_{t,H} \tag{2.75}$$

The translational energy eigenvalue ϵ_t uses the form of the infinite potential well, the rotational energy eigenvalue ϵ_r the form of the rigid motor, and the vibrational energy eigenvalue ϵ_v the form of the harmonic oscillator, i.e.,

$$\epsilon_t(n_x, n_y, n_z) = \frac{\hbar^2}{8m}\left(\left(\frac{n_x}{L_x}\right)^2 + \left(\frac{n_y}{L_y}\right)^2 + \left(\frac{n_z}{L_z}\right)^2\right) \tag{2.76}$$

$$\epsilon_r(j, m) = \frac{j(j+1)\hbar^2}{2I} = \frac{j(j+1)\hbar^2}{2\mu r^2} \tag{2.77}$$

$$\epsilon_v(\nu) = \left(\nu + \frac{1}{2}\right)\hbar\omega + E_d \tag{2.78}$$

where n_x, n_y, and n_z are the quantum numbers for the translational degrees of freedom; j and m are the quantum numbers for the rotational degrees of freedom; and ν is the quantum number for the vibrational degrees of freedom. ϵ_d is the disassociation energy of a given molecule (e.g. H_2 and FH). Each combination of quantum numbers corresponds to one energy eigenlevel of reac-

tant or product without degeneracy (provided the rotational state is distinguished by the magnetic quantum number m). The system energy eigenlevels are formed by all the available energy eigenlevels of reactants and products. The separation of the two subspaces $\{\epsilon^{reactant}\}$ and $\{\epsilon^{product}\}$ is kept to maintain their clear physical meaning. In the modeling, these two subspaces serve as two subsystems in the discussion of system non-equilibrium state.

2.4.1.2 Density of state

For temperatures higher than the characteristic temperatures of translation and rotation, the energy eigenlevels distribute from the ground state to infinity with high density. These spectrums can be approximated to be continuous. The densities of states of translational and rotational energy for species A are given by

$$D_{t,A}(\epsilon)d\epsilon = \frac{2\pi V}{h^3}(2m_A)^{\frac{3}{2}}\epsilon^{\frac{1}{2}}d\epsilon \tag{2.79}$$

$$D_{r,A}(\epsilon)d\epsilon = \frac{2I_A}{\hbar^2}d\epsilon \tag{2.80}$$

In contrast, that for vibration is assumed to be discrete. To describe the available energy eigenlevels, density of states instead of individual energy eigenlevels are used because of the extremely large number of the latter. Similar to the way of dealing with individual energy eigenlevels, the density of states is calculated separately for reactants and products. The joint density of states from the densities of states of M independent energy forms can be calculated from

$$D(E)dE = \int_{\sum_{i=1}^{M} e_i = E} D_1(e_1)D_2(e_2)\cdots D_M(e_M)de_1de_2\cdots de_M \tag{2.81}$$

$$= dE\int_{E_1^g}^{E} de_1 \int_{E_2^g}^{E-e_1} de_2 \cdots \int_{E_M^g}^{E-\sum_{i=1}^{M-2}} de_{M-1}D_1(e_1)D_2(e_2)\cdots D_{M-1}(e_{M-1})D_M(E-\sum_{i=1}^{M-1} e_i)$$

where E_i^g is the ground state for the i^{th} density of states.

Specifically, the density of states for one subsystem of the system studied can be calculated by

$$D_{reac}(E)dE = \int_{\epsilon_{t,H_2}+\epsilon_{r,H_2}+\epsilon_{v,H_2}+\epsilon_{t,F}=E} D_{t,H_2}(\epsilon_{t,H_2})D_{r,H_2}(\epsilon_{r,H_2})D_{v,H_2}(\epsilon_{v,H_2})D_{t,F}(\epsilon_{t,F}) \times d\epsilon_{t,H_2}d\epsilon_{r,H_2}d\epsilon_{v,H_2}d\epsilon_{t,F} \tag{2.82}$$

$$D_{prod}(E)dE = \int_{\epsilon_{t,FH}+\epsilon_{r,FH}+\epsilon_{v,FH}+\epsilon_{t,H}=E} D_{t,FH}(\epsilon_{t,FH})D_{r,FH}(\epsilon_{r,FH})D_{v,FH}(\epsilon_{v,FH})D_{t,H}(\epsilon_{t,H}) \times d\epsilon_{t,FH}d\epsilon_{r,FH}d\epsilon_{v,FH}d\epsilon_{t,H} \tag{2.83}$$

The joint distribution of the density of states of translational and rotational energy eigenlevels takes the form

$$D_{t,r}^{reac}(E)dE = \int_{\epsilon_{t,H_2}+\epsilon_{r,H_2}+\epsilon_{t,F}=E} D_{t,H_2}(\epsilon_{t,H_2})D_{r,H_2}(\epsilon_{r,H_2})D_{t,F}(\epsilon_{t,F})d\epsilon_{t,H_2}d\epsilon_{r,H_2}d\epsilon_{t,F}$$
$$= \frac{2\pi V}{h^3}(2m_{H_2})^{\frac{3}{2}}\frac{2\pi V}{h^3}(2m_F)^{\frac{3}{2}}\frac{2I_{H_2}}{\hbar^2}\frac{1}{3}B(\frac{3}{2},\frac{3}{2})E^3dE \tag{2.84}$$

$$D_{t,r}^{prod}(E)dE = \int_{\epsilon_{t,FH}+\epsilon_{r,FH}+\epsilon_{t,H}=E} D_{t,FH}(\epsilon_{t,FH})D_{r,FH}(\epsilon_{r,FH})D_{t,H}(\epsilon_{t,H})d\epsilon_{t,FH}d\epsilon_{r,FH}d\epsilon_{t,H}$$
$$= \frac{2\pi V}{h^3}(2m_{FH})^{\frac{3}{2}}\frac{2\pi V}{h^3}(2m_H)^{\frac{3}{2}}\frac{2I_{FH}}{\hbar^2}\frac{1}{3}B(\frac{3}{2},\frac{3}{2})E^3dE \tag{2.85}$$

where $B(\dots,\dots)$ is the beta function. Generally, the energy eigenlevels for a subspace are constructed from t translational and r rotational degrees of freedom, and the density of states for the subsystem built from these eigenlevels takes the form

$$D_{t,r}(E)dE \propto E^{\frac{1}{2}t+r-1}dE \tag{2.86}$$

For temperatures not much greater than or less than or equal to the characteristic temperature of the vibrational degrees of freedom, the form of the density of state for each subsystem is, respectively,

$$D^{reac}(E-\epsilon_{d,H_2})dE = D_{t,r}^{reac}(E)dE \tag{2.87}$$

$$D^{prod}(E-\epsilon_{d,FH})dE = D_{t,r}^{reac}(E)dE \tag{2.88}$$

where ϵ_{d,H_2} and $\epsilon_{d,FH}$ are the ground energy of vibrational degrees of freedom of H_2 and FH,

which are approximated by the disassociation energies of H_2 and FH.

For temperatures much greater than the characteristic temperature of the vibrational degrees of freedom, the form of the density of state for each subsystem is, respectively,

$$D^{reac}(E)dE = dE \sum_{\nu,\epsilon_{\nu,H_2}<E} D^{reac}_{t,r}(E - \epsilon_{\nu,H_2}) \tag{2.89}$$

$$D^{prod}(E)dE = dE \sum_{\nu,\epsilon_{\nu,FH}<E} D^{prod}_{t,r}(E - \epsilon_{\nu,FH}) \tag{2.90}$$

Finally, the energy eigenlevel information for reactant ($\{\epsilon_i^{reactant}\}$ and $\{n_i^{reactant}\}$) and product ($\{\epsilon_j^{product}\}$ and $\{n_j^{product}\}$) is obtained. The system has energy eigenlevels, $\{\epsilon_i^{reactant}, \epsilon_j^{product}\}$ and density of states $\{n_i^{reactant}, n_j^{product}\}$.

2.4.2 Numerical Process

2.4.2.1 Cut-off energy

With the density of states for each subspace, the cut-off energy for the system at a fixed energy corresponding to an initial state or that of stable equilibrium can easily be calculated. Given the density of states $n(E)$ of a subsystem and a type of probability distribution with parameter θ which takes the form that reduces to the canonical distribution when $\theta = 0$, i.e.,

$$p(E) \propto D(E)E^{\theta}e^{-\beta E} \tag{2.91}$$

the cumulative distribution function becomes

$$F(E) \propto \int_{E_{ground}}^{E} D(E')E^{\theta}e^{-\beta E'}dE' \tag{2.92}$$

The cut-off energy is then the inverse of the cumulative distribution function F where δ is a very small number, namely,

$$E_{cut} = F^{-1}(1 - \delta) \tag{2.93}$$

As an example, take a system consisting of an ideal gas mixture that has a temperature lower than the characteristic temperature of vibration but higher than that of translation and rotation. This is indicative of the conditions for a very large number of ideal gas applications ($10^2 \sim 10^3$ K). The

energy eigenlevels for a subspace are constructed from t translational and r rotational degrees of freedom, and the density of states for the subsystem built from these eigenlevels takes the form

$$D_{t,r}(E) = C_0 E^{\frac{1}{2}t+r-1} \tag{2.94}$$

where the procedure for determining C_0 is given in previous section [e.g., see Eqs. (2.84) and (2.85)]. If the probability distribution in the subsystem is a gamma function with parameter β and θ then

$$p(E) \propto D_{t,r}(E) E^{\theta} e^{-\beta E} \propto E^{\alpha+\theta-1} e^{-\beta E} \propto \Gamma(\alpha+\theta,\beta) \tag{2.95}$$

The distribution among the subsystem energy eigenlevels yields to the gamma distribution $\Gamma(\alpha+\theta,\beta)$ with the following parameter definitions:

$$\alpha = \frac{1}{2}t + r, \beta = \frac{1}{k_b T} \tag{2.96}$$

The distribution and cumulative distribution functions then take the form

$$p(E) = \frac{E^{\alpha+\theta-1}e^{-\beta E}}{\int_0^{\infty} E'^{\alpha+\theta-1}e^{-\beta E'}dE'} = \frac{\beta^{\alpha+\theta}}{\Gamma(\alpha+\theta)} E^{\alpha+\theta-1}e^{-\beta E} \tag{2.97}$$

$$F(E) = \frac{\int_{\approx 0}^{E} E'^{\alpha+\theta-1}e^{-\beta E'}dE'}{\int_0^{\infty} E'^{\alpha+\theta-1}e^{-\beta E'}dE'} = \frac{\gamma(\alpha+\theta,\beta E)}{\Gamma(\alpha+\theta)} \tag{2.98}$$

where $\Gamma(\alpha+\theta)$ is the gamma function evaluated at $\alpha+\theta$, and $\gamma(\alpha+\theta,\beta E)$ is the lower incomplete gamma function. The energy of the ground state is approximately zero. The cut-off energy is found from the inverse of the cumulative distribution function such that

$$E_{cut} = F^{-1}(1-\delta;\alpha+\theta,\beta) \tag{2.99}$$

2.4.2.2 Pseudo-system

Since there are two subspaces for the chemically reactive system considered here, i.e., one for reactants and the other for products, two cut-off energies are calculated; and the larger one is used to truncate the open interval of infinite energy eigenlevels into a closed one. To establish the pseudo-system, an energy interval ΔE is chosen according to the quasi-continuous condition, Eq. (2.55). Two pseudo-subsystems are then set up, one for the reactants and the other for the

products. The pseudo-system for the composite system is the combination of the two pseudo subsystems. The energy eigenvalue and degeneracy for one pseudo-subsystem corresponding to the i^{th} interval are then determined by integrating Eqs. (2.50) and (2.51) over that interval where the summations are replaced by integrals using the density of states $D(E)$ so that

$$N_i = \int_{e_i}^{e_i+\Delta E} D(E)dE \tag{2.100}$$

$$E_i = \frac{1}{N_i}\int_{e_i}^{e_i+\Delta E} D(E)EdE \tag{2.101}$$

Using Eq. (2.86) and considering only translational and rotational degrees of freedom, the energy eigenvalue and degeneracy for the i^{th} energy interval is

$$N_i = C_0\int_{e_i}^{e_i+\Delta E} E^{\alpha-1}dE = \frac{C_0}{\alpha}[(e_i+\Delta E)^\alpha - e_i^\alpha] \tag{2.102}$$

$$E_i = \frac{C_0}{N_i}\int_{e_i}^{e_i+\Delta E} E^{\alpha}dE = \frac{\alpha}{\alpha+1}\frac{(e_i+\Delta E)^{\alpha+1} - e_i^{\alpha+1}}{(e_i+\Delta E)^\alpha - e_i^\alpha} \tag{2.103}$$

where C_0 and α are defined by Eqs. (2.94) and (96), respectively, and calculated via Eqs. (2.82) and (83). Once the pseudo-system has been defined in this way, the evolution of the isolated chemically reactive system can be determined.

2.4.3 Initial condition

We provide the analytical solution for an initial condition when the vibrational energy is frozen.

2.4.3.1 Initial condition 1: 2^{nd}-order hypo-equilibrium

For a 2^{nd}-order hypo-equilibrium state, it is assumed that the reactant energy eigenlevels and product energy eigenlevels form subspaces, respectively. In either subspace, the distribution is proportional to the canonical distribution. Using Eqs. (2.84) to (85) and (87) to (88),

$$p^{reac}(E-\epsilon_{d,H_2})dE = p_{t,r}^{reac}(E)dE \propto D_{t,r}^{reac}(E)e^{-\beta E}dE \propto E^3e^{-\beta E}dE \tag{2.104}$$

$$p^{prod}(E-\epsilon_{d,FH})dE = p_{t,r}^{prod}(E)dE \propto D_{t,r}^{prod}(E)e^{-\beta E}dE \propto E^3e^{-\beta E}dE \tag{2.105}$$

Both distributions are $\Gamma(4,\beta)$ gamma distributions and both normalization constants are $\beta^4/\Gamma(4)$, where $\Gamma(4)$ is calculated from the gamma function.

2.4.3.2 Initial condition 2: The gamma distribution

If the initial condition for one subspace (reactant or product) takes the general form of a gamma distribution, then, for example, the reactant subspace distribution is given by

$$p^{reac}(E-\epsilon_{d,H_2})dE \propto E^{3+\theta}e^{-\beta E}dE \tag{2.106}$$

since the product has little probability initially. Equation (2.106) is the gamma distribution $\Gamma(4+\theta, 1/\beta)$. The mean and variance of E takes the form

$$Mean = \frac{4+\theta}{\beta} \tag{2.107}$$

$$Var = \frac{4+\theta}{\beta^2} \tag{2.108}$$

By varying θ, the influence of the initial condition can be studied. For instance, the effusion process can result in a gamma distribution if the probability distribution of one of the reactant's (e.g., F) energy eigenlevels is

$$p^F(E)dE = p_t^F(E)dE = \beta^2 E e^{-\beta E}dE \tag{2.109}$$

This is the energy distribution of an effusion particle, which can be acquired from the velocity distribution

$$F(v)dv \propto v f_M(v)dv \propto v \times v^2 e^{-\frac{mv^2}{2k_bT}}dv \tag{2.110}$$

where f_M is the Maxwellian velocity distribution. The other reactant H_2 has the Maxwellian probability distribution of its energy eigenlevels given by

$$p_{t,r}^{H_2}(E)dE = \frac{D_{t,r}^{H_2}(E)e^{-\beta E}}{Z_{t,r}^{H_2}(\beta)}dE = \frac{\beta^{5/2}}{\Gamma(5/2)}E^{3/2}e^{-\beta E}dE \tag{2.111}$$

where $D_{t,r}^{H_2}$ is the density of state for H_2 with vibrational degrees of freedom frozen, and $Z_{t,r}^{H_2}$ is the partition function. This results in a gamma distribution for $\theta = 0.5$ in Eq. (2.106). The initial reactant state is then

$$p^{reac}(E-\epsilon_{d,H_2})dE = p_{t,r}^{reac}(E) = \int_0^E p^F(E-e_1)p^{H_2}(e_1)de_1 = \frac{\beta^{9/2}}{\Gamma(9/2)}E^{7/2}e^{-\beta E}dE \tag{2.112}$$

2.5 Results and discussion

2.5.1 2^{nd}-order hypo-equilibrium initial condition

The fundamental theoretical result for the SEA equation of motion is composed of two parts: the non-equilibrium kinetic trajectory in state space and the subsystem temperatures. SEA predicts a unique trajectory for non-equilibrium state evolution (*Section* 2.2.5), while the definition of subsystem and subsystem temperature (*Section* 2.2.6) provide a good framework for studying the trajectory. Unlike phenomenological definitions of non-equilibrium temperature, the subsystem temperature defined here is fundamental and has a clear physical picture: the temperature is defined via the canonical distribution. Furthermore, the principle of SEA leads to a set of very well-defined physical and mathematical features for subsystem temperature, which allow subsystem hypo-equilibrium state and temperature to be reasonable generalizations of the existing concepts of state and temperature at stable equilibrium. In order to illustrate the above ideas, the non-equilibrium behavior of the isolated chemically reactive system introduced earlier is modeled using the SEAQT framework. A discussion of results for the state evolution trajectory in state space and on an energy-entropy (E-S) diagram is given first followed by a discussion of results for the total probability and temperature of the subsystems.

The initial state of the system is chosen to be a 2^{nd}-order hypo-equilibrium state, and the two subsystems are the reactant and product subspaces. The temperatures of the two subsystems for the initial non-equilibrium state are selected to be 300 K and 400 K, respectively. Although it would be more reasonable to choose the same temperature, the temperatures chosen here are to better illustrate subsystem temperature evolution. The total probability in the reactant subsystem is 0.9999, and that in the product subsystem 0.0001. The cut-off energy is 5.76×10^{-19} J, and the energy interval is 8.84×10^{-23} J. As a comparison, the real energy eigenlevel interval is 2.62×10^{-43} J, and the interval calculated with the initial temperature is $1/\beta(t=0) = 6.9 \times 10^{-21}$ J. Thus, the quasi-continuous condition holds. There are $14,127$ energy eigenlevels in the reactant subspace (or subsystem) and $16,666$ energy eigenlevels in the product subspace (or subsystem). At the initial state, the system has more than a 0.999999 probability of being distributed in the 3500 energy eigenlevels below the cut-off energy of 5.76×10^{-19} J. Thus, a total of $30,793$ levels are used to represent with great accuracy (as demonstrated below) the estimated 10^{130} levels of the actual

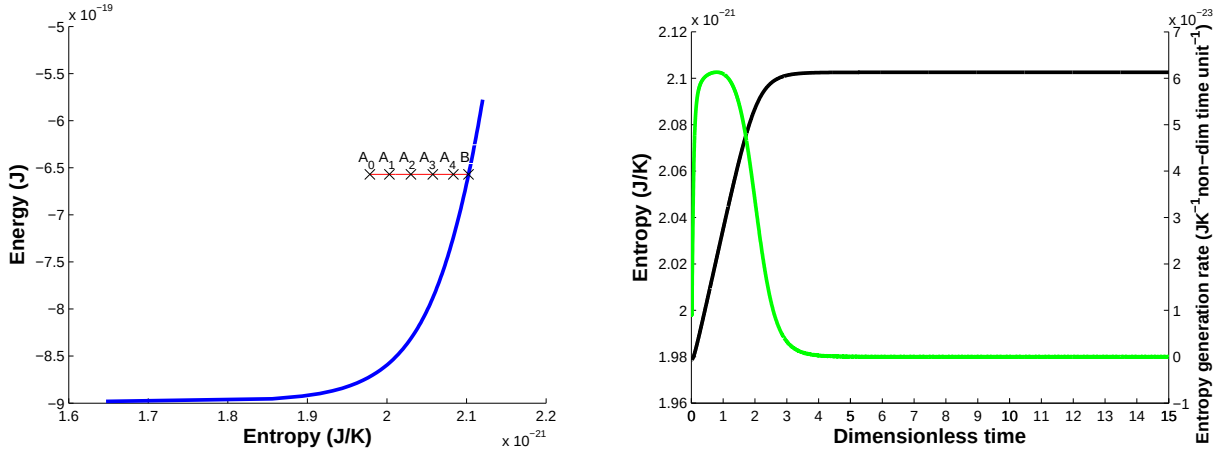

Figure 2.1. e

volutions as a function of dimensionless time.](a:top) System state evolution trajectory on an energy-entropy diagram; (b:bottom) entropy (black line) and entropy generation rate [green (light gray) line] evolutions as a function of dimensionless time.

system. The relaxation time is chosen to be 1 so that the kinetics of state evolution is studied using dimensionless time.

Fig. 2.1a shows the system state evolution trajectory on an energy-entropy diagram [48]. For any state of the system (non-equilibrium or equilibrium), the system state can be mapped to one point on the energy-entropy diagram. The bold solid concave curve is the stable equilibrium curve, and any point on the curve represents a stable equilibrium state. Because the stable equilibrium state has the maximum entropy at a given energy, composition, and volume, there is no system state available to the right of the stable equilibrium curve. Point A_0 is the initial state in the chemically reactive model. If the system state evolution trajectory is mapped from state space to the energy-entropy diagram, the trajectory is a horizontal line (red line) at a given energy. Points A_1 to A_4 are four intermediate non-equilibrium states on the evolution trajectory, and point B on the concave curve is the stable equilibrium state.

Fig. 2.1b shows the changes in the entropy and entropy generation rate values as the system state evolves along the trajectory. The entropy generation rate is not constant along the dimensionless time axis. According to SEA, the entropy generation rate is proportional to $\boldsymbol{g}_{\boldsymbol{S}\perp L(\boldsymbol{g}_{\boldsymbol{I}},\boldsymbol{g}_{\boldsymbol{E}})}$, which lies parallel to the constant probability and constant energy hyper-surface and is the perpendicular component of the entropy gradient to the manifold $L(\boldsymbol{g}_{\boldsymbol{I}},\boldsymbol{g}_{\boldsymbol{E}})$. Thus, the entropy generation rate reveals the entropy gradient changes along the trajectory in state space.

Fig. 2.2a shows the probability distribution among the energy eigenlevels when the system is at

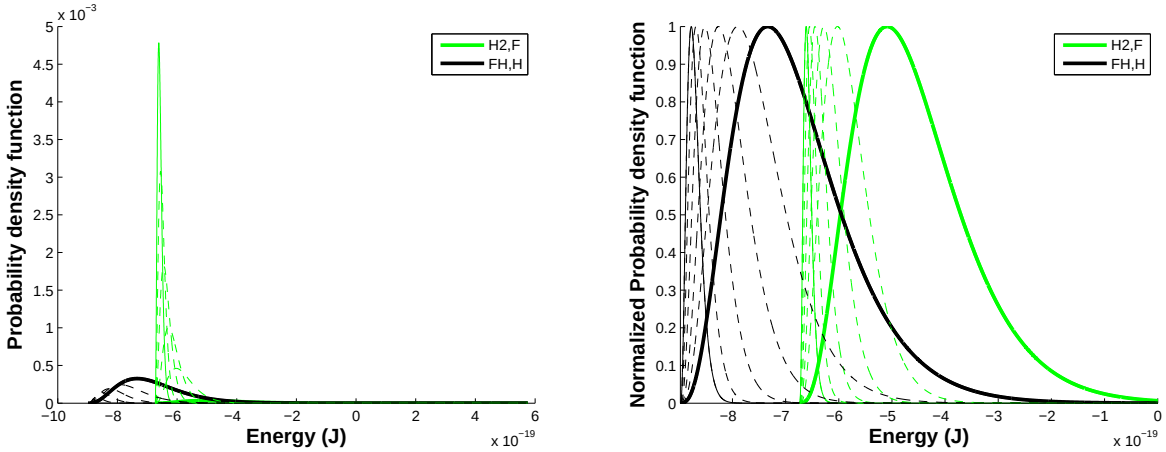

Figure 2.2. System trajectory in state space represented by (a:top) the evolution of the probability distribution among the energy eigenlevels and by (b:bottom) the evolution of the normalized distributions. The four dashed lines correspond to four of the non-equilibrium states along the trajectory (states A_1 to A_4 in Fig. 2.1), while the single narrow solid line is the distribution for the initial state (A_0) and the single bold solid line is that for the equilibrium state (B).

states A_0 to A_4 and B in Fig. 2.1a. In order to better show each distribution's evolution, each curve is normalized by its peak and the result shown in Fig. 2.2b. In Fig. 2.2a, one can observe that the system probability transfers from the reactant subsystem to the product subsystem. At the same time, the distributions of both subsystems evolve from narrow to wider distributions, indicating that the temperature is increasing. The distributions remain canonical at all times. The distribution evolution for each subsystem is more clearly seen in Fig. 2.2b.

As discussed in *Section* 2.2.6, the non-equilibrium evolution of state can be described via the evolutions of $\alpha_p(t)Z_p(\beta_p(t))$ and $\beta_p(t)$, which correspond to the particle number $N_p(t)$ and temperature $T_p(t) = 1/k_b\beta_p(t)$. Z_p is the partition function of the subsystem. Given the evolution of the particle number and temperature, one can rebuild the probability distribution via Eq. (2.38). Fig. 2.3a shows the particle number evolution for the process in which reactant changes to product. Fig. 2.3b shows the temperature evolution. The energy released by the chemical reaction heats up both the reactant and product, and the manner in which the temperature increases follows the SEA trajectory. At the end, when the system reaches stable equilibrium, the temperatures of the subsystems are equal, and the non-equilibrium temperatures converge to that for stable equilibrium. As already indicated in the discussion above surrounding Fig. 2.2b, the physical meaning of this temperature increase is a broadening in the probability distribution among the energy eigenlevels.

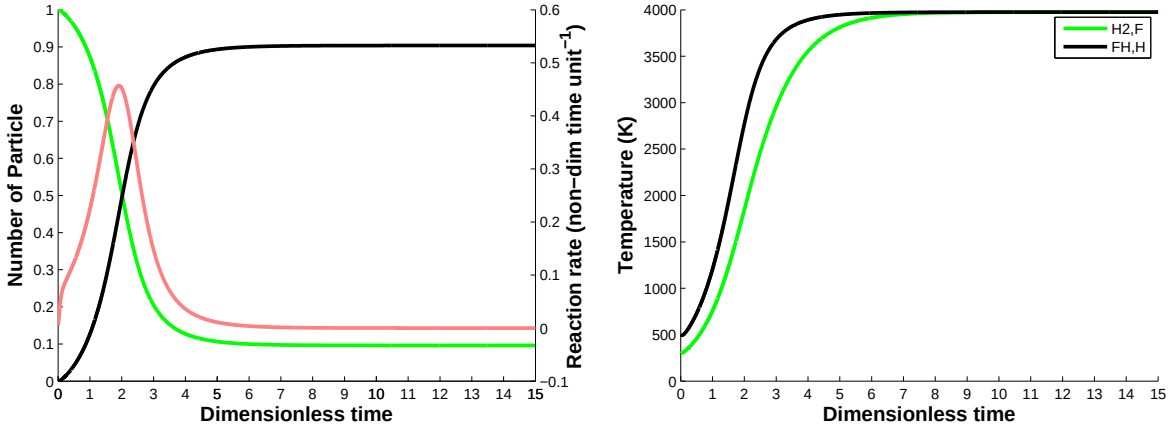

Figure 2.3. (a:top) Evolutions of particle number and reaction rate and (b:bottom) the evolution of temperature. For the line colors in (a), the black line and the green (light gray) line represent the FH, H and H_2, F, respectively, and the red (dark gray) line represents reaction rate.

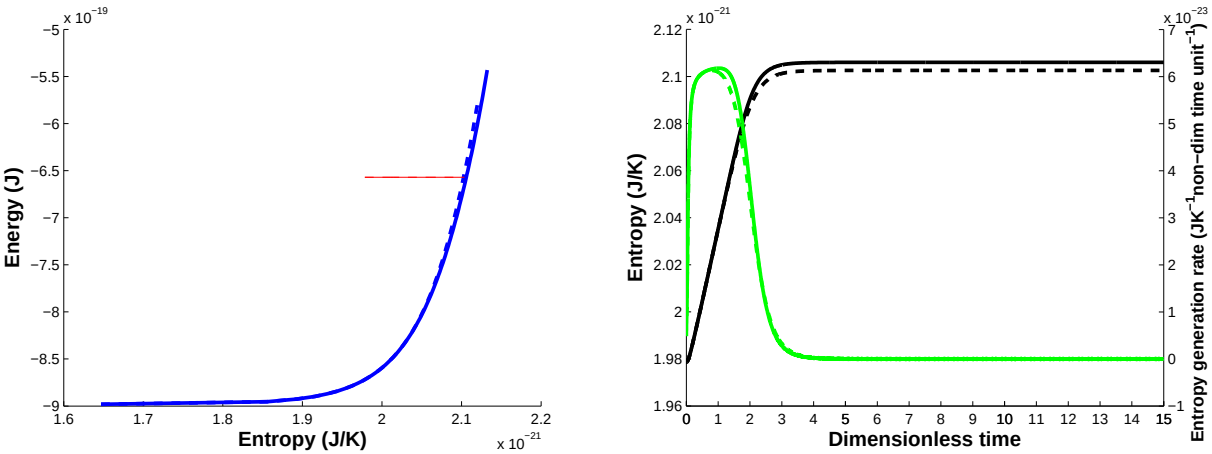

Figure 2.4. e

volutions for a system with and without vibrational degrees of freedom.]Comparison of (a:top) the energy-entropy diagrams and (b:bottom) the entropy (black line) and entropy generation rate [green (light gray) line] evolutions for a system with and without vibrational degrees of freedom. The solid lines are for the system with vibrational energy eigenlevels, while the dash lines are for the system without vibrational levels.

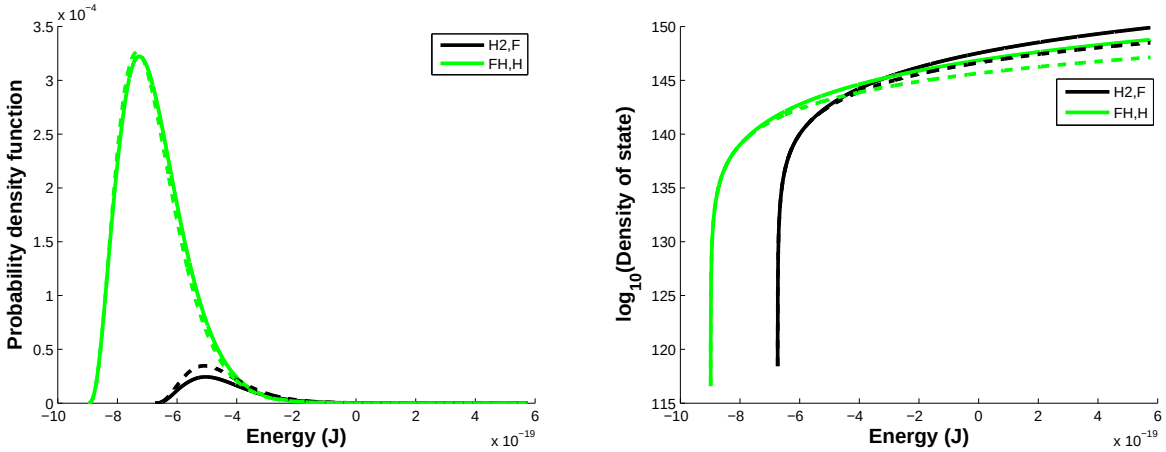

Figure 2.5. Comparison of (a:top) the stable equilibrium distributions and (b:bottom) the density of states for the systems with (solid line) and without (dashed line) vibrational energy eigenlevels.

2.5.2 Influence of the density of states

Using a comparison of system state evolution with and without vibrational energy eigenlevels included in the system description, one can study how the density of states influences system behavior. Fig. 2.4a shows the comparison of the corresponding stable equilibrium curves and the evolution trajectory using the same initial subsystem temperatures. Because the stable equilibrium temperature is less than 4000 K (Fig. 2.3b) and the characteristic temperature of vibration is about 6000 K, the stable equilibrium curves show some difference, which is consistent with the result found from equilibrium thermodynamics. Fig. 2.4b, in contrast, shows the difference of the two systems in the non-equilibrium region. At the beginning, the two systems perform the same. As the entropy generation rate approaches the maximum, the two systems perform differently and the system with vibrational energy eigenlevels exhibits a larger entropy and entropy generation rate. This phenomenon can be explained using subsystem temperature. The initial temperature is about one order of magnitude less than the characteristic temperature of vibration, which leads to the vibrational energy eigenlevels being frozen. Thus, the two systems perform similarly. However, as each subsystem temperature increases (Fig. 2.3b), the vibrational energy eigenlevels are activated, resulting in a difference in performance between the two systems.

Fig. 2.5a shows the difference in the system stable equilibrium distributions with and without vibrational energies. Fig. 2.5b shows the density of states difference. One can observe that although total properties such as the entropy change little, the probability distribution and even the equilibrium particle number changes are somewhat more significant. All the differences result

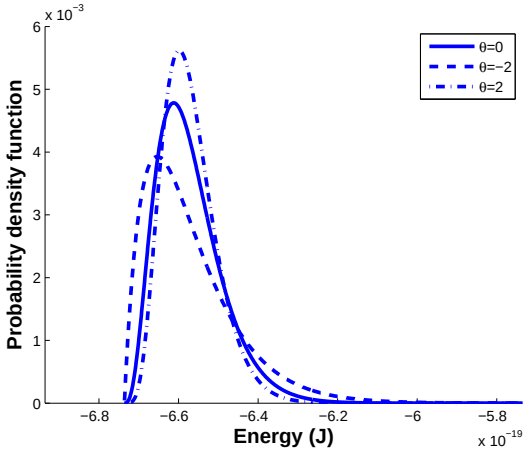

Figure 2.6. Initial distribution in reactant subspace for $\theta = 0$ (solid line), $\theta = -2$ (dashed line) and $\theta = 2$ (dashed-dotted line).

from the density of states changing.

2.5.3 Influence of the initial condition on the trajectory

Another important study is for the case when the initial condition is a very high order hypo-equilibrium state. In that case, although the theoretical discussion in *Section* 2.2.6 is still valid, the number of subsystem divisions of the system may be so high that characterizing each non-equilibrium state as an M^{th}-order hypo-equilibrium state may no longer be practical. However, the density of states method still permits the solution of the equation of motion to very high accuracy. This section uses the general gamma distribution to study the influence of initial condition on the non-equilibrium trajectory by varying θ in Eq. (2.106). The mean value of the energy for three cases with different θs is chosen to be the same in order to ensure the same system total energy and the same final stable equilibrium state. From Eqs. (2.111) and (2.112), the ratio of β in the three cases is $\beta_{-2} : \beta_0 : \beta_2 = 1 : 2 : 3$ and the ratio of the variance of energy is $Var_{-2} : Var_0 : Var_2 = 1 : 1/2 : 1/3$. The initial distribution for the reactant subspace is shown in Fig. 2.6, which takes 0.9999 of the total probability. It can be observed that for lower θ, there is more probability distributed in the higher energy eigenlevels (energies greater than -6.4×10^{-19} J) and the energy variance is larger.

The evolution in dimensionless time is studied in Fig 7. In order to facilitate the comparison, all the curves are shifted such that time 0 is the dimensionless time when the maximum reaction rate is reached, and both Figs. 2.7a and 2.7b use the same 0 time. In Fig. 2.7a, it is observed

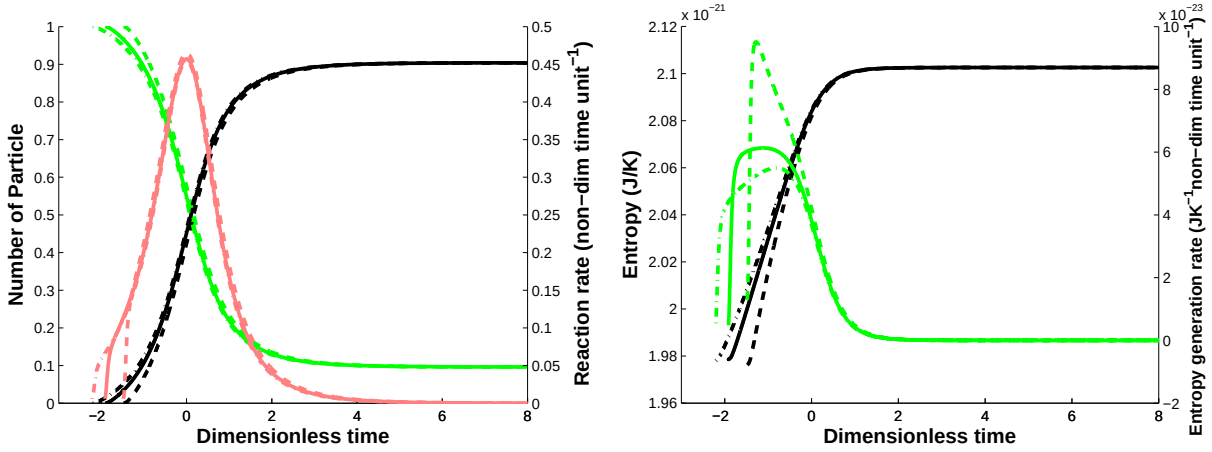

Figure 2.7. .

](a:top) Evolutions of particle number and reaction rate. For the line colors in (a), the black line and green (light gray) line represent the FH, H and H_2, F, respectively, and the red (dark gray) line represents reaction rate. (b:bottom) Evolutions of entropy (black line) and entropy generation rate [green (light gray) line]. For the line styles in both figures, $\theta = 0$ (solid line), $\theta = -2$ (dashed line) and $\theta = 2$ (dashed-dotted line). The dimensionless time when the maximum reaction rate is reached is set to be 0.

that the beginning of the three cases are quite different, while the reaction processes after time 0 are similar. Furthermore, the negative θ case takes less time to arrive at stable equilibrium than the zero θ case (Maxwellian distribution), and the positive θ case takes even more. In Fig. 2.7b, the entropy evolution is also similar after time 0. However, the beginning parts of the evolution exhibit three features. The first is that the initial entropy of the negative and positive θ cases are both smaller than that for $\theta = 0$, since the Maxwellian distribution provides the largest entropy for given energy. That also means that the initial entropy cannot decide how fast the reaction process is, which instead is decided by the value and the sign of θ. The second feature is that for negative θ, the entropy evolution is faster than that for the zero θ case, and the maximum of the entropy generation rate is larger than that for the zero θ case. The opposite is the case for the positive θ case. Both Figs. 2.7a and 2.7b show that the negative θ provides the faster reaction process. One possible explanation is that for lower θ, more probability is distributed in the higher energy eigenlevels, which accelerates the reaction process. Another view is that the lower θ case has lower β, which phenomenologically can be explained as higher temperature. The final or third feature is that in the evolution after time 0, the probability distributions for the positive and negative cases are not Maxwellian distributions in the strict sense used in the next section even though the particle number and entropy evolution are almost the same. However, as shown in Figs. 2.7 and 2.8, a

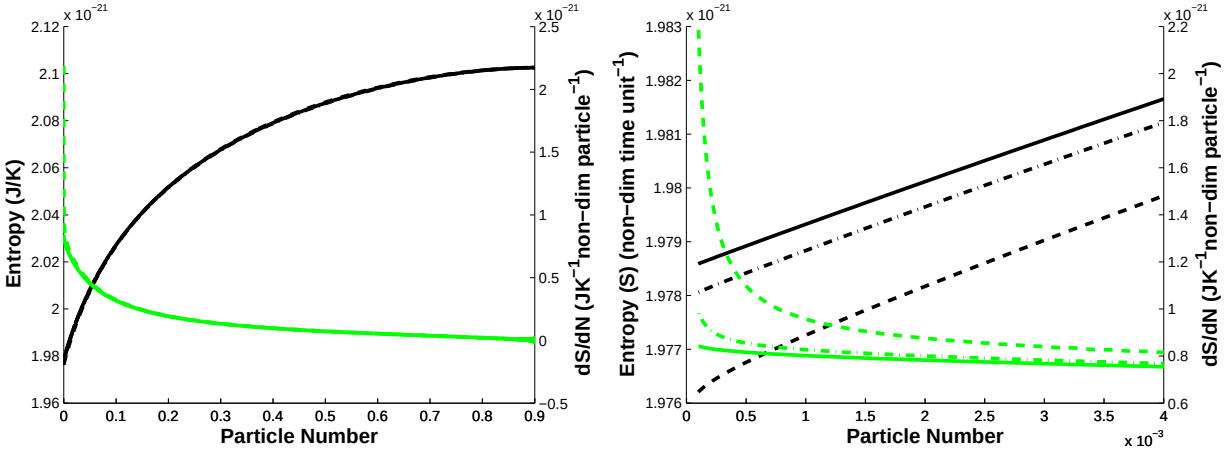

Figure 2.8. Trajectory representation using product particle number and entropy. Range of product particle number (a:top) from 0 to 0.9 and (b:bottom) from 0 to 0.004. The black line and the green (light gray) line represent entropy (S) and dS/dN, respectively. For the line styles, $\theta = 0$ (solid line), $\theta = -2$ (dashed line) and $\theta = 2$ (dashed-dotted line).

Maxwellian distribution in each subspace, for a 2^{nd}-order hypo-equilibrium state can be a very good approximation for studying a reaction's intermediate non-equilibrium states.

In Fig. 2.8, the trajectory of the chemical reaction is illustrated using the product particle number and system entropy. The particle number of the product can be regarded as an equivalent variable to the reaction coordinate here. By using product particle number instead of dimensionless time, only the information of the intermediate states is kept. It must be pointed out here that in Fig. 2.8, any trajectory with a positive dS/dN, i.e., a monotonically increasing function linking the initial state and stable equilibrium, does not violate the second law of thermodynamics. However, the trajectories plotted are not just any trajectories but those uniquely predicted by SEA, the maximum-entropy-production (MEP) trajectories. It can be observed that the trajectories for the three θ's chosen are very similar in Fig. 2.8a except at the very beginning (shown in Fig. 2.8b). As mentioned before, even though the probability distributions do not become 2^{nd}-order hypo-equilibrium distributions until very late (after the product particle number reaches 0.5), the 2^{nd}-order hypo-equilibrium state can provide a very good approximation of the intermediate non-equilibrium states. In addition, in Fig. 2.8b, one can observe that the zero θ case has the largest initial entropy and lowest dS/dN. The trajectories at the beginning can be separated into two parts by the state which the particle number reaches at 0.002. From 0 to 0.002, dS/dN for the non-zero θ case has a huge difference with that for the zero θ case. If the entropy is used as the measure of the difference of the distributions, the larger difference results in a greater speed of the non-

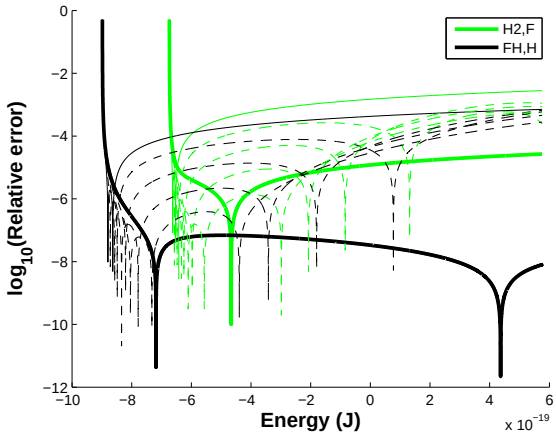

Figure 2.9. Relative error for the probability distribution.

Maxwellian distribution approaching Maxwellian one. In this process, the degree of reaction only changes a little when compared with the change in the total particle number of the product. After the particle number reaches 0.002, there is little difference in dS/dN between the three cases, even though the difference in entropy lasts until the system distribution reaches that for a 2^{nd}-order hypo-equilibrium state. However, this difference is small when compared with the total system entropy. Recall from Fig. 2.7 that there is quite a big difference in the state evolutions for the three cases until time 0, when the product particle number reaches about 0.5. For the range of product particle number from 0.002 to 0.5, the difference in entropy is negligible for the intermediate states of the trajectory but nonetheless has a large influence on the evolution in dimensionless time.

2.5.4 Numerical error

In Fig. 2.9, the state of the system without vibrational energy eigenlevels is compared with the analytical solution of the state, the gamma function, since the analytical solution for a system with vibrational levels is difficult to acquire. Fig. 2.9 shows the relative difference of the numerical solution with the analytical solution at states A_0 to A_4 and B. The relative errors of almost all the energy eigenlevels are less than 10^{-2}. There are 14 out of the $30,793$ eigenlevels where the relative error is larger than 10^{-2}. However, the total probability for these levels is less than 6.5×10^{-8}. The error is larger for these energy eigenlevels, since they coincide with the region where the density of states is lower and increasingly steep. Thus, this error can be explained by truncation error. It is also observed that the error is larger at the initial state than that at stable equilibrium. In addition, the states at lower subsystem temperatures have narrower distributions, whose accuracy

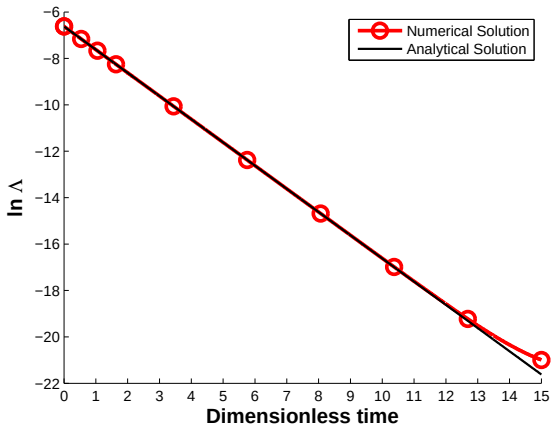

Figure 2.10. Time evolution of Λ.

is limited by the quasi-continuous condition. The energy interval chosen is about 10^{-2} times lower than $1/\beta = k_b T$, and that accuracy sets an upper limit on the relative error at the initial state. In conclusion, the density of states method developed and used here provides a very accurate numerical solution to the SEAQT equation of motion for a system with a very large number of energy eigenlevels. Furthermore, the criterion used in the previous section to check whether a distribution is Maxwellian or not is determined from the study here, i.e., if a distribution of energy has its distribution across most of the energy eigenlevels (for example, 99% of them) very close to the Maxwellian distribution (relative difference less than 1%) with the same mean value of energy, the distribution is regarded as a Maxwellian distribution.

Finally, validation of the numerical accuracy of the time evolution can be acquired through a value defined by

$$\Lambda = k_b(\beta^{product} - \beta^{reactant}) = 1/T^{product} - 1/T^{reactant} \tag{2.113}$$

According to *Section* 2.2.6, $\beta^{product}$ and $\beta^{product}$ yield to ODE Eq. (2.42) with different initial temperatures. Subtracting the ODE equations for $\beta^{product}$ and $\beta^{product}$ results in

$$\frac{d\Lambda}{dt} = -\frac{1}{\tau}\Lambda, \ \Lambda(0) = 1/300 - 1/500 \tag{2.114}$$

Using the dimensionless time scale for $\tau = 1$, the analytical solution of $\ln \Lambda$ yields

$$\ln \Lambda(t) = \ln(1/300 - 1/500) - t = -6.6201 - t \tag{2.115}$$

Plotting $\ln \Lambda$ as a function of dimensionless time as is done in Fig. 2.10 shows the accuracy of the numerical solution for different times. The deviation starts from time 12 onward. At dimensionless time 12, Λ, which is the difference in the inverse of the reactant and product temperatures, has a value smaller than 10^{-8}. Thus, this validation proves that the density of states method can provide a accurate numerical solution for the equation of motion.

2.6 Conclusions

In the preceding study, the non-equilibrium state evolution trajectory for a chemical reaction process is predicted using a first-principles, thermodynamic-ensemble based approach, which provides a computationally simpler, alternative global method for predicting the chemical kinetics of systems. This is well illustrated via the definition of hypo-equilibrium state and the existence of canonical distributions outside the realm of stable equilibrium. The nature of the SEA equation of motion directly leads to the existence of a unique non-equilibrium evolution trajectory in state space, which represents the kinetics. With the categorization of non-equilibrium states by different ordered hypo-equilibrium states, subsystem and subsystem temperatures serve as a good description of the trajectory in high-dimensional state space, whose properties are ensured by the equation of motion or the principle of SEA. In addition, with the goal of being able to model systems with a very large number of energy eigenlevels (for the system considered here, on the order of 10^{130}), the concepts of degeneracy and density of states are utilized, and the equation of motion for the degenerate system is developed. The equation of motion for an energy interval is presented and the numerical process to solve it introduced.

The clear physical meaning of the evolution trajectory, subsystem, and subsystem temperature are shown in the results as are the chemical reaction process via particle number evolution and subsystem heating via temperature evolutions. This work provides a reasonable generalization of the concept of temperature at stable equilibrium and offers a framework to describe and study non-equilibrium states and their relaxation process. In addition, even if the order of the hypo-equilibrium state is very high so that using this concept in such a case may not be practical, the density of state method still permits solution of the equation of motion so that the non-equilibrium thermodynamic trajectory, especially that for the intermediate states of the system, can be determined with the SEAQT equation of motion. As to the influence of the initial state, it is shown that

a 2^{nd} order hypo-equilibrium state is a good approximation for determining the non-equilibrium thermodynamic trajectory when the initial condition or state is that of a gamma distribution for the two subsystems. It is worthy noting that although the results given in this paper are based on a two-subsystem division and 2^{nd} order hypo-equilibrium state, the approach presented here can be easily applied to a system with a much higher number of subsystems. What order of hypo-equilibrium state is sufficient for arriving at an approximation is left as an open question for future work.

Finally, different from other methods for studying non-equilibrium systems, which are phenomenological or based on mechanics, this paper introduces a practical alternative approach based on a first-principle thermodynamic framework for studying the relaxation of non-equilibrium states.

Appendix A

A.1 Pseudo system

In this appendix, a system property calculated by the density of states method developed here is proven to be a good approximation of the property's true value. For the moment of energy in each interval of a given subspace (subsystem),

$$\begin{aligned}\sum_j n_j^i(\epsilon_j^i)^\theta &= E_i^\theta \sum_j n_j^i \frac{(\epsilon_j^i)^\theta}{E_i^\theta} = E_i^\theta \sum_j n_j^i (1 - \frac{\epsilon_j^i - E_i}{E_i})^\theta \\ &= E_i^\theta \sum_j n_j^i (1 - \theta \frac{\epsilon_j^i - E_i}{E_i}) = N_i E_i^\theta \end{aligned} \tag{2.116}$$

$$\begin{aligned}\sum_j n_j^i(\epsilon_j^i)^\theta \ln(\epsilon_j^i) &= \ln(E_i) \sum_j n_j^i(\epsilon_j^i)^\theta + n_j^i(\epsilon_j^i)^\theta \ln(\frac{\epsilon_j^i}{E_i}) \\ &= \ln(E_i) \sum_j n_j^i(\epsilon_j^i)^\theta (-\frac{\epsilon_j^i - E_i}{E_i}) = N_i E_i^\theta \ln(E_i) \end{aligned} \tag{2.117}$$

The third equal sign of Eq. (2.116) and the second of Eq. (2.117) hold when

$$\frac{\epsilon_j^i - E_i}{E_i} \ll 1 \tag{2.118}$$

which is the case for the intervals other than the lowest ones. In Fig. 2.9, it is shown that those intervals account for only a very small probability, if the probabilities of the original system and pseudo system have the forms

$$p_j^i = C n_j^i (\epsilon_j^i)^\theta e^{-\epsilon_j^i \beta} \tag{2.119}$$

$$\hat{P}_i = C N_i (E_i)^\theta e^{-E_i \beta} \tag{2.120}$$

For the properties of each interval of a given subspace (subsystem),

$$\begin{aligned} P_i &= \sum_j p_j^i = C \sum_j n_j^i (\epsilon_j^i)^\theta e^{-\epsilon_j^i \beta} = C \sum_j n_j^i (\epsilon_j^i)^\theta e^{-E_i \beta} e^{-(\epsilon_j^i - E_i)\beta} = C \sum_j n_j^i (\epsilon_j^i)^\theta e^{-E_i \beta} \\ &= C e^{-E_i \beta} \sum_j n_j^i (\epsilon_j^i)^\theta = C N_i E_i^\theta e^{-E_i \beta} = \hat{P}_i \end{aligned} \tag{2.121}$$

$$\begin{aligned} \langle e \rangle_i &= \sum_j p_j^i \epsilon_j^i = C \sum_j n_j^i (\epsilon_j^i)^{\theta+1} e^{-\epsilon_j^i \beta} = C \sum_j n_j^i (\epsilon_j^i)^{\theta+1} e^{-E_i \beta} e^{-(\epsilon_j^i - E_i)\beta} \\ &= C \sum_j n_j^i (\epsilon_j^i)^{\theta+1} e^{-E_i \beta} = C e^{-E_i \beta} \sum_j n_j^i (\epsilon_j^i)^{\theta+1} = C N_i E_i^{\theta+1} e^{-E_i \beta} = \langle \hat{e} \rangle_i \end{aligned} \tag{2.122}$$

$$\begin{aligned} \langle s \rangle_i &= -\sum_j p_j^i \ln \frac{p_j^i}{n_j^i} = -\beta \langle e \rangle_i + P_i \ln C - \sum_j p_j^i \theta \ln(\epsilon_j^i) \\ &= -\beta \langle e \rangle_i + P_i \ln C - P_i \theta \ln(E_i) = \langle \hat{s} \rangle_i \end{aligned} \tag{2.123}$$

The fourth equal sign in Eqs. (2.121) and (2.122) results from the quasi-continuous condition given by

$$\frac{1}{\beta} \gg |E_{i+1} - E_i| > |\epsilon_j^i - E_i| \tag{2.124}$$

$$e^{-(\epsilon_j^i - E_i)\beta} \doteq 1 \tag{2.125}$$

In addition, under the quasi-continuous condition and the assumption that the probability distribution p_j^i or the distribution P_i or $\hat{P}_i$ have the property of higher order moment convergence at least to the 2^{nd} order in energy (e.g., as for the case of an ideal gas), the summation of discrete energy eigenlevels can be approximated by an integral over a continuous spectrum. Thus, properties for a

given subsystem are found from

$$\begin{aligned}\langle es\rangle_K &= \sum_i \sum_j p_j^i \epsilon_j^i \ln \frac{p_j^i}{n_j^i} = \sum_i \sum_j n_j^i \epsilon_j^i e^{-\beta\epsilon_j^i}(-\beta\epsilon_j^i + \ln C - \theta \ln(\epsilon_j^i)) \\ &= C \int n(E)E(-\beta E + \ln C - \theta \ln(E))e^{-\beta E} dE \qquad (2.126)\\ \langle \hat{es}\rangle_K &= \sum_i \hat{P}_i E_i \ln \frac{\hat{P}_i}{N_i} = \sum_i N_i E_i e^{-\beta E_i}(-\beta E_i + \ln C - \theta \ln(E_i)) \\ &= C \int n(E)E(-\beta E + \ln C - \theta \ln(E))e^{-\beta E} dE = \langle es\rangle_K \\ \langle e^2\rangle_K &= \sum_i \sum_j p_j^i (\epsilon_j^i)^2 = \int E^2 p(E) dE = C \int n(E) E^{\theta+2} e^{-\beta E} dE \qquad (2.127)\\ \langle \hat{e^2}\rangle_K &= \sum_i \sum_j \hat{P}_i (E_i)^2 = \int E^2 p(E) dE = C \int n(E) E^{\theta+2} e^{-\beta E} dE = \langle e^2\rangle_K \qquad (2.128)\end{aligned}$$

Note that both discrete summations of the original and pseudo systems can be regarded as the Riemann summation of the integral, and the difference of the Riemann summation and the integral is of 2^{nd} order or greater for the energy interval. This means that the difference between both Riemann summations (original and pseudo system) is of 2^{nd} order or greater when the quasi-continuous condition hold. The properties for the system as a whole are then given by

$$\langle e\rangle = \sum_K^M (\sum_i \langle e\rangle_i)_K \ , \quad \langle \hat{e}\rangle = \sum_K^M (\sum_i \langle \hat{e}\rangle_i)_K \qquad (2.129)$$

$$\langle s\rangle = \sum_K^M (\sum_i \langle s\rangle_i)_K \ , \quad \langle \hat{s}\rangle = \sum_K^M (\sum_i \langle \hat{s}\rangle_i)_K \qquad (2.130)$$

$$\langle es\rangle = \sum_K^M \langle es\rangle_K \ , \quad \langle \hat{es}\rangle = \sum_K^M \langle \hat{es}\rangle_K \qquad (2.131)$$

$$\langle e^2\rangle = \sum_K^M \langle e^2\rangle_K \ , \quad \langle \hat{e^2}\rangle = \sum_K^M \langle \hat{e^2}\rangle_K \qquad (2.132)$$

where the summation is over all subsystems. With these expressions and the proof above linking the original and pseudo-subsystem properties, it is also clear that $\langle \hat{A}_1\rangle$, $\langle \hat{A}_2\rangle$ and $\langle \hat{A}_3\rangle$ are equal to $\langle A_1\rangle$, $\langle A_2\rangle$ and $\langle A_3\rangle$ under the quasi-continuous condition. Thus, the solution of the equation of motion for the pseudo-system, Eq. (2.71), can be used as a numerical approximation of that for the original system Eq. (2.70).

A.2 Onsager investigation

Some results of the Onsager investigation using the concepts of hypo-equilibrium state and non-equilibrium intensive properties found in [16, 17] are given below. For a general discussion of the Onsager relations in SEAQT using the language of quantum mechanics, the reader is referred to [42]. If the system is in an M^{th}-order hypo-equilibrium state, the probability evolution yields Eq. (2.32). For simplicity, the following definition is made:

$$\alpha^K = \ln Z^K - \ln p^K \tag{2.133}$$

Thus, the probability evolution of one energy eigenlevel is given by

$$p_i^K(t) = \frac{p^K(t)}{Z^K(\beta^K(t))} n_i^K e^{-\beta^K(t)\epsilon_i^K} = n_i^K e^{-\alpha^K(t)-\beta^K(t)\epsilon_i^K} \tag{2.134}$$

α^K and β^K are non-equilibrium intensive properties in the K^{th} subspace, corresponding to the extensive properties of p^K and E^K. Furthermore, by defining

$$\alpha = \frac{A_2}{A_1}, \quad \beta = -\frac{A_3}{A_1} \tag{2.135}$$

the particle number and energy evolution of the K^{th} subspace can be acquired from Eq. (2.36) by summation over one subspace, i.e.,

$$\frac{dp^K}{dt} = \frac{1}{\tau} p^K(\alpha^K - \alpha) + \frac{1}{\tau} E^K(\beta^K - \beta) \tag{2.136}$$

$$\frac{dE^K}{dt} = \frac{1}{\tau} E^K(\alpha^K - \alpha) + \frac{1}{\tau} \langle e^2 \rangle^K(\beta^K - \beta) \tag{2.137}$$

where $\langle e^2 \rangle^K$ is defined by Eq. (2.61) and p^K and E^K are the probability and energy in the K^{th} subspace. When a system is in a M^{th}-order hypo-equilibrium state and goes through a pure relaxation process, a relation for the evolution of extensive properties evolution in one subspace exists and is expressed as

$$\frac{dS^K}{dt} = \beta^K \frac{dE^K}{dt} + (\alpha^K - 1)\frac{dp^K}{dt} \tag{2.138}$$

where S^K is the entropy in the K^{th} subspace. This is the Gibbs relation for the subspace. The physical meaning of β^K and α^K is then given by

$$\beta^K = \left(\frac{\partial S^K}{\partial E^K}\right)_{p^K} = \frac{1}{T^k} \tag{2.139}$$

$$\alpha^K - 1 = \left(\frac{\partial S^K}{\partial p^K}\right)_{E^K} = -\frac{\mu^K}{T^k},\ \mu^K = \left(\frac{\partial E^K}{\partial p^K}\right)_{S^K} \tag{2.140}$$

where T^K is the subspace temperature and μ^K is its chemical potential with respect to the subspace probability p^K. The differential change in the total entropy, which for a pure relaxation process is equivalent to the entropy generation, is then written as

$$\begin{aligned} dS &= \sum_K dS^K = \sum_K \beta^K dE^K + \sum_K (\alpha^K - 1) dp^K \\ &= \sum_K (\beta^K - \beta) dE^K + \sum_K (\alpha^K - \alpha) dp^K \end{aligned} \tag{2.141}$$

where both energy ($\sum dE^K = 0$) and probability ($\sum dp^K = 0$) conservation have been applied. The Casimer condition holds and $J_E^K = dE^K/dt$ and $J_p^K = dp^K/dt$ are defined to be the internal fluxes of energy and probability inside the system, while $X_p^K = \beta^K - \beta$ and $X_E^K = \alpha^K - \alpha$ are the conjugate forces. Thus,

$$\frac{dS}{dt} = \sum_K X_E^K J_E^K + \sum_K X_p^K J_p^K \tag{2.142}$$

The Onsager relations are acquired from Eq. (2.137) and (138) in the form of $\mathbf{J} = \mathbf{\Lambda X}$, where $\mathbf{\Lambda}$ is symmetric and positive definite, so that

$$J_p^K = \frac{1}{\tau} p^K X_p^K + \frac{1}{\tau} E^K X_E^K \tag{2.143}$$

$$J_E^K = \frac{1}{\tau} E^K X_p^K + \frac{1}{\tau} \langle e^2 \rangle^K X_E^K \tag{2.144}$$

while the quadratic dissipation potential in force representation [44, 45] is given by

$$\begin{aligned} \Xi(\mathbf{X}, \mathbf{X}) &= \frac{1}{2} \langle \mathbf{X}, \mathbf{\Lambda X} \rangle = \frac{1}{2\tau} \sum_K [p^K (\alpha^K - \alpha)^2 \\ &+ 2E^K (\alpha^K - \alpha)(\beta^K - \beta) + \langle e^2 \rangle^K (\beta^K - \beta)^2] \end{aligned} \tag{2.145}$$

Furthermore, even though the following constraints apply to the fluxes:

$$\sum_K J_p^K = 0, \sum_K J_E^K = 0 \tag{2.146}$$

the reciprocity seen in Eqs. (2.144) to (2.146) is fully consistent with the Onsager theory since according to Gyarmati [44] *the validity of Onsager's reciprocal relations is not influenced by a linear homogeneous dependence valid amongst the fluxes*. Thus, the physical interpretation of Eqs. (2.144) to (2.146) in terms of hypo-equilibrium state and non-equilibrium intensive properties does not require a reformulation in terms of independent fluxes even though this could be done.

Thus, from the entropy generation of a non-equilibrium isolated system derived from the relaxation gradient dynamics, which are based on the geometry of system state space, one is able to arrive at the Onsager relations and the quadratic dissipation potential using the concepts of hypo-equilibrium state and non-equilibrium intensive properties. Alternatively, one can arrive as these relations and this potential using a variational principle in system state space as is done in [42]. Of course, the Onsager relations and quadratic dissipation potential also correspond to a variational principle in the space spanned by conjugate forces and fluxes [44].

Chapter 3

Atomistic-Level Non-equilibrium Model for Chemically Reactive Systems Based on Steepest-Entropy-Ascent Quantum Thermodynamics

3.1 Introduction

Studying the kinetics and dynamics of an atomistic-level system is a central topic of interest in physics and thermodynamics. Classical mechanics and quantum mechanics, which are built on Newton's and Schrödinger's equations of motion, respectively, provide an almost perfect description of the zero-entropy phenomena occurring in nature. However, both lack the 2^{nd} law of thermodynamics and are, thus, unable to provide a description of states at stable equilibrium with non-zero values of the entropy. To do so, both statistical thermodynamics (ST) and intrinsic quantum thermodynamics (IQT) use principles derived from the 2^{nd} law, namely, the maximum entropy and minimum energy principles, to arrive in constrained optimizations at a description of such states. However, this still leaves a gap not described between the zero-entropy and the maximum-entropy worlds, a gap which is important for a complete understanding of system behavior since it contains information about the kinetics and dynamics of non-equilibrium, non-zero-entropy, system-state evolutions. To fill this gap, IQT [26–30, 32, 36, 37, 40, 42, 46, 49–67] has emerged over the last

several decades as a theory which unifies quantum mechanics and thermodynamics and provides a complete picture of the kinetics and dynamics of system behavior in this region [65].

Of course, underlying any such description is the 2^{nd} law of thermodynamics and the dissipative phenomena which occur in a realm where the beautiful symmetry of the time reversibility of classical mechanics and quantum mechanics and that of the quasi-equilibrium processes of classical thermodynamics is broken. A traditional way of studying the state evolutions in this region is that of quantum thermodynamics (QT) [68, 69], which discards the isolation of the system, forming a so-called “open-system" model that includes “weak-interactions" with the environment. This approach places the system into a larger composite of system plus environment so that the dynamics of the dissipative phenomena present can be modeled as linear in the near-equilibrium realm of the composite. Thus, the QT master equations of the Lindblad type [70–73] retain the linear and reversible characteristics of the Schrödinger equation of motion, viewing dissipative phenomena as effects external to the system. This limits, among other things, this theory to the near-equilibrium and weak-interaction regimes and eschews entropy and entropy generation as intrinsic to the system.

In contrast, IQT regards the entropy and entropy generation as intrinsic and directly incorporates the irreversible and non-linear features of the dissipative process into the theory and its equation of motion. In this way, IQT avoids the necessity of introducing an external environment and does not limit itself to the near-equilibrium realm of weak system-environment interactions. Furthermore, in the limit of time reversibility, the IQT equation of motion reduces to the linear Schrödinger-von Neumann equation of quantum mechanics, which describes the linear dynamics of zero-entropy-state evolutions.

Now, of all the non-equilibrium phenomena of interest, those of chemically reactive systems are some of the most frequently studied in science and engineering. Starting with the Van’t Hoff-Arrhenius law [74, 75], the study of the kinetics and dynamics of chemical reactions remains an important topic of theoretical chemistry even today [76, 77]. The result is a set of theories which attempt to explain the mechanisms of chemical reactions and to predict their properties using classical mechanics or quantum mechanics or a mix of both.

Conventional theory describes the kinetic features of a reactive system using configuration space (or phase space), while potential energy surfaces (PESs) serve as constraints in configuration space. In this space, the chemical reaction is regarded as a motion from the reactant region to

the product region, and the kinetics are represented by a path found, for example, via the Minimum Energy Principle [78] or by a group of possible trajectories [79, 80] on the PES. The associated dynamics of each reaction mechanism is then viewed as resulting from inelastic collisions and the motions of single particles for which temperature plays an important role [81]. In contrast, the kinetics of each reaction mechanism provides the 'environment' for particle motion and contributes to the important concepts of potential energy barrier [82] and activated complex (e.g, in Transition State Theory) [83, 84], which underlie the exponential term in the Van't Hoff-Arrhenius law. With the microscopic velocities and a reaction path or set of trajectories known, a reaction rate calculation can be made via the kinetics in configuration space. Taking into account the uncertainty in the position or momentum of each particle, an ensemble of reactant particles resulting in a Maxwellian velocity distribution can be used to arrive at reasonable expectation values for reactant concentrations, which in turn provides a link to the statistical thermodynamic value of the entropy. Of course, quantum theory can be used to modify and improve, for example, the classical calculations [82] of the PES in order to include important quantum effects such as tunneling and the discrete nature of the energy spectrum of each particle. These so-called quasi-classical calculations can then be further improved by replacing them with a fully quantum calculation using quantum scattering theory based on either the time-dependent or time-independent Schrödinger equation [85, 86].

These conventional theories, whether classical, quasi-classical, or quantum, suffer from two disadvantages. First, both temperature and the Maxwellian velocity distribution play an important role in the theories but are valid only at stable equilibrium. The problem with this is that stable equilibrium only exists at the end of the reaction process whereas all prior states are in non-equilibrium, possibly very far from equilibrium. Second, the chemical reaction process in these theories is described by motion in configuration or phase space and the evolution of particle position and momentum is the principal driving force for the chemical reaction. This evolution is determined using an equation of motion which classically is given by Hamilton's equations or quantum mechanically by Schrödinger's equation. Either is reversible and, thus, there is the inevitable contradiction of using a reversible equation of motion to describe what inherently is an irreversible process. This compromise is made since the theories lack an equation of motion at a fundamental level of description for dissipative processes. Of course, turning at a classical level to the Boltzmann equation of motion, which only provides a phenomenological description, or at the

quantum level to QT and its master equations of the Lindblad type, which do provide a fundamental description, only begs the question since both suffer from the so-called Loschmidt paradox [87] of how an underlying dynamics, which for both is reversible or unitary, can lead to an irreversible result.

These two essential weaknesses are addressed in IQT and its mathematical framework steepest-entropy-ascent quantum thermodynamics (SEAQT). To begin with, the SEAQT framework links the zero-entropy and maximum entropy worlds by providing a comprehensive description of the non-equilibrium states of the system. Entropy, which is universally defined and intrinsic to the system, is used instead of temperature to provide information for the microscopic description. All the necessary information for system state evolution is derived from the energy eigenstructure and entropy of the system via the non-linear SEAQT equation of motion. Furthermore, the irreversibility of the chemical reaction is no longer regarded as a phenomenon resulting from particle collisions and the movement of single microscopic particles although both can be present and taken into account but instead as a dissipative process derived from the principle of steepest entropy ascent (SEA) or local maximal entropy generation (LMEG), which is a macroscopic or group effect at a fundamental level of description. Second, the SEAQT framework describes the system in a state space spanned by eigenstates of the reactants and products and not in a configuration or phase space. Recalling that quantum effects are very important at the atomistic level, the use of state space has the advantage of directly representing the uncertain position and momentum of each energy eigenstate. Furthermore, the energy eigenstructure, which is a fundamental feature of the system, is described by eigenlevels of the system Hamiltonian and does not require the very time consuming calculation of a PES and of particle or wave packet trajectories on the PES (also very time consuming).

With these advantages in mind, the SEAQT framework is applied here to the well-studied chemical reaction mechanism $F + H_2 \leftrightarrow FH + H$. A system using a finite number of energy eigenlevels as its energy eigenstructure is used and compared with one based on an infinite number of energy eignlevels. In *Section* 3.2, the mathematics for expressing system states in state space is described and the energy eignstructure of the system is built from single particle eigenstates. The SEAQT equation of motion is then presented and briefly discussed. In *Section* 3.3, results are presented which demonstrate the crucial role that entropy plays in dissipation phenomena. Results for the chemical reaction path and reaction rate are also presented and linked to experimental data.

The chemical kinetic results for the finite-level system are then compared to those for the infinite-level system. *Section* 3.4 provides some further discussion and conclusions.

3.2 Method

3.2.1 State description

The description of state of a chemically reactive system is at the core of the SEAQT framework [46, 66, 67]. The SEAQT description is based on an algebraic representation, which is quite different from the conventional description in configuration space (e.g., as in Transition State Theory) or the wave packet description using multi-body eigenfunctions (e.g., as in the Quantum Scattering Method). This avoids having to express particle position and momentum under conditions of uncertainty and brings to the fore the energy and entropy as being of primary significance. Thus, the kinetics and dynamics in the SEAQT framework depend principally on the critical concepts of energy and entropy for defining coordinates in state space and not on momentum and position as in phase space or configuration space. This provides a clearer vantage point from which to see the driving role, which entropy plays in the non-equilibrium evolutions of state of chemically reactive systems. The behavior in phase space or configuration space, which is not fundamental but which is extremely complex, is simply another view of system state evolution.

The state space of the chemically reactive system is spanned by the eigenstates of the reactants and those of the products. Intermediate states between reactants and products are represented by a mixture of reactant states and product states. This state space can be represented by the Hilbert space $\mathcal{H}$ as follows:

$$\mathcal{H} = \mathcal{H}_1 \oplus \mathcal{H}_2 \tag{3.1}$$

where $\mathcal{H}_1$ is the subspace of reactants and $\mathcal{H}_2$ is the subspace of products. Each subspace of the state is generated from single molecular state spaces by the cross product. In this paper, the reaction

$$F + H_2 \leftrightarrow FH + H \tag{3.2}$$

is modeled so that each subspace is given by

$$\mathcal{H}_1 = \mathcal{H}_{H_2} \otimes \mathcal{H}_F \tag{3.3}$$

$$\mathcal{H}_2 = \mathcal{H}_{FH} \otimes \mathcal{H}_H \tag{3.4}$$

The eigenstate of each molecule is generated from the one-particle eigenstates available to each molecule. For example, the state space of H_2 is expanded to include degrees of freedom for translation, rotation, vibration such that

$$\mathcal{H}_{H_2} = span\{|t_x t_y t_z\rangle_{H_2} \otimes |lm\rangle_{H_2} \otimes |\nu\rangle_{H_2}\} \tag{3.5}$$

where $|t_x t_y t_z\rangle$ represents the translational eigenstates, $|lm\rangle$ the rotational ones, and $|\nu\rangle$ the vibrational ones. Inside each *ket* are the quantum numbers for the one-particle eigenstate.

Starting from the one-particle eigenstates, one can represent the system-level eigenstate $|\vec{n}\rangle$ of the reactants or products by a quantum number group composed of translational, rotational, and vibrational one-particle eigenstates, i.e.,

$$|\vec{n}\rangle = |1(t_x t_y t_z lm\nu)_{H_2}(t_x t_y t_z)_F\rangle \quad \text{for the reactants} \tag{3.6}$$

$$|\vec{n}\rangle = |2(t_x t_y t_z lm\nu)_{FH}(t_x t_y t_z)_H\rangle \quad \text{for the products} \tag{3.7}$$

In Eqs. (3.6) and (3.7), each eigenstate for the reaction mechanism of Eq. (3.2) of the chemically reactive system is represented by a total of 10 indices. The first refers to the subspace (1 or 2), 6 to the quantum numbers for the diatomic molecules H_2 and FH, and 3 to the quantum numbers for the monatomic molecules H and F. The thermodynamic state of the system can then be written in a superposition of system eigenstates such that

$$|\Psi\rangle = \sum_{\vec{n}} \gamma(\vec{n})|\vec{n}\rangle \tag{3.8}$$

where $\gamma(\vec{n}) = \sqrt{p(\vec{n})}$ is the square root of the probability $p(\vec{n})$ of system energy eigenlevel $|\vec{n}\rangle$. Given the energy eigenstructure of the system, the system's thermodynamic state can also be represented by the probability distribution $p(\vec{k})$ where the $\vec{k}$ are all of the possible quantum number groups of $\vec{n}$.

3.2.2 Energy eigenstructure

As developed in [46] for chemically reactive systems, the Hamiltonian and identity operators are the generators of motion in the kinetics and dynamics of the SEAQT framework. In addition, the state of the system is represented by a probability distribution of available energy eigenlevels. The evolution of system state results in a different distribution for each state at every instant of time. Thus, generating the system-level energy eigenstructure of available levels for the chemically reactive system is an important step in the development of the SEAQT model for the system. This system-level structure is constructed from sets of one-particle eigenlevels, which for the reactive systems based on Eq. (3.1) considered here consist of the translational energies of the center of mass (ϵ_t), rotational energies (ϵ_r), and vibrational energies (ϵ_v). For F and H, which lack an internal structure, only translational energies need be considered. For translation,

$$\epsilon_t(t_x, t_y, t_z) = \frac{\hbar^2}{8m}\left(\left(\frac{t_x}{L_x}\right)^2 + \left(\frac{t_y}{L_y}\right)^2 + \left(\frac{t_z}{L_z}\right)^2\right) \tag{3.9}$$

where ϵ_t is the one-particle translational energy eigenvalue; $\hbar$ Plank's modified constant; m the center of mass of the particle; (t_x, t_y, t_z) the quantum numbers in the x, y, and z directions; and (L_x, L_y, L_z) the dimensions of system volume in the x, y, and z directions.

For the internal structure of the diatomic molecules H_2 and FH, the one-particle rotational energy eigenvalue is given by

$$\epsilon_r(l, m) = \frac{l(l+1)\hbar^2}{2I} = \frac{l(l+1)\hbar^2}{2\mu r^2} \tag{3.10}$$

where μ the reduced mass of the diatomic molecule, r the distance between the two atoms of the diatomic molecule, l the azimuthal quantum number, and m the magnetic quantum number. For vibration, the one-particle energy eigenvalue from the oscillator potential is written as

$$\epsilon_v(\nu) = \left(\nu + \frac{1}{2}\right)\hbar\omega \tag{3.11}$$

where ω is the angular frequency of the potential and ν the quantum number for vibration.

The system-level energy eigenvalues for each subspace can now be found from

$$\begin{aligned} E_{\vec{n}} &= E(|1(t_x t_y t_z lm\nu)_{H_2}(t_x t_y t_z)_F\rangle) \\ &= \epsilon_{t,H_2}(t_x, t_y, t_z) + \epsilon_{t,FH}(t_x, t_y, t_z) + \epsilon_{r,H_2}(l, m) + \epsilon_{\nu,H_2}(\nu) \end{aligned} \tag{3.12}$$

for subspace 1 and from

$$\begin{aligned} E_{\vec{n}} &= E(|2(t_x t_y t_z lm\nu)_{FH}(t_x t_y t_z)_H\rangle) \\ &= \epsilon_{t,FH}(t_x, t_y, t_z) + \epsilon_{t,H}(t_x, t_y, t_z) + \epsilon_{r,FH}(l, m) + \epsilon_{\nu,FH}(\nu) \end{aligned} \tag{3.13}$$

for subspace 2. Combining these values from the two subspaces results in the system energy eigenstructure.

3.2.3 Property operators

In quantum mechanics, an observable is represented by a single Hermitian operator. In a like manner, the SEAQT framework is written in terms of operators. To begin with, the density operator of the system is given by

$$\rho = \sum_{\vec{n}} p(\vec{n}) P_{\vec{n}} \tag{3.14}$$

where $P_{\vec{n}}$ is the projector of a given eigenstate $|\vec{n}\rangle$ of the system expressed as

$$P_{\vec{n}} = |\vec{n}\rangle\langle\vec{n}| \tag{3.15}$$

Since $P_{\vec{n}}$ is the basis in operator space, all other operators can be written as a superposition of the projector. Thus, the particle number operators are given by

$$N_{H_2} = N_F = \sum_{\vec{n} \text{ of reactant}} |\vec{n}\rangle\langle\vec{n}| \tag{3.16}$$

$$N_{FH} = N_H = \sum_{\vec{n} \text{ of product}} |\vec{n}\rangle\langle\vec{n}| \tag{3.17}$$

while the Hamiltonian operator is expressed as

$$H = \sum_{\vec{n}} E_{\vec{n}} |\vec{n}\rangle\langle\vec{n}| \tag{3.18}$$

As to the reaction coordinate and reaction rate operators for the system considered here, they are written as

$$\epsilon = N_{FH} \tag{3.19}$$

$$r = \frac{dN_{FH}}{dt} \tag{3.20}$$

Of course, the SEAQT framework as presented above provides only a very brief outline of the overall framework. A more general and comprehensive treatment can be found in Beretta and von Spakovsky [46] as well as in Al-Abbasi [67].

Finally, for any observable A, its expectation value can be calculated at any given instant of time by

$$\langle A\rangle = Tr(\rho A) \tag{3.21}$$

since $\rho = \rho(t)$ is known via the SEAQT equation of motion. Here $Tr(\centerdot)$ is the trace of the operator. Equation (3.21) is equally applicable for the observables of finite- and infinite-level systems with the exception of the entropy for which the expectation value for a finite-level system in a state of non-equilibrium is determined from

$$\langle S\rangle = -k_b Tr(\rho \ln \rho) \tag{3.22}$$

Here k_b is the Boltzmann constant. For an infinite-level system in a non-equilibrium state, however, Eq. (3.22) must be modified as explained in the following section.

3.2.4 Density of states method

To deal with an infinite-level system in the non-equilibrium realm, the expression for the expectation value of the entropy is modified using the density of states method developed by the first and third authors. The details of this method will be reported in a future paper, which is now in preparation. The same approach can be used for a continuous energy eigenspectrum system as

well as a degenerate system. Using this method, the energy eigenstructure can be approximated by a degenerate group of sampled energy eigenlevels where the degeneracy is proportional to the density of state of each sample energy value. As will be shown in a future paper, a set of energy eigenlevels in a small interval can be approximated by one energy value with degeneracy to an accuracy on the order of the length of the interval. With this modification, each degenerate energy value is equivalent to the set of energy eigenlevels for a given interval and contributes to the SEAQT equation of motion and the modified system entropy, i.e.,

$$\langle S \rangle = -k_b Tr(\rho \ln \frac{\rho}{N(\vec{n})}) \tag{3.23}$$

with the same kinetics and dynamics that would be present if all the infinite number of energy eigenlevels were explicitly taken into account. Note that $N(\vec{n})$ is the degeneracy for energy level $|\vec{n}\rangle$.

3.2.5 SEAQT equation of motion

The SEAQT equation of motion is presented directly here without derivation. For details of the derivation, the reader is referred to [46, 63, 67]. The equation of motion for a reactive system is written here in operator form and is expressed as

$$\frac{d\rho}{dt} = -\frac{i}{\hbar}[H, \rho] + \frac{1}{2k_b\tau}\{\Delta M, \rho\} \tag{3.24}$$

where the first term on the right captures the linear Hamiltonian dynamics and the second the non-linear dissipative dynamics. When the system is in a zero-entropy state, the second term vanishes, and the SEAQT equation of motion reduces to the time-dependent Schrödinger-von Neumann equation. In the dissipative term, τ is a relaxation time, which is the characteristic time of the dissipation process and can either be a constant or a function of ρ. $\{\}$ is the anti-commutator operator, while $\Delta M = M - \langle M \rangle$ is the deviation from the mean of the non-equilibrium Massieu operator defined as $M = S - H/\theta_H$ where $\theta_H = \langle \Delta H \Delta H \rangle / \langle \Delta S \Delta H \rangle$ is a constant-energy, non-equilibrium temperature and S and H are the entropy and Hamiltonian operators, respectively.

3.2.6 Initial state generation

To generate an initial density or state operator $\rho^{in}(\vec{n})$ for the SEAQT equation of motion, the following procedure is used. It is assumed that the reactants are a Gibbs-Dalton mixture of ideal gases in an isolated container. Initially, the mixture is in a state of stable equilibrium of a non-reactive system at some temperature T. The mixture is then ignited to move the state of the system into a state of non-equilibrium at which point the system becomes chemically reactive. The physical meaning of such a system can be that of a reactive system that requires ignition or a system whose reaction speed is much smaller than its diffusion speed. The initial canonical or stable equilibrium distribution $\rho^{se}(\vec{n})$ in reactant subspace at temperature T can be represented by

$$\rho^{se}(\vec{n}) = \frac{e^{-\beta E_{\vec{n}}}}{\sum e^{-\beta E_{\vec{n}}}} \quad \text{for } \vec{n} \text{ and } \vec{k} \text{ in the reactant subspace} \tag{3.25}$$

where $\beta = 1/k_b T$. Initially, this distribution is that of the system as a whole as well since only reactants are present. The ignition process is described by a perturbation of this canonical distribution $\rho^{se}(\vec{n})$ in both the reactant and product subspaces such that

$$\rho^{in}(\vec{n}) = \frac{(1-\delta)e^{-\beta E_{\vec{n}}}}{\sum e^{-\beta E_{\vec{n}}}} \quad \text{for } \vec{n} \text{ and } \vec{k} \text{ in the reactant subspace} \tag{3.26}$$

$$\rho^{in}(\vec{n}) = \frac{\delta e^{-\beta E_{\vec{n}}}}{\sum e^{-\beta E_{\vec{n}}}} \quad \text{for } \vec{n} \text{ and } \vec{k} \text{ in the product subspace} \tag{3.27}$$

where δ is a very small number.

3.2.7 Numerical approach

Initially, the system under study here and in [66, 67] contains one H_2 molecule and one F atom. Since the number of system energy eigenlevels is extremely large, a finite number from all possible $|\vec{n}\rangle$ is chosen for the finite-level system model. This finite number is sufficient to describe the entropy-driven phenomena of the reactive system and link the predicted results with published experimental data. The energy eigenlevels chosen are listed in Table 3.1. For the infinite-level system, the density of state method briefly described above in *Section* 3.2.4 is used. The kinetics for both systems is the same. Differences in results manifest themselves in the dynamics with the latter system, of course, more closely representing the actual reactive system.

As to the equation of motion, it is solved here using a fourth order Runge-Kutta explicit scheme [88–90] with the relative tolerance error set to 10^{-5}.

Table 3.1. Equilibrium temperatures and relaxation times of the SEAQT infinite-level model matched to the experimental values of the reaction rate constants found in Heidner et al. [91].

Species	Translational quantum nos.*	Vibrational quantum nos.	Rotational quantum nos.
F	$t = 1, \cdots, 5500$		
H_2	$t = 1, \cdots, 1000$	$\nu = 0$	$J = 0, 1, 2, 3$
FH	$t = 1, \cdots, 1000$	$\nu = 0, 1, 2, 3, 4$	$J = 0, 1, \cdots, 10$
H	$t = 1, \cdots, 5000$		

* Although the translational principal quantum number t (defined as the square root of $t_x^2 + t_y^2 + t_z^2$) varies here in the range shown in the second column of the table for each species, only a sampling (10) of these quantum numbers across this range is used for each species in the SEAQT model.

3.3 Results

3.3.1 Entropy and concentration evolution

The SEAQT chemical reaction model is based on the idea that the entropy generation via the principle of steepest entropy ascent is the driving force behind the chemical reaction. The reactive system considered here initially consists of 1 mol of H_2 and 1 mol of F contained in a cubic tank, 10 cm on a side.

Fig. 3.1 shows the evolution in time of the expectation values of the entropy and the particle number. It is evident that the expectation values of the species particle numbers evolve in a fashion similar to that of the entropy and that this is consistent with the idea that the entropy generation is the driving force of the chemical reaction. The entropy is, thus, not simply a phenomenological property calculated to check whether or not a system behaves consistently with the 2^{nd} law of thermodynamics but instead a means for applying the 2^{nd} law to the description and prediction of the non-equilibrium kinetics and dynamics of chemically reactive systems. In addition, note that Fig. 3.1b verifies that the mass of the system is conserved at every instant of time throughout

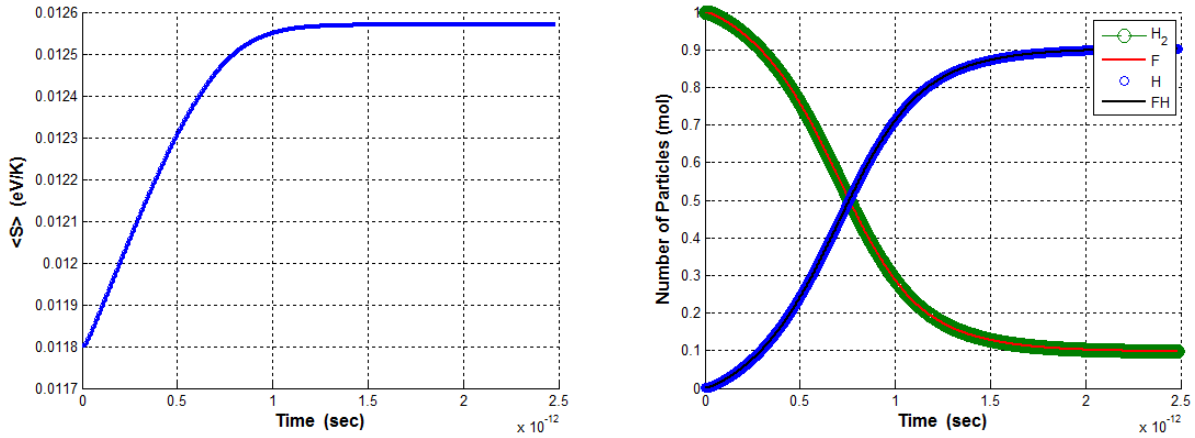

Figure 3.1. Evolution of the expectation values of system (a:left) entropy and (b:right) species particle number for the infinite energy eigenlevel system initially at a temperature of 298 K.

the evolution of state of the system. Although not shown here, similar graphs for the expectation values of the energies of the species show that energy is also conserved at every instant of time throughout the evolution.

3.3.2 Chemical reaction rate

Solution of SEAQT equation of motion provides system information at every instant of time, which can be used to calculate the chemical reaction rate. The traditional reaction rate constant $k(T)$ or thermal rate constant reported in the literature is a function of the initial stable equilibrium temperature of the reactive system and is a single value for each temperature, i.e., it does not vary in time during the reaction since it is a value gleamed from the initial reaction rate. In contrast, the SEAQT framework is able to predict the reaction rate constant at every instant of time independent of temperature, referencing this temperature only in a post-processing procedure which allows the SEAQT results to be compared to those in the literature. The SEAQT framework is, thus, consistent with the fact that the chemical reaction process is a non-equilibrium process for which no temperature is defined. Moreover, the state of a chemically reactive system varies a lot not only with respect to the species concentrations but as well with respect to the entropy generation. The SEAQT framework, therefore, provides a more complete picture of all the intermediate states of the system and the instantaneous chemical reaction rates in the non-equilibrium region.

Now, for the reaction mechanism considered here, i.e., $H_2 + F \leftrightarrow FH + H$, the reaction rate

is given by

$$r(t) = r_f(t) - r_b(t) \tag{3.28}$$

$$r_f(t) = k_f[F(t)][H_2(t)] \tag{3.29}$$

$$r(t) = k_b[FH(t)][H(t)] \tag{3.30}$$

where r is the net reaction rate, r_f the forward reaction rate, and r_b the backward reaction rate. k_f and k_b are the forward and backward reaction rate "constants", while $[A(t)]$ is the concentration of species A, which can be found from its particle number expectation value and the geometric dimensions of the system. The reaction order for each species in the reaction coincides here with the stoichiometric coefficient of each species in the reaction mechanism. However, this is not generally the case [92].

At stable equilibrium, Eqs. (3.28) to (3.30) provide a zero rate condition. With this condition and the assumption that the detailed balance condition also holds for the time-dependent rate constant, another relation is found, i.e.,

$$\frac{k_f(t)}{k_b(t)} = \frac{k_f(t^{se})}{k_b(t^{se})} = \frac{[F(t^{se})][H_2(t^{se})]}{[FH(t^{se})][H(t^{se})]} \tag{3.31}$$

which can be used with Eqs. (3.28) to (3.30) to calculate the $k_f(t)$ and $k_b(t)$ at every instant of time. In this last equation, t^{se} is the time at stable equilibrium.

The reaction rate constant values provided in the literature are those for the forward reaction at the beginning of the reaction process when the backward reaction is negligible. To make a comparison with the experimental data found in Heidner et al. [91], initial values for $k_f(t = t_0) = k_f(T^{in})$ for different initial equilibrium temperatures are calculated with the SEAQT equation of motion by adjusting the relaxation time τ in the equation of motion to match the experimental data. The results for the infinite-level system are presented in Table 3.2, which lists the relaxation time calculated from the experimental data and the T^{eq}. The latter are the final stable equilibrium temperatures of the system corresponding to each initial stable equilibrium temperature. Of course, it is important to point out that the kinetic path of the chemical reaction process predicted by the SEAQT framework is independent of the speed of system state evolution, i.e., of the relaxation time. No matter which relaxation time we use, the non-equilibrium path in state space remains the

same. This result can be shown from the equation of motion where the relaxation time does not influence the relative value of each probability. We fit the relaxation time with the experimental data in order to show our state-space path result in the proper time scale.

Table 3.2. Quantum numbers considered for each of the molecules and atoms in the SEAQT model [66, 67].

T^{in}(K)	T^{eq}(K)	$k_f(T^{in})/10^{-11}$(cm^3/molecule-sec)[91]	$\tau/10^{-14}$(sec)
298	3906.84	2.93	15.3045
400	3981.67	4.88	7.4923
500	4054.37	6.57	4.7362
600	4126.64	8.01	3.4038
700	4198.57	9.23	2.6453

Fig. 3.2 shows a typical temperature evolution for the chemically reactive system. As mentioned above, intermediate states are non-equilibrium states for which the temperature is not defined. Nonetheless, using the surrogate system approach outlined in [67], a stable equilibrium temperature can be associated with each of these system states by using the entropy of each intermediate state at a given system energy and the fundamental relation for the entropy of a Gibbs-Dalton mixture of ideal gases to solve for the corresponding equilibrium temperature. For the infinite-level system, this temperature can also be gleamed from the slope of the curve of stable equilibrium states in the energy-entropy plane corresponding to the surrogate system [67] associated with a given intermediate (i.e., non-equilibrium) state at given values of the energy and entropy. In Fig. 3.3a, the characteristics of the reaction rates in the non-equilibrium realm for the infinite-level system are presented. The rates show a behavior similar to that for the entropy generation rate, which puts in evidence once more the idea that the chemical reaction is driven by the entropy generation. The evolutions of the forward and backward reaction rates are consistent with what would be expected for a chemical reaction, namely, that the forward reaction rate dominates initially and then begins to diminish its dominance over the backward rate as the reaction proceeds until both cancel each other at stable equilibrium consistent with the initial detailed balance assumption.

Finally, Fig. 3.3b shows an extension of the conventional reaction rate “constant" to one that

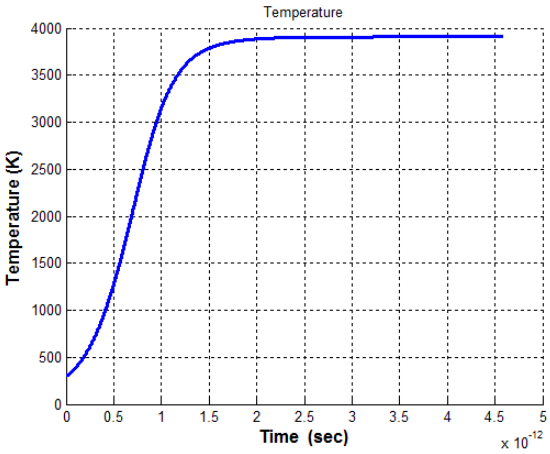

Figure 3.2. Evolution of temperature for the infinite-level system initially at a temperature of 298 K.

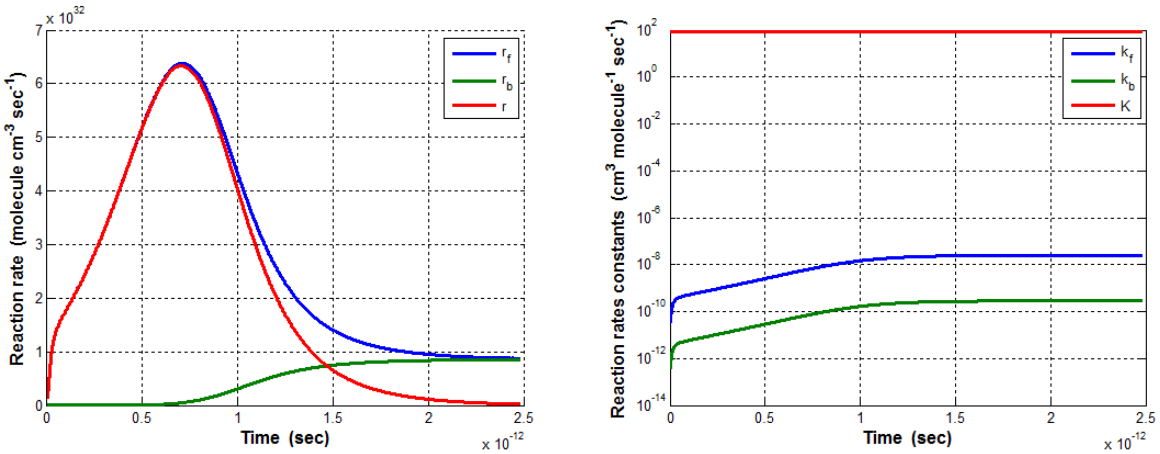

Figure 3.3. (a:left) Chemical reaction rates and (b:right) reaction rate constants for the infinite-level system initially at a temperature of 298 K.

has a different value at every instant of time. This more complete description of the reaction process has a clear physical meaning, namely, that the evolving state of the system in a dissipative process results in varying reaction speeds. This is consistent with the temperature evolution shown in Fig. 3.2, i.e., that the rapid rate of increase in temperature seen initially coincides with the rapid increase in the net reaction rate after which it slows as the net reaction rate decreases.

3.3.3 Comparison of infinite-level model and finite-level model

Use of the density of states approach that we have developed has allowed us to extend the finite-level system approach reported in [46, 66, 67] from the microscale to the macroscale. However, to demonstrate the improvement of the infinite-level model results over that for the finite-level model,

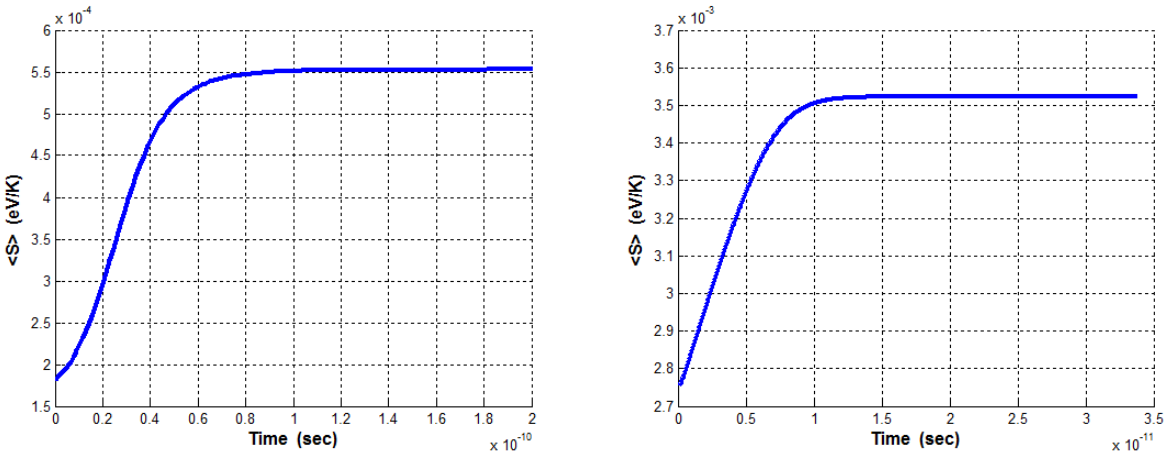

Figure 3.4. Evolution of the expectation values of system entropy for (a:left) the finite energy eigenlevel system and (b:right) the infinite energy eigenlevel system initially at a temperature of 298 K.

the number of particles considered and the size of the system are reduced to 1 particle ($1H_2$, $1F$) and a box with dimensions 4 nm by 2 nm by 2 nm. Anything larger results in computational convergence problems with the finite-level system.

Figs. 3.4 and 3.5 show the evolution in time of the expectation values of the entropy and entropy generation rate for the finite- and infinite-level systems. A number of differences can be seen. The first is that the maximum entropy value and the entropy generation peak value for the finite-level system are more than one order of magnitude smaller than that for the infinite-level system. In contrast, the evolution time to stable equilibrium for the infinite-level system is somewhat less than one order of magnitude smaller than that for the finite-level system. In addition, although the shapes of the entropy generation rate curves are similar for the two systems, that for the latter is much more asymmetric with a wider peak than that for the former suggesting that the irreversible phenomena present differ much more in intensity throughout the evolution in state of the latter system.

Clearly, for a fixed system energy, the more energy eigenlevels available over which the energy can be distributed, the higher the system entropy. In fact, using the infinite-level model, one can validate the SEAQT model prediction of the expectation value of the entropy at stable equilibrium by comparing it with that found from standard calculations using the maximum entropy principle of ST or IQT. Indeed good agreement is seen. Similarly, the larger the number of energy eigenlevels available, the larger the entropy generation is expected to be and the faster the dynamics. Again, this is indeed what is observed.

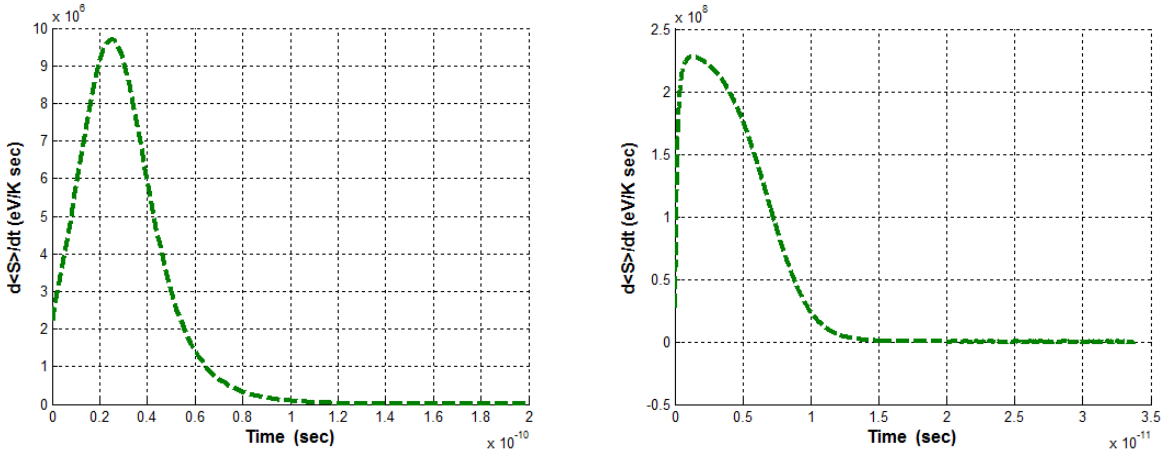

Figure 3.5. Entropy generation for (a:left) the finite energy eigenlevel system and (b:right) the infinite energy eigenlevel system initially at a temperature of 298 K.

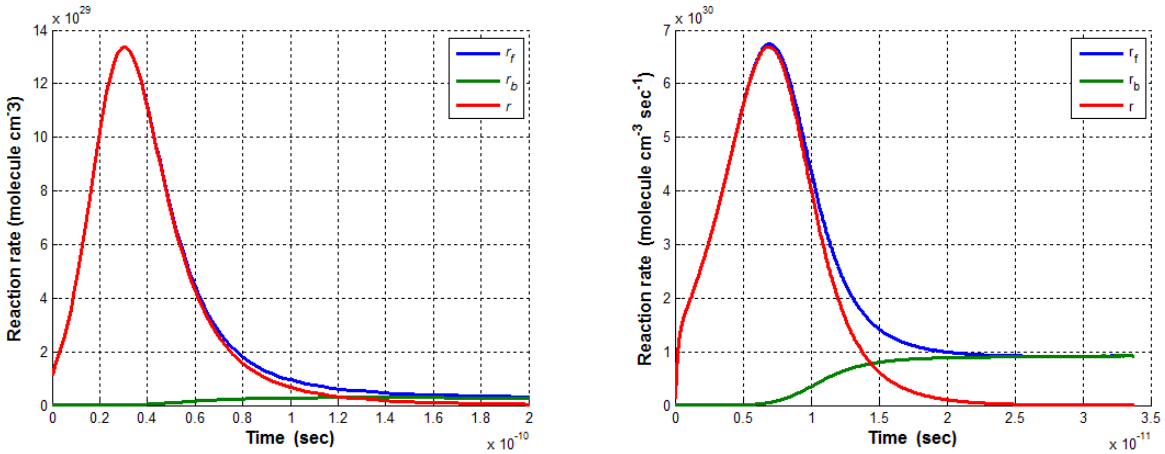

Figure 3.6. Chemical reaction rates for (a:left) the finite energy eigenlevel system and (b:right) is for infinite energy eigenlevel system initially at a temperature of 298 K.

Finally, Figs. 3.6 and 3.7 show the reaction rates and reaction rate constants for the finite- and infinite-level systems, respectively. Clearly, as seen in Fig. 3.6, the reaction rates for the latter system are about an order of magnitude large than those for the former, which explains the order of magnitude reduction in the evolution time for the latter seen here and in previous figures. As expected, the trends are comparable to those seen for the entropy generation rates in Fig. 3.5. The differences in the reaction rate constants k_f and k_b seen in Fig. 3.7 are, on the other hand, much more pronounced, showing differences of as much as two orders of magnitude between the finite- and infinite-level systems and between k_f and k_b, given that the initial forward reaction rate constants k_f are set to be the same.

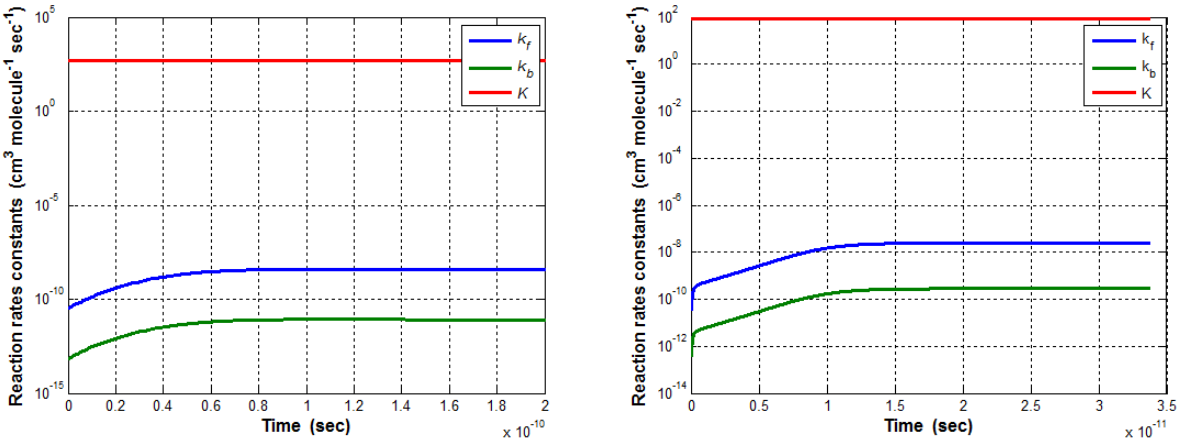

Figure 3.7. Reaction rate constant for (a:left) the finite energy eigenlevel system and (b:right) the infinite energy eigenlevel system initially at a temperature of 298 K.

3.4 Conclusion

The SEA-IQT chemical reaction framework provides a new fundamental approach to studying chemically reactive systems, especially their non-equilibrium behaviour. A major benefit of this framework is that it accounts for both the quantum mechanical and thermodynamic features of the system and the process it undergoes. It is different from conventional state-to-state chemical reaction models in that it uses the system energy eigenstructure and a non-linear equation of motion to quickly and straightforwardly establish the reaction characteristics of a system in the non-equilibrium realm, providing access to detailed information about the reaction process, which would otherwise not be available. In addition, the evolution of key system properties provides a clearer physical picture of non-equilibrium behaviour and leads to a deeper understanding of the role played by the 2^{nd} law of thermodynamics in the dissipative process.

A final point is that the computational burden involved in these calculations is minimal when compared to comparable methods in the literature. To date, model predictions have been made on a PC workstation and complete in a matter of seconds to a few hours depending on the complexity of the chemical reaction pathways that are considered. For those produced for this paper, the computational times are at the lower end. For a multi-phase, multi-component, nano-scale system with heat conduction, external applied field, diffusion, and multiple coupled electrochemical reaction pathways, the computational times are at the upper end. This is a huge advantage compared to the computational cost required by, for example, scattering calculations. Furthermore, since the

solution is obtained via solving a set of first order ordinary differential equations, the memory requirement for solving the system models formulated using this framework is minimal, which contrasts with methods that depend on 3D grids of configurational space where the dimensionality grows exponentially. For this reason and the others demonstrated above, the SEAQT framework has a great potential to contribute to the field of reaction kinetics for all phases of matter.

Chapter 4

Steepest-Entropy-Ascent Quantum Thermodynamic Modeling of Heat and Mass Diffusion in a Far-from-equilibrium System Based on a Single Particle Ensemble

4.1 Introduction

The study of non-equilibrium relaxation processes including chemical kinetics, mass diffusion, and heat diffusion is typically accomplished using approaches based on microscopic mechanics or thermodynamics. With the former, system state space is spanned by microstates and the governing equation is based on the dynamics of classical mechanics (e.g., molecule dynamics [6] or kinetic theory [4]), quantum mechanics (e.g., non-equilibrium Green's functions [1] or the quantum Boltzmann equation, i.e., the Uehling-Unlenbeck-Boltzmann equation [93–95]) or a stochastic process (e.g., Monte Carlo simulation of the Ising model [7]). These approaches provide complete information of the microscopic process such as individual particle collisions or quantum state scattering. However, the large amount of very detailed information required inevitably results in large computational burdens, which limit the applicability of these approaches.

Approaches based on thermodynamics, on the other hand, are not similarly burdened and are able to generally capture the features of the relaxation process is of interest via, for example, the

Onsager relation. Approaches of this type include non-equilibrium thermodynamics [44, 96], linear response functions and the fluctuation-dissipation theorem [97], stochastic thermodynamics [98], extended irreversible thermodynamics [99], etc. The thermodynamic features captured can be regarded as a coarse graining of the microscopic dynamics or as a pattern in ensemble evolution [20, 21], which computationally is more efficient. However, most of these approaches have limited or no applicability in the far-from-equilibrium realm, since the local or near-equilibrium assumption is needed or analytical solutions are only available at steady state. In addition, their governing equations are phenomenological or stochastic in nature and, thus, do not have a first-principle basis. To address these issues and push the application of thermodynamic principles further into the non-equilibrium realm, it is of great importance to find a general and simple description of non-equilibrium state corresponding to a thermodynamic pattern of the microscopic description, to fundamentally define the macroscopic properties of any thermodynamic state (i.e., extensive or intensive properties for both equilibrium and non-equilibrium states), and to use a thermodynamic governing equation based on first principles.

Steepest-entropy-ascent quantum thermodynamics (SEAQT), which is a first-principle, thermodynamic-ensemble based approach, addresses all of the issues raised above, providing a governing equation able to describe the non-equilibrium process from an entropy generation viewpoint. The description of system state is based on the density operator of quantum mechanics or probability distribution in state space of classical mechanics. The macroscopic properties of entropy, energy, and particle number, which are well defined for any state of any system [33], are used to develop the governing equation and describe system state evolution. Recently, this description has been simplified via the concept of hypo-equilibrium state [14], which captures the global features of the microscopic description for the relaxation process. In addition, the concept of non-equilibrium intensive properties introduced in [14] based on the concept of hypo-equilibrium state enables a complete description of the non-equilibrium evolution of state when combined with the set of non-equilibrium extensive properties. Unlike the intensive property definitions of other non-equilibrium thermodynamic approaches (definitions which require local-equilibrium, near-equilibrium, or steady state assumption or a phenomenological basis), the definitions in the SEAQT framework are fundamental and available to all non-equilibrium states and are especially suitable for the description of the evolution in state of relaxation processes. Both of these concepts enable the generalization of many equilibrium (or near-equilibrium) thermodynamic relations such as the Gibb's relation, the

Clausius inequality, and the Onsager relations into the far-from-equilibrium realm.

To describe the SEAQT framework, the paper starts with a derivation in *Sections* 4.2.1 and 4.2.2 of the SEAQT relaxation dynamics starting from the geometry of system state space. Some useful mathematical features of the relaxation process are then presented in *Section* 4.2.3, enabling the definition of the concepts of hypo-equilibrium state and non-equilibrium intensive properties. As an alternative to the geometric derivation from state space, the relaxation dynamics of SEAQT can also be derived using a variational principle in system state space as is done in *Section* 4.2.4. *Section* 4.3 then follows with a discussion of mass diffusion in a local, isolated system in non-equilibrium. Subsequently, the transport equations, the Gibbs relation, and the Onsager relations are generalized for the non-equilibrium relaxation process, and the dissipation potential is given to complete the link from the variational principle in system state space to that for the conjugate fluxes and/or forces [44]. *Section* 4.4 discusses the process of heat diffusion by choosing a set of system constraints different from those used for mass diffusion. In *Section* 4.5, the SEAQT model is applied to the study of the heat and mass diffusion of a simple system consisting of ideal gas (hydrogen), which can be represented by a single-particle ensemble. Linear behavior in the near-equilibrium realm provides the phenomenological transport equations, and higher-order, non-linear behavior in the near-equilibrium realm is also studied. Finally, *Section* 4.6 concludes the paper with some final comments.

4.2 Theory: SEAQT Equation of motion

The basic framework of SEAQT is introduced in this section. This framework describes the relaxation process of a local, isolated system in non-equilibrium based on thermodynamic concepts. To begin with, the equation of motion for such a system is derived in *Section* 4.2.1 from the geometric principle of steepest entropy ascent. This is followed in *Section* 4.2.2 by a discussion of the kinetics and dynamics of the relaxation process, which enable the study of the thermodynamic trajectory regardless of the details of the microscopic interactions. A description of non-equilibrium state and its evolution for the relaxation process is then given in *Section* 4.2.3 using the concepts of hypo-equilibrium state and non-equilibrium intensive properties. Finally, in *Section* 4.2.4, a presentation of the variational principle of steepest entropy ascent is used to derive the SEAQT equation of motion for the local system.

4.2.1 SEAQT equation of motion for an isolated system

Based on the discussion by Grmela [20, 21, 35] and Beretta [24, 34], the general form of a non-equilibrium framework is a combination of both irreversible relaxation and reversible symplectic dynamics. If written in the generalized form of the Ginzburg-Landau equation [20, 34], the equation of motion takes the following form:

$$\frac{d}{dt}\phi(t) = X^H_{\phi(t)} + Y^H_{\phi(t)} \tag{4.1}$$

where $\phi(t)$ represents the state evolution trajectory, $X^H_{\phi(t)}$ and $Y^H_{\phi(t)}$ are functions of the system state $\phi(t)$ and represent the reversible symplectic dynamics and irreversible relaxation dynamics, respectively. In the SEAQT framework, the system state is represented by the density operator $\hat{\rho}$, $X^H_{\phi(t)}$ follows the Schrödinger equation, and $Y^H_{\phi(t)}$ is derived from the SEA principle. Thus,

$$\frac{d\hat{\rho}}{dt} = \frac{1}{i\hbar}[\hat{\rho}, \hat{H}] + \frac{1}{\tau(\hat{\rho})}\hat{D}(\hat{\rho}) \tag{4.2}$$

where $\hat{D}$ is the dissipation operator determined via a constrained gradient in Hilbert space. A metric tensor must be specified in the derivation of this dissipation term, since it describes the geometric features of the Hilbert space [24]. τ is the relaxation time, which represents the speed of system evolution in Hilbert space.

In the application here to the modeling of heat and mass diffusion, the system is restricted to the class of dilute-Boltzmann-gas states in which the particles have no quantum correlation between eigenstates, and are independently distributed [28]. Such states can be represented by a single-particle density operator that is diagonal in the basis of the single-particle energy eigenstates. The Hilbert space metric chosen here is the Fisher-Rao metric, which is uniform in different dimensions of Hilbert space. Under these conditions, the symplectic Schödinger term in the equation of motion vanishes. Thus, the focus is this paper is on the irreversible relaxation process only.

A group of energy eigenlevels $\{\epsilon_i, i = 1, 2, ...\}$ is determined from the system Hamiltonian. The state of the system can then be represented by a probability distribution among the energy eigenlevels $\{p_i, i = 1, 2, ...\}$, which is the diagonal terms of the density operator. Using the Fisher-Rao metric of the probability space $\{p_i, i = 1, 2, ...\}$, one can define the distance in probability space, which can be used as the state distance. Equivalently, the square root of the probability

distribution $\{x_i, i = 1, 2, ...\}$ can be used to represent the system state with the result that the Fisher-Rao metric of the probability space becomes the Euclidean metric in square root of the probability space of $\{x_i, i = 1, 2, ...\}$. The later representation is used in the paper. Both are expressed as follows:

$$\text{State: } \{p_i, i = 1, 2, ...\}, \quad \text{Distance: } dl = \frac{1}{2}\sqrt{\sum_i p_i (\frac{dlnp_i}{d\theta})^2 d\theta} \tag{4.3}$$

$$\text{State: } \{x_i, i = 1, 2, ...\}, \quad \text{Distance: } dl = \sqrt{\sum_i (dx_i)^2} \tag{4.4}$$

where dl is the distance between $p(\theta + d\theta)$ and $p(\theta)$ or $x(\theta + d\theta)$ and $x(\theta)$, and θ is a continuous parameter. An extensive property of the system can then be defined as a function of the state $\{x_i\}$ such that

$$I = \sum_i x_i^2 \tag{4.5}$$

$$E = \langle e \rangle = \sum_i \epsilon_i x_i^2 \tag{4.6}$$

$$S = \langle s \rangle = \sum_i -x_i^2 \ln(x_i^2) \tag{4.7}$$

where $\langle \cdot \rangle$ means the ensemble average. The von Neumann formula for entropy is used, because as shown in [32], it has all the properties required by thermodynamics. The gradient of a given property in state space is then expressed by

$$\boldsymbol{g_I} = \sum_i \frac{\partial I}{\partial x_i} \hat{e}_i = \sum_i 2 x_i \hat{e}_i \tag{4.8}$$

$$\boldsymbol{g_E} = \sum_i \frac{\partial E}{\partial x_i} \hat{e}_i = \sum_i 2 \epsilon_i x_i \hat{e}_i \tag{4.9}$$

$$\boldsymbol{g_S} = \sum_i \frac{\partial S}{\partial x_i} \hat{e}_i = \sum_i [-2x_i - 2x_i \ln(x_i^2)] \hat{e}_i \tag{4.10}$$

where $\hat{e}_i$ is the unit vector for each dimension. Furthermore, for an isolated system, the system satisfies the conservation laws for probability and energy, i.e.,

$$I = \sum_i x_i^2 = 1, \quad E = \sum_i \epsilon_i x_i^2 = \text{constant} \tag{4.11}$$

The principle of SEA upon which the equation of motion is based is defined as the system state evolving along the direction that at any instant of time has the largest entropy gradient consistent with the conservation constraints. The equation of motion is given by

$$\frac{d\boldsymbol{x}}{dt} = \frac{1}{\tau(x)} \boldsymbol{g_{S\perp L(g_I,g_E)}} \tag{4.12}$$

where τ, which is a function of system state, is the relaxation time which describes the speed at which the state evolves in state space in the direction of steepest entropy ascent. $L(\boldsymbol{g_I}, \boldsymbol{g_E})$ is the manifold spanned by $\boldsymbol{g_I}$ and $\boldsymbol{g_E}$, and $\boldsymbol{g_{S\perp L(g_I,g_E)}}$ is the perpendicular component of the gradient of the entropy to the hyper-surface that conserves the probability and energy. It takes the form of a ratio of Gram determinants expressed as

$$\boldsymbol{g_{S\perp L(g_I,g_E)}} = \frac{\begin{vmatrix} \boldsymbol{g_S} & \boldsymbol{g_I} & \boldsymbol{g_E} \\ (\boldsymbol{g_S},\boldsymbol{g_I}) & (\boldsymbol{g_I},\boldsymbol{g_I}) & (\boldsymbol{g_E},\boldsymbol{g_I}) \\ (\boldsymbol{g_S},\boldsymbol{g_E}) & (\boldsymbol{g_I},\boldsymbol{g_E}) & (\boldsymbol{g_E},\boldsymbol{g_E}) \end{vmatrix}}{\begin{vmatrix} (\boldsymbol{g_I},\boldsymbol{g_I}) & (\boldsymbol{g_E},\boldsymbol{g_I}) \\ (\boldsymbol{g_I},\boldsymbol{g_E}) & (\boldsymbol{g_E},\boldsymbol{g_E}) \end{vmatrix}} \tag{4.13}$$

where $(,)$ denotes the scalar product of two vectors in state space. The explicit form of Eq. (4.13) for $\{p_j\}$ is, thus, [28]

$$\frac{dp_j}{dt} = \frac{1}{\tau} \frac{\begin{vmatrix} -p_j \ln p_j & p_j & \epsilon_j p_j \\ \langle s \rangle & 1 & \langle e \rangle \\ \langle es \rangle & \langle e \rangle & \langle e^2 \rangle \end{vmatrix}}{\begin{vmatrix} 1 & \langle e \rangle \\ \langle e \rangle & \langle e^2 \rangle \end{vmatrix}} \tag{4.14}$$

where

$$\langle e^2 \rangle = \sum_i \epsilon_i^2 x_i^2, \quad \langle es \rangle = \sum_i -\epsilon_i x_i^2 \ln(x_i^2) \tag{4.15}$$

The state representation and the equation of motion can be simplified by combining degenerate energy eigenlevels [14]. The system is defined by a group of different energy eigenlevels $\{\epsilon_i, i = 1, 2, ...\}$ and their degeneracy $\{n_i, i = 1, 2, ...\}$. The state of the system is described by a probability distribution among the energy eigenlevels $\{p_i, i = 1, 2, ...\}$ or square root of the

probability $\{x_i, i = 1, 2, ...\}$. As a result, the equation of motion changes to

$$\frac{dp_j}{dt} = \frac{1}{\tau} \frac{\begin{vmatrix} -p_j \ln \frac{p_j}{n_j} & p_j & \epsilon_j p_j \\ \langle s \rangle & 1 & \langle e \rangle \\ \langle es \rangle & \langle e \rangle & \langle e^2 \rangle \end{vmatrix}}{\begin{vmatrix} 1 & \langle e \rangle \\ \langle e \rangle & \langle e^2 \rangle \end{vmatrix}} \tag{4.16}$$

where the properties are defined by

$$\langle e \rangle = \sum_i \epsilon_i x_i^2, \ \langle s \rangle = \sum_i -x_i^2 \ln(\frac{x_i^2}{n_i}), \ \langle e^2 \rangle = \sum_i \epsilon_i^2 x_i^2, \ \langle es \rangle = \sum_i -\epsilon_i x_i^2 \ln(\frac{x_i^2}{n_i}) \tag{4.17}$$

4.2.2 Non-equilibrium evolution: Kinetics and Dynamics

In general, the equation of motion for a system with a given group of conservation laws has the form:

$$\frac{dp_j}{dt} = \frac{1}{\tau(\mathbf{p})} D_j(\mathbf{p}) \tag{4.18}$$

where $D_j(\mathbf{p})$ is calculated from the conservation laws and the principle of steepest entropy ascent [42]. Specifically, it takes the form of Eq. (4.14) for an isolate system yielding to mass and energy conservation.

Since for a given initial state of the system, the non-equilibrium thermodynamic path of state evolution is uniquely solved from this equation, Eq. (4.18), the path can be used to define a new parameter $\tilde{\tau}$ given by

$$d\tilde{\tau} = \frac{1}{\tau(\mathbf{p}(t))} dt, \quad \text{or} \quad \tilde{\tau} = \int_{path} \frac{1}{\tau(\mathbf{p}(t'))} dt' = \tilde{\tau}(t) \tag{4.19}$$

where $\tilde{\tau}$ is called the dimensionless time. With this time, the independent variable for the equation of motion can be changed so that

$$\frac{dp_j}{d\tilde{\tau}} = D_j(\mathbf{p}) \tag{4.20}$$

The solution of this equation is written as:

$$p_j = p_j(\tilde{\tau}) \tag{4.21}$$

Independent of how the relaxation time τ depends on the real time t and the state, the equation of motion can always be transformed to Eq. (4.20) with the parameter change defined by Eq. (4.19). Furthermore, the evolution of system state will follow the same function (Eq. (4.21)) in $\tilde{\tau}$. Physically, this means that the system follows the same trajectory in state space. By using this transformation, the kinetics and dynamics of the system are separated. The former is found via Eqs. (4.20) and (4.21) and result in the trajectory in state space based on the parameter $\tilde{\tau}$ or a constant relaxation time τ. The dynamics are found via Eq. (4.18) and the functional dependence $\tau = \tau(p)$ (Eq. (4.19)) and result in the trajectory in state space based on the real time t.

In the discussion on mass diffusion (*Section* 4.3) and heat diffusion (*Section* 4.4), it is shown that the kinetics (or its associated trajectory) of the non-equilibrium relaxation results in a generalized Gibbs relation and the Onsager relations in the far-from-equilibrium realm and in linear phenomenological equations in the near-equilibrium realm, which are independent of the dynamics. The kinetics appears as a system feature or pattern of the thermodynamics in the sense of the GENERIC [20, 21, 35], which is an ensemble or group feature. Information about the mechanical details (e.g., how the particles interact in the system mechanically) can be included in the dynamics (e.g., by how τ is chosen) when the state evolution in time t is studied. The focus of this paper, however, is on the thermodynamic features of the non-equilibrium relaxation so that τ is set equal to 1. More discussion on how τ is chosen using the mechanics and on the dynamics of non-equilibrium is left for a future paper.

4.2.3 Non-equilibrium state and state evolution description: Hypo-equilibrium

The solution of the SEA-QT equation of motion exhibits some good properties, which allows for a complete description of non-equilibrium state and the general definition of non-equilibrium temperature. More discussion is presented in reference [14], and an example is provided below. The energy eigenlevels of the system $\{\epsilon_i, i = 1, 2, 3...\}$ with degeneracy $\{n_i, i = 1, 2, 3...\}$ can be divided into to M sets $\{\epsilon_i^K\}$ (degeneracy $\{n_i^K\}$) with $i = 1, 2, 3, ...,\ K = 1, 2, ..., M$, so that the state space of the system (the Hilbert space) $\mathcal{H}$ can be represented by the sum of M subspaces $\mathcal{H}_K$,

with $K = 1, 2, ..., M$, i.e.,

$$\mathcal{H} = \bigoplus_{K=1}^{M} \mathcal{H}_K \tag{4.22}$$

To be complete, M can be infinite. The system state can be represented by the distributions in M subspace energy eigenlevels $\{p_i^K, K = 1, ..., M\}$. If the probability distribution in one subspace, for example, the K^{th} subspace yields to the canonical distribution of parameter β_K, the temperature of the K^{th} subspace is defined to be $T_K = 1/\beta_K$. Given a way to divide the energy eigenlevels, if the system probability distributions in the M subspaces are all canonical distribution, the state of the system is called a M^{th}-order hypo-equilibrium state [14], which can be described uniquely by the total probability in each subspace ($\{p^K = \sum p_i^K, K = 1, ..., M\}$) and the temperature of each of the subspaces ($\{T_K, K = 1, ..., M\}$). If the initial state of the system is a M^{th}-order hypo-equilibrium state then

$$p_i^K(t = 0) = \frac{p^K n_i^K}{Z^K(\beta^K)} e^{-\beta_K \epsilon_i^K}, i = 1, 2, 3, ... \tag{4.23}$$

where k_b is the Boltzmann constant, $Z^K(\beta^K)$ is the partition function of subspace K at temperature T^K. A more general form to represent any non-equilibrium state is given in [42] using the language of quantum mechanics. Li and von Spakovsky [14] have proven that the system retains a M^{th}-order hypo-equilibrium state throughout the non-equilibrium relaxation process if it initial starts out in such a state. The solution to Eq. (4.18), thus, becomes

$$p_i^K(t) = \frac{p^K(t)}{Z^K(\beta^K(t))} n_i^K e^{-\beta^K(t)\epsilon_i^K}, i = 1, 2, 3, n_K \tag{4.24}$$

As a result, each subspace has temperature defined throughout the entire non-equilibrium relaxation process. This result applies to an isolate system with probability and energy conservation. For a system with a different set of conservation laws, a similar relation exists. However, the general proof is left for a future paper. The proof for a system with heat diffusion only is given in the *Appendix* B.1.

4.2.4 Local variational principle in thermodynamic state space

According to Beretta [28], the equation of motion can be derived from a local variational principle, which can be regarded as the variational form of the steepest entropy ascent principle, i.e.,

$$\begin{aligned}&\text{Maximize: } \dot{S}(\dot{\mathbf{x}}) = (\dot{\mathbf{x}}, \mathbf{g_S}) \text{ subject to } \dot{E} = (\dot{\mathbf{x}}, \mathbf{g_E}) = 0,\ \dot{I} = (\dot{\mathbf{x}}, \mathbf{g_I}) = 0,\ (\dot{\mathbf{x}},\ \dot{\mathbf{x}}) = \xi(\mathbf{x}) \\ &\text{with } \delta\dot{\mathbf{x}} \neq 0,\ \delta\mathbf{x} = 0\end{aligned} \tag{4.25}$$

The third constraint on $\dot{\mathbf{x}}$ indicates that only the direction of $\dot{\mathbf{x}}$ is of interest. This variational principle is in microscopic state space, which contrasts with the variational principle in the space spanned by conjugate fluxes and forces presented later for the Onsager relations.

4.3 Theory: Diffusion in a non-equilibrium system

In the next two sections, *Sections* 4.3 and 4.4, two interactions are studied with the SEAQT framework. The theory for mass diffusion in a local, isolated system in non-equilibrium is presented in this section, *Section* 4.3. The Gibbs relation, the entropy generation for a non-quasi-equilibrium process, and the Onsager relations are derived based on the concept of hypo-equilibrium state and intensive properties. The variational principle using conjugate forces is given at the end of *Section* 4.3.

4.3.1 Equation of motion for mass diffusion

The mass (or probability) diffusion across energy eigenlevels (or across subspaces) can be studied for an isolated system in non-equilibrium. Using Eq. (4.14), one energy eigenlevel in the K^{th} subspace yields to the following equation of motion:

$$\frac{dp_j^K}{dt} = \frac{1}{\tau}(-p_j^K \ln \frac{p_j^K}{n_j^K} - p_j^K \frac{A_2}{A_1} + \epsilon_j p_j^K \frac{A_3}{A_1}) \tag{4.26}$$

where

$$A_1 = \begin{vmatrix} 1 & \langle e \rangle \\ \langle e \rangle & \langle e^2 \rangle \end{vmatrix}, A_2 = \begin{vmatrix} \langle s \rangle & \langle e \rangle \\ \langle es \rangle & \langle e^2 \rangle \end{vmatrix}, A_3 = \begin{vmatrix} \langle s \rangle & 1 \\ \langle es \rangle & \langle e \rangle \end{vmatrix} \tag{4.27}$$

Summation over all energy eigenlevels in the K^{th}subspace yields the evolution of the probability in the K^{th} subspace, represented by p^K, namely,

$$\frac{dp^K}{dt} = \frac{1}{\tau}(-p^K \ln p^K + p^K \langle \tilde{s} \rangle^K - p^K \frac{A_2}{A_1} + p^K \langle \tilde{e} \rangle^K \frac{A_3}{A_1}) \tag{4.28}$$

where $\langle \tilde{\cdot} \rangle^K$ is the specific property in the K^{th} subspace. To calculate the specific property, the probability distribution in the K^{th} subspace is found from

$$p^K \equiv \sum_j p_j^K, \quad \tilde{p}_j^K \equiv \frac{p_j^K}{p^K} \tag{4.29}$$

where p^K is the particle number in the K^{th} subspace. The specific property in the K^{th} subspace is then expressed as

$$\langle \tilde{e} \rangle^K \equiv \sum_j \epsilon_j^K \tilde{p}_j^K \tag{4.30}$$

$$\langle \tilde{s} \rangle^K \equiv -\sum_j \tilde{p}_j^K \ln \frac{\tilde{p}_j^K}{n_j^K} \tag{4.31}$$

4.3.2 Particle number and temperature evolution when the initial state is a hypo-equilibrium state

If the system is in a M^{th}-order hypo-equilibrium state, the probability evolution yields Eq. (4.24). For simplicity, the following definition is made:

$$\alpha^K = \ln Z^K - \ln p^K \tag{4.32}$$

With this definition, the probability evolution of one energy eigenlevel is given by

$$p_i^K(t) = \frac{p^K(t)}{Z^K(\beta^K(t))} n_i^K e^{-\beta^K(t)\epsilon_i^K} = n_i^K e^{-\alpha^K(t) - \beta^K(t)\epsilon_i^K} \tag{4.33}$$

α^K and β^K are non-equilibrium intensive properties of the K^{th} subspace, corresponding to the extensive properties p^K and $E^K \equiv p^k\langle\tilde{e}\rangle^K$. Furthermore, by defining

$$\alpha = \frac{A_2}{A_1}, \quad \beta = -\frac{A_3}{A_1} \tag{4.34}$$

the particle number and energy evolution of the K^{th} subspace can be acquired from Eq. (4.26), i.e.,

$$\frac{dp^K}{dt} = \frac{1}{\tau}p^K(\alpha^K - \alpha) + \frac{1}{\tau}p^K\langle\tilde{e}\rangle^K(\beta^K - \beta) \tag{4.35}$$

$$\frac{d\langle e\rangle^K}{dt} = \frac{1}{\tau}p^K\langle\tilde{e}\rangle^K(\alpha^K - \alpha) + \frac{1}{\tau}p^K\langle\tilde{e^2}\rangle^K(\beta^K - \beta) \tag{4.36}$$

From Eqs. (4.24) and (4.26), the intensive properties α^K and β^K obey the evolutions (see *Appendix* B.2 for the derivation)

$$\frac{d\alpha^K}{dt} = -\frac{1}{\tau}(\alpha^K - \alpha) \tag{4.37}$$

$$\frac{d\beta^K}{dt} = -\frac{1}{\tau}(\beta^K - \beta) \tag{4.38}$$

The authors prove that α and β have the physical meaning of intensive properties from measurements of a non-equilibrium state [17]. At stable equilibrium, the intensive properties in any subsystem obey the following relations:

$$\alpha(t = t^{eq}) = \alpha^K(t = t^{eq}) = \alpha^{eq} \tag{4.39}$$

$$\beta(t = t^{eq}) = \beta^K(t = t^{eq}) = \beta^{eq} \tag{4.40}$$

4.3.3 Gibbs relation, entropy generation for a non-quasi-equilibrium process, and the Onsager relations in the nonlinear realm

Differential changes of the extensive properties in the K^{th} subspace are written as

$$dE^K = \sum_i d(\epsilon_j^K p_j^K) \tag{4.41}$$

$$dS^K = \sum_i \frac{d}{dt}(-p_j^K \ln \frac{p_j^K}{n_j^K}) = \sum_i (-\ln \frac{p_j^K}{n_j^K} - 1)\frac{dp_j^K}{dt} \tag{4.42}$$

where E^K and $S^K \equiv p^K \langle \tilde{s} \rangle^K$ are the energy and entropy in the K^{th} subspace, respectively.

When a system is in a M^{th}-order hypo-equilibrium state and undergoes a pure relaxation process, a relation for property evolution in one subspace is acquired by using relation of Eq. (4.33), namely,

$$\frac{dS^K}{dt} = \sum (\epsilon_j^K \beta^K + \alpha^K - 1)\frac{dp_j^K}{dt} = \beta^K \frac{dE^K}{dt} + (\alpha^K - 1)\frac{dp^K}{dt} \tag{4.43}$$

The proof of this relation for one subspace applies to any differential changes (not only the time derivative). Thus, a generalization of the Gibbs relation to the K^{th} subspace of a system in non-equilibrium, is expressed by

$$dS^K = \beta^K dE^K + (\alpha^K - 1)dp^K \tag{4.44}$$

Thus, from the Gibbs relation at stable equilibrium written as

$$dS = \frac{1}{T}dE - \frac{\mu}{T}dN \tag{4.45}$$

the physical meaning of β^K and α^K is shown to be

$$\beta^K = \left(\frac{\partial S^K}{\partial E^K}\right)_{p^K} = \frac{1}{T^k} \tag{4.46}$$

$$\alpha^K - 1 = \left(\frac{\partial S^K}{\partial p^K}\right)_{E^K} = -\frac{\mu^K}{T^k},\ \mu^K = \left(\frac{\partial E^K}{\partial p^K}\right)_{S^K} \tag{4.47}$$

where T^K is subspace temperature and μ^K is subspace chemical potential with respect to subspace probability p^K. The total differential entropy change for the system, which for a pure non-

equilibrium relaxation process corresponds to the entropy generation, is

$$dS = \sum_K dS^K = \sum_K \beta^K dE^K + \sum_K (\alpha^K - 1) dp^K = \sum_K (\beta^K - \beta) dE^K + \sum_K (\alpha^K - \alpha) dp^K \quad (4.48)$$

where both energy ($\sum E^K = 0$) and probability ($\sum p^K = 0$) conservations have been applied. The Casimir condition holds and $J_E^K = dE^K/dt$ and $J_p^K = dp^K/dt$ are defined to be the internal fluxes of energy and probability inside the system, while $X_p^K = \beta^K - \beta$ and $X_E^K = \alpha^K - \alpha$ are the conjugate forces. The result is

$$\sigma(\mathbf{J}, \mathbf{X}) = \frac{dS}{dt} = \sum_K X_E^K J_E^K + \sum_K X_p^K J_p^K \quad (4.49)$$

The Onsager relations are then acquired from Eqs. (4.35) and (4.36) in the form of $\mathbf{J} = \mathbf{\Lambda X}$, where $\mathbf{\Lambda}$ is a symmetric and positive definite operator. Thus,

$$J_p^K = \frac{1}{\tau} p^K X_p^K + \frac{1}{\tau} E^K X_E^K \quad (4.50)$$

$$J_E^K = \frac{1}{\tau} E^K X_p^K + \frac{1}{\tau} \langle e^2 \rangle^K X_E^K \quad (4.51)$$

The quadratic dissipation potential using force representation [44, 45] is written as

$$\Xi(\mathbf{X}, \mathbf{X}) = \frac{1}{2} \langle \mathbf{X}, \Lambda \mathbf{X} \rangle = \frac{1}{2\tau} \sum_K [p^K (\alpha^K - \alpha)^2$$
$$+ 2E^K (\alpha^K - \alpha)(\beta^K - \beta) + \langle e^2 \rangle^K (\beta^K - \beta)^2] \quad (4.52)$$

Using force representation, the variational principle is given by

$$\delta[\sigma(\mathbf{J}, \mathbf{X}) - \Xi(\mathbf{X}, \mathbf{X})]_{\mathbf{J}} = 0, \ \mathbf{J} = \text{const}, \ \delta\mathbf{J} = 0, \ \delta\mathbf{X} \neq 0 \quad (4.53)$$

where the $\sigma(\mathbf{J}, \mathbf{X})$ and $\Xi(\mathbf{X}, \mathbf{X})$ are given by Eqs. (4.49) and (4.52). Furthermore, even though the following constraints apply to the fluxes:

$$\sum_K J_p^K = 0, \ \sum_K J_E^K = 0 \quad (4.54)$$

The reciprocity seen in Eqs. (4.50) and (4.51) is completely consistent with the Onsager theory

since according to Gyarmati [44], *the validity of Onsager's reciprocal relations is not influenced by a linear homogeneous dependence valid amongst the fluxes*. Thus, the physical interpretation given here is fully consistent with other investigations [17] and does not require a reformulation in terms of independent fluxes even though this could be done. In addition, it is from the gradient dynamics of the non-equilibrium relaxation process that the entropy generation, the Onsager relations, and the quadratic dissipation potential of a local, isolated system in non-equilibrium have been derived using the geometric principle of SEA as well as the concepts of hypo-equilibrium state and non-equilibrium intensive properties. Alternatively, the variational principle of SEA in system state space can be used to arrive at these relations as is done in [42] using the language of quantum mechanics. Of course, these relations also correspond to the variational principle in the space spanned by conjugate forces and fluxes [44].

4.4 Theory: Heat diffusion in a non-equilibrium system

A local, isolated system in non-equilibrium with heat diffusion only is considered in this section. This requires a model with a different set of constraints (i.e., the probability redistribution is only allowed in each subspace) then when only heat diffusion is considered. The entropy change of the system and subspaces due to heat diffusion for non-quasi-equilibrium process is given and the relationship between the SEAQT equation of motion and the phenomenological diffusion equation is presented.

4.4.1 Equation of motion for heat diffusion

Different from previous forms of the equation of motion, that for pure heat diffusion yields to a different set of conservation equations. If the system is separated into M subspaces with energy flow but no probability flow across the subspaces, there are $M + 1$ conservation laws. System probability conservation is replaced by that for M individual subspaces. In *Appendix* B.1, it is proven that the concept of hypo-equilibrium state and non-equilibrium temperature are also well

defined under these new constraints given by

$$I^K = \sum_i (x_i^K)^2 = p^K,\ K = 1, 2, ...M \tag{4.55}$$

$$E = \sum_i \epsilon_i x_i^2 = \text{constant} \tag{4.56}$$

For simplicity, a 2^{nd}-order hypo-equilibrium state is studied first. The system is separated into 2 subspaces (subspace a and subspace b) so that the equation of motion takes the form

$$\frac{dp_j^a}{dt} = \frac{1}{\tau} \frac{\begin{vmatrix} p_j^a s_j^a & p_j^a & 0 & \epsilon_j^a p_j^a \\ \langle s \rangle^a & p^a & 0 & \langle e \rangle^a \\ \langle s \rangle^b & 0 & p^b & \langle e \rangle^b \\ \langle es \rangle & \langle e \rangle^a & \langle e \rangle^b & \langle e^2 \rangle \end{vmatrix}}{\begin{vmatrix} p^a & 0 & \langle e \rangle^a \\ 0 & p^b & \langle e \rangle^b \\ \langle e \rangle^a & \langle e \rangle^b & \langle e^2 \rangle \end{vmatrix}} \tag{4.57}$$

where the contribution of each subspace to the total property is defined by

$$\langle s \rangle = \langle s \rangle^a + \langle s \rangle^b,\ \langle s \rangle^a = \sum p_i^a s_i^a,\ \langle s \rangle^b = \sum p_i^b s_i^b \tag{4.58}$$

$$\langle e \rangle = \langle e \rangle^a + \langle s \rangle^b,\ \langle e \rangle^a = \sum p_i^a \epsilon_i^a,\ \langle e \rangle^b = \sum p_i^b \epsilon_i^b \tag{4.59}$$

where

$$s_j^{a(b)} = -\ln \frac{p_j^{a(b)}}{n_j^{a(b)}} = \tilde{s}_j^{a(b)} - \ln p^{a(b)},\ \tilde{s}_j^{a(b)} \equiv -\ln \frac{\tilde{p}_j^{a(b)}}{n_j^{a(b)}} \tag{4.60}$$

By defining

$$B_1 = \begin{vmatrix} p^a & 0 & \langle e\rangle^a \\ 0 & p^b & \langle e\rangle^b \\ \langle e\rangle^a & \langle e\rangle^b & \langle e^2\rangle \end{vmatrix}, B_2^a = \begin{vmatrix} \langle s\rangle^a & 0 & \langle e\rangle^a \\ \langle s\rangle^b & p^b & \langle e\rangle^b \\ \langle es\rangle & \langle e\rangle^b & \langle e^2\rangle \end{vmatrix}$$
$$B_2^b = \begin{vmatrix} \langle s\rangle^b & 0 & \langle e\rangle^b \\ \langle s\rangle^a & p^a & \langle e\rangle^a \\ \langle es\rangle & \langle e\rangle^a & \langle e^2\rangle \end{vmatrix}, B_3 = \begin{vmatrix} \langle s\rangle^a & p^a & 0 \\ \langle s\rangle^b & 0 & p^b \\ \langle es\rangle & \langle e\rangle^a & \langle e\rangle^b \end{vmatrix} \tag{4.61}$$

Eq. (4.57) can be simplified to

$$\frac{dp_j^a}{dt} = \frac{1}{\tau}(p_j^a s_j^a - p_j^a \frac{B_2^a}{B_1} - \epsilon_j^a p_j^a \frac{B_3}{B_1}) \tag{4.62}$$

Moreover, the equation of motion for the probability distribution in one subspace can also be written in terms of the normalized probability by dividing both sides of Eq. (4.62) by p^a so that

$$\frac{d\tilde{p}_j^a}{dt} = \frac{1}{\tau}(\tilde{p}_j^a s_j^a - \tilde{p}_j^a \frac{B_2^a}{B_1} - \epsilon_j^a \tilde{p}_j^a \frac{B_3}{B_1}) \tag{4.63}$$

Furthermore, if the system is in a 2^{nd}-order hypo-equilibrium initially so that each subspace has a canonical distribution, Eq. (4.63) can be simplified further to arrive at the form

$$\frac{d\tilde{p}_j^a}{dt} = \frac{1}{\tau}\tilde{p}_j^a[(\tilde{s}_j^a - \langle\tilde{s}\rangle^a) - \beta(\epsilon_j^a - \langle\tilde{e}\rangle^a)] \tag{4.64}$$

where $\tilde{s}_j^a$ is defined by Eq. (4.60) and $\langle\tilde{s}\rangle^a$ and $\langle\tilde{e}\rangle^a$ are defined by Eqs. (4.30) and (4.31). The parameter β is given

$$\beta \equiv \frac{B_3}{B_1} = \frac{p^a \tilde{A}_1^a \beta^a + p^b \tilde{A}_1^b \beta^b}{p^a \tilde{A}_1^a + p^b \tilde{A}_1^b} \tag{4.65}$$
$$B_1 = p^a p^b (p^a \tilde{A}_1^a + p^b \tilde{A}_1^b) \tag{4.66}$$
$$B_3 = p^a p^b (p^a \beta^a \tilde{A}_1^a + p^b \beta^b \tilde{A}_1^b) \tag{4.67}$$

is a weighted average of the inverse temperatures of the subsystems relative to the mole fractions and the energy fluctuation (or non-dimensional specific heat at constant volume) of the subspaces

written as

$$\tilde{A}_1^{a(b)} = \langle \tilde{e^2} \rangle^{a(b)} - (\langle \tilde{e} \rangle^{a(b)})^2 = -\frac{\partial \langle \tilde{e} \rangle^{a(b)}}{\partial \beta^{a(b)}} = \frac{C_V^{a(b)}}{(\beta^{a(b)})^2} \tag{4.68}$$

$$C_V^{a(b)} \equiv \frac{1}{k_b} \frac{\partial \langle \tilde{e} \rangle^{a(b)}}{\partial T^{a(b)}} \tag{4.69}$$

For the more general case of a M^{th}-order hypo-equilibrium state and the system separated into M subspaces, equation (4.63) remains the same but with

$$\beta \equiv \frac{B_3}{B_1} = \frac{\sum_K^M p^K \tilde{A}_1^K \beta^K}{\sum_K^M p^K \tilde{A}_1^K} \tag{4.70}$$

A given interaction type (e.g., heat diffusion) results in a given relaxation time τ (see *Section* 4.2.2), while the ratio B_3/B_1 provides an average temperature based on subspace mole fractions and energy fluctuations. At stable equilibrium, $\beta = \beta^{eq}$. Now, if one subspace R is attached to a reservoir, the evolution of the other subspaces behave according to the equation of motion, Eq. (4.63), with β^R constant. For example, only part of the energy eigenlevels can absorb energy from the environment. Mathematically, if subspace R yields to one of two conditions,

$$\forall K \neq R, C_V^R \gg C_V^K, \quad p^R \gg p^K \tag{4.71}$$

the relation $\beta = \beta^R$ holds and subspace $K(\neq R)$ yields to the equation of motion.

$$\frac{d\tilde{p}_j^K}{dt} = \frac{1}{\tau} \tilde{p}_j^K [(-\ln \frac{\tilde{p}_j^K}{n_j^K} - \langle \tilde{s} \rangle^K) - \beta^R (\epsilon_j^K - \langle \tilde{e} \rangle^K)] \tag{4.72}$$

Note that in this equation, the only parameter related to subspace R is the reservoir temperature β^R. The energy eigenstructure of subspace R plays no role!

4.4.2 Property of heat diffusion: non-quasi-equilibrium process and 2^{nd} of thermodynamics

Based on Eq. (4.62), the total entropy and energy evolution in one subspace can be determined via

$$\frac{dS^K}{dt} = \frac{d\langle s\rangle^K}{dt} = p^K \frac{d\langle \tilde{s}\rangle^K}{dt} = \frac{1}{\tau} p^K (\beta^K - \beta)\beta^K \tilde{A}_1^K \tag{4.73}$$

$$\frac{dE^K}{dt} = \frac{d\langle e\rangle^K}{dt} = p^K \frac{d\langle \tilde{e}\rangle^K}{dt} = \frac{1}{\tau} p^K (\beta^K - \beta)\tilde{A}_1^K \tag{4.74}$$

Dividing Eq. (4.73) by (4.74) yields

$$\frac{dS^K}{dE^K} = \frac{dS^K}{dt} / \frac{dE^K}{dt} = \beta^K \tag{4.75}$$

The equation is a generalized form of the differential entropy transfer due to heat diffusion using the non-equilibrium temperature for each subspace, i.e.,

$$dS^K = \beta^K dE^K = \frac{\delta Q^K}{k_b T} \tag{4.76}$$

Moreover, Eq. (4.76) can applied to all kinds of thermodynamic processes, and is not limited to quasi-equilibrium processes. This argument comes from the universal definition of non-equilibrium temperature provided in this paper.

4.5 Model: Composite system in a non-equilibrium state

Interacting systems can form a composite non-equilibrium system with the interaction resulting in the non-equilibrium relaxation process for the composite. Using the SEA equation of motion, the state evolution of the composite system can be determined. Proper division of this composite allows the subspaces to be viewed as the interacting subsystems within the composite. The behavior of each subsystem, thus, can be studied by an analysis of the state evolution of each subspace. In particular, if two individual subsystems involved in an interaction both have canonical state distributions, and each subsystem's energy eigenvectors span one subspace, the composite system is in a 2^{nd}-order hypo-equilibrium state. On the other hand, if each individual subsystem's state cannot be described by a canonical distribution, a higher-order hypo-equilibrium state will be required.

In the following section, (*Section* 4.5.1), the SEAQT framework using single particle energy eigenlevels is applied to the study of a simple system. *Section* 4.5.2 then explains the process of subspace division followed in *Section* 4.5.3 by a comparison with the phenomenological equations for mass and heat diffusion. In *Section* 4.5.4, the physical details of the system used are described. Finally, in *Section* 4.5.5, the coupling of mass and heat diffusion is modeled and discussed.

4.5.1 Multi-particle classical simple system

Theoretically and in general, the SEAQT equation of motion is applicable to multi-particle systems provided that energy eigenstructure of the system is known [17]. However, for a multi-particle classical simple system, the energy eigenstructure of a single particle and its associated equation of motion can be used to study the system, since all of the particles (or particle groups) have the same energy eigenlevels $\{\epsilon_i, i = 1, 2, 3, ...\}$ and degeneracy $\{n_i, i = 1, 2, 3, ...\}$. Thus, the system state can be represented by the particle number (or particle group number) at each energy eigenlevel $\{m_i, i = 1, 2, 3, ...\}$. The mole fraction of particles at the i^{th} energy eigenlevel is given by $y_i = m_i / \sum m_i$. The extensive property constraints of the system are then

$$M = \sum_i m_i = \text{constant} \tag{4.77}$$

$$E = \sum_i \epsilon_i m_i = \text{constant} \tag{4.78}$$

$$S = \sum_i -m_i \ln \frac{y_i}{n_i} \tag{4.79}$$

Dividing the constraints by the total particle number $\sum m_i$, the system state can be represented by the mole fractions $\{y_i, i = 1, 2, 3, ...\}$, which is equivalent to the single-particle probability distribution $\{p_i, i = 1, 2, 3, ...\}$. For an isolated system the constraints become

$$I = \sum_i y_i = \sum_i p_i = \text{constant} \tag{4.80}$$

$$\langle e \rangle = \frac{E}{M} = \sum_i \epsilon_i y_i = \sum_i \epsilon_i p_i = \text{constant} \tag{4.81}$$

$$\langle s \rangle = \frac{S}{M} = \sum_i -y_i \ln \frac{y_i}{n_i} = \sum_i -p_i \ln \frac{p_i}{n_i} \tag{4.82}$$

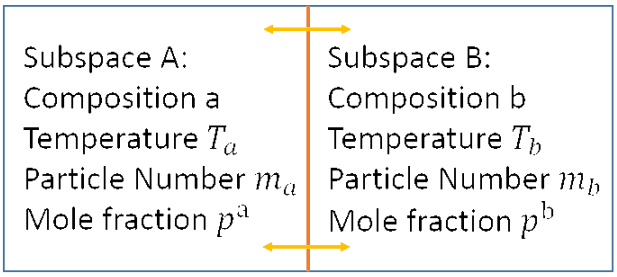

Figure 4.1. Partition in simple system. For mass diffusion, mass flow and energy flow are both allowed across the partition. For heat diffusion, only energy flow is allowed.

$\langle \cdot \rangle$ represents an average specific property. The constraints and equation of motion reduce to the single-particle case (Eqs. (4.5) to (4.7) and (4.14)) when $y_i = p_i, i = 1, 2, 3, ...$

In general, a system's energy eigenstructure and extensive properties are a function of the total particle number of each constituent. This is also true of its specific properties in the presence of a mass interaction or chemical reaction if the system is partitioned and not simple [48], since partitioning influences each partition's energy eigenstructure. Thus, for mass diffusion, the framework outlined here requires an invariant eigenstructure and as a consequence the simple system assumption. With this assumption, particle number no longer influences the specific properties. This same assumption, however, is not required in the case of heat diffusion since the total number of particles for each system partition (i.e., subsystem) does not change.

4.5.2 Interacting systems

It is assumed that a group of observable operators $\hat{F}$ commuting with the Hamiltonian operator $\hat{H}$ exists. The degenerate energy eigenlevels of the system can be distinguished by eigenvalues of the observations of $\hat{F}$, which have values $F_1, F_2, \cdots, F_M$, so that the system energy eigenlevels can be separated into M sets $\{\epsilon_i^K, i = 1, 2, 3, ...\}$ with degeneracy $\{n_i^K, i = 1, 2, 3...\}$, where $K = 1, \cdots, M$. In each set, every energy eigenlevel represents an eigenstate common to both $\hat{F}$ and $\hat{H}$ with the same eigenvalue of $\hat{F}$. Eigenstates in each of the sets can be spanned into a subspace of the system state space and can be designed as a subsystem.

Practically, by choosing the observable operator, the system can be view as an composite system whose subsystems can be properly arranged to study specific phenomena. For the kinetics of a chemical reaction, F can be chosen to be an observable operator of species, whose eigenvalues are "$Reactant$" and "$Product$". In heat and mass diffusion, the observable operator F is chosen to be the relative location to a partition, with eigenvalue of "$left$" (left of the partition) and "$right$"

(right of the partition). The partition allows mass and heat diffusion (see Fig. 4.1).To be more precise, it is assumed that the de Brogli wavelength λ is much smaller than the distance ΔL between the center of the subsystem on the "$left$" and that on the "$right$". This wavelength represents the classical limit, i.e.,

$$p_v = \sqrt{2mk_bT}, \quad \lambda = \frac{h}{p_v} = \frac{h}{\sqrt{2mk_bT}}, \quad \Delta L \gg \lambda \tag{4.83}$$

where p_v is the expectation value of the particle momentum for a system at temperature T.

4.5.3 Phenomenological transport equation

With the assumption that the two subspaces of the system are two subsystems at two positions, the phenomenological transport equations of mass and heat diffusion can be derived.

4.5.3.1 Mass diffusion

Using Eq. (4.28), the equations of motion for two subspaces are written as

$$\frac{d\ln p^a}{dt} = -\frac{1}{\tau}\ln p^a + \frac{1}{\tau}(\langle\tilde{s}\rangle^a - \frac{A_2}{A_1} + \langle\tilde{e}\rangle^a\frac{A_3}{A_1}) \tag{4.84}$$

$$\frac{d\ln p^b}{dt} = -\frac{1}{\tau}\ln p^b + \frac{1}{\tau}(\langle\tilde{s}\rangle^b - \frac{A_2}{A_1} + \langle\tilde{e}\rangle^b\frac{A_3}{A_1}) \tag{4.85}$$

When the two subspaces of the system have the same eigenstructure and temperature, subtracting Eq. (4.85) from Eq. (4.84) yields

$$\frac{d}{dt}(\ln p^a - \ln p^b) = -\frac{1}{\tau}(\ln p^a - \ln p^b) \tag{4.86}$$

Substituting the subspace probability (or mole fraction), Eq. (4.87) into Eq. (4.86) results in

$$p^a = \frac{n^a}{n^a + n^b}, \quad p^b = \frac{n^b}{n^a + n^b} \tag{4.87}$$

$$\frac{d}{dt}(\ln\frac{n^a}{n^b}) = -\frac{1}{\tau}(\ln\frac{n^a}{n^b}) \tag{4.88}$$

If the global mass distribution is continuous, and position A and position B are close enough,

$$n^a = n^b + \Delta n \tag{4.89}$$

which transforms Eq. (4.88) into

$$\frac{d}{dt}(\frac{\Delta n}{n^b}) = -\frac{1}{\tau}\frac{\Delta n}{n^b} \tag{4.90}$$

$$J^{a(b)} \equiv \frac{1}{2A}\frac{d}{dt}(n^a - n^b) = -\frac{n^a - n^b}{2\tau A} = -\frac{\delta x}{2\tau A}\frac{dn}{dx} \tag{4.91}$$

where the approximation $\ln(1+x) \simeq x$ for small x has been used and higher-order terms dropped to arrive at Eq. (4.90). In Eq. (4.91), δx is the distance between two positions, A is the cross-sectional area of the interacting surface, and $J^{a(b)}$ is the flow of particle number equal to $(dn^a/dt)/A$ or $(-dn^b/dt)/A$ (hence the division by 2 in Eq. (4.91)). Eq. (4.91) recovers Fick's law with the diffusion coefficient (diffusivity) given by $D = \frac{\delta x}{2\tau A}$. The specific form of D is directly related to the form of τ, which contains the detailed mechanical information. The phenomenological linear equation can be derived without the form of τ, which is a pure thermodynamic feature or pattern of the non-equilibrium relaxation process. In addition to results such as these for the near-equilibrium realm, thermodynamic features or patterns in the far-from-equilibrium realm can also be studied using Eqs. (4.35) and (4.36) provided the initial state is a hypo-equilibrium state. For the case when it is not, Eq. (4.14) can directly be used as is done, for example, in [14].

4.5.3.2 Heat diffusion

For system in which the only interaction is that of heat diffusion, Eq. (4.76) captures the energy flow between two subsystems, i.e.,

$$\dot{Q} = J_E^{a(b)} = -\kappa'\delta x A\frac{dT}{dx} = \frac{1}{\tau}p^a(\beta^a - \beta)\tilde{A}_1^a = \frac{1}{\tau}\frac{p^a p^b \tilde{A}_1^a \tilde{A}_1^b}{p^a\tilde{A}_1^a + p^b\tilde{A}_1^b}(\beta^a - \beta^b) \tag{4.92}$$

where $\dot{Q}$ is the rate of energy transferred, $J_E^{a(b)}$ is the heat flux, A is the cross-sectional area of the interacting surface, T^a and T^b are temperature of the two subsystems, and Eq. (4.65) has been substituted for β. Eq. (4.92) recovers Fourier's law of heat diffusion (conduction). The thermal

conductivity per unit length κ' and thermal conductivity κ are expressed as:

$$\kappa' = \frac{1}{\tau}\frac{p^a p^b \beta^a \beta^b \tilde{A}_1^a \tilde{A}_1^b}{p^a \tilde{A}_1^a + p^b \tilde{A}_1^b}\frac{1}{A}, \quad \kappa = \kappa' \delta_x \tag{4.93}$$

In the near-equilibrium region with the same constituent in the two subsystems,

$$p^a = p^b = \frac{1}{2}, \quad C_V^a = C_V^b = C_V \tag{4.94}$$

and the thermal conductivity per unit length and the thermal conductivity are expressed in terms of the energy fluctuation (or non-dimensional specific heat at constant volume) of the subspaces, i.e.,

$$\kappa' = \frac{1}{2\tau} C_V \frac{1}{A}, \quad \kappa = \frac{1}{2\tau}\frac{\delta_x}{A} C_V \tag{4.95}$$

The above formulation is applicable for any kind of interaction resulting in a flow of energy only. Furthermore, if the heat and mass diffusion are affected via the same kind of micro-mechanical interactions such as the collision of particles, it can be assumed that the same τ is applicable when the system is in the near-equilibrium region near to the same stable equilibrium point. In this case, $\kappa = C_V D$. This last result is the same as that found from classical transport theory and is a direct consequence of the thermodynamic features of the system minus any direct knowledge of the details of the micro-mechanical interactions taking place.

4.5.4 Mass and heat diffusion of hydrogen

To model the mass and heat diffusion for a specific case, a composite system of hydrogen is set up with two subspaces corresponding to subsystems on two sides of a partition. The energy eigenlevels of the two subsystems together form the energy eigenlevels for the composite system as a whole. Denoting the state space of the subsystem on the "$left$" by $\mathcal{H}^a$ and that on the "$right$" by $\mathcal{H}^b$, the composite system state space $\mathcal{H}$ takes the form

$$\mathcal{H} = \mathcal{H}^a \oplus \mathcal{H}^b \tag{4.96}$$

The available energy eigenvalues for one subspace ("$left$" or "$right$") are constructed from the energy eigenvalues of each degree of freedom for translation and rotation, i.e., from

$$\epsilon^{a(b)} = \epsilon_{t,H_2} + \epsilon_{r,H_2} \tag{4.97}$$

The translational energy eigenvalue ϵ_t uses the form of the infinite potential well, while the rotational energy eigenvalue ϵ_r uses the form of the rigid motor. These are expressed as follow:

$$\epsilon_t(n_x, n_y, n_z) = \frac{\hbar^2}{8m}\left(\frac{n_x^2}{L_x^2} + \frac{n_y^2}{L_y^2} + \frac{n_z^2}{L_z^2}\right) \tag{4.98}$$

$$\epsilon_r(j, m) = \frac{j(j+1)\hbar^2}{2I} \tag{4.99}$$

where n_x, n_y, and n_z are the quantum numbers for the translational degrees of freedom, j and m are the quantum numbers for the rotational degrees of freedom, I is the moment of inertia and L_x, L_y, and L_z are chosen based on mean-free-path of the particles in each subsystems (e.g., the dimension of subsystem is used for an ideal gas). The vibrational energy are not included since the temperature in the study is below its characteristic temperature. For more discuss on the vibrational energy, reader is refereed to [14]. The disassociated energy is not included by selection of the proper energy reference. Each combination of quantum numbers and position corresponds to one energy eigenlevel in the subspaces (or subsystems). The composite system energy eigenlevels are formed by all the available energy eigenlevels of the "$left$" and the "$right$".

A 2^{nd}-order hypo-equilibrium state with the subspace division of "$left$" and "$right$" is chosen to be the initial condition, which means that two subsystems are in local equilibrium states. The non-quasi-equilibrium process of mass and heat diffusion is studied using Eqs. (4.26) and (4.62). For the case when the subsystems are not in states of local equilibrium, the two subspaces can be divided further. For example, if the "$left$" subsystem is a M^{th}-order hypo-equilibrium state, this subspace, subspace a, can be divided into M subspaces according to the initial condition. However, the evolution of each subspace, regardless of whether or not the subsystem is in a state of local equilibrium, yields to the same form of the equations of motion, Eqs. (4.26) and (4.62). For the case considered here, the initial condition is given by (4.23), i.e., by

$$p_i^{a(b)}(t=0) = \frac{p^{a(b)} n_i^{a(b)}}{Z^{a(b)}\left(\beta^{a(b)}\right)} e^{-\beta^{a(b)}\epsilon_i^{a(b)}} \tag{4.100}$$

The time evolution is acquired by solving Eqs. (4.26) and (4.62). For a more general initial condition, such as that for an infinite-order hypo-equilibrium state, the equation of motion can be solved using the density of states method developed in [14].

The specific properties of the individual subsystems at a given temperature and volume are given

$$Z^{a(b)}(\beta^{a(b)}, V) = Z^t Z^r = V(\frac{m}{2\pi\hbar^2\beta^{a(b)}})^{\frac{3}{2}}\frac{2I}{\beta^{a(b)}\hbar^2} = C_Z V(\beta^{a(b)})^{-5/2} \tag{4.101}$$

$$\langle\tilde{e}\rangle^{a(b)}(\beta^{a(b)}) = \frac{5}{2}k_b T^{a(b)} = \frac{5}{2\beta^{a(b)}} = \frac{C_V}{\beta^{a(b)}} \tag{4.102}$$

$$\begin{aligned}\langle\tilde{s}\rangle^{a(b)}(\beta^{a(b)}, V) &= \beta^{a(b)}\langle\tilde{e}\rangle^{a(b)} + \ln Z^{a(b)} = -\frac{5}{2}\ln\beta^{a(b)} + \ln V + C_s \\ &= -C_V \ln\beta^{a(b)} + \ln V + C_s \end{aligned} \tag{4.103}$$

where C_Z and C_s are constants determined from Eqs. (4.101) to (4.103).

4.5.5 Mass and heat diffusion coupling

For mass diffusion with no temperature difference, as shown in Eq. (4.37), the temperature difference remains zero, and only the particle number difference changes and Eq. (4.35) reverts to the linear transport equation in the near-equilibrium realm. The more complex case occurs when mass diffusion takes place in the presence of a temperature difference is of interest in which case coupling effects may be present.

The mass flow between two subsystems is determined by subtracting the probability evolution of one (Eq. (4.35)) from the other with the result that.

$$\begin{aligned}2J_p^{b\to a} &= \frac{dp^a}{dt} - \frac{dp^a}{dt} = \frac{1}{\tau}p^a(\alpha^a - \alpha) + \frac{1}{\tau}p^a\langle\tilde{e}\rangle^a(\beta^a - \beta) \\ &-\frac{1}{\tau}p^b(\alpha^b - \alpha) - \frac{1}{\tau}p^b\langle\tilde{e}\rangle^b(\beta^b - \beta)\end{aligned} \tag{4.104}$$

The coupling effects come from the differences in both of the non-equilibrium intensive properties α and β. To study the effect of temperature on the probability (mass) flow, the two subsystems start from the same initial probability ($p^a = p^b = p^{eq} = 0.5$) but different temperatures. For the case of a perfect gas (i.e., ideal gas with constant specific heats), the final stable equilibrium temperature

T^{eq} is an average of the initial temperatures of the two subsystems, namely,

$$T^{eq} = (T^a + T^b)/2,\ \xi \equiv \Delta T/T^{eq},\ T^a = T^{eq} + \Delta T,\ T^b = T^{eq} - \Delta T \tag{4.105}$$

Thus, Eq. (4.104) can be simplified to

$$J_p^{b\to a} = \frac{1}{2\tau} p^{eq}[(\langle\tilde{s}\rangle^a - \langle\tilde{s}\rangle^b) - \beta(\langle\tilde{e}\rangle^a - \langle\tilde{e}\rangle^b)] \tag{4.106}$$

where $\langle\tilde{s}\rangle^{a(b)}$ and $\langle\tilde{e}\rangle^{a(b)}$ are the specific entropy and energy of subsystem a(b) defined by Eqs.(4.30) and (4.31). Substituting Eqs. (4.102) and (4.103) yields

$$\begin{aligned} J_p^{b\to a} &= \frac{1}{2\tau} p^{eq}[C_V(\ln\frac{1}{\beta^a} - \ln\frac{1}{\beta^b}) - \beta(\frac{C_V}{\beta^a} - \frac{C_V}{\beta^b})] \\ &= \frac{C_V p^{eq}}{2\tau}[(\ln T^a - \ln T^b) - \frac{1}{T}(T_a - T_b)] \end{aligned} \tag{4.107}$$

where $T = 1/(k_b\beta)$ and the relation $T/T^{eq} = 1 + \xi^2 + O(\xi^4)$ holds when $p^a = p^b$. The mass (probability) flux due to a temperature difference is then written as

$$J_p^{b\to a} = \frac{dp^a}{dt}\frac{C_V p^{eq}}{\tau}[\frac{\Delta T}{T^{eq}} + \frac{\Delta T^3}{(T^{eq})^3} - \frac{\Delta T}{T}] = \frac{4}{3}\frac{C_V p^{eq}}{\tau}(\frac{\Delta T}{T^{eq}})^3 + O(\lambda^5) \tag{4.108}$$

and the temperature evolution, Eq. (4.38), reduces to

$$\frac{dT^a}{dt} = -\frac{1}{\tau}\Delta T \tag{4.109}$$

In the near-equilibrium region where only small temperature differences exist ($\xi \ll 1$), higher-order nonlinear temperature difference effects, which influence the probability (mass) flux, are negligible and can, thus, be ignored. For this case, the temperature evolution equation (Eq. (4.109)) and the probability (mass) evolution equation (Eq. (4.108)) due to a temperature difference are effectively decoupled. In far-from-equilibrium realm, however, higher-order temperature difference nonlinearities may be significant in which case coupling effects become important. In Fig. 4.2, the thermodynamic trajectories of three different cases for which the initial probabilities for the two subsystems are the same are plotted on a temperature-particle number diagram. For each case, the

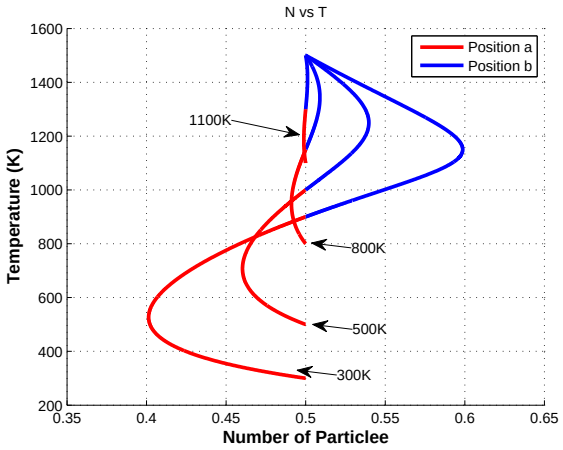

Figure 4.2. Thermodynamic trajectories on a temperature-particle number diagram with only temperature difference. The initial probabilities for the two subsystems are the same, while the initial temperature of subsystem b is 1500 K, while that for subsystem a is 300 K, 500 K, 800 K and 1100 K, respectively.

trajectory consists of two lines, one for each subsystem, with each point on each line representing an intermediate state for a given subsystem. The two subsystems start from opposite ends of the two colored lines and evolve towards the common end of the lines, which is the state of stable equilibrium for the system. As can be seen in the figure, when the temperature difference is small, the maximum of the concentration difference through the evolution approaches zero very quickly. Since the lowest order terms of Eqs. (4.108) and (4.109) have different signs, the nonlinear effects of temperature drive the probability (mass) flux towards the higher temperature subsystem. This phenomena can be explained from an entropy generation standpoint. The higher temperature subsystem has a higher specific entropy so that the probability (mass) flux towards it results in entropy generation for the system. On the other hand, the temperature evolution is explained by the fact that the heat diffusion towards the lower temperature subsystem increases the specific entropy in the lower temperature subsystem, which in turn results in entropy generation for the system.

When probability (mass) and temperature differences exist at the same time, it is the combined effect (i.e., the coupling) from the probability and the temperature, which determines the probability flow, since the lower order terms of Eqs. (4.91) and (4.108) have opposite signs. In Fig. 4.3, the trajectory for Case 1 shows a competition effect between the probability and temperature, while the trajectory of Case 3 shows a cooperation effect. Both of these can be explained via the effects discussed relative to Fig. 4.2. in addition, as a validation, Fig. 4.4 provides the entropy generation rate for the three cases along with the entropy trajectories. All exhibit monotonic increases in the

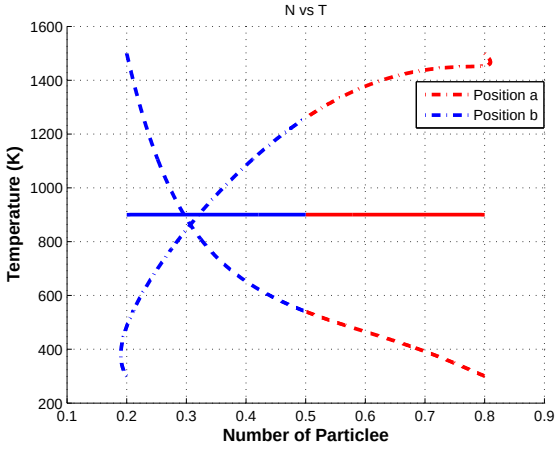

Figure 4.3. Thermodynamic trajectories on a temperature-particle number diagram with probability and temperature difference. Case 1: $p^a = 0.8$, $p^b = 0.2$,$T^a = 1500$ K, $T^b = 300$ K (dashed-dotted line); Case 2: $p^a = 0.8$, $p^b = 0.2$, $T^a = 900$ K, $T^b = 900$ K (solid line); and Case 3: $p^a = 0.2$, $p^b = 0.8$, $T^a = 1500$ K, $T^b = 300$ K (dashed line). The red lines are the trajectory of subsystem a, and the blue lines are the trajectory of subsystem b.

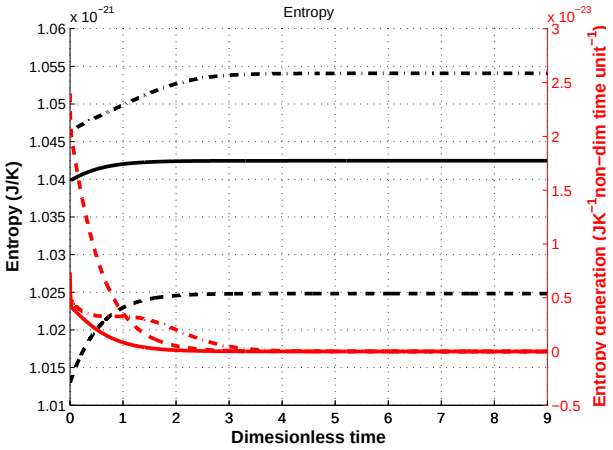

Figure 4.4. Entropy evolution and entropy generation in dimensionless time of the three cases of Fig. 4.3. Case 1: $p^a = 0.8$, $p^b = 0.2$,$T^a = 1500$ K, $T^b = 300$ K (dashed-dotted line); Case 2: $p^a = 0.8$, $p^b = 0.2$, $T^a = 900$ K, $T^b = 900$ K (solid line); and Case 3: $p^a = 0.2$, $p^b = 0.8$, $T^a = 1500$ K, $T^b = 300$ K (dashed line). The black lines are the entropy evolutions relative to the vertical axis on the left, and the red lines are the entropy generation rates relative to the vertical axis on the right.

entropy over time. Comparing to the diffusion case (Case 2) without temperature difference, the case for which the temperature effect is competitive (Case 1) results in a greater variation in the entropy generation rate, while the case for which the temperature effect is cooperative results in a much steeper drop in the entropy generation rate.

4.6 Conclusion

This paper investigates the relaxation process of local, isolated systems in non-equilibrium using the SEAQT framework. The mass and heat diffusion inside the system, which are the mass and energy redistribution among the system subspaces (or equivalent, energy eigenlevels), are described by defining conjugate forces and conjugate fluxes using the concepts of hypo-equilibrium state and non-equilibrium intensive properties. These thermodynamic features or patterns of the non-equilibrium relaxation process are used to generalize the Gibbs relation, the Clausius inequality, and the Onsager relations to the far-from-equilibrium realm and for quasi-non-equilibrium processes. The variational principle in the spaces spanned by conjugate forces and conjugate fluxes is derived from the variational principle in system state space (i.e., from the principle of steepest entropy ascent). As an application, the mass diffusion of a simple system consisting of hydrogen is studied. The study results in decoupled mass and energy transport equations and their associated phenomenological coefficients in the near-equilibrium realm. In far-from-equilibrium realm, the coupling phenomena and the nonlinear effects for mass and energy transport are derived.

From this investigation it is evident that the introduction of the concepts of hypo-equilibrium state and non-equilibrium intensive properties into the SEAQT framework provides a novel and fundamental vantage point from which to describe non-equilibrium states and their evolution during a relaxation process. In addition to the study presented here, additional work using the density of states method developed in [14], has permitted the wide application of the SEAQT framework to the study of non-equilibrium, systems in which complex, coupled reaction diffusion pathways are modeled and compared with experiment [9, 10]. chemical reaction, mass and heat diffusion. As a complement to the present paper, [17] continues our study of the quasi-non-equilibrium process of two interacting systems and completes the discussion of Onsager type of investigation of the relaxation process with both fluxes inside a non-equilibrium system and those across different systems. All of these studies show SEAQT to be a powerful approach applicable to the study of

non-equilibrium phenomena across all temporal and spatial scales.

Appendix B

B.1 Hypo-equilibrium for heat diffusion

In this appendix, it is proven that for a system with heat diffusion only, if the initial state is given by Eq. (4.23), the system evolution is also given by Eq. (4.24), and the non-equilibrium temperature is well-defined. The proof follows the same process as in [14] for a system with probability and energy conservations. To show this, Eq. (4.62) is reformulated such that

$$\frac{d}{dt}\ln\frac{p_j^a}{n_j^a} = \frac{1}{\tau}(-\ln\frac{p_j^a}{n_j^a} - \frac{B_2^a}{B_1} + \epsilon_j^a\frac{B_3}{B_1}) \tag{4.110}$$

where it is noted that $d(\ln n_j^a)/dt$ is zero and that B_1, B_2^a, and B_3 are the same for all chosen energy eigenlevels p_j^a from subspace a and only a function of the entire probability distribution at a given instant of time. Subtracting the equations of motion for the i^{th} and k^{th} energy eigenlevels results in

$$\frac{d}{dt}(\ln\frac{p_j^a}{n_j^a} - \ln\frac{p_k^a}{n_k^a}) = -\frac{1}{\tau}(\ln\frac{p_j^a}{n_j^a} - \ln\frac{p_k^a}{n_k^a}) + \frac{1}{\tau}\frac{B_3}{B_1}(\epsilon_j^a - \epsilon_k^a) \tag{4.111}$$

Defining a new variable

$$W_{jk} = \frac{1}{\epsilon_j^a - \epsilon_k^a}(\ln\frac{p_j^a}{n_j^a} - \ln\frac{p_k^a}{n_k^a}) \tag{4.112}$$

the time evolution of W_{jk} yields to the ordinary differential equation

$$\frac{dx}{dt} = -\frac{1}{\tau}x + \frac{1}{\tau}\frac{B_3}{B_1} \tag{4.113}$$

If p_j^a and p_k^a are in the same subsystem for which the initial probability distribution is a canonical one, i.e., if

$$p_j^a(t=0) = \alpha^a n_j^a e^{-\epsilon_j^a\beta^a}, \quad p_k^a(t=0) = \alpha^a n_k^a e^{-\epsilon_k^a\beta^a} \tag{4.114}$$

then

$$W_{jk}(t=0) = \frac{1}{\epsilon_j^a - \epsilon_k^a}(\ln\frac{p_j^a}{n_j^a} - \ln\frac{p_k^a}{n_k^a}) = -\beta^a \tag{4.115}$$

For $\forall p_j^a, p_k^a$ in the same subsystem a, the time evolution of W_{jk} yields to the same ordinary differential equation (ODE) with the same initial value, namely,

$$\frac{dx}{dt} = -\frac{1}{\tau}x + \frac{1}{\tau}\frac{B_3}{B_1},\ x = W_{jk}(t=0) = -\beta^a \tag{4.116}$$

so that the solution of W_{jk} is the same $W_{jk}(t) = \beta^a(t)$. Therefore, the probability distribution in this subsystem maintains the canonical distribution with the parameter $\beta^a(t)$ given by

$$p_j^a(t) = \alpha^a(t) n_j e^{-\epsilon_j^a \beta^a(t)} \tag{4.117}$$

In addition, the temperature of the subsystem at time t is defined by

$$T^a(t) = \frac{1}{k_b \beta^a(t)} \tag{4.118}$$

Thus, for a system in a non-equilibrium state, the hypo-equilibrium temperature for each subsystem is defined. This temperature can be the same or different from that of any other subsystem. If a system is in a M^{th}-order hypo-equilibrium state, it remains at least of order M throughout as well as after the evolution, and the probability distribution of each subsystem remains canonical.

B.2 Evolution of intensive properties

In this appendix, the evolutions of intensive properties are given for the system with probability and energy conservations. Eq. (4.26) is reformulated such that

$$\frac{d}{dt}\ln\frac{p_j^K}{n_j^K} = \frac{1}{\tau}(-\ln\frac{p_j^K}{n_j^K} - \frac{A_2}{A_1} + \epsilon_j^a\frac{A_3}{A_1}) \tag{4.119}$$

Using Eqs. (4.33) and (4.34) yields

$$\frac{d}{dt}(-\alpha^K(t) - \beta^K(t)\epsilon_i^K) = \frac{1}{\tau}(\alpha^K(t) + \beta^K(t)\epsilon_i^K - \alpha - \epsilon_j^K\beta) \tag{4.120}$$

Subtracting the equations of motion for the i^{th} and j^{th} energy eigenlevels results in

$$\frac{d}{dt}(-\beta^K(t)\epsilon_i^K + \beta^K(t)\epsilon_j^K) = \frac{1}{\tau}(\beta^K(t)\epsilon_i^K - \beta^K(t)\epsilon_j^K) - \frac{1}{\tau}\beta(\epsilon_i^K - \epsilon_j^K) \tag{4.121}$$

If $i \neq j$, dividing both sides by $(\epsilon_i^K - \epsilon_j^K)$ results in the evolution for β^K, namely,

$$\frac{d\beta^K}{dt} = -\frac{1}{\tau}(\beta^K - \beta) \tag{4.122}$$

Finally, subtracting Eq. (4.122) from (4.120) gives the evolution for α^K, i.e.,

$$\frac{d\alpha^K}{dt} = -\frac{1}{\tau}(\alpha^K - \alpha) \tag{4.123}$$

Chapter 5

Steepest-Entropy-Ascent Quantum Thermodynamic Modeling of the Far-from-equilibrium Interactions between Non-equilibrium Systems of Indistinguishable Particle Ensembles

5.1 Introduction

The study of non-equilibrium relaxation processes - including chemical kinetics, mass diffusion, and heat diffusion - is typically accomplished using approaches based on microscopic mechanics [1, 4, 6, 7] or thermodynamics [44, 96–99]. Approaches based on thermodynamics are able to generally capture the features of the relaxation process via, for example, the Onsager relations. The thermodynamic features captured can be regarded as a coarse graining of the microscopic dynamics or as a pattern in ensemble evolution [20, 21], which computationally is more efficient. However, most of these approaches have limited or no applicability in the far-from-equilibrium realm, since the local or near-equilibrium assumption is needed or only analytical solutions at steady state are available. In addition, their governing equations are phenomenological or stochastic in nature and, thus, do not have a first-principle basis. To address these issues and push the application of ther-

modynamic principles further into the non-equilibrium realm, it is of great importance to find a general and simple description of non-equilibrium state corresponding to a thermodynamic pattern of the microscopic description, to fundamentally define the macroscopic properties of any thermodynamic state (i.e., extensive or intensive properties for both equilibrium and non-equilibrium states), and to use a thermodynamic governing equation based on first principles.

Steepest-entropy-ascent quantum thermodynamics (SEAQT), which is a first-principle, thermodynamic-ensemble based approach, addresses all of the issues raised above, providing a governing equation able to describe the non-equilibrium process from an entropy generation viewpoint. The macroscopic properties of entropy, energy, and particle number, which are well defined for any state of any system [33], are used to develop the governing equation and describe system state evolution. Recently, this description has been further simplified via the concept of hypo-equilibrium state [14, 16], which captures the global features of the microscopic description for the relaxation process. In addition, the concept of non-equilibrium intensive properties introduced in [14, 16] based on the concept of hypo-equilibrium state enables a complete description of the non-equilibrium evolution of state when combined with the set of non-equilibrium extensive properties. Unlike the intensive property definitions of other non-equilibrium thermodynamic approaches (definitions which require the local-equilibrium, near-equilibrium, or steady state assumption or a phenomenological basis), the definitions in the SEAQT framework are fundamental and available to all non-equilibrium states and are especially suitable for the description of the evolution in state of relaxation processes. Both of these concepts enable the generalization of many equilibrium (or near-equilibrium) thermodynamic relations such as the Gibbs relation, the Clausius inequality, and the Onsager relations into the far-from-equilibrium realm as well as for non-quasi-equilibrium processes.

In this paper, SEAQT is applied to the study of the interaction of systems using the grand partition function. The system studied can be any distinguishable or indistinguishable system with or without long distance intermolecular interaction. The evolution of two systems can be a non-quasi-equilibrium process. In *Section* 5.2, the equation of motion and the concepts of hypo-equilibrium state and non-equilibrium intensive properties are introduced. In *Section* 5.3, interacting systems with heat diffusion only are studied. The Onsager relations and a thermodynamic explanation of measurement (of a system in equilibrium or non-equilibrium) and reservoir is given. In *Section* 5.4, interacting systems with heat and mass diffusion are studied followed in *Section* 5.5 by the

study of a system interacting with multiple systems and a discussion of the applicability of the SEAQT framework to the network of non-equilibrium systems.

5.2 SEAQT equation of motion

5.2.1 General equation of motion

In this section, the system and state description in SEAQT is given, and the equation of motion, is presented. Based on the discussion by Grmela [20, 21, 35] and Beretta [24, 34] the general form of a non-equilibrium framework is a combination of both irreversible relaxation and reversible symplectic dynamics. If written in a generalized form of Ginzburg-Landau equation [20, 34], the equation of motion takes the following form:

$$\frac{d}{dt}\phi(t) = X^H_{\phi(t)} + Y^H_{\phi(t)} \tag{5.1}$$

where $\phi(t)$ represents the state evolution trajectory, $X^H_{\phi(t)}$ and $Y^H_{\phi(t)}$ are functions of the system state $\phi(t)$ and represent the reversible symplectic and irreversible relaxation dynamics, respectively. In the SEAQT framework, the system is defined by the Hamiltonian operator $\hat{H}$, the system state is represented by the density operator $\hat{\rho}$, $X^H_{\phi(t)}$ follows the Schrödinger equation, and $Y^H_{\phi(t)}$ is derived from the SEA principle. To describe the evolutionary process, conservation laws are explicitly required in order to construct the equation of motion, which is given by [42]

$$\frac{d\hat{\rho}}{dt} = \frac{1}{i\hbar}[\hat{\rho}, \hat{H}] + \frac{1}{\tau}\hat{D} \tag{5.2}$$

where the first term is the Schrödinger term, and the second is the dissipation term. If the system is in pure (zero-entropy) state, $\hat{\rho}\hat{\rho} = \hat{\rho}$, and, the equation of motion reverts back to the Schrödinger equation of quantum mechanics. If the system is in a so-called mixed (nonzero-entropy) state and $\hat{\rho}$ is diagonal in the energy eigenstate basis, $\hat{H}$ commutes with $\hat{\rho}$ and the Schrödinger term goes to zero even though $\hat{\rho}$ may not be a Maxwellian distribution among the energy eigenlevels. The state evolution of such a mixed-state operator cannot be captured by the Schrödinger term and is instead given by the second term to the right of the equals, the dissipation term, which captures the probability redistribution towards the Maxwellian distribution. The dissipation term is constructed

using a set of operators called the 'generators of the motion'. Each generator corresponds to one of the conservation laws to which the system is subjected. For example, an non-reacting isolated system is subject to two conservation laws, probability normalization and energy conservation, so that the generators of the motion are $\{\hat{I}, \hat{H}\}$.

In the study of two interacting systems, the system state space is given by

$$\mathcal{H} = \mathcal{H}_a \otimes \mathcal{H}_b \tag{5.3}$$

where $\mathcal{H}_{a(b)}$ are the Hilbert space of two systems $a(b)$ (for a general system with a variable number of indistinguishable particle, $\mathcal{H}_{a(b)}$ will be Fock space) and the initial state of density operator is chosen to be

$$\hat{\rho} = \hat{\rho}_a \otimes \hat{\rho}_b \tag{5.4}$$

Note that it does not include a correlation term. The Hamiltonian operator of the system is then

$$\hat{H} = \hat{H}_a \otimes \hat{I}_b + \hat{I}_a \otimes \hat{H}_b \tag{5.5}$$

where no inter-particle interaction term has been included. If we assume both system a and system b to consist of a dilute-Boltzmann gas that give the diagonal density operators $\hat{\rho}_a$ and $\hat{\rho}_b$, the equation of motion reduces to

$$\frac{dp_i^{a(b)}}{dt} = \frac{1}{\tau} D_i^{a(b)}(\mathbf{p}) \tag{5.6}$$

where $p_i^a(b)$ is the i^{th} diagonal term of $\hat{\rho}^{a(b)}$ in the energy eigenstates basis and represents the probability of the system $a(b)$ being in the eigenstate associated with the i^{th} energy eigenlevel, $\mathbf{p}$ represents the distributions $\{p_i^a,\, i = 1, \cdots\}$ and $\{p_j^b\, j = 1, \cdots\}$ for system a and b, and τ is the relaxation time.

5.2.2 Non-equilibrium state and state evolution description: Hypo-equilibrium

The thermodynamic features of the non-equilibrium relaxation process generated by the SEAQT framework have a number of useful characteristics, which lead to a complete description of non-equilibrium state and the general fundamental definition of non-equilibrium intensive properties. This description is based on two key concepts, which are briefly discussed below.

For a given system, such as system a, represented by an energy eigenlevel set $\Omega^a = \{(n_i^a, \epsilon_i^a, N_i^a)\}$, where each energy eigenlevel is represented by a triplet of energy (ϵ_i^a) and particle number (N_i^a) eigenvalues and by its degeneracy (n_i^a), the system can be divided into M_a subsystems $\Omega_K^a = \{(n_i^{a,K}, \epsilon_i^{a,K}, N_i^{a,K})\}, K = 1, \cdots, M_a$, so that the state space of system a (Hilbert space) $\mathcal{H}^a$ can be represented by the sum of M_a subspaces $\mathcal{H}_K^a$ with $K = 1, 2, ..., M_a$.

$$\mathcal{H}^a = \bigoplus_{K=1}^{M_a} \mathcal{H}_K^a \tag{5.7}$$

To be complete, M_a can be infinite. The state of system a can be represented by the distributions in M_a subspace energy eigenlevels $\{p_i^{a,K}, K = 1, ..., M_a\}$.

If the probability distribution in each subsystem yields to a grand canonical distribution, the system is designated as being in an M_a^{th}-order hypo-equilibrium state. Based on this definition, it can be shown that any state of the system a is a hypo-equilibrium state with order M_a, where M_a is less than or equal to the number of system eigenlevels [14, 16]. A hypo-equilibrium state of order 1 corresponds to a state in stable equilibrium. The probability distribution of the K^{th} subspace of the M_a^{th}-order hypo-equilibrium state takes the form

$$p_i^{a,K} = \frac{p^{a,K}}{\Xi^{a,K}(\beta^{a,K}, \gamma^{a,K})} e^{-\beta^{a,K}\epsilon_i^{a,K} - \gamma^{a,K} N_i^{a,K}} \tag{5.8}$$

where $\beta^{a,K}$ and $\gamma^{a,K}$ are parameters, $p^{a,K}$ is the total probability in subspace K of system a, and $\Xi^{a,K}(\beta^{a,K}, \gamma^{a,K})$ is the grand partition function of the subspace with parameters $\beta^{a,K}$ and $\gamma^{a,K}$. To be complete, $\beta^{a,K} = 0$ and $\gamma^{a,K} = 0$ if $\#(\mathcal{H}_a^K) = 1$, $\gamma^{a,K} = 0$ if $\#(\mathcal{H}_a^K) = 2$ and the $\#(\mathcal{H}_a^K)$ can be infinite. The grand partition function is written as

$$\Xi^{a,K}(\beta^{a,K}, \gamma^{a,K}) = \sum_{K=1}^{\#(\mathcal{H}_a^K)} n_i^{a,K} e^{-\beta^{a,K}\epsilon_i^{a,K} - \gamma^{a,K} N_i^{a,K}} \tag{5.9}$$

Then, defining

$$\alpha^{a,K} = \ln \Xi^{a,K}(\beta^{a,K}, \gamma^{a,K}) - \ln p^{a,K} \tag{5.10}$$

so that the probability distribution of the K^{th} subspace can be represented using $\{(\alpha^{a,K}, \beta^{a,K}, \gamma^{a,K}), K = 1, \cdots, M_a\}$, i.e.,

$$p_i^{a,K} = n_i^{a,K} e^{-\alpha^{a,K}} e^{-\epsilon_i^{a,K}\beta^{a,K}} e^{-N_i^{a,K}\gamma^{a,K}} \tag{5.11}$$

For a given M_a^{th}-order hypo-equilibrium state, the intensive properties of the subspaces can be represented by $\beta^{a,K}$ and $\gamma^{a,K}$ or equivalently using temperature and chemical potential defined by

$$T^{a,K} = \frac{1}{k_b \beta^{a,K}}, \quad \mu^{a,K} = \gamma^{a,K} T^{a,K} \tag{5.12}$$

A M_a^{th}-order hypo-equilibrium state can then be represented by a division $\{\Omega_K = (n_i^{a,K}, \epsilon_i^{a,K}, N_i^{a,K}) , \ K = 1, ..., M_a\}$ of the system and a corresponding triplet set $\{(\alpha^{a,K}, \beta^{a,K}, \gamma^{a,K}), \ k = 1, ..., M_a\}$. The intensive property set $\{(T^{a,K}, \mu^{a,K}), \ K = 1, ..., M_a\}$ is a generalization of the definition of intensive property at stable equilibrium (T^{eq}, μ^{eq}), which itself is a 1^{st}-order hypo-equilibrium state. *Appendix* C.1 proves that for the equation of motions used in this paper, if a system begins in a M_a^{th}-order hypo-equilibrium state, it remains in a M_a^{th}-order hypo-equilibrium state throughout the state evolution as long as the same subsystem division is maintained. Thus, the time evolution of the distribution is given by

$$p_i^{a,K}(t) = n_i^{a,K} e^{-\alpha^{a,K}(t) - \beta^{a,K}(t)\epsilon_i^{a,K} - \gamma^{a,K}(t) N_i^{a,K}} \tag{5.13}$$

The intensive property set $\{(T^{a,K}(t), \mu^{a,K}(t)), \ i = 1, ..., M\}$ is well defined throughout the entire state evolution. This system state evolution can also be represented by the evolution of the triplet set $\{(\alpha^{a,K}(t), \beta^{a,K}(t), \gamma^{a,K}(t)), \ K = 1, ..., M\}$. In the discussions below, the triplet $(\alpha^{a,K}, \beta^{a,K}, \gamma^{a,K})$ are also called intensive properties, since they are equivalent to temperature and chemical potential.

5.3 Interacting systems with heat diffusion only

In this section, system a and system b form a composite system, and only heat diffusion is allowed between them. Both system a and system b can be in non-equilibrium states, and are represented by the probability distribution among the energy eigenlevels of system a and b, i.e., by $\{p_i^a\}$ and $\{p_i^b\}$.

5.3.1 Equation of motion

For the case when only heat diffusion is present, five conservation laws hold: probability and particle number conservation for both system a and system b, and total energy conservation of the composite system. Thus, the generators of motion are $\{\hat{I}_a, \hat{I}_b, \hat{N}_a, \hat{N}_b, \hat{H}\}$ constrained by

$$I^a = \sum_i p_i^a = 1 \tag{5.14}$$

$$I^b = \sum_i p_i^b = 1 \tag{5.15}$$

$$N^a = \sum_i N_i^a p_i^a = \text{constant} \tag{5.16}$$

$$N^b = \sum_i N_i^b p_i^b = \text{constant} \tag{5.17}$$

$$E = \sum_i \epsilon_i^a p_i^a + \sum_i \epsilon_i^b p_i^b = \text{constant} \tag{5.18}$$

Based on the derivation in *Appendix* C.2, the equation of motion for system a takes the form

$$\frac{dp_j^a}{dt} = \frac{1}{\tau} \frac{\begin{vmatrix} -p_j^a \ln \frac{p_j^a}{n_j^a} & p_j^a & N_j^a p_j^a & 0 & 0 & \epsilon_j^a p_j^a \\ \langle s \rangle^a & 1 & \langle N \rangle^a & 0 & 0 & \langle e \rangle^a \\ \langle Ns \rangle^a & \langle N \rangle^a & \langle N^2 \rangle^a & 0 & 0 & \langle eN \rangle^a \\ \langle s \rangle^b & 0 & 0 & 1 & \langle N \rangle^b & \langle e \rangle^b \\ \langle Ns \rangle^b & 0 & 0 & \langle N \rangle^b & \langle N^2 \rangle^b & \langle eN \rangle^b \\ \langle es \rangle & \langle e \rangle^a & \langle eN \rangle^a & \langle e \rangle^b & \langle eN \rangle^b & \langle e^2 \rangle \end{vmatrix}}{\begin{vmatrix} 1 & \langle N \rangle^a & 0 & 0 & \langle e \rangle^a \\ \langle N \rangle^a & \langle N^2 \rangle^a & 0 & 0 & \langle eN \rangle^a \\ 0 & 0 & 1 & \langle N \rangle^b & \langle e \rangle^b \\ 0 & 0 & \langle N \rangle^b & \langle N^2 \rangle^b & \langle eN \rangle^b \\ \langle e \rangle^a & \langle eN \rangle^a & \langle e \rangle^b & \langle eN \rangle^b & \langle e^2 \rangle \end{vmatrix}} \tag{5.19}$$

The numerator of the ratio of determinants on the right can be expanded to yield

$$\det = -p_j \ln \frac{p_j^a}{n_j^a} C_1 - p_j^a C_2^a + N_j^a p_j^a C_3^a - \epsilon_j^a p_j^a C_4 \tag{5.20}$$

where $|C_1|$, $|C_2^a|$, $|C_3^a|$, and $|C_4|$ are the cofactors of the first line of the determinant. By defining

$$\frac{C_2^a}{C_1} = \alpha_a^0, \quad \frac{C_3^a}{C_1} = -\gamma_a^0, \quad \frac{C_4}{C_1} = \beta^0, \tag{5.21}$$

the equation of motion transforms to

$$\frac{dp_j^a}{dt} = \frac{1}{\tau}(-p_j^a \ln \frac{p_j^a}{n_j^a} - p_j^a \alpha_a^0 - N_j^a p_j^a \gamma_a^0 - \epsilon_j^a p_j^a \beta^0) \tag{5.22}$$

Now, defining a row vector of extensive properties

$$\vec{l}_j^a = \begin{bmatrix} 1 & N_j^a & \epsilon_j^a \end{bmatrix} \tag{5.23}$$

where the subscript j refers to the j^{th} energy eigenlevel and defining a column vector of intensive properties

$$\vec{\mu}_a^0 = \begin{bmatrix} \alpha_a^0 \\ \gamma_a^0 \\ \beta^0 \end{bmatrix} \tag{5.24}$$

the equation of motion can be written as

$$\frac{dp_j^a}{dt} = \frac{1}{\tau}(-p_j^a \ln \frac{p_j^a}{n_j^a} - p_j^a \vec{l}_j^a \cdot \vec{\mu}_a^0) \tag{5.25}$$

In stable equilibrium, each element of $\vec{\mu}_a^0$ turns out to be an intensive property of the composite system.

5.3.2 Hypo-equilibrium state and non-equilibrium intensive properties

We assume that the initial state of system a is a M_a^{th}-order hypo-equilibrium state, and that the probability for the i^{th} energy eigenlevel represented by the triplet $(n_i^{a,K}, \epsilon_i^{a,K}, N_i^{a,K})$, where $i = 1, 2, \cdots$, $K = 1, 2, \cdots M_a$, is given by

$$p_i^{a,K} = n_i^{a,K} e^{-\alpha^{a,K}} e^{-\epsilon_i^{a,K} \beta^{a,K}} e^{-N_i^{a,K} \gamma^{a,K}} \tag{5.26}$$

where the triplet $\{(\alpha^{a,K}, \beta^{a,K}, \gamma^{a,K}),\ K = 1, \cdots, M_a\}$ has been used in the representation. This can be rewritten in terms of row vector of extensive properties and column vector of intensive properties such that

$$\ln \frac{p_i^{a,K}}{n_i^{a,K}} = -\alpha^{a,K} - \epsilon_i^{a,K}\beta^{a,K} - N_i^{a,K}\gamma^{a,K} = -\vec{l}_j^{a,K} \cdot \vec{\mu}^{a,K} \tag{5.27}$$

where the superscripts refer to system a and the K^{th} subspace of system a, and the subscript to the i^{th} energy eigenlevel in the K^{th} subspace. The row and column vectors are defined as

$$\vec{l}_i^{a,K} = \begin{bmatrix} 1 & N_i^{a,K} & \epsilon_i^{a,K} \end{bmatrix} \tag{5.28}$$

$$\vec{\mu}^{a,K} = \begin{bmatrix} \alpha^{a,K} \\ \beta^{a,K} \\ \gamma^{a,K} \end{bmatrix} \tag{5.29}$$

In *Appendix* C.1, it is proven that if the initial state is an hypo-equilibrium state, the system remains in an hypo-equilibrium state with the same subsystem division, which means that the time evolution of the distribution of system a takes the form

$$p_i^{a,K}(t) = n_i^{a,K} e^{-\alpha^{a,K}(t)} e^{-\epsilon_i^{a,K}\beta^{a,K}(t)} e^{-N_i^{a,K}\gamma^{a,K}(t)} = n_i^{a,K} e^{-\vec{l}_i^{a,K}\cdot\vec{\mu}^{a,K}(t)} \tag{5.30}$$

where the evolution of the intensive properties $\alpha^{a,K}(t),\ \beta^{a,K}(t),\ \gamma^{a,K}(t)$ are the solutions to (see *Appendix* C.1)

$$\frac{d\vec{\mu}^{a,K}(t)}{dt} = -\frac{1}{\tau}(\vec{\mu}^{a,K}(t) - \vec{\mu}_a^0(t)) \tag{5.31}$$

and the equation of motion Eq.(25), is expressed as

$$\frac{dp_i^{a,K}}{dt} = \frac{1}{\tau} p_i^{a,K} \vec{l}_i^{a,K} \cdot (\vec{\mu}^{a,K} - \vec{\mu}_a^0) \tag{5.32}$$

Thus, if the initial state of system a is a M_a^{th}-order hypo-equilibrium and that of system b is a M_b^{th}-order hypo-equilibrium, only $3(M_a + M_b)$ ODEs need to be solved in order to determine the non-equilibrium evolution.

5.3.3 Time evolution of subsystem extensive property and Onsager relations

Based on the row vector for extensive properties of one energy eigenlevel, the vector of system a properties can be defined as a row vector as well such that

$$\vec{L}^{a,K} = \sum_i p_i^{a,K} \vec{l}_i^{a,K} = \left[\begin{array}{ccc} p^{a,K} & E^{a,K} & N^{a,K} \end{array} \right] \tag{5.33}$$

where $p^{a,K}$, $E^{a,K}$, and $N^{a,K}$ are the contributions of the K^{th} subspace to the total extensive properties of system a and are defined by

$$p^{a,K} = \sum p_i^{a,K} \tag{5.34}$$

$$E^{a,K} = \langle e \rangle^{a,K} = \sum \epsilon_i^{a,K} p_i^{a,K} \tag{5.35}$$

$$N^{a,K} = \langle N \rangle^{a,K} = \sum N_i^{a,K} p_i^{a,K} \tag{5.36}$$

The evolutions of these extensive properties and others are governed by

$$\frac{d\vec{L}^{a,K}(t)}{dt} = -\frac{1}{\tau}(\vec{\mu}^{a,K}(t) - \vec{\mu}_a^0(t))^T [C_1]^{a,K} \tag{5.37}$$

where

$$[C_1]^{a,K} = \left[\begin{array}{ccc} p^{a,K} & \langle e \rangle^{a,K} & \langle N \rangle^{a,K} \\ \langle e \rangle^{a,K} & \langle e^2 \rangle^{a,K} & \langle eN \rangle^{a,K} \\ \langle N \rangle^{a,K} & \langle eN \rangle^{a,K} & \langle N^2 \rangle^{a,K} \end{array} \right] \tag{5.38}$$

Here $\langle \cdot \rangle^{a,K}$ is the contribution of the K^{th} subspace to the total extensive property $\langle \cdot \rangle^a$ of system a.

The rate of entropy change of the K^{th} subsystem is then

$$\begin{aligned} \frac{dS^{a,K}}{dt} &= \frac{d\langle s \rangle^{a,K}}{dt} = \sum_i \frac{d}{dt}(-p_i^{a,K} \ln \frac{p_i^{a,K}}{n_i^{a,K}}) = \sum_j (-\ln \frac{p_i^{a,K}}{n_i^{a,K}} - 1)\frac{dp_i^{a,K}}{dt} \\ &= \sum_j (\vec{l}_i^{a,K} \cdot \vec{\mu}^{a,K} - 1)\frac{dp_i^{a,K}}{dt} = \frac{d\vec{L}^{a,K}}{dt} \cdot \vec{\mu}^{a,K} - \frac{dp^{a,K}}{dt} \end{aligned} \tag{5.39}$$

and for system a

$$\frac{dS^a}{dt} = \sum_K \frac{dS^{a,K}}{dt} = \sum_K \frac{d\vec{L}^{a,K}}{dt} \cdot \vec{\mu^{a,K}} \tag{5.40}$$

where probability conservation for system a has been used. The rate of system entropy is then for the composite system is

$$\frac{dS}{dt} = \sum_a \frac{dS^a}{dt} = \sum_a \sum_K \frac{d\vec{L}^{a,K}}{dt} \cdot \vec{\mu^{a,K}} = \sum_a \sum_K \frac{d\vec{L}^{a,K}}{dt} \cdot (\vec{\mu}^{a,K} - \vec{\mu}_a^0) \tag{5.41}$$

where in the last equal sign, the conservation laws has been applied. Defining conjugate fluxes and conjugate forces, respectively, as

$$\vec{J}^{a,K} = \frac{d\vec{L}^{a,K}}{dt},\ \vec{X}^{a,K} = \vec{\mu}^{a,K} - \vec{\mu}_a^0 \tag{5.42}$$

the evolutions of the extensive properties can be written from Eqs. (5.37) and (5.40) as

$$\vec{J}^{a,K} = \vec{X}^{a,K} \cdot [C_1]^{a,K} \tag{5.43}$$

$$\frac{dS}{dt} = \sum_a \sum_K \vec{J}^{a,K} \vec{X}^{a,K} \tag{5.44}$$

Since $[C_1]^{a,K}$ is positive definite and symmetric, the Onsager relations are acquired. Specifically, due to the conservation laws, probability and particle number fluxes occur within a given system a or b, while the energy fluxes can cross from one system to the next. Thus, the Onsager relations hold here for the relaxation process of system a and for the non-quasi-equilibrium process between systems a and b.

5.3.4 Linkage between two systems: Measurement and reservior

The conservation of probability and particle number for system a leads to

$$\frac{dp^a}{dt} = \sum_K \frac{dp^{a,K}}{dt} = 0 \tag{5.45}$$

$$\frac{d\langle N\rangle^a}{dt} = \sum_K \frac{d\langle N\rangle^{a,K}}{dt} = 0 \tag{5.46}$$

which can be written as

$$\sum_K (\alpha^{a,K} - \alpha_a^0) p^{a,K} + \sum_K \langle e \rangle^{a,K} (\beta^{a,K} - \beta^0) + \sum_K \langle N \rangle^{a,K} (\gamma^{a,K} - \gamma_a^0) = 0 \tag{5.47}$$

$$\sum_K (\alpha^{a,K} - \alpha_a^0) \langle N \rangle^{a,K} + \sum_K \langle eN \rangle^{a,K} (\beta^{a,K} - \beta^0) + \sum_K \langle N^2 \rangle^{a,K} (\gamma^{a,K} - \gamma_a^0) = 0 \tag{5.48}$$

α_a^0 and γ_a^0 can then be determined from Eqs. (5.47) and (5.48), i.e.,

$$\alpha_a^0 = \sum_K \alpha^{a,K} p^{a,K} + \sum_K \langle e \rangle^{a,K} \beta^{a,K} + \sum_K \langle N \rangle^{a,K} \gamma^{a,K} - \beta^0 \langle e \rangle^a - \gamma_a^0 \langle N \rangle^a \tag{5.49}$$

$$A_{NN}^a \gamma_a^0 = \sum_K \alpha^{a,K} \langle N \rangle^{a,K} + \sum_K \langle eN \rangle^{a,K} \beta^{a,K} + \sum_K \langle N^2 \rangle^{a,K} \gamma^{a,K} - A_{eN}^a \beta^0 \tag{5.50}$$

where $A_{NN}^a = \langle N^2 \rangle^a - \langle N \rangle^a \langle N \rangle^a$ and $A_{eN}^a = \langle eN \rangle^a - \langle e \rangle^a \langle N \rangle^a$ Thus, γ_a^0 and α_a^0 are only a function of β^0 and system a properties. Furthermore, the evolutions of subsystem properties can be calculated by

$$\frac{d\alpha^{a,K}}{dt} = -\frac{1}{\tau}(\alpha^{a,K} - \alpha_a^0) \tag{5.51}$$

$$\frac{d\gamma^{a,K}}{dt} = -\frac{1}{\tau}(\gamma^{a,K} - \gamma_a^0) \tag{5.52}$$

$$\frac{d\beta^{a,K}}{dt} = -\frac{1}{\tau}(\beta^{a,K} - \beta^0) \tag{5.53}$$

Thus, the time evolution of $\alpha^{a,K}$, $\gamma^{a,K}$ and $\beta^{a,K}$ can be determined using properties of system a and β^0 only. The influence of system b is only via β^0 so that if a different system b can provide the same β, the time evolution of system a is the same.

To study the linkage between systems a and b, the explicit form of $\beta^0 = |C_4|/|C_1|$ is given

using fluctuations of the extensive properties of energy and particle number, i.e.,

$$|C_1| = \begin{vmatrix} A^a_{NN} & 0 & A^a_{Ne} \\ 0 & A^b_{NN} & A^b_{Ne} \\ A^a_{Ne} & A^b_{Ne} & A_{ee} \end{vmatrix} \tag{5.54}$$

$$|C_4| = \begin{vmatrix} A^a_{Ns} & A^a_{NN} & 0 \\ A^b_{Ns} & 0 & A^b_{NN} \\ A_{es} & A^a_{Ne} & A^b_{Ne} \end{vmatrix} \tag{5.55}$$

where

$$A^{a(b)}_{UV} = \langle UV \rangle^{a(b)} - \langle U \rangle^{a(b)} \langle V \rangle^{a(b)},\ A_{UV} = A^a_{UV} + A^b_{UV} \tag{5.56}$$

and $A^{a(b)}_{UV}$ is the fluctuation of extensive properties U and V in system $a(b)$, while A_{UV} is the sum of the fluctuations of systems a and b.

Now, if system b is much smaller than system a, i.e., if $A^a_{UV} \gg A^b_{UV}$ for any set of extensive properties, $\beta^0 \to \tilde{\beta}^a$ where

$$\tilde{\beta}^a \equiv \lim_{\frac{A^b_{UV}}{A^a_{UV}} \to 0} |C_4| \,/\, |C_1| = \begin{vmatrix} A^a_{es} & A^a_{Ne} \\ A^a_{Ns} & A^a_{NN} \end{vmatrix} \Big/ \begin{vmatrix} A^a_{ee} & A^a_{eN} \\ A^a_{eN} & A^a_{NN} \end{vmatrix} \tag{5.57}$$

The stable equilibrium temperature of system b is $\tilde{\beta}^a$ if the state of system a remains in a non-equilibrium state (for example, if system a relaxes much slower than system b or is controlled by some external interaction). Thus, $\tilde{\beta}^a$ is a temperature measurement of system a, which can be used as an expression for the experimental measurement of system a in non-equilibrium. In addition, $\tilde{\beta}^a$ also turns out to be the β^0 in the equation of motion for a single system relaxation, i.e., when system b is not present.

Now, if the system b is in stable equilibrium and much larger than system a, i.e., $A^a_{UV} \ll A^b_{UV}$ for any set of extensive properties, $\beta^0 \to \tilde{\beta}^b = 1/k_b T_b$, and T_b is the temperature of system b. In this case, system b acts as a heat reservoir at temperature T_b.

5.4 Equation of motion for interacting systems with heat and mass diffusion

For the case when both heat and mass diffusion are present, four conservation laws hold: probability conservation for both system a and system b, and total energy and total particle number conservation for the composite system. Thus, the generators of motion are $\{\hat{I}_a, \hat{I}_b, \hat{N}, \hat{H}\}$ constrained by

$$I^a = \sum_i p_i^a = 1 \tag{5.58}$$

$$I^b = \sum_i p_i^b = 1 \tag{5.59}$$

$$N = \sum_i N_i^a p_i^a + \sum_i N_i^b p_i^b = \text{constant} \tag{5.60}$$

$$E = \sum_i \epsilon_i^a p_i^a + \sum_i \epsilon_i^b p_i^b = \text{constant} \tag{5.61}$$

Similar to the derivation in *Appendix* C.2, the equation of motion for the case is

$$\frac{dp_j^a}{dt} = \frac{1}{\tau} \frac{\begin{vmatrix} -p_j^a \ln \frac{p_j^a}{n_j^a} & p_j^a & 0 & \epsilon_j^a p_j^a & N_j^a p_j^a \\ \langle s \rangle^a & 1 & 0 & \langle e \rangle^a & \langle N \rangle^a \\ \langle s \rangle^b & 0 & 1 & \langle e \rangle^b & \langle N \rangle^b \\ \langle es \rangle & \langle e \rangle^a & \langle e \rangle^b & \langle e^2 \rangle & \langle eN \rangle \\ \langle Ns \rangle & \langle N \rangle^a & \langle N \rangle^b & \langle eN \rangle & \langle N^2 \rangle \end{vmatrix}}{\begin{vmatrix} 1 & 0 & \langle e \rangle^a & \langle N \rangle^a \\ 0 & 1 & \langle e \rangle^b & \langle N \rangle^b \\ \langle e \rangle^a & \langle e \rangle^b & \langle e^2 \rangle & \langle eN \rangle \\ \langle N \rangle^a & \langle N \rangle^b & \langle eN \rangle & \langle N^2 \rangle \end{vmatrix}} \tag{5.62}$$

The numerator of a ratio of determinants on the right can be expanded to yield

$$\det = -p_j^a \ln \frac{p_j^a}{n_j} C_1 - p_j^a C_2^a - \epsilon_j^a p_j^a C_3 + N_j^a p_j^a C_4 \tag{5.63}$$

where $|C_1|$, $|C_2^a|$, $|C_3|$, and $|C_4|$ are the cofactors of the first line of the determinant. By defining

$$\frac{C_2^a}{C_1} = \alpha_a, \quad \frac{C_3}{C_1} = \beta, \quad \frac{C_4}{C_1} = -\gamma \tag{5.64}$$

the equation of motion transforms into

$$\frac{dp_j^a}{dt} = \frac{1}{\tau}(-p_j^a \ln \frac{p_j^a}{n_j} - p_j^a \alpha_a - \epsilon_j^a p_j^a \beta - N_j^a p_j^a \gamma) \tag{5.65}$$

Using the row vector $\vec{l}_j^a$ of Eq. (5.24) and defining a new column vector $\vec{\mu}_a^0$ of intensive properties, the equation of motion changes to

$$\frac{dp_j^a}{dt} = \frac{1}{\tau}(-p_j^a \ln \frac{p_j^a}{n_j} - p_j^a \vec{l}_j^a \cdot \vec{\mu}_a^0) \tag{5.66}$$

where the column vector is defined as

$$\vec{\mu}_a^0 = \begin{bmatrix} \alpha_a \\ \beta^0 \\ \gamma^0 \end{bmatrix} \tag{5.67}$$

Thus, the discussion using the concept of hypo-equilibrium state given in *Sections* 5.3.2 and 5.3.3 can be repeated here with the only difference being the definition of $\vec{\mu}_a^0$. Furthermore, the discussion in *Section* 5.3.4 is simplified here since only probability conservation holds for system a with the consequence that

$$\frac{dp^a}{dt} = \sum_K \frac{dp^{a,K}}{dt} = 0 \tag{5.68}$$

from which, α_a can be calculated, i.e.,

$$\alpha_a = \sum_K \alpha^{a,K} p^{a,K} + \sum_K \langle e \rangle^{a,K} \beta^{a,K} + \sum_K \langle N \rangle^{a,K} \gamma^{a,K} - \beta^0 \langle e \rangle^a - \gamma^0 \langle N \rangle^a \tag{5.69}$$

Here, α_a is a function of β^0, γ^0, and system a properties. Furthermore, the evolutions of subsystem (i.e., subspace) properties can be determined from

$$\frac{d\alpha^{a,K}}{dt} = -\frac{1}{\tau}(\alpha^{a,K} - \alpha_a) \tag{5.70}$$

$$\frac{d\gamma^{a,K}}{dt} = -\frac{1}{\tau}(\gamma^{a,K} - \gamma^0) \tag{5.71}$$

$$\frac{d\beta^{a,K}}{dt} = -\frac{1}{\tau}(\beta^{a,K} - \beta^0) \tag{5.72}$$

For this case, the time evolution of $\alpha^{a,K}$, $\gamma^{a,K}$ and $\beta^{a,K}$ are determined using properties of system a and β^0 and γ^0 only. The influence of system b is via β^0 and γ^0, which relates to the energy and particle number fluxes between the two systems.

To study the linkage between systems a and b, the explicit form of $\beta^0 = |C_3|/|C_1|$ is given using fluctuations of the extensive properties, i.e.,

$$|C_1| = \begin{vmatrix} A_{ee} & A_{eN} \\ A_{Ne} & A_{NN} \end{vmatrix}, |C_3| = \begin{vmatrix} A_{es} & A_{eN} \\ A_{Ns} & A_{NN} \end{vmatrix}, |C_4| = \begin{vmatrix} A_{es} & A_{ee} \\ A_{Ns} & A_{eN} \end{vmatrix} \tag{5.73}$$

The measurements of the intensive properties $\tilde{\beta}^a$ and $\tilde{\gamma}^a$ of system a are given as

$$\tilde{\beta}^a \equiv \lim_{\frac{A^b_{UV}}{A^a_{UV}} \to 0} |C_3| \,/\, |C_1| = \begin{vmatrix} A_{es} & A_{eN} \\ A_{Ns} & A_{NN} \end{vmatrix} / \begin{vmatrix} A^a_{ee} & A^a_{eN} \\ A^a_{eN} & A^a_{NN} \end{vmatrix} \tag{5.74}$$

$$\tilde{\gamma}^a \equiv \lim_{\frac{A^b_{UV}}{A^a_{UV}} \to 0} |C_4| \,/\, |C_1| = \begin{vmatrix} A_{es} & A_{ee} \\ A_{Ns} & A_{eN} \end{vmatrix} / \begin{vmatrix} A^a_{ee} & A^a_{eN} \\ A^a_{eN} & A^a_{NN} \end{vmatrix} \tag{5.75}$$

When system b is in stable equilibrium and much larger than system a, system b acts as a heat and mass reservoir.

5.5 System interacting with multiple systems

If there are R different kinds of interactions, which system a experiences, the equation of motion changes to

$$\frac{dp_j^a}{dt} = \sum_{r=1}^{R}(\frac{1}{\tau^r}(-p_j^a \ln \frac{p_j^a}{n_j^a} - p_j^a \vec{l}_j^a \cdot \vec{\mu}_a^r)) \tag{5.76}$$

Defining

$$\frac{1}{\tilde{\tau}} = \sum_{r=1}^{R} \frac{1}{\tau^r}, \ \frac{\vec{\tilde{\mu}}_a^0}{\tilde{\tau}} = \sum_{r=1}^{R} \frac{\vec{\mu}_a^r}{\tau^r} \tag{5.77}$$

the equation of motion is rewritten as

$$\frac{dp_j^a}{dt} = \frac{1}{\tilde{\tau}}(-p_j^a \ln \frac{p_j^a}{n_j^a} - p_j^a \vec{l}_j^a \cdot \vec{\tilde{\mu}}_a^0) \tag{5.78}$$

which recovers the form of Eq. (5.25). Thus, the discussion in *Sections* 5.3.2 and 5.3.3 and in *Appendix* C.1 still hold. The evolution of hypo-equilibrium state and the definition of non-equilibrium intensive properties can be applied to the study a network of non-equilibrium systems with non-quasi-equilibrium interactions.

5.6 Conclusions

This paper provides a thermodynamic investigation of interacting systems undergoing heat and/or mass interactions. In order to apply the SEAQT framework to all kinds of systems, the grand canonical ensemble and the grand partition function are used. The evolutions of intensive and extensive properties as well as the Onsager relations of the relaxation process of non-quasi-equilibrium processes in general are discussed. Both temperature and chemical potential measurements to a system in non-equilibrium is explained from a thermodynamic viewpoint, independent of the microscopic interactions taking place in the measurement. The investigation presented here provides a first-principle explanation for the experimental phenomenological measurement. In addition, both heat and mass reservoirs are defined thermodynamically. Finally, a system interacting with

multiple systems is discussed showing how the SEAQT framework and the concepts of hypo-equilibrium state and non-equilibrium intensive properties can be applied to studying a network of non-equilibrium system, which in turn permits the study of a macro/mesoscopic system with discrete local systems in non-equilibrium.

Appendix C

C.1 Hypo-equilibrium state evolution

The equation of motions of every energy eigenlevel in the K^{th} subspace of system a take the form

$$\frac{dp_j^{a,K}}{dt} = \frac{1}{\tau}(-p_j^{a,K}\ln\frac{p_j^{a,K}}{n_j^{a,K}} - p_j^{a,K}\alpha - \epsilon_j^{a,K}p_j^{a,K}\beta - N_j^{a,K}p_j^{a,K}\gamma) \tag{5.79}$$

Defining

$$\vec{l}_j^{a,K} = \begin{bmatrix} 1 & \epsilon_j^{a,K} & N_j^{a,K} \end{bmatrix}, \vec{\mu}^{a,K} = \begin{bmatrix} \alpha^{a,K} \\ \beta^{a,K} \\ \gamma^{a,K} \end{bmatrix}, \vec{\mu}_a^0 = \begin{bmatrix} \alpha \\ \beta \\ \gamma \end{bmatrix} \tag{5.80}$$

the equation of motion is written as

$$\frac{dp_j^{a,K}}{dt} = \frac{1}{\tau}(-p_j^{a,K}\ln\frac{p_j^{a,K}}{n_j^{a,K}} - p_j^{a,K}\vec{l}_j^{a,K}\cdot\vec{\mu}_a^0) \tag{5.81}$$

For the K^{th} subspace of system a, the probability distribution, grand partition function and $\alpha^{a,K}$ are given by

$$p_j^{a,K} = n_j^{a,K}e^{-\alpha^{a,K}}e^{-\epsilon_j^{a,K}\beta^{a,K}}e^{-N_j^{a,K}\gamma^{a,K}} \tag{5.82}$$

$$\Xi^{a,K}(\beta^{a,K},\gamma^{a,K}) = \sum_{i=1}^{\#(\mathcal{H}_a^K)} n_i^{a,K}e^{-\beta^{a,K}\epsilon_i^{a,K}-\gamma^{a,K}N_i^{a,K}} \tag{5.83}$$

$$\alpha^{a,K} = \ln\Xi^{a,K}(\beta^{a,K},\gamma^{a,K}) - \ln p^{a,K} \tag{5.84}$$

The equation of motion then simplifies to

$$\frac{dp_j^{a,K}}{dt} = \frac{p_j^{a,K}}{\tau}\vec{l}_j^{a,K} \cdot (\vec{\mu}^{a,K} - \vec{\mu}_a^0) \tag{5.85}$$

Using the relation

$$\ln \frac{p_j^{a,K}}{n_j^{a,K}} = -\mu^{a,K} - \epsilon_j^{a,K}\beta^{a,K} - N_j^{a,K}\gamma^{a,K} - \vec{l}_j^{a,K} \cdot \vec{\mu}^{a,K} \tag{5.86}$$

and the fact that the degeneracy $n_j^{a,K}$ is a constant, the equation of motion can also be written as

$$-\frac{d}{dt}(\vec{l}_j^{a,K} \cdot \vec{\mu}^{a,K}) = \frac{1}{\tau}(\vec{l}_j^{a,K} \cdot \vec{\mu}^{a,K} - \vec{l}_j^{a,K} \cdot \vec{\mu}_a^0) \tag{5.87}$$

$$\vec{l}_j^{a,K} \cdot (\frac{d\vec{\mu}^{a,K}}{dt} + \frac{1}{\tau}\vec{\mu}^{a,K} - \frac{1}{\tau}\vec{\mu}_a^0) = 0 \tag{5.88}$$

For any equation of motion that can reduce to the form of Eq. 5.88 above (e.g., multiple interacting non-equilibrium systems), the system remains in a hypo-equilibrium state throughout its evolution provided the system's initial state is a hypo-equilibrium state. The solution of this equation is,

$$p_j^{a,K} = n_j^{a,K} e^{-\vec{l}_j^{a,K} \cdot \mu^{a,K}(t)} \tag{5.89}$$

and $\mu^{a,K}(t)$ is found from

$$\frac{d\vec{\mu}^{a,K}(t)}{dt} = -\frac{1}{\tau}(\vec{\mu}^{a,K}(t) - \vec{\mu}_a^0(t)) \tag{5.90}$$

which governs the evolutions of the non-equilibrium intensive properties.

For any three eigenstates, p_i, p_j, and p_k, of system a, represented by $\vec{l_i}$, $\vec{l_j}$, and $\vec{l_k}$ where for simplicity the superscripts have been omitted, the following relation is found

$$\ln \frac{p_j}{n_j} = -\vec{l_j} \cdot \vec{K}^{ijk} \tag{5.91}$$

provided $\vec{l}_i$, $\vec{l}_j$, and $\vec{l}_k$ are linearly independent, i.e.,

$$\begin{vmatrix} 1 & \epsilon_i & N_i \\ 1 & \epsilon_j & N_j \\ 1 & \epsilon_k & N_k \end{vmatrix} \neq 0, \quad \text{or} \quad \begin{vmatrix} \epsilon_j - \epsilon_i & N_j - N_i \\ \epsilon_k - \epsilon_i & N_k - N_i \end{vmatrix} \neq 0 \tag{5.92}$$

In Eq. (5.91), $\vec{K}^{ijk}$ is defined as

$$\vec{K}^{ijk} \equiv \begin{bmatrix} 1 & \epsilon_i & N_i \\ 1 & \epsilon_j & N_j \\ 1 & \epsilon_k & N_k \end{bmatrix}^{-1} \begin{bmatrix} -\ln \frac{p_i}{n_i} \\ -\ln \frac{p_j}{n_j} \\ -\ln \frac{p_k}{n_k} \end{bmatrix} \tag{5.93}$$

The time evolution of these three energy eigenlevels (or eigenstates) obeys the following equations:

$$-\frac{d}{dt}(\vec{l}_j \cdot \vec{K}^{ijk}) = \frac{1}{\tau}(\vec{l}_j \cdot \vec{K}^{ijk} - \vec{l}_j \cdot \vec{\mu}) \tag{5.94}$$

$$\vec{l}_j \cdot (\frac{d\vec{K}^{ijk}}{dt} + \frac{1}{\tau}\vec{K}^{ijk} - \frac{1}{\tau}\vec{\mu}) = 0 \tag{5.95}$$

Because $\vec{l}_i$, $\vec{l}_j$, and $\vec{l}_k$ are linearly independent,

$$\frac{d\vec{K}^{ijk}}{dt} + \frac{1}{\tau}\vec{K}^{ijk} - \frac{1}{\tau}\vec{\mu} = 0 \tag{5.96}$$

If $\vec{l}_i$, $\vec{l}_j$, and $\vec{l}_k$ are in the same K^{th} subspace of system a which is in hypo-equilibrium with intensive properties $\vec{\mu}^{a,K}$, the initial condition for the equation of motion of $\vec{K}^{ijk}$ is

$$\vec{K}^{ijk}(t=0) = \vec{\mu}^{a,K} \tag{5.97}$$

Thus, the $\vec{K}^{ijk}$ from any three independent energy eigenlevels in the K^{th} subspace of system a follows the same ordinary differential equation, i.e., the same time evolution,

$$\vec{K}^{ijk}(t) = \vec{\mu}^{a,K}(t) \tag{5.98}$$

and, therefore, the system keeps is always in a hypo-equilibrium state. If no linearly independent

triplet of $\vec{l}_i$, $\vec{l}_j$, and $\vec{l}_k$ exists in the subspace, one can set $\gamma = 0$ or $\beta = 0$ for the case when two linearly independent $\vec{l}_i$ and $\vec{l}_j$ exist in the subspace and set both $\gamma = 0$ and $\beta = 0$ for the case of a single eigenlevel in the subspace.

C.2 Equation of motion

The energy eigenlevels of system a and b are represented by $\{(n_i^a, \epsilon_i^a, N_i^a)\}$ and $\{(n_j^a, \epsilon_j^a, N_j^a)\}$. The state of the system can be represented by two probability distributions among the energy eigenlevels of systems a and b given by $\{p_i^a, p_j^b,\, i, j = 1, 2, \cdots\}$. The distance between two states is defined here as the Fisher-Rao metric. Equivalently, the square root of the probability distribution $\{p_i^a, p_j^b,\, i, j = 1, 2, ...\}$ can be used to represent the system state. One can prove that the Fisher-Rao metric of the probability space becomes the Euclidean metric in the space of $\{x_i^a, x_j^b, i, j = 1, 2, ...\}$. The distance between states for both representations is given by

$$dl = \frac{1}{2}\sqrt{(\sum_i p_i^a (\frac{d \ln p_i^a}{d\theta})^2 + \sum_j p_j^b (\frac{d \ln p_j^b}{d\theta})^2) d\theta} \tag{5.99}$$

$$dl = \sqrt{(\sum_i x_i^a (\frac{d \ln x_i^a}{d\theta})^2 + \sum_j x_j^b (\frac{d \ln x_j^b}{d\theta})^2) d\theta} \tag{5.100}$$

where dl is the distance between $p(\theta + d\theta)$ and $p(\theta)$ or $x(\theta + d\theta)$ and $x(\theta)$, and θ is a continuous parameter. A property of the system can be defined as a function of state $\{x_i^a, x_j^b\}$ such that:

$$I^a = \sum_i (x_i^a)^2 = 1 \tag{5.101}$$

$$I^b = \sum_j (x_j^b)^2 = 1 \tag{5.102}$$

$$N^a = \langle N \rangle^a = \sum_i N_i^a (x_i^a)^2 = \text{constant} \tag{5.103}$$

$$N^b = \langle N \rangle^b = \sum_j N_j^b (x_j^b)^2 = \text{constant} \tag{5.104}$$

$$E = \langle e \rangle^a + \langle e \rangle^b = \sum_i \epsilon_i^a (x_i^a)^2 + \sum_j \epsilon_j^b (x_j^b)^2 = \text{constant} \tag{5.105}$$

$$S = \langle s \rangle^a + \langle s \rangle^b = -\sum_i (x_i^a)^2 \ln(x_i^a)^2 - \sum_j (x_j^b)^2 \ln(x_i^a)^2 \tag{5.106}$$

where $\langle\cdot\rangle^{a(b)}$ indicates the expectation value in system $a(b)$. For interacting systems with heat diffusion only, there are five conservation laws for the first five properties (Eqs. (5.101) to (5.105)). The von Neumann formula for the entropy is used. For a detailed discussion of why, the reader is referred to [32]. The gradient of a given property in state space is then expressed by

$$\boldsymbol{g_{I^a}} = \sum_i \frac{\partial I^a}{\partial x_i^a}\hat{e_i^a} + \sum_j \frac{\partial I^a}{\partial x_j^b}\hat{e_j^b} = \sum_i 2x_i^a\hat{e_i^a} \tag{5.107}$$

$$\boldsymbol{g_{I^b}} = \sum_i \frac{\partial I^b}{\partial x_i^a}\hat{e_i^a} + \sum_j \frac{\partial I^b}{\partial x_j^b}\hat{e_j^b} = \sum_j 2x_j^b\hat{e_j^b} \tag{5.108}$$

$$\boldsymbol{g_{N^a}} = \sum_i \frac{\partial N^a}{\partial x_i^a}\hat{e_i^a} + \sum_j \frac{\partial N^a}{\partial x_j^b}\hat{e_j^b} = \sum_i 2x_i^a N_i^a\hat{e_i^a} \tag{5.109}$$

$$\boldsymbol{g_{N^b}} = \sum_i \frac{\partial N^b}{\partial x_i^a}\hat{e_i^a} + \sum_j \frac{\partial N^b}{\partial x_j^b}\hat{e_j^b} = \sum_j 2x_j^b N_j^b\hat{e_j^b} \tag{5.110}$$

$$\boldsymbol{g_E} = \sum_i \frac{\partial E}{\partial x_i^a}\hat{e_i^a} + \sum_j \frac{\partial E}{\partial x_j^b}\hat{e_j^b} = \sum_i 2x_i^a\epsilon_i^a\hat{e_i^a} + \sum_j 2x_j^b\epsilon_j^b\hat{e_j^b} \tag{5.111}$$

$$\begin{aligned}\boldsymbol{g_S} = \sum_i \frac{\partial S}{\partial x_i^a}\hat{e_i^a} + \sum_j \frac{\partial S}{\partial x_j^b}\hat{e_j^b} = \sum_i[-2x_i^a - 2x_i^a\ln(x_i^a)^2]\hat{e_i^a} \\ + \sum_j[-2x_j^b - 2x_j^b\ln(x_j^b)^2]\hat{e_j^b}\end{aligned} \tag{5.112}$$

where $\hat{e}_i^a(b)$ is the unit vector for each dimension.

The principle of SEA upon which the equation of motion is based is defined as the direction at any instant of time along which the system state evolves, which has the largest entropy gradient consistent with the conservation constraints. The resulting equation of motion is then expressed as

$$\frac{d\boldsymbol{x}}{dt} = \frac{1}{\tau(x)}\boldsymbol{g_{S\perp L(g_{I^a},g_{I^b},g_{N^a},g_{N^b},g_E)}} \tag{5.113}$$

where τ, which is a function of system state, is the relaxation time that describes the speed at which the state evolves in state space in the direction of steepest entropy ascent. $L = L(\boldsymbol{g_{I^a}}, \boldsymbol{g_{I^b}}, \boldsymbol{g_{N^a}}, \boldsymbol{g_{N^b}}, \boldsymbol{g_E})$ is the manifold spanned by the first five gradients, and $\boldsymbol{g_{S\perp L}}$ is the perpendicular component of the gradient of the entropy to the hyper-surface that yields to the five conservation laws. The right hand side of Eq. (5.113) takes the form of a ratio of Gram determinants. The explicit form of this equation using $\{p_i^a, p_j^b\}$ is given by Eq. (5.19).

Chapter 6

Thermodynamic Trajectory Study on Size Effects in Heat and Mass Diffusion of Identical Particles using Steepest-Entropy-Ascent Quantum Thermodynamics

6.1 Introduction

In addition to the phenomenological approach of studying heat and mass diffusion using empirical equations, there also exist numerous methods for modeling such non-equilibrium phenomena from a first-principles standpoint with each restricted to its own applicable set of spatial and temporal scales. At the macroscopic level, continuum non-equilibrium thermodynamics with the local equilibrium assumption is used but cannot generally be applied at atomistic/mesoscopic scales since the small dimensions of the system result in quantum and for that matter classical effects that the continuum assumption cannot address. Moreover, non-equilibrium processes in the far-from-equilibrium realm make the application of the continuum formulation of non-equilibrium thermodynamics, i.e., the so-called Onsager formulation (e.g., [96]), questionable due to its underlying assumption of linearity or near-equilibrium behavior. Furthermore, each specific set of

spatial and temporal scales usually entails a different kinematic and dynamic description of system state and its motion. Thus, a general approach which could provide a thermodynamic analysis of non-equilibrium evolution, especially that far-from-equilibrium, across different spatial and temporal scale has been lacking, even though the general system properties of energy and entropy are well defined [33] and their evolutions observable.

To arrive at a general study of non-equilibrium state evolution (i.e., of the entropy generation process), a mathematical framework with a single kinematic and dynamic description that crosses all temporal and spatial scales and accounts for both non-continuum quantum and classical effects is needed. At the same time, retaining the advantage of the equilibrium thermodynamic approach, which is able to provide system property information phenomenologically, is also desirable as is providing thermodynamic features of system state and state evolution as a non-equilibrium relaxation pattern (in the sense of GENERIC [20, 21]), which captures the complex and detailed dynamic balance of particles or quantum states independent of the exact details of the micro-mechanical interactions taking place. Such a framework must also avoid the computational burdens inherent to existing methods based on mechanics (e.g., the Boltzmann equation [4, 100, 101] and molecular dynamics [6]) or quantum mechanics (e.g., 'open-system' quantum thermodynamics [68, 73, 102–105], "closed quantum systems" [106], heat reservoirs mediated by quantum systems [107], quantum non-equilibrium Green's function equations of motion [1, 108, 109], and the quantum Boltzmann equation, i.e., the Uehling-Uhlenbeck-Boltzmann equation [93–95]) that require detailed interaction information of particles or quantum states.

A mathematical framework that meets these requirements is that of steepest-entropy-ascent quantum thermodynamics (SEAQT) [24, 26–29, 39]. It can be used to model non-equilibrium processes (even those far-from equilibrium) from the atomistic to the macroscopic level [15, 36–38, 110]. SEAQT bases its framework on properties well-defined at all scales for equilibrium as well as non-equilibrium states, such as the energy, particle number and entropy [33]. The non-linear dynamics of state evolution are characterized by the entropy generation, which results from the principle of steepest entropy ascent. This principle forms the basis of the equation of motion that tracks the evolution of energy and entropy in state space. Using the concept of hypo-equilibrium state (i.e., a non-equilibrium relaxation pattern), the non-equilibrium trajectory of system state evolution for a large range of initial conditions can be fully described [14]. In this way, the thermodynamic analysis of both reactive and non-reactive non-equilibrium phenomena, including

heat and mass diffusion, can be studied within a single framework. This characteristic of SEAQT enables the comparative study of non-equilibrium trajectories for coupled and uncoupled heat and mass diffusion at different spatial scales. In addition, SEAQT is a first-principle, thermodynamic-ensemble based approach, which views the non-equilibrium relaxation process from the point of view of an ensemble entity and as a result, avoids the computational burdens inherent to existing approaches. Its equation of motion is, thus, able to provide trajectories in thermodynamic state space independent of the mechanical details of the relaxation process, i.e., of the details of specific microscopic interactions. Non-equilibrium features of system behavior are nonetheless clearly revealed.

In the following, how the dimensions of a system influence the heat and mass diffusion process is illustrated. Note that the SEAQT framework requires no assumptions of equilibrium nor of near-equilibrium. Furthermore, system energy eigenstructure changes and entropy generation play key roles since system dimensions influence the eigenstructure, while the eigenstructure determines the topology of eigenstates that can be accessed by any given thermodynamic state at any instant of time along the non-equilibrium trajectory of state evolution. Size effects can, thus, be studied from the point of view of thermodynamics. The present study focuses on the effects of system size on the kinetics of the non-equilibrium state evolution, specifically, the trajectory in thermodynamic state space. The discussion is limited to the condition that the temperature is high and the concentration of the particle is not too high when the state is not in the strong degenerate limit [needs a reference]. Results for fermions and bosons are included here. Two kinds of size effects are presented, i.e., those due to concentration and those due to volume.

The paper starts with an introduction of the SEAQT equation of motion in *Section* 6.2. Next, the important concepts of the kinetics and dynamics of the non-equilibrium evolution are presented in *Section* 6.2.1. This is followed in *Section* 6.2.2 by an illustration of hypo-equilibrium and non-equilibrium intensive properties in order to give a complete description of non-equilibrium state evolution. *Section* 6.3 then provides a discussion of how interactions between systems are captured within the SEQT framework followed in *Section* 6.4 with results from the application of the SEAQT framework to the prediction of the heat and mass diffusion of fermion and boson systems. *Section* 6.5 then ends with some conclusions.

6.2 SEAQT equation of motion

In this section, the system and state description in SEAQT is given, and the equation of motion, is presented. Based on the discussion by Grmela [20, 21, 35] and Beretta [24, 34] the general form of a non-equilibrium framework is a combination of both irreversible relaxation and reversible symplectic dynamics. If written in a generalized form of Ginzburg-Landau equation [20, 34], the equation of motion takes the following form:

$$\frac{d}{dt}\phi(t) = X^H_{\phi(t)} + Y^H_{\phi(t)} \tag{6.1}$$

where $\phi(t)$ represents the state evolution trajectory, $X^H_{\phi(t)}$ and $Y^H_{\phi(t)}$ are functions of the system state $\phi(t)$ and represent the reversible symplectic dynamics and irreversible relaxation process, respectively. In the SEAQT framework, the system is defined by the Hamiltonian operator $\hat{H}$, the system state is represented by the density operator $\hat{\rho}$, $X^H_{\phi(t)}$ follows the Schr"odinger equation, and $Y^H_{\phi(t)}$ is derived from the SEA principle. To describe the evolutionary process, conservation laws are explicitly required in order to construct the equation of motion, which is given by [42]

$$\frac{d\hat{\rho}}{dt} = \frac{1}{i\hbar}[\hat{\rho}, \hat{H}] + \frac{1}{\tau}\hat{D} \tag{6.2}$$

where the first term is the Schrödinger term, and the second is the dissipation term. If the system is in a pure (zero-entropy) state, $\hat{\rho}\hat{\rho} = \hat{\rho}$, and the equation of motion reverts back to the Schrödinger equation of quantum mechanics. If the system is in a so-called mixed (nonzero-entropy) state and $\hat{\rho}$ is diagonal in the energy eigenstate basis, $\hat{H}$ commutes with $\hat{\rho}$ and the Schrödinger term goes to zero even though $\hat{\rho}$ may not be a Maxwellian distribution among the energy eigenlevels. The state evolution of such a mixed-state operator cannot be captured by the Schrödinger term and is instead given by the second term to the right of the equals, the dissipation term, which captures the probability redistribution towards the Maxwellian distribution. The dissipation term is constructed using a set of operators called the ‘generators of the motion’. Each generator corresponds to one of the conservation laws to which the system is subjected. For example, an isolated system is subject to two conservation laws, probability normalization and energy conservation, so that the generators of the motion are $\{\hat{I}, \hat{H}\}$. For the case when $\hat{\rho}$ is diagonal in the energy eigenstate basis,

the equation of motion takes the form [28]

$$\frac{dp_j}{dt} = \frac{1}{\tau}\frac{\begin{vmatrix} -p_j \ln p_j & p_j & \epsilon_j p_k \\ \langle s \rangle & 1 & \langle e \rangle \\ \langle es \rangle & \langle e \rangle & \langle e^2 \rangle \end{vmatrix}}{\begin{vmatrix} 1 & \langle e \rangle \\ \langle e \rangle & \langle e^2 \rangle \end{vmatrix}} = \frac{1}{\tau} D_j(\mathbf{p}) \tag{6.3}$$

where p_j is the diagonal term of $\hat{\rho}$ in the energy eigenstates basis and represents the probability of the system being in the eigenstate associated with the j^{th} energy eigenlevel, $\mathbf{p}$ represents the vector $\{p_j\}$, $\langle \cdot \rangle$ is the expectation value of the property given $\hat{\rho}$, and τ is the relaxation time.

6.2.1 Non-equilibrium evolution: kinetics and dynamics

In general, the equation of motion for a system with a given group of conservation laws has the form

$$\frac{dp_j}{dt} = \frac{1}{\tau(\mathbf{p})} D_j(\mathbf{p}) \tag{6.4}$$

where D_j and τ can be a function of $\mathbf{p}$. $D_j(\mathbf{p})$ is calculated from the conservation laws and the principle of SEA [42]. Specifically, it reduces to Eq. (6.2) for an isolated system subject to mass and energy conservation.

The solution of this ordinary differential equation is

$$p_j = p_j(t) \tag{6.5}$$

where the time evolution of probability can be regarded as a parametric equation with parameter t. If t is the real time, the solution of Eq. (6.3) provides both the trajectory in state space and the system state at any instant of time.

In general, the relaxation time τ can be a function of system state such that

$$\tau = \tau(\mathbf{p}(t)) \tag{6.6}$$

Since for a given initial state of the system, the non-equilibrium path of state evolution is uniquely

solved from the equation of motion, Eq. (6.3), this path can be used to define a new parameter $\tilde{\tau}$ such that

$$d\tilde{\tau} = \frac{1}{\tau(\mathbf{p}(t))}dt, or \quad \tilde{\tau} = \int_{path} \frac{1}{\tau(\mathbf{p}(t'))}dt' = \tilde{\tau}(t) \tag{6.7}$$

where $\tilde{\tau}$ is called the dimensionless time. With this time, the independent variable for the equation of motion can be changed so that

$$\frac{dp_j}{d\tilde{\tau}} = D_j(\mathbf{p}) \tag{6.8}$$

The solution for this equation is written as

$$p_j = p_j(\tilde{\tau}) \tag{6.9}$$

No matter how the relaxation time τ depends on the real time t and the state, the equation of motion can always be transformed to Eq. (6.7) with the parameter change defined by Eq. (6.6). Furthermore, the evolution of system state follows the same function (Eq. (6.8)) in $\tilde{\tau}$. Physically, this means that it follows the same trajectory in state space. If the relaxation time is chosen to be a constant, Eq. (6.2) gives the same parametric equation, Eq. (6.7), with a parametric scaling in the relaxation time τ.

By doing the preceding, the kinetics and dynamics of the system are separated. The former is found via Eqs. (6.7) and (6.8), and results in a unique trajectory in state space based on the parameter $\tilde{\tau}$. This trajectory gives the intermediate states through which the system goes during state relaxation, and the sequence in which they occur. The dynamics is found via Eq. (6.3) and the functional dependence $\tau = \tau(p)$ (Eq. (6.5)) and results in the same trajectory in state space but based this time on the real time t. In this paper, the discussion focuses on the kinetics of the system state evolution, which decided by Eqs. (6.2) and (6.7). The kinetics of the relaxation process can be regarded as a thermodynamic property of the system's non-equilibrium evolution. For different forms of τ, the system relaxation may be due to different forms of microscopic interactions such as, for example, different types of collisions. Faster relaxations correspond to smaller τ's, while slower ones correspond to larger τ's. If the relaxation speed depends on system state, τ has a functional dependence on $\mathbf{p}$. Otherwise, τ is a constant. However, no matter what kind of microscopic interaction causes the relaxation, a system's non-equilibrium state evolution follows the same trajectory, one decided by its eigenstructure. In this way, the thermodynamic

features of relaxation are revealed without going into the detailed microscopic mechanics of the system.

6.2.2 Non-equilibrium state and state evolution description: hypo-equilibrium

The thermodynamic features of the non-equilibrium relaxation process generated by the SEAQT framework have a number of useful characteristics, which lead to a complete description of non-equilibrium state and the general fundamental definition of non-equilibrium intensive properties. This description is based on two key concepts, which are briefly discussed below. For proofs and a more detailed discussion, the reader is referred to [14, 17].

For a given system represented by an energy eigenlevel set $\Omega = \{(\epsilon_k, N_k)\}$, where each energy eigenlevel is represented by a pair of energy and particle number eigenvalues, the system can be divided into M subsystems $\Omega_i = \{(\epsilon_k^i, N_k^i)\}$, $\Omega_i \cap \Omega_j = \emptyset$ and $\Omega = \bigcup \Omega_i$. For system with E and N conserved (or only E conserved), if the probability distribution in each subsystem yields to a grand canonical distribution (or canonical distribution), the system is designated as being in an M^{th}-order hypo-equilibrium state. Based on this definition, it can be shown that any state of the system is a hypo-equilibrium state with order M, where M is less than or equal to the number of system eigenlevels [14, 17]. A hypo-equilibrium state of order 1 corresponds to a state in stable equilibrium. For system with E and N conserved, the probability distribution of the M^{th}-order hypo-equilibrium state takes the form

$$\forall i = 1, 2, ..., M,\ p_k^i = \frac{p^i}{\Xi^i(\beta^i, \gamma^i)} e^{-\beta^i \epsilon_k^i - \gamma^i N_k^i},\ k = 1, 2, ..., w_i \tag{6.10}$$

where β^i and γ^i are parameters, p^i is the total probability in subsystem i, and $\Xi^i(\beta^i, \gamma^i)$ is the grand partition function of the subsystem with parameters β^i and γ^i. To be complete, $\beta^i = 0$ and $\gamma^i = 0$ if $w_i = 1$, and w_i can be infinite. The grand partition function is written as

$$\Xi^i(\beta^i, \gamma^i) = \sum_{k=1}^{w_i} e^{-\beta^i \epsilon_k^i - \gamma^i N_k^i} \tag{6.11}$$

For a given M^{th}-order hypo-equilibrium state, the intensive properties of the subsystems can

be represented by β^i and γ^i, or equivalently using temperature and chemical potential defined by

$$T^i = \frac{1}{k_b \beta^i}, \quad \mu^i = \gamma^i T^i \tag{6.12}$$

A M^{th}-order hypo-equilibrium state can then be represented by a division $\{\Omega_i = (\epsilon_k^i, N_k^i),\ i = 1, ..., M\}$ of the system and a corresponding triplet set $\{(p^i, \beta^i, \gamma^i),\ i = 1, ..., M\}$. The intensive property set $\{(T^i, \mu^i),\ i = 1, ..., M\}$ is a generalization of the definition of intensive property at stable equilibrium (T^{eq}, μ^{eq}), which is also a 1^{st}-order hypo-equilibrium state. Li and von Spakovsky have proven that if a system begins in an M^{th}-order hypo-equilibrium state, it will remain in an M^{th}-order hypo-equilibrium state throughout the state evolution as long as the same subsystem division is maintained. Thus, the time evolution of the distribution has the form

$$\forall i = 1, 2, ..., M,\ p_k^i(t) = \frac{p^i(t)}{\Xi^i(\beta^i(t), \gamma^i(t))} e^{-\beta^i(t)\epsilon_k^i - \gamma^i(t) N_k^i},\ k = 1, 2, ..., w_i \tag{6.13}$$

The intensive property set $\{(T^i(t), \mu^i(t)),\ i = 1, ..., M\}$ is also well defined throughout the entire evolution, and the system evolution can also be represented by the evolution of the triplet set $\{(p^i(t), \beta^i(t), \gamma^i(t)),\ i = 1, ..., M\}$.

6.3 SEAQT for interacting systems

6.3.1 Heat and mass interaction

The equation of motion is designed to study the non-equilibrium relaxation process of an isolate system. However, since interacting systems can be view as a composite isolated non-equilibrium system of subsystems whose interactions cause the relaxation process of the composite, the SEAQT equation of motion calculate can be used to determine the evolution of these interacting systems as well. Furthermore, if the subsystems of the composite are themselves not in grand canonical (or canonical) distribution (i.e., they are in non-equilibrium states), higher order hypo-equilibrium states [14, 17] can be applied, and used to study the composite system and its subsystem interactions.

The SEAQT framework, thus, explains these interactions on the basis of thermodynamics. This contrasts with other non-equilibrium approaches, which attempt to predict the non-equilibrium

relaxation process on the basis of mechanical microscopic interactions. It is also contrasts with traditional thermodynamics, which necessarily limits its description to quasi-equilibrium processes and the near-equilibrium realm. The SEAQT framework, on the other hand, is able to not only describe these processes and this realm but non-quasi-equilibrium processes and the far-from-equilibrium realm as well.

Now, consider two interacting systems (system a and system b). The composite system is not in stable equilibrium, and its state is represented by the probability distributions $\{p_i^a\}$ in system a and $\{p_i^b\}$ in system b together. There are four conservation laws: probability normalization of system a, probability normalization of system b, energy conservation of the composite system, and particle number conservation of the composite system. Based on SEA and the conservation laws, $\{I^a, I^b, E, N\}$ serve as the generators of the motion and the equation of motion for system a takes the form [17, 42]

$$\frac{dp_j^a}{dt} = \frac{1}{\tau}\frac{\begin{vmatrix} -p_j^a \ln p_j^a & p_j^a & 0 & \epsilon_j^a p_j^a & N_j^a p_j^a \\ \langle s\rangle^a & 1 & 0 & \langle e\rangle^a & \langle N\rangle^a \\ \langle s\rangle^b & 0 & 1 & \langle e\rangle^b & \langle N\rangle^b \\ \langle es\rangle & \langle e\rangle^a & \langle e\rangle^b & \langle e^2\rangle & \langle eN\rangle \\ \langle Ns\rangle & \langle N\rangle^a & \langle N\rangle^b & \langle eN\rangle & \langle N^2\rangle \end{vmatrix}}{\begin{vmatrix} 1 & 0 & \langle e\rangle^a & \langle N\rangle^a \\ 0 & 1 & \langle e\rangle^b & \langle N\rangle^b \\ \langle e\rangle^a & \langle e\rangle^b & \langle e^2\rangle & \langle eN\rangle \\ \langle N\rangle^a & \langle N\rangle^b & \langle eN\rangle & \langle N^2\rangle \end{vmatrix}} \tag{6.14}$$

where $\langle\cdot\rangle^{a(b)}$ is the expectation value of a property in system a(b), and $\langle\cdot\rangle = \langle\cdot\rangle^a + \langle\cdot\rangle^b$ is the expectation value of the total property of the composite system. The numerator of the fraction to the right of the equals can be expanded by the elements of the first row and their cofactors such that

$$\det = -p_j^a \ln p_j^a C_1 + p_j^a C_2^a + \epsilon_j^a p_j^a C_3 + N_j^a p_j C_4 \tag{6.15}$$

where C_1, C_2, C_3, C_4 are the cofactor of the first line of the determinant. By defining

$$\frac{C_2}{C_1} = -\alpha, \quad \frac{C_3}{C_1} = -\beta, \quad \frac{C_4}{C_1} = -\gamma \tag{6.16}$$

the equation of motion transforms to

$$\frac{dp_j^a}{dt} = \frac{1}{\tau}(-p_j^a \ln p_j^a - p_j^a \alpha - \epsilon_j^a p_j^a \beta - N_j^a p_j^a \gamma) \tag{6.17}$$

If the two systems are in stable equilibrium states, the composite system is in a 2^{nd}-order hypo-equilibrium state. Li and von Spakovsky [17] have proven that the conclusions in previous section relative to the hypo-equilibrium state still hold for the composite system. Thus, the time evolution of the two systems takes the form

$$\text{System a: } p_j^a(t) = \frac{1}{\Xi^a(\beta^a(t), \gamma^a(t))} e^{-\gamma^a(t) N_j^a - \beta^a(t)\epsilon_j^a} \tag{6.18}$$

$$\text{System b: } p_j^b(t) = \frac{1}{\Xi^b(\beta^b(t), \gamma^b(t))} e^{-\gamma^b(t) N_j^b - \beta^b(t)\epsilon_j^b} \tag{6.19}$$

The time evolution of $\beta^a(t)$, $\beta^b(t)$, $\gamma^a(t)$, and $\gamma^b(t)$ can be solved from the equation of motion for intensive properties [17] such that

$$\text{System a: } \frac{d\beta^a(t)}{dt} = \frac{1}{\tau}(\beta^a(t) - \beta(t)) \tag{6.20}$$

$$\text{System a: } \frac{d\gamma^a(t)}{dt} = \frac{1}{\tau}(\gamma^a(t) - \gamma(t)) \tag{6.21}$$

$$\text{System b: } \frac{d\beta^b(t)}{dt} = \frac{1}{\tau}(\beta^b(t) - \beta(t)) \tag{6.22}$$

$$\text{System b: } \frac{d\gamma^b(t)}{dt} = \frac{1}{\tau}(\gamma^b(t) - \gamma(t)) \tag{6.23}$$

where β and γ are given by Eq. (6.15). For the general form where two systems are in non-equilibrium states, the reader is referred to the detailed discussion given in [17].

6.3.2 Many particle system

For a many particle system, the occupation number representation is used, and the state space is a Fock space, which is the sum of N-particle state spaces [111]. The N-particle basis state is

$$|n_{\nu_1}, n_{\nu_2}, n_{\nu_3}, \cdots\rangle, \quad \sum_j n_{\nu_j} = N \tag{6.24}$$

The space spanned by the occupation number basis is the Fock space $\mathcal{F}$

$$\mathcal{F} = \bigoplus_{N=0}^{\infty} \mathcal{F}_N, \quad \text{where } \mathcal{F}_N = \text{span}\{|n_{\nu_1}, n_{\nu_2}, n_{\nu_3}, \cdots\rangle \,|\, \sum_j n_{\nu_j} = N\} \tag{6.25}$$

For independent particles, the occupation number basis is also the energy eigenlevels of the Hamiltonian. The occupation number n_{ν_j} is the particle number distributed in single-particle energy eigenlevels ν_j with values of

$$\text{fermions: } n_{\nu_j} = 0, 1 \tag{6.26}$$

$$\text{bosons: } n_{\nu_j} = 0, 1, 2, \cdots \tag{6.27}$$

In order to get system properties, the grand partition function is calculated, which is defined by

$$\Xi(\beta, \gamma) = \sum_N e^{-\gamma N} \sum_{S_N} e^{\beta E_{S_N}} \tag{6.28}$$

The sum over S_N is a summation is over N-particle energy eigenlevels. The natural logarithm of the partition function takes the form

$$\text{fermions: } \ln \Xi(\beta, \gamma) = \sum_k \ln(1 + e^{-\gamma - \beta\epsilon_k}) \tag{6.29}$$

$$\text{bosons: } \ln \Xi(\beta, \gamma) = -\sum_k \ln(1 - e^{-\gamma - \beta\epsilon_k}) \tag{6.30}$$

where the summation is over the single-particle energy eigenlevels.

The single-particle energy eigenlevels are chosen to be those for free particles in a box, Helium 3 as fermions and Helium 4 as bosons. Thus,

$$\epsilon(n_x, n_y, n_z) = \frac{\hbar^2}{8m}\left(\left(\frac{n_x}{L_x}\right)^2 + \left(\frac{n_y}{L_y}\right)^2 + \left(\frac{n_z}{L_z}\right)^2\right) \tag{6.31}$$

where n_x, n_y, n_z are the quantum numbers for the transnational energy eigenlevels, L_x, L_y, L_z are the three dimensions of the box, $\hbar$ is the reduced Plank's constant, and m is the mass of a particle.

The volume is given by $V = L_x L_y L_z$. If the system yields to the two conditions

$$e^{-\gamma} < 1,\ \beta \ll \frac{1}{\Delta\epsilon} = \frac{8mL^2}{\hbar^2} \tag{6.32}$$

which mean that the concentration is not too high (weak degenerate condition) and the temperature is much higher than the characteristic temperature (quasi-continuous condition). The natural logarithm of the partition function can then be calculated using

$$\text{fermions: } \ln \Xi(\beta,\gamma) = -\frac{V}{\lambda_T^3}(2s+1)Li_{5/2}(-e^{-\gamma}) \tag{6.33}$$

$$\text{bosons: } \ln \Xi(\beta,\gamma) = \frac{V}{\lambda_T^3}(2s+1)Li_{5/2}(e^{-\gamma}) \tag{6.34}$$

where s is the spin of a particle, $(2s+1)$ is the degeneracy from spin, and $Li_s(z)$ is the polylogarithm function defined by

$$Li_s(z) = \sum_k^\infty \frac{z^k}{k^s} \tag{6.35}$$

and λ_T, a function of β, is the de Broglie wavelength of the thermal energy defined by

$$\lambda_T = \frac{h}{\sqrt{2\pi m k_b T}} = \frac{h}{\sqrt{2\pi m/\beta}} \tag{6.36}$$

The properties for system a are then given by

$$\langle N\rangle^a = -\frac{\partial}{\partial\gamma}\ln\Xi^a = \mp\frac{V}{\lambda_T^3}(2s+1)Li_{3/2}(\mp e^{-\gamma^a}) \tag{6.37}$$

$$\langle e\rangle^a = -\frac{\partial}{\partial\beta}\ln\Xi^a = \mp\frac{V}{\lambda_T^3}\frac{3}{2\beta^a}(2s+1)Li_{5/2}(\mp e^{-\gamma^a}) \tag{6.38}$$

$$\langle s\rangle^a = k_b(\ln\Xi^a - \gamma^a\frac{\partial}{\partial\gamma}\ln\Xi^a - \beta^a\frac{\partial}{\partial\beta}\ln\Xi^a) = k_b(\frac{5}{2}\ln\Xi^a + \gamma^a\langle N\rangle^a) \tag{6.39}$$

$$\langle e^2\rangle^a = (\langle E\rangle^a)^2 + \frac{\partial^2}{\partial^2\beta}\ln\Xi^a = (\langle E\rangle^a)^2 + \frac{15}{4(\beta^a)^2}\ln\Xi^a \tag{6.40}$$

$$\langle N^2\rangle^a = (\langle N\rangle^a)^2 + \frac{\partial^2}{\partial^2\gamma}\ln\Xi^a = (\langle N\rangle^a)^2 \mp \frac{V}{\lambda_T^3}(2s+1)Li_{1/2}(\mp e^{-\gamma^a}) \tag{6.41}$$

$$\langle eN\rangle^a = \langle E\rangle^a\langle N\rangle^a + \frac{\partial^2}{\partial\beta\partial\gamma}\ln\Xi^a = \langle E\rangle^a\langle N\rangle^a \mp \frac{V}{\lambda_T^3}\frac{3}{2\beta^a}(2s+1)Li_{3/2}(\mp e^{-\gamma^a}) \tag{6.42}$$

$$\langle sN\rangle^a = k_b(\beta^a\langle eN\rangle^a + \gamma^a\langle N^2\rangle^a + \ln\Xi^a\langle N\rangle^a) \tag{6.43}$$

$$\langle es\rangle^a = k_b(\beta^a\langle e^2\rangle^a + \gamma^a\langle eN\rangle^a + \ln\Xi^a\langle e\rangle^a) \tag{6.44}$$

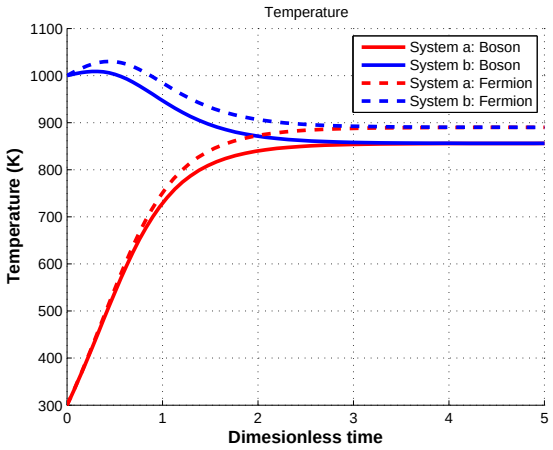

Figure 6.1. Temperature evolution for the boson systems (solid line) and that for the fermion systems (dashed line) with high concentration ($e^{\gamma} \sim 10$).

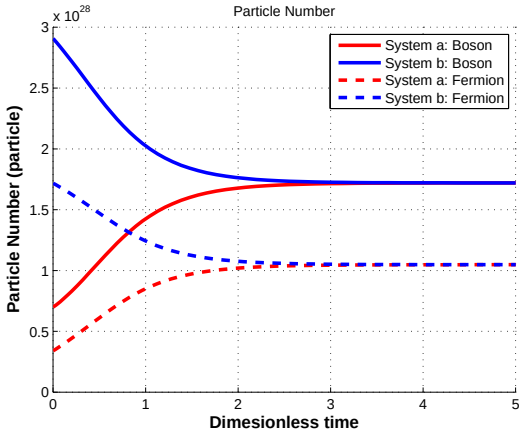

Figure 6.2. Particle number evolution for the boson systems (solid line), and that for the fermion systems (dashed line) with high concentration ($e^{\gamma} \sim 10$).

where fermions take the minus sign and bosons the plus sign. The properties for system b have the same form. These properties are used to calculate the β and γ in Eq. (6.15). From Eq. (6.36), one can arrive at the expression for the particle number concentration, namely,

$$n^a = \mp \frac{(2s+1) Li_{3/2}(\mp e^{-\gamma^a})}{\lambda_T^3} \tag{6.45}$$

where again fermions take the minus sign and bosons the plus sign.

6.4 Results and discussion

The SEAQT model is applied to study the size effects on heat and mass diffusion. The discussion of size effects focuses on their influence on the thermodynamic properties or kinetics of the relax-

ation process since the results are shown in dimensionless time. There are two ways for quantum mechanics to influence the thermodynamic properties of the system. One is from the fact that energy eigenlevels are discrete at temperatures close to or lower than the characteristic temperature for a given energy mode (e.g., that of translation, rotation, vibration, etc.). The other is from the indistinguishable feature of a particle, where statistical correlations are important. The results presented here are limited to the realm where Eq. (6.31) holds, i.e., where the temperature is significantly higher than the characteristic temperature for translation (condition #2 of Eq. (6.31)) and the chemical potential is not too low (condition #1 of Eq. (6.31)) so that the system is in the weak degenerate realm. For strong degenerate effects, such as Bose–Einstein condensation, Eqs. (6.32) and (6.33) need an additional term for energy ground state, but this is left for a future paper. However, the indistinguishable feature of the particles still influences the non-equilibrium relaxation process in the realm where e^{γ} is not too high. Furthermore, since the temperature is much higher than the characteristic temperature, the quantum effect from discrete energy eigenlevels is not studied here and is also left for a future paper. This also means that the summations in Eqs. (6.28) and (6.29) cannot be calculated by the polylogarithm function.

The particle number evolutions and temperature evolutions for bosons and fermions is shown in Figs. 6.1 to 6.4. The temperatures of system a and system b are chosen to be 300 K and 1000 K, respectively. In Fig. 6.1 and Fig. 6.2, the e^{γ} of system a and system b are chosen to be 1.2 and 1.5, respectively. In Fig. 6.3 and Fig. 6.4, the e^{γ} of system a and system b are chosen to be 1.2×10^5 and 1.5×10^5. The solid line is for the interacting boson systems, and the dashed line is for the interacting fermion systems. In order to make a comparison, in all four figures (Fig. 6.1 to 6.4), fermions and bosons are assumed to have the same particle mass m_{He_3} and the same box size of $10^{-3}m^3$. This comparison also necessitates removing the degenerate influence, which requires that the particle number, Eq. (6.36), for system a and the particle number for system b be divided by their respective degeneracies, which for a single particle with spin s is $2s + 1$. From these four figures, one can observed that the difference in the behavior of fermions and bosons decreases, as e^{γ} increases which in turn means that the concentration (Eq. (6.44)) decreases. At the low concentration limit, $e^{\gamma} \gg 1$, both fermions and bosons go back to being classical particles.

In Fig. 6.5 and Fig. 6.6, four cases for the boson systems are modeled in order to study the size effect due to concentration changes. The temperatures of the two systems are those for Figs.

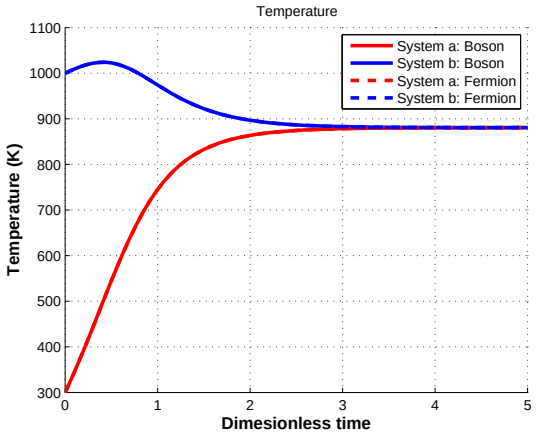

Figure 6.3. Temperature evolution for the boson systems (solid line) and that for the fermion systems (dashed line) with low concentration ($e^{\gamma} \gg 1$). The solid line and the dashed line converge.

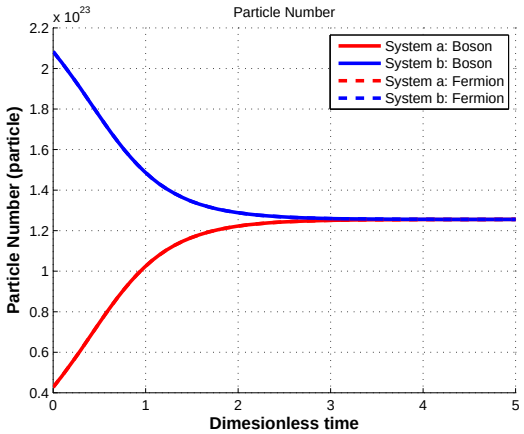

Figure 6.4. Particle number evolution for the boson systems (solid line) and that for fermion systems (dashed line) with low concentration ($e^{\gamma} \gg 1$). The solid line and the dashed line converge.

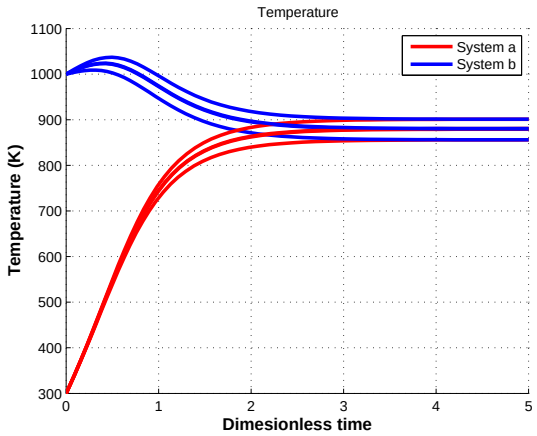

Figure 6.5. Temperature evolution for the boson systems for the four cases. γ^a and γ^b increase and, thus, concentration decreases from the bottom blue curve to the top one and from the top of the red curve to the bottom one. $\gamma^a - \gamma^b$ is kept constant. The curves for the two low concentration cases converge.

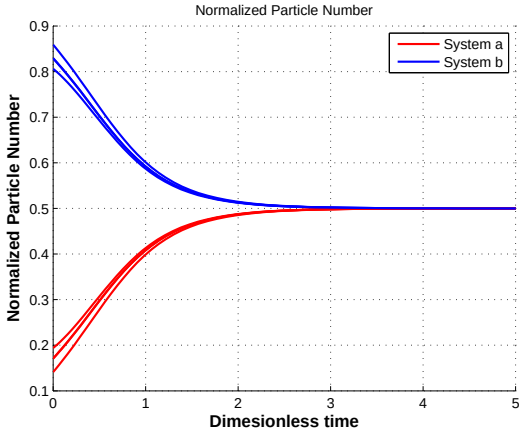

Figure 6.6. Normalized particle number evolution for the boson systems for the four cases. γ^a and γ^b increase and, thus, concentration decreases from the bottom blue curve to the top one and from the top of the red curve to the bottom one. $\gamma^a - \gamma^b$ is kept constant. The curves for the two low concentration cases converge.

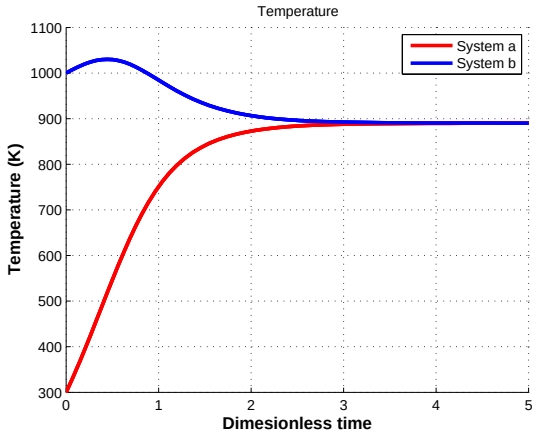

Figure 6.7. Temperature evolution for boson systems for different volume and same (γ^a, γ^b). The curves of the three cases converge.

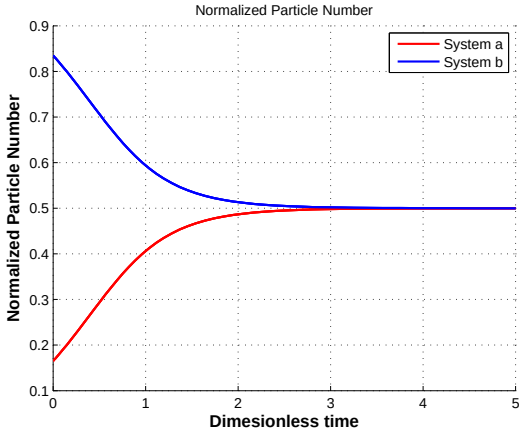

Figure 6.8. Normalized particle number evolution evolution for boson systems for different volume and same (γ^a, γ^b). The curves of the three cases converge.

6.1 to 6.4. $(e^{\gamma^a}, e^{\gamma^a})$ are chosen to be $(1.2, 1.5)$, $(12, 15)$, $(1200, 1500)$ and $(1.2 \times 10^5, 1.5 \times 10^5)$, where the difference $\gamma^a - \gamma^b$ remains the same. It can be observed that the size effect influences the thermodynamic trajectory of the non-equilibrium evolution via changes in γ (chemical potential) or equivalently via changes in concentration (Eq. (6.44)). This particular size effect is a concentration effect, and systems with same particle number but different concentrations follow this type of behavior.

The size effect can also appear in another way: systems with the same concentration but different volumes. This effect is called the volume effect. Fig. 6.7 and Fig. 6.8 show the particle number evolution and temperature evolution for boson system interactions for the different volumes, and γ^a and γ^b (or equivalently, the concentrations of two the systems) and other parameters are kept constant. The particle number curves are normalized by the total particle number at any instant of

time. The e^{γ} of system a and system b are chosen to be 1.2 and 1.5, and their temperatures to be 300 K and 1000 K. The volumes of systems are chosen to be 10^{-3} m^3, 10^{-9} m^3, and 10^{-18} m^3. It is can be observed that there is no difference in normalized trajectory. This can be proven by plugging Eq. (6.36)-(6.43) in Eq. (6.15) to acquire the explicit expression for β and γ. Actually, under conditions of Eq. (6.31), β and γ do not depend on V explicitly. Thus, the trajectory is not influenced by volume. However, for the case when the conditions of Eq. (6.31) do not hold, the natural logarithm of the grand partition function no longer depends linearly on volume as it does in Eqs. (6.32) and (6.33). In this case, volume effect may appear and the summation of Eqs. (6.28) and (6.29) cannot be calculated by polylogarithm function. Moreover, the volume effect can also appear when the study is conducted in real time. However, this volume effect can only influence the speed of the system going through the trajectory but cannot change the trajectory or intermediate states of system state evolution.

6.5 Conclusions

The SEAQT framework is a powerful and novel approach for studying non-equilibrium phenomena, even far-from-equilibrium phenomena, from the atomistic level up to the macroscopic. With this framework, heat and mass diffusion, even in realms far-from-equilibrium, can be modeled. Furthermore, with the concepts of hypo-equilibrium state and non-equilibrium intensive property, a description of non-equilibrium states comparable to that at stable equilibrium is now available. To illustrate this framework and these concepts, the kinetics of the non-equilibrium evolutions of heat and mass diffusion are predicted for interacting boson as well as fermion systems, and their state evolution trajectories in thermodynamic state space determined. Emphasis is placed on the thermodynamic features of the trajectories with each revealing through which intermediate thermodynamic states the system evolves and by which sequence these states occur.

In addition, two kinds of size effects influencing non-equilibrium trajectories have been studied. The concentration effect is shown to influence the state evolution trajectory in the weak degenerate realm, which comes from the indistinguishable feature of the particles. In contrast, volume changes show no influence on these trajectories in the high temperature limit where the discrete energy eigenlevels are treated as continuous. This is the case even though these changes influence system properties via the grand partition function.

Chapter 7

Steepest-Entropy-Ascent Model of Reservoir and Engine Cycle in Non-equilibrium Using Hypo-equilibrium State and an Isothermal-Isobaric Ensemble

7.1 Introduction

Numerous methods for modeling non-equilibrium phenomena exist with each is restricted to its own applicable set of spatial and temporal scales. At the macroscopic level, continuum non-equilibrium thermodynamics with the local equilibrium assumption is used but cannot generally be applied at atomistic/mesoscopic levels since the small dimensions of a system result in quantum and for that matter classical effects that the continuum assumption cannot address. Furthermore, non-equilibrium processes in the far-from-equilibrium realm make the application of the continuum formulation of non-equilibrium thermodynamics, i.e., the so-called Onsager formulation (e.g., [96]) questionable due to its underlying assumption of linearity or near-equilibrium behavior. In addition, each method uses a different kinematic and dynamic description of system state and its motion. Thus, a general approach that provides a thermodynamic analysis of non-equilibrium evolution, especially that far-from-equilibrium, across different spatial and temporal scales has been lacking even though general system properties such as the energy and entropy are well defined

[33] and their evolutions observable. Steepest-entropy ascent quantum thermodynamics (SEAQT) [24, 26–29, 39] addresses these issues providing a mathematical framework with a single kinematics and dynamics that crosses all temporal and spatial scales and accounts for both non-continuum quantum and classical effects. At the same time, it is able to provide system property information phenomenologically and thermodynamic system features from non-equilibrium relaxation patterns (in the sense of GENERIC [20, 21]), which capture the dynamic balance of detailed and complex microscopic single particle or quantum state evolutions. These patterns represent a reduction of a system's microscopic kinematics, appear to be general, and are independent of the microscopic dynamics, i.e., of the exact form of the micro-mechanical interactions. One of the benefits of this is that the SEAQT framework is able to avoid the computational burdens inherent to existing methods based on mechanics (e.g., the Boltzmann equation [4, 100, 101] and molecular dynamics [6]) or quantum mechanics (e.g., 'open-system' quantum thermodynamics [68, 73, 102–105], 'closed quantum systems' [106], heat reservoirs mediated by quantum systems [107], quantum non-equilibrium Green's function equations of motion [1, 108, 109], and the quantum Boltzmann equation, i.e., the Uehling-Uhlenbeck-Boltzmann equation [93–95]) that require detailed interaction information of the particles or quantum states.

To date, SEAQT has successfully been used to model non-equilibrium processes (even those far-from equilibrium) from the atomistic to the macroscopic level [15, 36–38, 110] and bases its framework on properties such as energy, particle number, and entropy, which as mentioned before, are well-defined at all scales for equilibrium as well as non-equilibrium states [33]. The non-linear dynamics of state evolution are characterized by the entropy generation, which results from the principle of steepest entropy ascent. This principle forms the basis of the equation of motion that tracks the evolution of energy and entropy in state space. Using the concept of hypo-equilibrium state (i.e., a non-equilibrium relaxation pattern), the non-equilibrium trajectory of system state evolution can be fully described across a wide range of initial conditions [14]. In this way, the thermodynamic analysis of non-equilibrium phenomena at different scales, whether classical or quantum, can be studied using a single framework, i.e., a single kinematics and dynamics.

Since an important part of thermodynamics is to study systems for which volume is the only parameter (in the sense of Gyftopoulos and Beretta, [32, 48]), a description of such a system undergoing a cyclic process in the non-equilibrium realm using SEAQT is presented here. Clearly, an important application of thermodynamics is to the study of such processes independent of the

exact nature of the microscopic interactions, which take place inside the system. Cyclic processes have been modeled both at the macroscopic as well as quantum levels[112–114] using equilibrium thermodynamics and quantum mechanics. The limitation with respect to the former is that the study of a cycle for such a system necessarily assumes that the system (e.g., that of a gas in a piston/cylinder device) is in a stable equilibrium state at any given instant of time and undergoes a quasi-equilibrium process, i.e., that system state evolution is very, very slow and that the process is reversible. To move the analysis into the practical realm requires the introduction of phenomenological parameters (e.g., experimental polytropic exponents, isentropic efficiencies) to help account for the effects of irreversibilities and, thus, model real engine cycles and guide device design. The limitation with respect to the latter, i.e., the use of approaches based on quantum mechanics (e.g., 'open quantum systems' [112, 113]) is that due to significant computational burdens the system model is necessarily limited to only a few energy eigenlevels and can, thus, not be extended across scales into the mesoscopic and macroscopic realms. Such approaches also cannot provide a general thermodynamic description (both kinematic and dynamic) applicable across all scales and in all regions even those far from equilibrium [39]. In contrast, the SEAQT framework provides a single theoretical model of irreversibility from the macroscopic to the atomistic level and overcomes the computational burdens of other approaches via the use of the concept of density of states [14, 15]. In addition, using the concepts of hypo-equilibrium state and non-equilibrium intensive properties, greater physical insight into the influence of non-equilibrium effects on system performance can be revealed.

In the following, unique thermodynamic trajectories for system state evolutions from some initial transient state to steady state are predicted for cyclic processes using the SEAQT equation of motion, which is introduced and discussed in *Sections* 7.2.1 to 7.2.3 along with the system and state space considered. To describe each trajectory in detail, the concepts of hypo-equilibrium state, temperature, and pressure for non-equilibrium states are introduced in *Section* 7.2.4 and are shown to be closely related to the isothermal-isobaric ensemble of stable equilibrium [115–119]. The definitions of temperature and pressure proposed for non-equilibrium states are fundamental rather than phenomenological and a generalization of these properties from those at stable equilibrium. The SEAQT equation of motion for two interacting systems and for a system interacting with a reservoir is then presented in *Section* 7.3 followed in *Section* 7.4 by a description of a system undergoing a non-quasi-equilibrium evolution in state. Finally, in *Section* 7.5, results are given for

the state time evolution of a system undergoing a transient cyclic process. How non-equilibrium phenomena influence the performance of the cycle is discussed.

7.2 SEAQT equation of motion

7.2.1 SEAQT equation of motion using a quantum mechanics description

In this section, the system and state description in SEAQT used here is given, and the equation of motion, is presented. Based on the discussion by Grmela and Öttinger [20, 21, 35] and Beretta *et al.* [24, 34] the general form of a non-equilibrium framework is a combination of both irreversible relaxation and reversible symplectic dynamics. If written in the generalized form of the Ginzburg-Landau equation [20, 34], the equation of motion takes the following form:

$$\frac{d}{dt}\phi(t) = X^H_{\phi(t)} + Y^H_{\phi(t)} \tag{7.1}$$

where $\phi(t)$ represents the state evolution trajectory and $X^H_{\phi(t)}$ and $Y^H_{\phi(t)}$ are functions of the system state $\phi(t)$ and represent the reversible symplectic and irreversible relaxation dynamics, respectively. In the SEAQT framework, the system is defined by the Hamiltonian operator $\hat{H}$, system state is represented by the density operator $\hat{\rho}$, $X^H_{\phi(t)}$ follows the Schrödinger equation, and $Y^H_{\phi(t)}$ is derived from the SEA principle. To describe the evolutionary process, conservation laws are explicitly required in order to construct the equation of motion, which is given by [42]

$$\frac{d\hat{\rho}}{dt} = \frac{1}{i\hbar}[\hat{\rho}, \hat{H}] + \frac{1}{\tau}\hat{D} \tag{7.2}$$

where the first term is the Schrödinger term, and the second the dissipation term. If the system is in a pure (zero-entropy) state, $\hat{\rho}\hat{\rho} = \hat{\rho}$, and the equation of motion reverts back to the Schrödinger equation of quantum mechanics. If the system is in a so-called mixed (nonzero-entropy) state and $\hat{\rho}$ is diagonal in the energy eigenstate basis, $\hat{H}$ commutes with $\hat{\rho}$ and the Schrödinger term goes to zero even though $\hat{\rho}$ may not be a Maxwellian distribution among the energy eigenlevels. The state evolution of such a mixed-state operator cannot be captured by the Schrödinger term and is instead given by the second term to the right of the equals, the dissipation term, which captures the probability redistribution towards the Maxwellian distribution. The dissipation term is constructed

using a set of operators called the 'generators of the motion'. Each generator corresponds to one of the conservation laws to which the system is subjected. For example, an isolated, non-reacting system is subject to two conservation laws, probability normalization and energy conservation, so that the generators of the motion are $\{\hat{I}, \hat{H}\}$. For the case when $\hat{\rho}$ is diagonal in the energy eigenstate basis, the equation of motion takes the form [28]

$$\frac{dp_j}{dt} = \frac{1}{\tau} \frac{\begin{vmatrix} -p_j \ln p_j & p_j & \epsilon_j p_k \\ \langle s \rangle & 1 & \langle e \rangle \\ \langle es \rangle & \langle e \rangle & \langle e^2 \rangle \end{vmatrix}}{\begin{vmatrix} 1 & \langle e \rangle \\ \langle e \rangle & \langle e^2 \rangle \end{vmatrix}} = \frac{1}{\tau} D_j(\mathbf{p}) \tag{7.3}$$

where p_j is the diagonal term of $\hat{\rho}$ in the energy eigenstates basis and represents the probability of the system being in the eigenstate associated with the j^{th} energy eigenlevel. Furthermore, $\mathbf{p}$ represents the vector $\{p_j\}$, $\langle \cdot \rangle$ is the expectation value of the property given $\hat{\rho}$, and τ is the relaxation time.

7.2.2 System description in phase space

Within the SEAQT framework, state space is most generally assumed to be a Hilbert space. Nonetheless, within this framework [24, 34], state space can also be represented using phase space for classical/semi-classical systems. For the purposes of this paper, the second choice is made since it facilities the inclusion of volume as an intensive property in the description of non-equilibrium state.

Now, consider that the system contains N particles with spin degrees of freedom. The microstate of the system is decided by the position, momentum and spin of every particle, so that the system microstate is labeled by $7N$ properties $\{p_{x,i}, q_{x,i}, p_{y,i}, q_{y,i}, p_{z,i}, q_{z,i}, s_i\}$, where $i = 1, 2, ..., N$. By defining a map from the microstate to the system macroscopic property (i.e., a bundle structure [20, 34]), each microstate gives a quartet of macroscopic properties , which defines a macrostate. The four properties are particle number (N), energy (e), volume (v) and magnetization (m). The number of microstate with the macroscopic property in the range $e < e' < e + de$, $v < v' < v + dv$ and $m < m' < m + dm$ is represented by $\Omega(N, e', v', m')dedvdm$, which is the

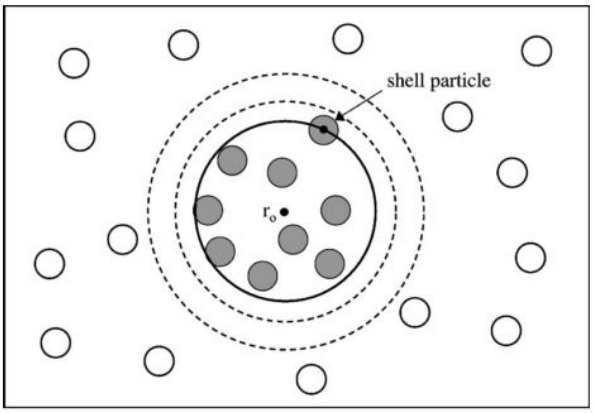

Figure 7.1. Definition of volume for a microstate in configuration space using a “shell particle". Reprinted with permission from [120] Copyright (2001) by the American Physical Society.

density of states. In defining the bundle projection from the space of the microstate to that of the macrostate, the total energy and total magnetization can be defined by

$$e = \sum_{i=1}^{N} (\frac{p_{x,i}^2}{2m_i} + \frac{p_{y,i}^2}{2m_i} + \frac{p_{z,i}^2}{2m_i}) \tag{7.4}$$

$$m = \sum_{i=1}^{N} s_i \tag{7.5}$$

A unique specification of the exact volume for any given microstate is of great significance to an accurate definition of macrostate. Classically, the volume for a given microstate is given through the concept of a ‘shell particle’, which can prevent redundancy in counting the configurations for one macrostate.

In Fig. 7.1, r_0 is the location of the center of mass. The volume uses a spherical shape and the boundary is decided by the ‘shell particle’. All the N particles (the shaded particles) of the system are in the volume $v + dv$ and at least one particle is within the shell volume dv, which describes the outer boundary of the volume v. In this way, the boundary of the system’s volume is the solid line, which is a unique choice among all the possible other boundary choices (dashed lines) that could be made that contain the N particles . For further discussion, the reader is refereed to [120–123].

7.2.3 SEAQT equation of motion

The SEAQT equation of motion in microstate space (phase space) takes the form

$$\frac{d\rho(p,q,s)}{dt} = \{\rho(p,q,s), H\} + \frac{1}{\tau} D(p,q,s) \tag{7.6}$$

where p, q, and s represents all the $7N$ variables in phase space and H is the free particle kinetic energy given by

$$H = \sum_{i=1}^{N} \left(\frac{p_{x,i}^2}{2m_i} + \frac{p_{y,i}^2}{2m_i} + \frac{p_{z,i}^2}{2m_i}\right) \tag{7.7}$$

The first term on the right in Eq. (7.6) is the symplectic term (Louisville's equation), while the second is the irreversible relaxation term. The former expressed in terms of the Poisson bracket is written as

$$\begin{aligned} \{\rho(p,q,s), H\} &= \sum_{i=1}^{3N} \left(\frac{\partial \rho}{\partial q_i}\frac{\partial H}{\partial p_i} - \frac{\partial \rho}{\partial p_i}\frac{\partial H}{\partial q_i}\right) = \sum_{i=1}^{3N} \frac{\partial \rho}{\partial q_i}\frac{\partial H}{\partial p_i} \\ &= \sum_{i=1}^{N} \left(\frac{p_{x,i}}{m_i}\frac{\partial \rho}{\partial q_{x,i}} + \frac{p_{y,i}}{m_i}\frac{\partial \rho}{\partial q_{y,i}} + \frac{p_{z,i}}{m_i}\frac{\partial \rho}{\partial q_{z,i}}\right) \end{aligned} \tag{7.8}$$

In order to arrive at the equation of motion in macrostate space from which macroscopic properties can directly be obtained, the probability distribution $\tilde{\rho}$ in energy and volume is defined as

$$\tilde{\rho}(e,v)dedv = \int_{e<e'<e+de, v<v'<v+dv} \rho(p,q,s)dpdqds \tag{7.9}$$

For the specific class of initial condition studied here in which a generalization of the equal-probability condition for the micro-ensemble holds, the following holds as a good approximation for an isotropic non-equilibrium state:

$$\rho(p,q,s) = \frac{\tilde{\rho}(e,v)}{\Omega(e,v)} \tag{7.10}$$

where

$$\Omega(e,v)dedv = \int_{e<e'<e+de, v<v'<v+dv} dpdqds \tag{7.11}$$

is the number of microstates satisfy the conditions $e < e' < e + de$ and $v < v' < v + dv$. As a result, the equation of motion in the energy and volume distribution takes the form

$$\frac{d\tilde{\rho}(e,v)}{dt} = \frac{1}{dedv}\int \{\rho(p,q,s), H\} dpdqds + \frac{1}{\tau dedv}\int D(p,q,s) dpdqds \tag{7.12}$$

Under the equal-probability condition

$$\rho(p,q,s) = \rho(-p,q,s) \tag{7.13}$$

the relation

$$\{\rho(p,q,s), H\} dpdqds = -\{\rho(-p,q,s), H\} dpdqds \tag{7.14}$$

holds. In addition, due to the symmetry of the equation of motion, Eq. (7.6), the equal-probability condition holds during the time evolution. Thus, the integral of the Poisson bracket term vanishes at the initial condition consistent with the equal-probability condition. The equation of motion, Eq. (7.12), thus, reduces to the form

$$\frac{d\tilde{\rho}(e,v)}{dt} = \frac{1}{\tau dedv}\int D(p,q,s) dpdqds \tag{7.15}$$

and the evolution in macrostate space reveals the irreversible process without the influence of the symplectic term, since it does not affect the system entropy under the conditions specified.

7.2.4 Non-equilibrium state and evolution description: Hypo-equilibrium

The thermodynamic features of the non-equilibrium relaxation process generated by the SEAQT framework have a number of useful characteristics, which lead to a complete description of non-equilibrium state and the general fundamental definition of non-equilibrium intensive properties for that state yielding to Eq. (7.10). This description is based on the key concept of hypo-equilibrium state. In this section, the theory is presented using a system whose state can be characterized by energy and volume. For proofs and a more detailed discussion, the reader is referred to [14, 17].

Any initial thermodynamic state of a system (system A or B) can be represented by a probability distribution $\rho(p,q,s)$ among all of the accessible microstates in phase space (represented by

$\mathcal{K}$). If an initial state satisfies the equal-probability condition of Eq. (7.10), the system state can be represented by a probability distribution $\tilde{\rho}(e, v, m)$ among the accessible set of macrostate (represented by $\mathcal{H}$ and and density of states $\Omega(e, v, m)$), where the constant property N is omitted for a closed system . Given an initial thermodynamic state $\tilde{\rho}(e, v, m)$, the macrostate set $\mathcal{H}$ can be separated into M sets (subsystems), and the division satisfies $\mathcal{H} = \bigcup_{i\in\mathcal{I}} \mathcal{H}_i$ and $\mathcal{H}_i \cap \mathcal{H}_j = \emptyset$, where $\mathcal{I}$ is a set of indices, which can be a countable or uncountable set. If the probability distribution in each subsystem yields to a canonical distribution for e and v, i.e.,

$$\forall i \in \mathcal{I},\ \tilde{\rho}(e^i, v^i, m^i) = \frac{\tilde{p}^i}{\Lambda^i(\beta^i, \theta^i)} e^{-\beta^i e^i - \theta^i e^i},\ (e^i, v^i, m^i) \in \mathcal{H}_i \tag{7.16}$$

the system is designated as being in an M^{th}-order e-v hypo-equilibrium state. Based on this definition, it can be shown that any thermodynamic state of the system is a hypo-equilibrium state in $\mathcal{H}$ with order M where M is less than or equal to the number of accessible system macrostates [14, 17]. A hypo-equilibrium state of order 1 corresponds to a state in stable equilibrium. In Eq. (7.16), (e^i, v^i, m^i) is the macrostate in $\mathcal{H}_i$, β^i and θ^i are parameters that correspond to the Lagrange multipliers of the energy and volume constraints, $\tilde{p}^i$ is the total probability in subsystem i, and $\Lambda^i(\beta^i, \theta^i)$ is the partition function of the subsystem with parameters β^i and θ^i. Note, that since spin is not conserved, there is no corresponding Lagrange multiplier and, thus, no parameter associated with the magnetization m^i. Furthermore, to be complete, $\beta^i = 0$ and $\theta^i = 0$ if $\#(\mathcal{H}_i) = 1$ (i.e., there is a single macrostate) and $\theta^i = 0$ if $\#(\mathcal{H}_i) = 2$. In addition, the $\#(\mathcal{H}_i)$ can be infinite so that any non-equilibrium state yielding to Eq. (7.10) can be regarded as a specific M^{th}-order e-v hypo-equilibrium state. Now, the partition function is written as

$$\Lambda^i(\beta^i, \theta^i) = \int_{\mathcal{H}^i} de^i dv^i dm^i \Omega(e^i, v^i, m^i) e^{-\beta^i e^i - \theta^i v^i} = \int_{\mathcal{K}^i} e^{-\beta^i e^i - \theta^i v^i} dpdqds \tag{7.17}$$

where the integral to the right of the first equal sign is over macrostate set $\mathcal{H}_i$, while that to the right of the second equal sign is over the microstate set $\mathcal{K}_i$, which contains all of the microstates leading to the macrostates in $\mathcal{H}_i$.

For a given M^{th}-order e-v hypo-equilibrium state, the intensive properties of the subsystems can be represented by β^i and θ^i, or equivalently using temperature and pressure by

$$T^i = \frac{1}{k_b \beta^i}, \quad P^i = \theta^i T^i \tag{7.18}$$

A M^{th}-order e-v hypo-equilibrium state can then be represented by a division $\{\mathcal{H}_i(\mathcal{K}_i),\ i \in \mathcal{I}\}$ of a system's accessible macrostate (microstate) set and a corresponding triplet set $\{(\tilde{p}^i, \beta^i, \theta^i),\ i \in \mathcal{I}\}$, where $\mathcal{I}$ is a parameter set that can be discrete or continuous. The intensive property set $\{(T^i, P^i),\ i \in \mathcal{I}\}$ is a generalization of the definition of intensive property at stable equilibrium (T^{eq}, P^{eq}). Li and von Spakovsky [14, 17] prove that if a system begins in an M^{th}-order hypo-equilibrium state, it will remain in an M^{th}-order hypo-equilibrium state throughout the state evolution as long as the same subsystem division is maintained. Thus, the time evolution of the distribution takes the form

$$\forall i \in \mathcal{I},\ (e^i, v^i, m^i) \in \mathcal{H}_i,\ \tilde{\rho}(e^i, v^i, m^i) = \frac{\tilde{p}^i(t)}{\Lambda^i(\beta^i(t), \theta^i(t))} e^{-\beta^i(t)e^i - \theta^i(t)e^i} \tag{7.19}$$

The intensive property set $\{(T^i(t), P^i(t)),\ i \in \mathcal{I}\}$ is also well defined throughout the entire evolution as is the triplet set $\{(\tilde{p}^i(t), \beta^i(t), \theta^i(t)),\ i \in \mathcal{I}\}$.

7.3 SEAQT for interacting systems

7.3.1 SEAQT for interacting systems

The equation of motion is designed to study the non-equilibrium relaxation process of an isolated system. However, since interacting systems can be viewed as a composite isolated non-equilibrium system of subsystems whose interactions cause the relaxation process of the composite, the SEAQT equation of motion can be used to determine the evolution of these interacting systems as well.

Now, consider two interacting systems (system A and system B). The composite system is not in stable equilibrium, and its state is represented by the probability distributions $\{\rho^a(p^a, q^a, s^a)\}$ for system A and $\{\rho^b(p^b, q^b, s^b)\}$ for system B together. There are four conservation laws, which must be satisfied: probability normalization of system A, probability normalization of system B, energy conservation of the composite system, and particle number conservation of the composite system. Based on SEA and the conservation laws, $\{I^a, I^b, E, V\}$ serve as the generators of the motion and the equation of motion for system A takes the form [17, 18, 42]

$$\frac{d\rho^a(p^a, q^a, s^a)}{dt} = \{\rho^a(p, q, s), H\} + \frac{1}{\tau} D^a(p, q, s) \tag{7.20}$$

where

$$H = H^a + H^b = \sum_{i=1}^{N_a}(\frac{p_{x,i}^2}{2m_i^a} + \frac{p_{y,i}^2}{2m_i^a} + \frac{p_{z,i}^2}{2m_i^a}) + \sum_{i=1}^{N_b}(\frac{p_{x,i}^2}{2m_i^b} + \frac{p_{y,i}^2}{2m_i^b} + \frac{p_{z,i}^2}{2m_i^b}) \tag{7.21}$$

and

$$D^a(p,q,s) = \frac{\begin{vmatrix} -\rho^a \ln \rho^a & \rho^a & 0 & e^a\rho^a & v^a\rho^a \\ \langle s\rangle^a & 1 & 0 & \langle e\rangle^a & \langle v\rangle^a \\ \langle s\rangle^b & 0 & 1 & \langle e\rangle^b & \langle v\rangle^b \\ \langle es\rangle & \langle e\rangle^a & \langle e\rangle^b & \langle e^2\rangle & \langle ev\rangle \\ \langle vs\rangle & \langle v\rangle^a & \langle v\rangle^b & \langle ev\rangle & \langle v^2\rangle \end{vmatrix}}{\begin{vmatrix} 1 & 0 & \langle e\rangle^a & \langle v\rangle^a \\ 0 & 1 & \langle e\rangle^b & \langle v\rangle^b \\ \langle e\rangle^a & \langle e\rangle^b & \langle e^2\rangle & \langle ev\rangle \\ \langle v\rangle^a & \langle v\rangle^b & \langle ev\rangle & \langle v^2\rangle \end{vmatrix}} \tag{7.22}$$

Here $\rho^{a(b)}$ is the probability distribution in phase space of system $a(b)$, $(p^{a(b)}, q^{a(b)}, s^{a(b)})$ are the variables in system A(B), and $(p,q,s) = (p^a, q^a, s^a, p^b, q^b, s^b)$ are all the variables in composite system. The macroscopic properties $e^a = e^a(p^a, q^a, s^a)$ and $v^a = v^a(p^a, q^a, s^a)$ are both functions of the microstate (p^a, q^a, s^a). $\langle\cdot\rangle^{a(b)}$ is the expectation value of a property in system A(B), and $\langle\cdot\rangle = \langle\cdot\rangle^a + \langle\cdot\rangle^b$ is the expectation value of the total property of the composite system. The numerator of the fraction to the right of the equals can be expanded by the elements of the first row and their cofactors such that

$$\det = -\rho^a \ln \rho^a C_1 + \rho^a C_2^a + e^a\rho^a C_3 + v^a\rho^a C_4 \tag{7.23}$$

where C_1, C_2^a, C_2^b, C_3, and C_4 are the determinants of the cofactors of the first line of the numerator's determinant. By defining

$$\frac{C_2^a}{C_1} = -\alpha_a, \quad \frac{C_2^b}{C_1} = -\alpha_b, \quad \frac{C_3}{C_1} = -\beta, \quad \frac{C_4}{C_1} = -\theta \tag{7.24}$$

the equation of motion of the two systems A and B takes the form

$$\frac{d\rho^a}{dt} = \{\rho^a, H\} + \frac{1}{\tau}(-\rho^a \ln \rho^a - \rho^a \alpha_a - e^a \rho^a \beta - v^a \rho^a \theta) \tag{7.25}$$

$$\frac{d\rho^b}{dt} = \{\rho^a, H\} + \frac{1}{\tau}(-\rho^b \ln \rho^b - \rho^b \alpha_b - e^b \rho^b \beta - v^b \rho^b \theta) \tag{7.26}$$

where β and θ are the same in the equations of motion for ρ^a and ρ^b, α_a specific to the equation of motion for ρ^a, and α_b is specific to the equation of motion for ρ^b.

Under the equal-probability condition

$$\rho^a(p^a, q^a, s^a) = \frac{\tilde{\rho}^a(e^a, v^a)}{\Omega^a(e^a, v^a)} \tag{7.27}$$

$$\rho^b(p^b, q^b, s^b) = \frac{\tilde{\rho}^b(e^b, v^b)}{\Omega^b(e^b, v^b)} \tag{7.28}$$

the Poisson bracket vanishes by integrating over all the microstates of the energy e and the volume v, and the equation of motion in energy-volume distribution is written for each system A and B as

$$\frac{d\tilde{\rho}^a}{dt} = \frac{1}{\tau}(-\tilde{\rho}^a \ln \frac{\tilde{\rho}^a}{\Omega^a} - \tilde{\rho}^a \alpha_a - e^a \tilde{\rho}^a \beta - v^a \tilde{\rho}^a \theta) \tag{7.29}$$

$$\frac{d\tilde{\rho}^b}{dt} = \frac{1}{\tau}(-\tilde{\rho}^b \ln \frac{\tilde{\rho}^b}{\Omega^b} - \tilde{\rho}^b \alpha_b - e^b \tilde{\rho}^b \beta - v^b \tilde{\rho}^b \theta) \tag{7.30}$$

In the application to an engine cycle, system B is assumed to be a temperature reservoir whose properties remain unchanged during its interactions with system A. The following discussion, thus, focuses on the time evolution of system A.

7.3.2 Equation of motion for two systems in hypo-equilibrium states

In order to study how a system in a non-equilibrium state evolves in a engine cycle, one of two interacting systems, namely, system A is initialized in a M^{th}-order e-v hypo-equilibrium state. The distribution of the macrostate $(e^{a,i}, v^{a,i}, m^{a,i}) \in \mathcal{H}_i^a$ for subsystem i ($i \in \mathcal{I}^a$) of system A is given by

$$\tilde{\rho}^{a,i}(e^{a,i}, v^{a,i}, m^{a,i}) = \frac{\tilde{p}^{a,i}}{\Lambda^{a,i}(\beta^{a,i}, \theta^{a,i})} e^{-\beta^{a,i} e^{a,i} - \theta^{a,i} e^{a,i}} \tag{7.31}$$

where the probability in the i^{th} subsystem (i.e., subsystem) of system A ($\tilde{p}^{a,i}$) and the two intensive properties ($\beta^{a,i}$ and $\theta^{a,i}$) define the state of the i^{th} subsystem of system A and $\Lambda^{a,i}$, which is the

partition function for the i^{th} subsystem, is expressed as

$$\begin{aligned}\Lambda^{a,i}(\beta^{a,i},\theta^{a,i}) &= \int\limits_{\mathcal{H}^{a,i}} de^{a,i}dv^{a,i}dm^{a,i}\Omega(e^{a,i},v^{a,i},m^{a,i})e^{-\beta^{a,i}e^{a,i}-\theta^{a,i}v^{a,i}} \\ &= \int_{\mathcal{K}^{a,i}} e^{-\beta^{a,i}e^{a,i}-\theta^{a,i}v^{a,i}}dpdqds \end{aligned} \tag{7.32}$$

Defining

$$\alpha^{a,i} = \ln\Lambda^{a,i}(\beta^{a,i},\theta^{a,i}) - \ln\tilde{p}^{a,i} \tag{7.33}$$

so the i^{th} subsystem state can be represented by

$$\tilde{\rho}^{a,i}(e^{a,i},v^{a,i},m^{a,i}) = e^{-\alpha^{a,i}}e^{-e^{a,i}\beta^{a,i}}e^{-v^{a,i}\theta^{a,i}} \tag{7.34}$$

With the additional property, i.e., the magnetization $m^{a,i}$, considered in the argument of $\tilde{\rho}$ in Eq. (7.34), the equation of motion (Eq. (7.29)) takes the form

$$\frac{d\tilde{\rho}^{a,i}}{dt} = \frac{1}{\tau}(-\tilde{\rho}^{a,i}\ln\frac{\tilde{\rho}^{a,i}}{\Omega^{a,i}} - \tilde{\rho}^{a,i}\alpha_a - e^{a,i}\tilde{\rho}^{a,i}\beta - v^{a,i}\tilde{\rho}^{a,i}\theta) \tag{7.35}$$

where another superscription 'i' indicates the i^{th} subsystem. As is proven in [14, 17], if the initial state is a hypo-equilibrium state, the system remains in an hypo-equilibrium state provided the same subsystem division is maintained. As a consequence, the time evolution of the distribution of the i^{th} subsystem of A takes the form

$$\tilde{\rho}^{a,i}(t) = e^{-\alpha^{a,i}(t)}e^{-e^{a,i}\beta^{a,i}(t)}e^{-v^{a,i}\theta^{a,i}(t)} \tag{7.36}$$

where $\alpha^{a,i}(t),\ \beta^{a,i}(t),\ \theta^{a,i}(t)$ are the solution of

$$\frac{d\alpha^{a,i}}{dt} = -\frac{1}{\tau}(\alpha^{a,i}-\alpha_a) \tag{7.37}$$

$$\frac{d\beta^{a,i}}{dt} = -\frac{1}{\tau}(\beta^{a,i}-\beta) \tag{7.38}$$

$$\frac{d\theta^{a,i}}{dt} = -\frac{1}{\tau}(\theta^{a,i}-\theta) \tag{7.39}$$

By solving these three equations of motions for each i^{th} subsystem, the time evolution of system A is obtained. The parameters β and θ, which are determined by Eq. (7.24), are expressed using

the intensive and extensive properties of both system A and system B.

7.3.3 Interacting with a reservoir

Assuming system B, which is in a stable equilibrium state with parameters β_r and θ_r to have a volume and energy much larger than that of system A, [17] proves that the parameters in Eqs. (7.38) and (7.39) take the form

$$\beta = \beta_r, \quad \theta = \theta_r \tag{7.40}$$

so that the equations of motion of the i^{th} subsystem of system A take the form

$$\frac{d\alpha^{a,i}}{dt} = -\frac{1}{\tau}(\alpha^{a,i} - \alpha_a) \tag{7.41}$$

$$\frac{d\beta^{a,i}}{dt} = -\frac{1}{\tau}(\beta^{a,i} - \beta_r) \tag{7.42}$$

$$\frac{d\theta^{a,i}}{dt} = -\frac{1}{\tau}(\theta^{a,i} - \theta_r) \tag{7.43}$$

where α_a determined from an expansion of the determinants that define the numerator and denominator of Eq. (7.24), The result using Eq. (7.40) reduces to the following:

$$\alpha_a = \sum_i \alpha^{a,i}\tilde{p}^i + \sum_i \langle e\rangle^{a,i}\beta^{a,i} + \sum_i \langle v\rangle^{a,i}\theta^{a,i} - \beta_r\langle e\rangle^a - \theta_r\langle v\rangle^a \tag{7.44}$$

Thus, the properties of the reservoir (system B) only appear in the equation of motion of system A in the form of the reservoir parameters β_r and θ_r.

7.4 Cycle of the system undergoing a non-quasi-equilibrium process

7.4.1 System description and initial state

The cyclic process is studied using a non-equilibrium system (system A) interacting with a series of reservoirs (systems B). System A consists of approximately 1 mole Helium-3 in a piston-cylinder with variable energy and volume interacting with a different temperature reservoir at each instant of time t. The reservoir at a given t has the intensive properties $(T(t), P(t))$, where T is the

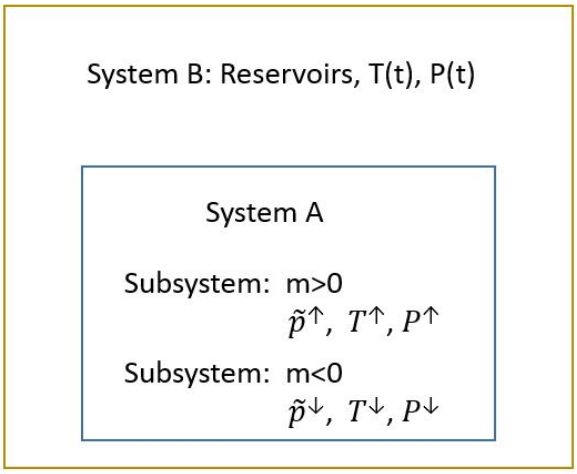

Figure 7.2. System model.

temperature and P the pressure. At any given instant of time, the interaction between system A and system B keeps the total energy and volume of the composite system of A and B conserved. When the temperature is not too low, Helium-3 performs as Maxwellian particle.

In order to simplify the discussion, an initial condition, whose analytical solution is available, is used. The number of particles in system A is assumed to be odd, and the initial state of system A is chosen to be a 2^{nd}-order e-v hypo-equilibrium state. The corresponding two subspaces are chosen to be the set of all macrostate with $m > 0$ so that $\{(e^{\uparrow}, v^{\uparrow}, \uparrow)\}$ and the set of all macrostate with $m < 0$ so that $\{(e^{\downarrow}, v^{\downarrow}, \downarrow)\}$. Higher order e-v hypo-equilibrium state can also be studied, and for more details, the reader is referred to [17]. The initial state can be represented by the macrostate probability distributions of each of the subspaces, i.e., by $\{\tilde{\rho}^{\uparrow}\}$ and $\{\tilde{\rho}^{\downarrow}\}$, where

$$\tilde{\rho}^{\uparrow} = \frac{\tilde{p}^{\uparrow}}{\Lambda^{\uparrow}(\beta^{\uparrow}, \theta^{\uparrow})} e^{-e^{\uparrow}\beta^{\uparrow}} e^{-v^{\uparrow}\theta^{\uparrow}} \tag{7.45}$$

$$\tilde{\rho}^{\downarrow} = \frac{\tilde{p}^{\downarrow}}{\Lambda^{\downarrow}(\beta^{\downarrow}, \theta^{\downarrow})} e^{-e^{\downarrow}\beta^{\downarrow}} e^{-v^{\downarrow}\theta^{\downarrow}} \tag{7.46}$$

Here $(\tilde{p}^{\uparrow}, \beta^{\uparrow}, \theta^{\uparrow})$ is the parameter triplet for the $m > 0$ subspace and $(\tilde{p}^{\downarrow}, \beta^{\downarrow}, \theta^{\downarrow})$ for the $m < 0$ subspace defined in *Section* 7.3.2. Both the partition function for the $m > 0$ subspace and that for the $m < 0$ subspace share the same functional form Λ_0 so that

$$\Lambda^{\uparrow(\downarrow)}(\beta^{\uparrow(\downarrow)}, \theta^{\uparrow(\downarrow)}) = \Lambda_0(\beta^{\uparrow(\downarrow)}, \theta^{\uparrow(\downarrow)}) \tag{7.47}$$

while the partition function for the total system is given by

$$\Lambda^{total}(\beta,\theta) = \Lambda^{\uparrow}(\beta,\theta) + \Lambda^{\downarrow}(\beta,\theta) = 2\Lambda_0(\beta,\theta) \tag{7.48}$$

where

$$\Lambda^{total}(\beta,\theta) = \int_{\mathcal{H}} dedvdm\Omega(e,v,m)e^{-\beta e-\theta v} = \int_{\mathcal{K}} e^{-\beta e-\theta v}dpdqds \tag{7.49}$$

Note that the evaluation of the partition function is based on the concept of the density of volume state [124] for an isothermal-isobaric ensemble partition function [120–123]. Thus, using the formulation provided in [121]

$$\Lambda^{total}(\beta,\theta) = \int_v \left(\frac{\partial \ln Q}{\partial v}\right)_{T,N} Qe^{-\theta v}dv = \int_v \left(\frac{\partial Q}{\partial v}\right)_{T,N} e^{-\theta v}dv = \int_v e^{-\theta v}dQ \tag{7.50}$$

where Q is the canonical ensemble partition function for a system containing N particles in a volume v at temperature T. For Maxwellian particles with spin degeneracy of 2, Q takes the following form by modifying the non-degenerate form given in [120]:

$$Q = \frac{2^N}{N!}(\frac{\sqrt{2\pi m}}{h})^{3N} v^N \beta^{-\frac{3}{2}N} \tag{7.51}$$

and Λ^{total} takes the form

$$\Lambda^{total}(\beta,\theta) = \frac{2^N}{(N-1)!}(\frac{\sqrt{2\pi m}}{h})^{3N}\beta^{-\frac{3}{2}N}\int_0^{\infty} v^{N-1}dve^{-\theta v} = \frac{2^N}{N!}(\frac{\sqrt{2\pi m}}{h})^{3N} v^N \beta^{-\frac{3}{2}N}\theta^{-N} \tag{7.52}$$

where m is the mass of a particle. Furthermore, the properties of one subsystem of system A and the properties of the entire system A are written as

$$\langle e\rangle^{\uparrow(\downarrow)} = p^{\uparrow(\downarrow)}\left(-\frac{1}{\Lambda^{\uparrow(\downarrow)}}\frac{\partial\Lambda^{\uparrow(\downarrow)}}{\partial\beta}\right) = \frac{3N\tilde{p}^{\uparrow(\downarrow)}}{2\beta^{\uparrow(\downarrow)}} \tag{7.53}$$

$$\langle V\rangle^{\uparrow(\downarrow)} = \tilde{p}^{\uparrow(\downarrow)}\left(-\frac{1}{\Lambda^{\uparrow(\downarrow)}}\frac{\partial\Lambda^{\uparrow(\downarrow)}}{\partial\theta}\right) = \frac{N\tilde{p}^{\uparrow(\downarrow)}}{\theta^{\uparrow(\downarrow)}} \tag{7.54}$$

$$\langle e\rangle = \langle e\rangle^{\uparrow} + \langle e\rangle^{\downarrow} \tag{7.55}$$

$$\langle v\rangle = \langle v\rangle^{\uparrow} + \langle v\rangle^{\downarrow} \tag{7.56}$$

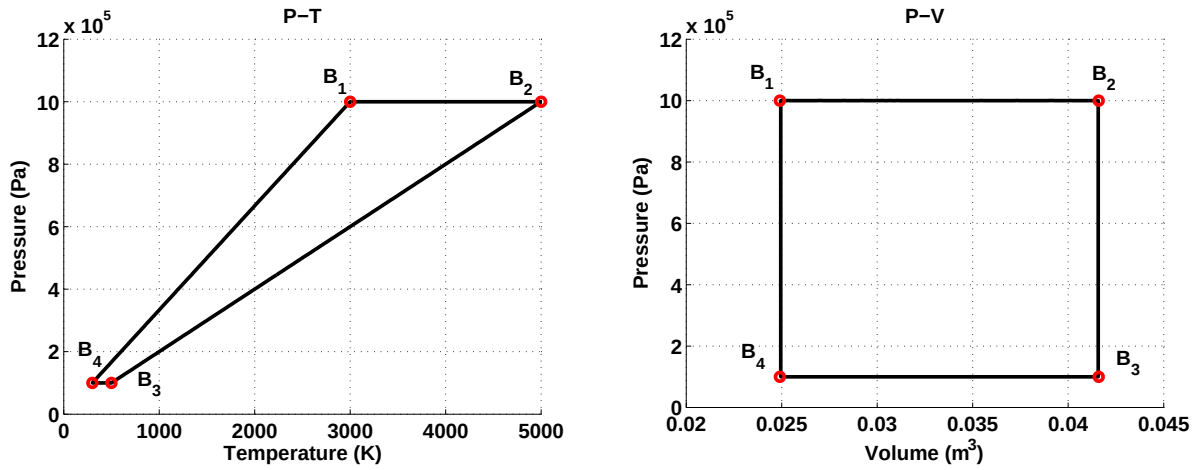

Figure 7.3. Reservoir locations on a P-T diagram and a P-V diagram. B_1 to B_4 represented the stable equilibrium state of the system at different (T, P). B_1: (3000K, 10^6Pa). B_2: (5000K, 10^6Pa). B_3: (500K, 10^5Pa). B_4: (300K, 10^6Pa).

Since the time evolution of a reservoir due to its interaction with system A is negligible, the study focuses on the evolution of system A provided by the equation of motion for system A (Eqs. (7.41) to (7.43)).

7.4.2 Reservoir

The reservoir series $(T(t), P(t))$ is defined to be a periodic function of time, with period τ_r where τ_r is the characteristic time of system B, i.e.,

$$T(t) = T(t - \tau_r) \tag{7.57}$$

$$P(t) = P(t - \tau_r) \tag{7.58}$$

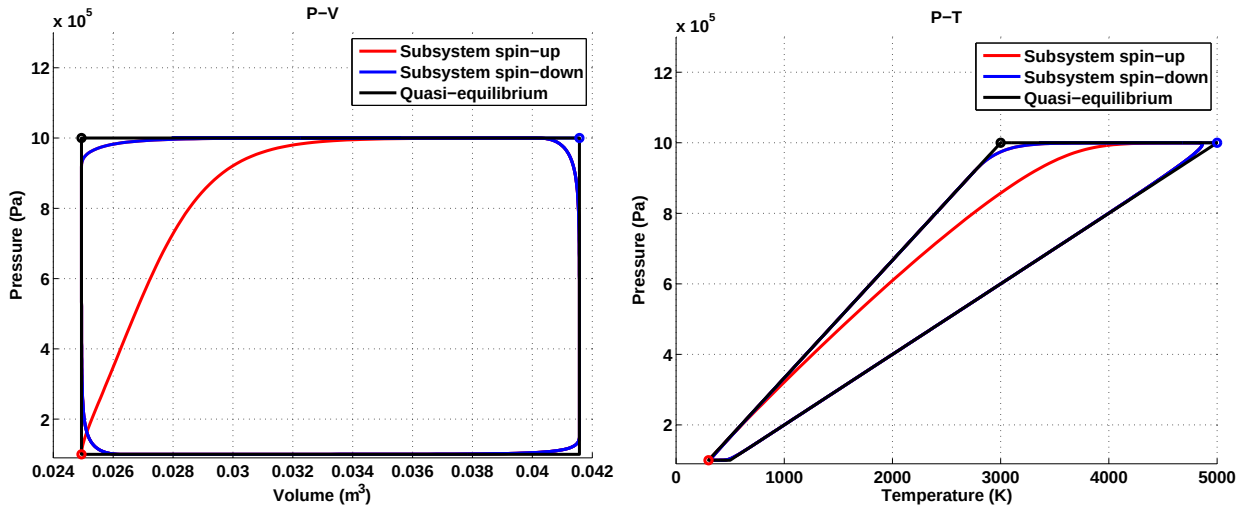

Figure 7.4. P-T and P-V cycle diagram for $\tau_r/\tau = 50$. The red/blue/black dots represent the initial states for the $m > 0$ subsystem, the $m < 0$ subsystem and system B, respectively. System B evolves clockwise.

For any given period τ_r, $(T(t), P(t))$ take the form

$$P(t) = \begin{cases} P_1 & \text{if } 0 \leq t < 0.25\tau_r \\ P_1 + (P_2 - P_1)\frac{t-0.25\tau_r}{0.25\tau_r} & \text{if } 0.25\tau_r \leq t < 0.5\tau_r \\ P_2 & \text{if } 0.5\tau_r \leq t < 0.75\tau_r \\ P_2 + (P_1 - P_2)\frac{t-0.75\tau_r}{0.25\tau_r} & \text{if } 0.75\tau_r \leq t < \tau_r \end{cases} \tag{7.59}$$

$$T(t) = \begin{cases} T_1 + (T_2 - T_1)\frac{t}{0.25\tau_r} & \text{if } 0 \leq t < 0.25 \\ P(t)T_2/P_1 & \text{if } 0.25\tau_r \leq t < 0.5\tau_r \\ T_3 + (T_4 - T_3)\frac{t-0.5\tau_r}{0.25\tau_r} & \text{if } 0.5\tau_r \leq t < 0.75\tau_r \\ P(t)T_4/P_2 & \text{if } 0.75\tau_r \leq t < \tau_r \end{cases} \tag{7.60}$$

The trajectory of $(T(t), P(t))$ on a P-T diagram is shown in the left of Fig. 7.3. If the intensive properties of system A were to proceed through a quasi-equilibrium process, its trajectory on a P-V diagram would be that shown in the right of Fig. 7.3.

7.5 Result

The SEAQT model is used to study how a system proceeds through a cycle formed by two constant-pressure and two constant-volume processes. The traditional way is to assume that the system is at stable equilibrium at every instant of time so that it follows the path of a quasi-equilibrium

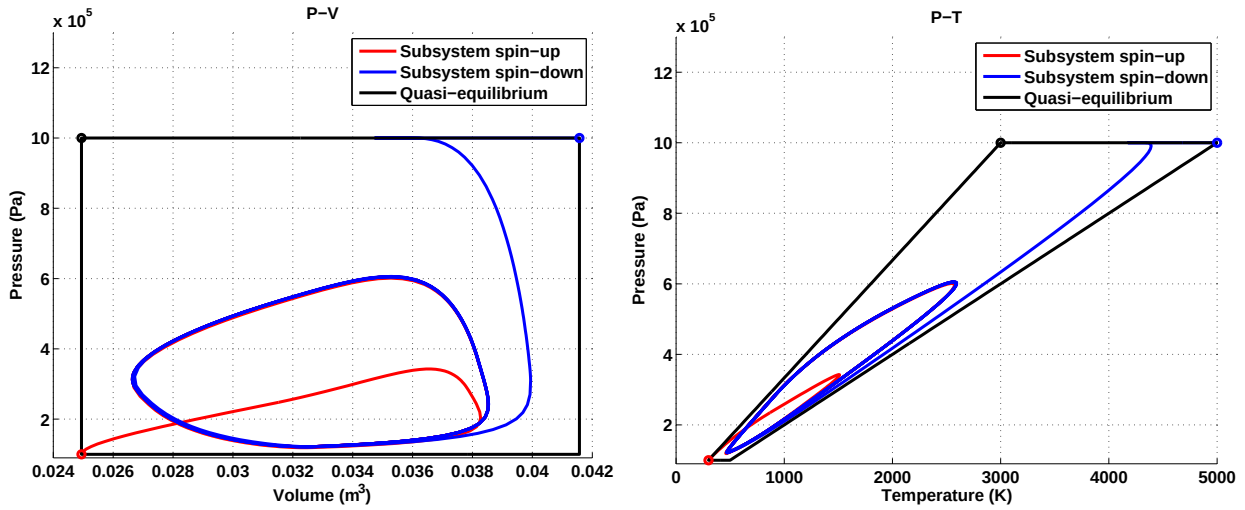

Figure 7.5. P-T and P-V cycle diagram for $\tau_r/\tau = 5$. The red/blue/black dots represent the initial states for the $m > 0$ subsystem, the $m < 0$ subsystem and system B, respectively. System B evolves clockwise.

process. Such a path is represented by the black lines in Figs. 7.3 to 7.6. As shown later, this is the limiting path that system B (i.e., the reservoirs) follows as it changes very, very slowly. In the general case, the non-equilibrium interactions of system A with the reservoir result in a different path. Using the SEAQT non-equilibrium model, three cases with different characteristic times for system B ($\tau_r/\tau = 50, 5, 0.5$) are simulated. The model predictions clearly illustrate that as system B changes more quickly, the behavior of system A departs ever further from the quasi-equilibrium process.

Cycle diagrams for systems A and B are given in Figs. 7.4 to 7.6. Since system is in a non-equilibrium state initially and throughout its state evolution, temperature and pressure are generally not defined. However, using a 2^{nd}-order e-v hypo-equilibrium state description as discussed in *Section* 7.2, the temperature and pressure for each subsystem can be found so that a comparison of the pressure and temperature evolutions for the $m > 0$ subsystem, $m < 0$ subsystem, and reservoir can be made. The contribution to the volume of system A can be calculated for each subsystem. Normalizing by the probabilities of each subsystems, the $m > 0$ subsystem, $m < 0$ subsystem, and system B (reservoirs) evolutions can also be compared on a P-V diagram.

There are two general features can be observed from the P-T and P-V diagrams in Figs. 7.4 to 7.6. The first is that the red and blue lines, which represent the $m > 0$ and $m < 0$ subsystems, respectively, start from two different locations on the diagrams and converge at the end. This represents the process of system A evolving from some non-equilibrium state to stable equilibrium

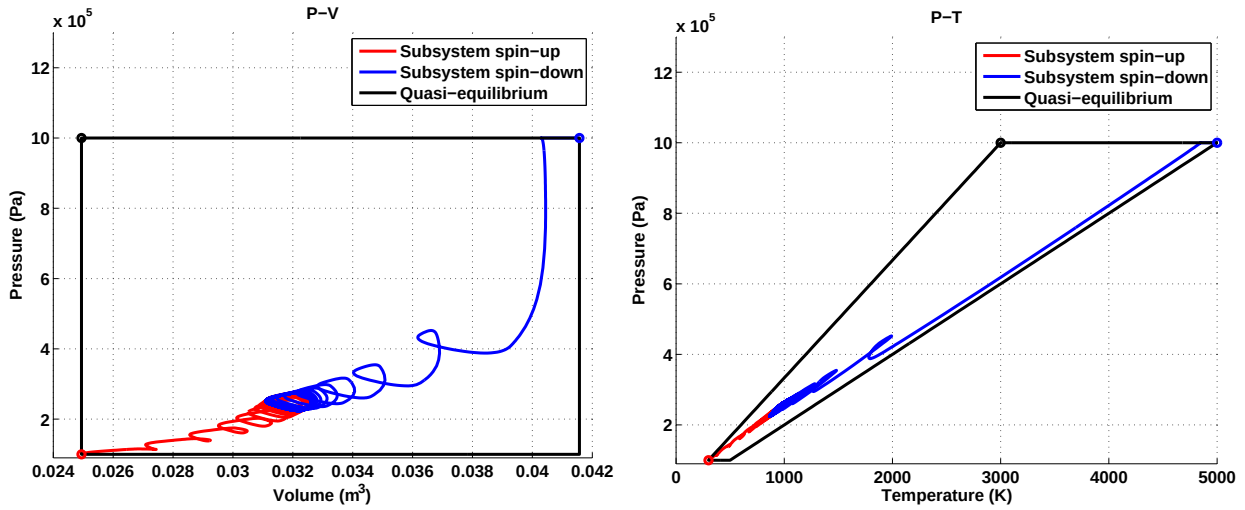

Figure 7.6. P-T and P-V cycle diagram for $\tau_r/\tau = 0.5$. The red/blue/black dots represent the initial states for the $m > 0$ subsystem, the $m < 0$ subsystem and system B, respectively. System B evolves clockwise.

or, equivalently, it is the process that the two subsystems of system A undergo to come to mutual stable equilibrium with each other.

The second general feature is that after the two subsystems arrive at mutual stable equilibrium, the two converged lines (i.e., the red and the blue) can be regarded as the quasi-equilibrium path that system A would follow if each of its states were in stable equilibrium at any instant of time. This path called the end-cycle (i.e., the steady as opposed to transient cycle) is generally different from the cycle path that system B takes. This end-cycle or steady cycle can have a great deal of overlap with the cycle path of system B such as occurs in Fig. 7.3 or it can have almost no overlap such as occurs in Figs. 7.5 and 7.6. Note that the composite system of A and B is in a non-equilibrium state, even one far from equilibrium so that, the interactions between system A and B are not restricted to those in the near-equilibrium region. The difference in the cycles of these two systems results from the fact that they are not in mutual equilibrium and from the fact that the non-equilibrium intensive properties of system A are very different from the equilibrium properties of system B. Furthermore, the ratio of τ_r to τ indicates how strong the interactions between system A and system B are compare to with how fast system B changes its state. If τ_r/τ is sufficeintly large, the interactions between A and B are strong enough to make systems A and B come to mutual stable equilibrium before there is a change in reservoir as seen in Fig. 7.3. In contrast, when this ratio is sufficiently small as in Figs. 7.4 and 7.5, systems A and B are not able to reach mutual stable equilibrium before there is a change in reservoir.

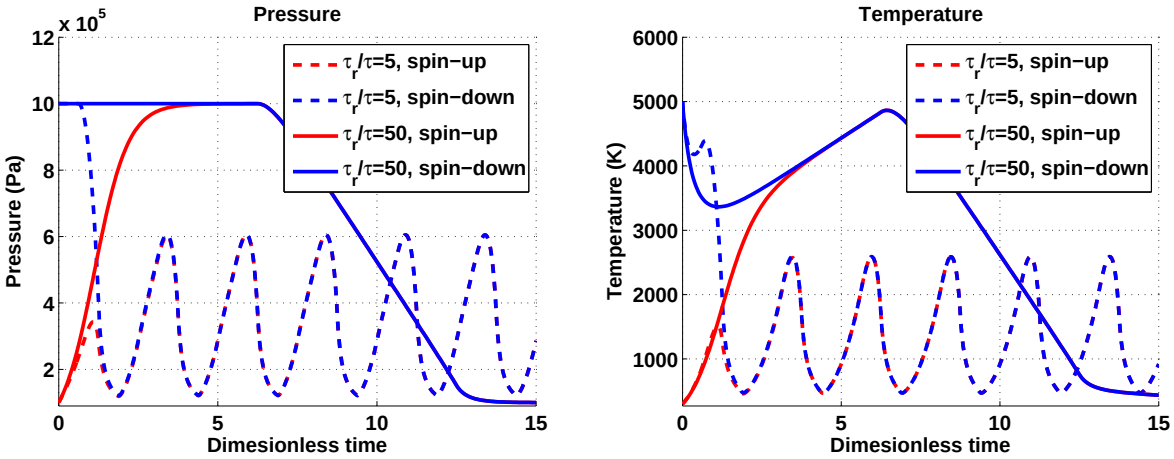

Figure 7.7. Pressure and temperature evolution for $\tau_r/\tau = 50$ and $\tau_r/\tau = 5$.

A comparison across Figs. 7.4 to 7.6 shows how the ratio τ_r/τ influences the end-cycle. When this ratio is small, so is the end-cycle resulting in less work produced by the cycle as indicated by the cycle area on the P-V diagram. In other words, as the characteristic time of the series of reservoirs represented by system B grows smaller, the work done by system A becomes smaller and the loss in work is the difference between the area of the end-cycle and that of the cycle of system B. To achieve a better cyclic device design, the characteristic time of the series of reservoirs should be considerably larger than the characteristic time for the interactions as is the case in Fig. 7.4. Furthermore, for the limiting case when τ_r/τ becomes small as in Fig. 7.6, system A interacts with a fast-changing system B (i.e., series of reservoirs), which is equivalent to the case when system A interacts with a single reservoir, whose intensive properties are the average of the system B cycle. Thus, changes of the single reservoir only appear as fluctuations.

Finally, in Fig. 7.7, the pressure and temperature evolutions for two cases, $\tau_r/\tau = 50$ and $\tau_r/\tau = 5$, are compared. As indicated earlier, the time for the red and blue lines to converge is the time for the two subsystems of system A to reach mutual stable equilibrium. This is also the approximate start time for the end-cycle (see Figs. 7.5 and 7.6). As seen in Fig. 7.7, for a ratio of $\tau_r/\tau = 50$, system A takes longer to arrive at the end-cycle (steady cycle) for the reason that the $m < 0$ subsystem is driven by the series of reservoirs to approach state B_2(5000 K, 10^6 Pa), while for the $\tau_r/\tau = 5$ case, this same subsystem is driven to approach state B_3(500 K, 10^5 Pa) because the constant-pressure process has already finished by the time that this subsystem's temperature has reached a peak at a dimensionless time of approximately 2. It is also observed that, for the steady cycle, the changing range of temperature and pressure for the $\tau_r/\tau = 5$ case is inside of

that for the $\tau_r/\tau = 50$ case. This is consistent with the result that end-cycle reduces for the former as seen in Figs. 7.4, 7.5 and 7.7 in which the end-cycle for the $\tau_r/\tau = 50$ case. This is consistent with the result from Fig. 7.4, Fig. 7.5 and Fig. 7.6 in which the end-cycle for the $\tau_r/\tau = 5$ case is inside of that for $\tau_r/\tau = 50$ case.

7.6 Conclusions

The SEAQT framework as demonstrated here and elsewhere is a first-principles, thermodynamic-ensemble based approach applicable to the entire non-equilibrium realm even that far-from-equilibrium. It furthermore provides a single kinematics and dynamics applicable across all temporal and spatial scales. Its application here to the modeling of an engine cycle is unlike that of traditional approaches based on equilibrium thermodynamics, which necessarily incorporate phenomenological parameters based on, for example, experiment to account for irreversibilities, or on so-called 'open quantum systems' which for a number of reasons including computational are limited in their applicability.

Using the concepts of hypo-equilibrium state and non-equilibrium intensive properties, the SEAQT framework is applied to a system with variable volume undergoing a cyclic process in which work is produced and energy in a heat interaction is exchanged with a series of reservoirs. The predictions made provide a clear description of the time evolution of the system from an initial transient cycle to an end-cycle, i.e., a steady cycle. As part of this description, intensive property evolutions of temperature, pressure, and volume on P-T and P-V diagrams are provided, which enhance an understanding of the system's non-equilibrium behavior and provide device design guidance without the need for phenomenological or experimental parameters, which capture the effects of irreversibilities. In addition, since the SEAQT framework is able to model the kinetics of a chemically reactive system, future work will make transient and steady cycle predictions of system behavior by replacing the heat reservoirs used in this study with a set of reaction mechanisms internal to the system.

Chapter 8

Multiscale Transient and Steady State Study of the Influence of Microstructure Degradation and Chromium Oxide Poisoning on SOFC Cathode Performance

8.1 Introduction

Among the different types of fuel cells, solid oxide fuel cells (SOFCs) have intensively been studied. A SOFC is composed of two porous electrodes and one ionic conductive electrolyte. The most common electrolyte material is ion conducting yttria-stabilized zirconia (YSZ), while perovskites such as strontium-doped lanthanum manganese (LSM) are used for the cathode and nickel/YSZ for the anode. Of the two electrodes, it is the oxygen reduction process at the cathode, which accounts for most of the performance losses. In order to improve cathode performance, new manufacturing techniques as well as the synthesis of new materials have been used to develop cathodes with greater stability and better electrical properties. For example, ABO_3 cubic perovskite-structured oxides are promising cathode materials for intermediate temperature SOFCs ($600°C$ to $800°C$). Among the various compositions, $La_{0.6}Sr_{0.4}Co_{0.2}Fe_{0.8}O_3$ (LSCF) has received significant attention due to its remarkable electrochemical properties such as high electronic and ionic conductivity (302 S/cm and 8×10^{-3} S/cm, respectively) at $800°C$ [125–127]. Additionally, the thermal ex-

pansion coefficient of LSCF is (17.5×10^{-6}/ K [128]) compatible with that of classic 8 mol% yttria-stabilized zirconia (YSZ, 10.5×10^{-6}/ K) electrolyte material [129]. LSCF is widely being used for SOFC operation at intermediate temperatures [130].

To help guide material development for improved oxygen reduction efficiencies, it is useful to study the oxygen reduction mechanism both via experiment and a theoretical model able to provide insight into the details of the phenomena which take place at the cathode. There are two differing views of what these phenomena entail [131]. The first is that they involve a mixed chemical/electrochemical process and the other is that the process is purely electrochemical. The main difference in the two is the presence of the charged oxygen ion O^-. O^- allows mass transfer via an additional charge transfer pathway other than that of neutral particle diffusion. There are many models based on one or the other of these two views. Gong *et al.* [132] have built a 1D continuum model in order to study the interaction between O^- formation and transport at the surface of the cathode material and O^X ($V_{\ddot{O}}$) diffusion in the bulk. Experimental observation is still needed to confirm the existence of the intermediate product O^- [131]. Nonetheless, for generality, it is included in the non-equilibrium steepest-entropy-ascent quantum thermodynamic (SEAQT) model presented here, which includes three mass transfer pathways: O_2 diffusion in the pore, O^- diffusion along the material surface, and O^X ($V_{\ddot{O}}$) diffusion in the bulk material.

Of course, improved material performance at the expense of material stability must also be dealt with since the development of LSCF cathodes has been hindered by their performance degradation due to the instability of the LSCF material [133, 134] and chromium poisoning from the interconnect [135, 136]. Thus, understanding how degradation mechanisms due to structural changes [126, 128, 129] and chromium oxide poisoning [137, 138] impact cathode lifetimes as well as performance is of great importance. The former has been studied experimentally and results show that they significantly influence cathode performance, while some theoretical studies of the kinetics of the poisoning process and its coupling with the oxygen reduction process have been made at a micro-scale using kinetic theory and the Lattice Boltzmann Method (LBM) [139, 140].

There are a number of approaches aimed at modeling non-equilibrium phenomena at different time and length scales [141] including that of the quantum Boltzmann equation [93–95], non-equilibrium quantum Green's function (NEGF)[1], and molecular dynamics (MD) [2] at the microscale; kinetic Monte Carlo (KMC) [3] and kinetic theory using the lattice Boltzmann method (LBM) [142] and direct simulation Monte Carlo (DSMC) [5, 41] at the mesoscale; and finite el-

ement (FE) [2], finite volume (FV) [143], and continuum electrochemical models [132] at the macroscale. However, a particular limitation of all of these approaches is that they are restricted to an effective time and length scale even though in many cases microscopic and mesoscopic level properties may have a strong influence on macroscopic performance. For example, chemical reactions and species transport are greatly affected by microstructure parameters [141]. The traditional solution to this dilemma is to define macroscopic phenomenological parameters (e.g., tortuosity, porosity, diffusivity, viscosity, thermal conductivity, etc.), which average atomistic-level dynamics and microscopic geometrical features, and incorporate them into the macroscopic-level model in order to capture microscopic and mesoscopic influences. At times, the microscopic and/or mesoscopic model can be incorporated into the macroscopic one to form a multiphysics, multiscale model in which the phenomenological parameters of the macroscopic description can be updated in real-time. Of course, in doing so, the issue of dealing with huge differences in both the description of the system and the equations of motion at different scales must be dealt with. For example, a macroscopic continuum model may use concentration and temperature as state variables and balance equations resulting from the laws of thermodynamics as stand-ins for an equation of motion. In contrast, microscopic MD lacks any thermodynamic information at all and uses particle position and momentum as state variables and the dynamics resulting from Newton's laws as its equation of motion. As a result, there is no shared form for the microscopic and macroscopic variables or properties, and, thus, a need exists for some sort of link between scales to transform property information at one scale into that at another. This is an important feature of any multi-physics, multiscale model.

To address these issues of time and length scales and the influence of microscopic and mesoscopic parameters, a novel approach based on the SEAQT mathematical framework of intrinsic quantum thermodynamics (IQT) [15, 24, 26–29, 36–40, 42, 110] is used here. The resulting model, which has a range of applicability from the equilibrium to the far-from equilibrium realm, can in a single coherent description deal with a much wider range of scales than that of previous models since the model consists of a set of local systems with length scales in the mesoscopic range, while each local system is characterized by particle energy eigenstate properties, which provide information about atomistic or microscopic features. Energy eigenstates are calculated from atomistic-level information, and microscopic parameters such as the mean free path of a particle or a microscopic potential well influence performance via the energy eigenstates. In the SEAQT

framework, the basic system state variables are energy and entropy, which are well defined at both the microscopic and mesoscopic levels and can even be extended to the macroscopic level. Using the same state variables at all scales of description permits the transfer of information between scales by simple scaling, which naturally extends the range of scales to which the SEAQT model can be applied. Furthermore, since the SEAQT framework uses the principle of steepest entropy ascent as the basis for its dynamics, its equation of motion is applicable from the atomistic to the macroscopic level, exhibiting the same basic features across different time and length scales. Thus, a consistent description and dynamics across scales makes this novel approach a good choice for studying microscopic parameter influences on mesoscopic and macroscopic system performance. It is also a good choice since it can predict system behavior in the presence of transport-reaction coupling both in the steady state and transient regime, even that far from equilibrium where non-linearities and entropy generation play a significant role. In this regard, it is particularly advantageous for studying the effects of chromium oxide poisoning on SOFC cathode performance since the presence of this oxide increases the complexity of the coupling, which exists between mass diffusion, chemical/electrochemical reactions, and heat diffusion phenomena.

Finally, the succeeding sections of the paper are organized as follow. *Section* 8.2 provides a brief description of the non-equilibrium SEAQT cathode model. A description of the experimental study on microstructure degradation is then introduced in *Section* 8.3 followed in *Section* 8.4 by a presentation and discussion of results for the prediction of cathode performance relative to the coupled oxygen and chromium oxide reduction-diffusion pathways. Included is a parametric study of the degradation effects on performance of microstructural changes as well as a qualitative comparison of our theoretical predictions with some of our experimental results. *Section* 8.5 concludes with a few final remarks.

8.2 Mathematical Modeling

8.2.1 SOFC cathode model

The following two sections describe both the oxygen reduction (*Section* 8.2.1.1) and chromium oxide poisoning (*Section* 8.2.1.2) models. The latter section also describes how these two models are combined.

8.2.1.1 Oxygen reduction pathway

The system studied is a 1D system from the interface of the interconnect with the cathode to the interface of the cathode with the electrolyte. There are three parallel regions in the system: the cathode pore, the surface of the cathode material, and the bulk of the cathode material. The O_2 molecule travels in the pore, the oxygen ion O^- along the surface of the material, and the oxygen ion O^X (or the vacancy $V_{\ddot{O},MIEC}$) inside the bulk of the material. The oxygen molecule O_2 enters the system through the pore at the interface of the cathode with the interconnect, and the oxygen ion O^X exits the system at the surface and from the bulk of the interface of the cathode with the electrolyte.

Table 8.1. Details of the three pathways for oxygen reduction in the cathode of the SOFC.

Pathway 1	
Step 1: Diffusion from $x = 0$ to $x = L$	O_2
Step 2: Chemical reaction at $x = L$	$O_2 \leftrightarrow 2O_{ad}$
Step 3: Electrochemical reaction at $x = L$	$O_{ad} + e^- \leftrightarrow O^-_{TPB}$
Step 4: Electrochemical reaction at $x = L$	$O^-_{TPB} + V_{\ddot{O},YSZ} + e^- \leftrightarrow O^X_{O,YSZ}$
Pathway 2	
Step 1: Chemical reaction at $x = 0$	$O_2 \leftrightarrow 2O_{ad}$
Step 2: Electrochemical reaction at $x = 0$	$O_{ad} + e^- \leftrightarrow O^-_{ad}$
Step 3: Diffusion from $x = 0$ to $x = L$	$O^-_{ad} \leftrightarrow O^-_{TPB}$
Step 4: Electrochemical reaction at $x = L$	$O^-_{TPB} + V_{\ddot{O},YSZ} + e^- \leftrightarrow O^X_{O,YSZ}$
Pathway 3	
Step 1: Chemical reaction at $x = 0$	$O_2 \leftrightarrow 2O_{ad}$
Step 2: Electrochemical reaction at $x = 0$	$O_{ad} + e^- \leftrightarrow O^-_{ad}$
Step 3: Electrochemical reaction at $x = 0$	$O^-_{ad} + V_{\ddot{O},MIEC} + e^- \leftrightarrow O^X_{O,MIEC}$
Step 4: Diffusion from $x = 0$ to $x = L$	$V_{\ddot{O},MIEC}$
Step 5: Diffusion at $x = L$	$O^X_{MIEC} \leftrightarrow O^X_{YSZ}$ or $(V_{\ddot{O},MIEC} \leftrightarrow V_{\ddot{O},YSZ})$

Based on a multi-step charge transfer model, three coupled pathways are considered sufficient for providing a sufficiently complete description of the oxygen reduction process. The three pathways are distinguished by where two steps of the reduction process occur. In the first pathway, O_2 diffuses through a nano-pore of the porous cathode electrode material to a three-phase boundary

(TPB) at or near the cathode-electrolyte interface after which a two-step charge transfer reaction reduces the oxygen molecule to $2O^X$ so that it can diffuse into the bulk electrolyte. A second pathway is for O_2 to be absorbed by the surface of the cathode material in the micro-pore after which it becomes $2O^-$ through a one-step charge transfer. This is followed by diffusion along the surface of the cathode material to a TPB where a one-step charge transfer transforms $2O^-$ into $2O^X$. This last species then diffuses into the bulk electrolyte. Finally, the third pathway is one where O_2 is absorbed by the surface of cathode material and through a two-step charge transfer becomes $2O^X$ in the bulk of the cathode material where it diffuses through the bulk to arrive at the electrolyte. The design of our system and its pathways is inspired by the work of Gong *et al.* [132]. Details of the three pathways are listed in Table 8.1. For the system results given in *Sections* 8.4.1, 8.4.2, and 8.4.3, adsorption sites are located at multiple positions from the interconnect to the electrolyte.

8.2.1.2 Chromium oxide poisoning pathway

The system for the chromium oxide pathway is composed of the same pore and cathode material surface that makes up the system for the oxygen reduction pathway. CrO_3 enters the pore and then diffuses towards the TPB. Simultaneously, part of the CrO_3 is reduced to Cr_2O_3, which accumulates on the surface of the cathode material. The chromium oxide poisoning pathway is listed in Table 8.2.

Table 8.2. Chromium Oxide Poisoning Pathway

Step 1: Diffusion from $x = 0$ to $x = L$	CrO_3
Step 2: Electrochemical reaction at x	$2CrO_3 + 3e^- \leftrightarrow Cr_2O_3 + 3O^-$

8.2.2 SEAQT model for the SOFC cathode: local system separation of pathways

The SOFC cathode system modeled consists of two types of pathways: three oxygen reduction pathways and one chromium oxide pathway. The oxygen reduction pathways are depicted in Fig 8.1. Each of the three oxygen reduction pathways, which corresponds to one region of the cathode, i.e., pore, surface, or bulk, is separated into 20 locations where each constituent forms one of the local systems. There are 82 local systems in total: 20 for the oxygen (O_2) in the pore region, 20 for the absorbed oxygen atom (O_{ad}) in the surface region, 20 for the ionized oxygen (O^-) in the

surface region, 20 for the oxygen ion inside the bulk material (O^X_{MIEC}), and two for the oxygen ion inside the YSZ (O^X_{YSZ}), which serves as the outlet.

The diffusion and chemical/electrochemical reactions are represented by the links (see Table 8.3) between the local systems. Every two linked local systems can have diffusion or a reaction occurring, and there is mass and/or energy transfer between them. These mass and energy fluxes are modeled by the SEAQT model using information from the linked local system states.

Table 8.3. Links in the oxygen reduction model.

Oxygen Reduction	
D1: Oxygen diffusion in the pore	$O_2(x) \leftrightarrow O_2(x+\delta x)$
D2: Oxygen ion diffusion on the cathode material surface	$O^-_{ad}(x) \leftrightarrow O^-_{ad}(x+\delta x)$
D3: Oxygen ion diffusion in the cathode material bulk	$O^X_{MIEC}(x) \leftrightarrow O^X_{MIEC}(x+\delta x)$ or $V_{\ddot{O},MIEC}(x) \leftrightarrow V_{\ddot{O},MIEC}(x+\delta x)$
R1: Oxygen adsorption by the adsorption site of the cathode material surface	$O_2 \leftrightarrow 2O_{ad}$
R2: Oxygen first step ionization	$O_{ad} + e^- \leftrightarrow O^-_{ad}$
R3: Oxygen second step ionization	$O^-_{ad} + V_{\ddot{O},MIEC} + e^- \leftrightarrow O^X_{O,MIEC}$
R4: Oxygen ion second step ionization into the electrolyte from cathode surface	$O^-_{TPB} + V_{\ddot{O},YSZ} + e^- \leftrightarrow O^X_{O,YSZ}$
R5: Oxygen ion diffusion into the electrolyte from cathode bulk	$O^X_{MIEC} \leftrightarrow O^X_{YSZ}$ or $V_{\ddot{O},MIEC} \leftrightarrow V_{\ddot{O},YSZ}$

The chromium oxide pathway is shown in Fig. 8.2. For this pathway, there are 20 local systems for the CrO_3 in the pore and 20 local systems for the Cr_2O_3 on the surface of the cathode material. Two different kinds of links between local systems exist as shown in Table 8.4. These represent diffusion of the CrO_3 and the chemical reaction, which generates the Cr_2O_3.

Table 8.4. Links in the chromium oxide poisoning model.

Chromium oxide reduction	
D4: CrO_3 diffusion in the pore	$CrO_3(x) \leftrightarrow CrO_3(x+\delta x)$
R6: Cr_2O_3 accumulation on the cathode material surface	$2CrO_3 + 3e^- \leftrightarrow Cr_2O_3 + 3O^-_{ad}$

To describe the communication between the chromium oxide and oxygen reduction pathways, parameter α, which describes the accumulation effectiveness of an adsorption site, can be defined

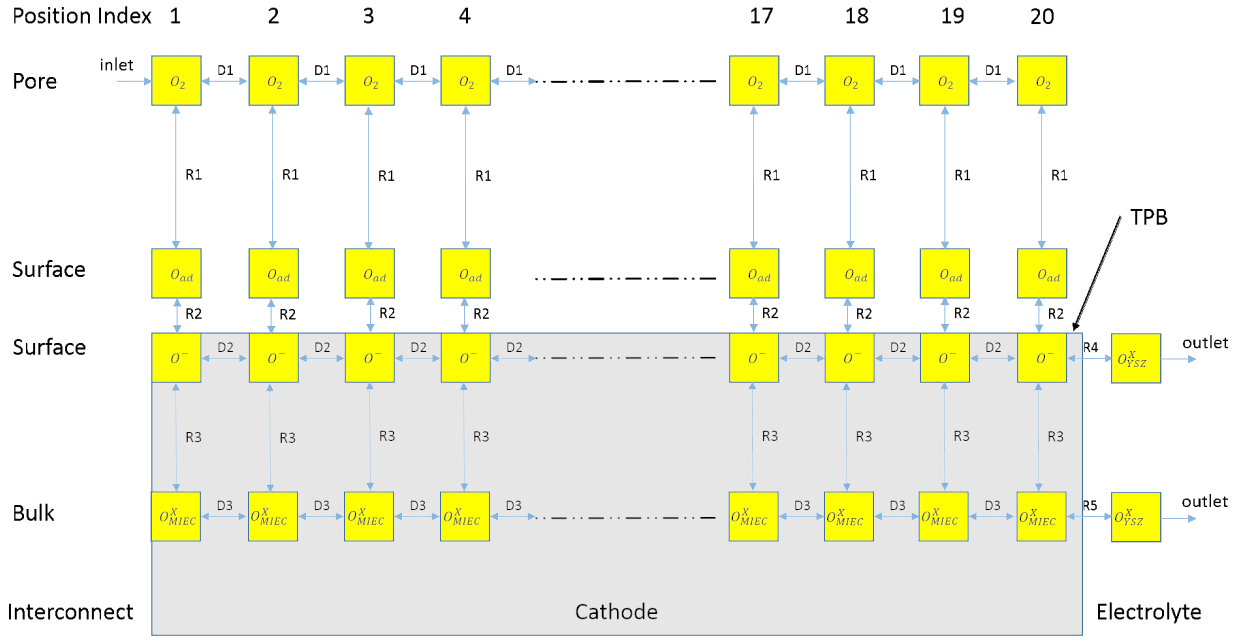

Figure 8.1. Diagram of pathways for the oxygen reduction model.

as a function of particle number of accumulated Cr_2O_3 such that

$$\alpha = \alpha(m_{Cr_2O_3}) \tag{8.1}$$

$$\left(\frac{dm_{O^-}}{dt}\right)_{actual} = \alpha_0^{O^-}\alpha\left(\frac{dm_{O^-}}{dt}\right)_{no\,loss} \tag{8.2}$$

$$\left(\frac{dm_{Cr_2O_3}}{dt}\right)_{actual} = \alpha_0^{Cr_2O_3}\alpha\left(\frac{dm_{Cr_2O_3}}{dt}\right)_{no\,loss} \tag{8.3}$$

where α_0 is the concentration effectiveness of an adsorption site and the subscript “no loss" indicates that the rate of change in mass of the species (O_2 or Cr_2O_3) is acquired directly from the SEAQT equation of motion for the case when $\alpha_0^{O^-} = \alpha_0^{Cr_2O_3} = \alpha = 1$, i.e., when there are no accumulation or concentration limitations relative to the site. The actual rates for oxygen adsorption in Eq. (8.2) and for Cr_2O_3 accumulation in Eq. (8.3) are scaled by α and α_0 to that actually absorbed and accumulated. The physical meaning for the dependence of α on $m_{Cr_2O_3}$ is that as the accumulation occurs, Cr_2O_3 covers the adsorption sites and gradually reduces the ability of the site to absorb and ionize the oxygen as well as the CrO_3. Thus, the greater the accumulation, the smaller the value of α is. In this paper, a linear form is chosen for α, namely,

$$\alpha(m_{Cr_2O_3}) = 1 - m_{Cr_2O_3}/m_0 \tag{8.4}$$

where $m_{Cr_2O_3}$ is the mass of Cr_2O_3 accumulated and m_0 is the threshhold value for the accumulated mass when the adsorption site is totally disabled. Another parameter in Eq. (8.2) is the concentration effectiveness $\alpha_0^{O^-}$, which is the original adsorption site effectiveness without degradation for the oxygen pathway. $\alpha_0^{O^-} = 1$ indicates that the O_2 molecules can find enough adsorption sites to react. However, since the number of adsorption sites to O_2 molecules present is very small in a real fuel cell, $\alpha_0^{O^-}$ is chosen to be a very small number, i.e., 0.0003, in Eq. (8.2) consistent with the current densities considered here. In contrast, due to the low concentration of Cr_2O_3, the concentration effectiveness for the chromium oxide molecules is chosen to be 1 in Eq. (8.3). More discussion about $\alpha_0^{O^-}$ is given in *Section* 8.4.4.3.

8.2.3 SEAQT chemical/electrochemical reaction and transport model: interaction calculation

After establishing the local systems (see Figs. 8.1 and 8.2), a model for the interactions between systems represented by the arrows in Figs. 8.1 and 8.2 is needed to calculate the mass and heat fluxes as well as the reactions. These interactions result in entropy generation, which is captured within the SEAQT framework by its equation of motion, which is used to model the kinetics and dynamics of the chemical and electrochemical reaction and diffusion pathways directly. This first principles approach incorporates quantum as well as classical microscopic information directly into the model via the system energy eigenstructure, which plays a key role in the equation of motion. A brief description of this equation and the principle of SEA upon which it is based is presented in the following section. This is followed in the subsequent sections by a description of the reaction and diffusion models.

8.2.3.1 Principle of SEA and the non-equilibrium SEAQT equation of motion

The underlying theory of our approach is introduced here using an isolated, finite energy eigenlevel quantum system. A discussion of how the theory applies more broadly to other kinds of systems is included in [14, 15, 39, 46] or in papers submitted for publication [16, 17]. A quantum system is well defined by a group of energy eigenstates and associated eigenvalues $\{e_i, i = 1, 2, \cdots\}$. A given thermodynamic (non-equilibrium or equilibrium) state of the system is uniquely defined by a probability distribution among the energy eigenstates denoted by $\{p_i, i = 1, 2, 3, \cdots\}$, and all

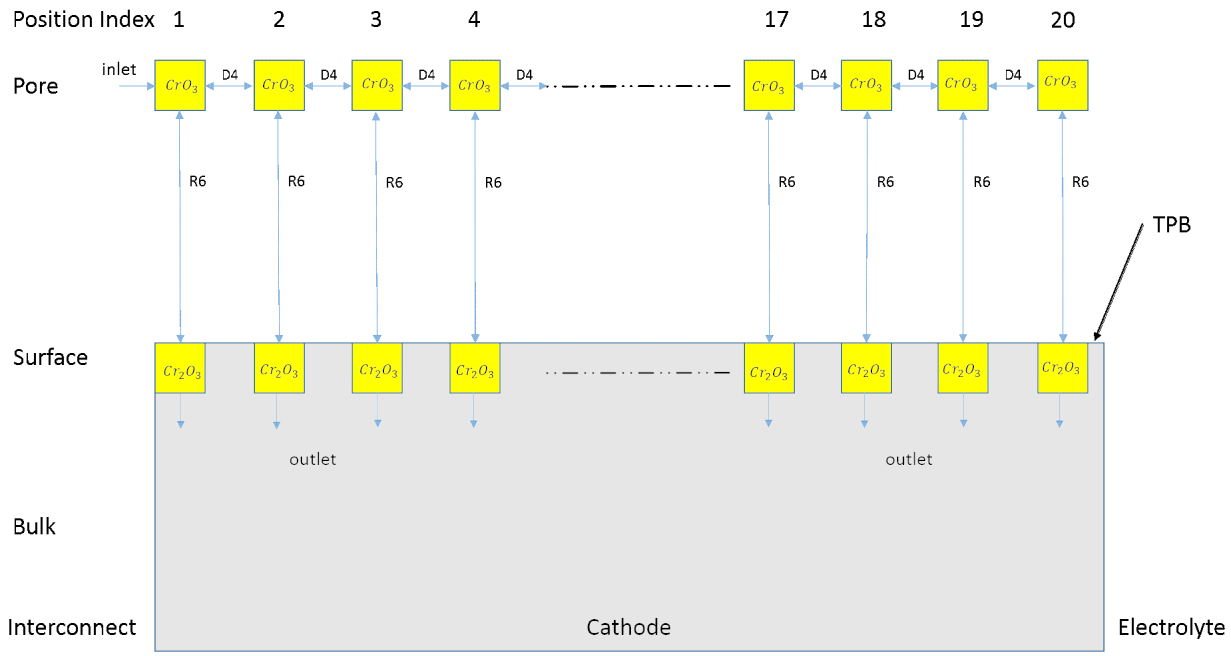

Figure 8.2. Diagram for the pathway of the chromium oxide poisoning model.

possible distributions form the state space of the system. In particular, the stable equilibrium state of an isolated system has a probability distribution described by the Maxwellian distribution. An evolution of state occurs when the system in a state of non-equilibrium evolves to one at stable equilibrium; and it is the given set of probability distributions predicted by the SEAQT equation of motion, which define the unique thermodynamic path that the system takes during the evolution.

For an isolated system, energy and mass conservation require, respectively, that

$$\sum e_i p_i = E \tag{8.5}$$

and

$$\sum p_i = 1 \tag{8.6}$$

The SEAQT equation of motion is constructed so that it takes the direction in state space, which coincides with that of steepest entropy ascent constrained by Eqs. (8.5) and (8.6). At this level of description, the entropy of the system takes the form

$$S = -k_b \sum p_i \ln p_i \tag{8.7}$$

where k_b is Boltzmann's constant. The equation of motion for an isolated system comprised of

a single elementary constituent (i.e., a single particle, a single assembly of indistinguishable particles, or a single field) is then written for the case when the state operator commutes with the Hamiltonian operator of energy eigenstates as

$$\frac{dp_j}{dt} = -\frac{1}{\tau}D = -\frac{1}{\tau}\frac{\begin{vmatrix} p_j \ln p_j & p_j & e_j p_j \\ \sum p_i \ln p_i & 1 & \sum e_i p_i \\ \sum e_i p_i \ln p_i & \sum e_i p_i & \sum e_i^2 p_i \end{vmatrix}}{\begin{vmatrix} 1 & \sum e_i p_i \\ \sum e_i p_i & \sum e_i^2 p_i \end{vmatrix}} \tag{8.8}$$

where the only generators of the motion are the identity and Hamiltonian operators. Unlike traditional equations of motion such as, for example, classical [144–146] and quantum [93–95] versions of the Boltzmann equation, Eq. (8.8) requires no near-equilibrium assumption. It can be used in the nonlinear, far-from-equilibrium realm without any theoretical ambiguities or violations of the laws of thermodynamics or of quantum mechanics. The only parameter, which must be estimated, is the relaxation time τ associated with the dissipation term D in Eq. (8.8). The latter predicts the rate of entropy generation for a given system evolving in time. The relaxation time can be realistically estimated using experimental data such as that for a reaction rate constant [15], diffusion coefficient, heat transfer coefficient, etc.

8.2.3.2 The non-equilibrium state description and solution of the equation of motion

The solution of the SEAQT equation of motion exhibits a number of convenient features, which lead to a complete description of each non-equilibrium state and a fundamental as opposed to phenomenological definition of non-equilibrium temperature. More discussion is presented in reference [14], and an example is provided below. The energy levels of the system $e_i, i = 1, 2, \cdots$ can be divided into to two sets $e_{iA}, i = 1, 2, \cdots$ and $e_{iB}, i = 1, 2, \cdots$ so that the system state space (Hilbert space) $\mathcal{H}$ can be expressed by the sum of the two subspaces $\mathcal{H}_A$ and $\mathcal{H}_B$ as follows:

$$\mathcal{H} = \mathcal{H}_A \oplus \mathcal{H}_B \tag{8.9}$$

The system state can then be represented by the distributions for the two subspaces' energy eigenlevels $\{p_{iA}, i = 1, 2, 3, \cdots\}$ and $\{p_{iB}, i = 1, 2, \cdots\}$. If the distribution in subspace A yields to the

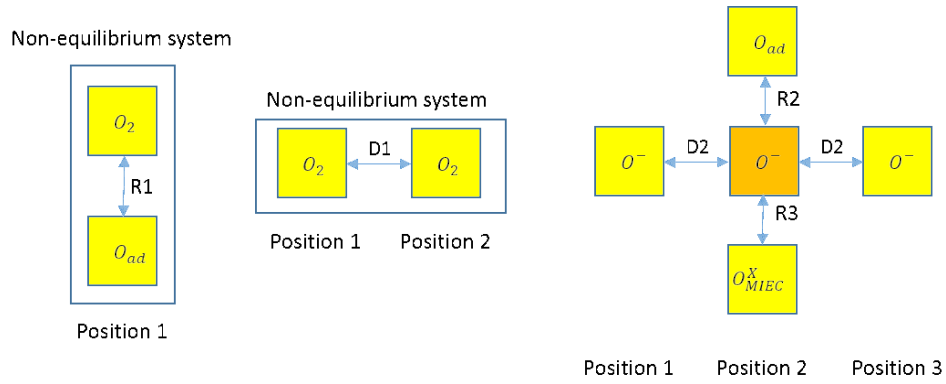

Figure 8.3. Calculation of the mass flux in Fig. 8.1. (a:left) Chemical reaction, (b:middle) diffusion, and (c:right) more than one interactions.

canonical distribution of temperature T_A, the temperature of subspace A is defined to be T_A. Given the division of the state space, Eq. (8.9), if the system probability distribution in the two subspaces are both canonical distributions, the state of the system is called a 2^{nd}-order hypo-equilibrium state, which can be described uniquely by the total probability in each subspace ($p^A = \sum_i p_{iA}$ and $p^B = \sum_i p_{iB}$) and the temperature of each subspace (T_A and T_B). If the initial state of the system is a 2nd- order hypo-equilibrium state

$$p_{iA}^{initial} = \frac{p^A}{Z^A(T_A)} e^{-\frac{e_{iA}}{k_b T_A}}, \quad i = 1, 2, \cdots, n_A \tag{8.10}$$

$$p_{iB}^{initial} = \frac{p^B}{Z^B(T_B)} e^{-\frac{e_{iB}}{k_b T_B}}, \quad i = 1, 2, \cdots, n_B \tag{8.11}$$

where k_b is Boltzmann's constant, n_A and n_B are the number of energy eigenlevels in each subspace, respectively, $Z^A(T_A)$ is the partition function of subspace A at temperature T_A, and $Z^B(T_B)$ is the partition function of subspace B at temperature T_B, Li and von Spakovsky [14] have proven using Eq. (8.8) that the system remains in a 2^{nd}-order hypo-equilibrium state throughout the non-equilibrium state evolution so that

$$p_{iA}(t) = \frac{p^A(t)}{Z^A(T_A(t))} e^{-\frac{e_{iA}}{k_b T_A(t)}}, \quad i = 1, 2, \cdots, n_A \tag{8.12}$$

$$p_{iB}(t) = \frac{p^B(t)}{Z^B(T_B(t))} e^{-\frac{e_{iB}}{k_b T_B(t)}}, \quad i = 1, 2, \cdots, n_B \tag{8.13}$$

Thus, each subspace has temperature defined throughout the whole non-equilibrium process of relaxation.

In calculate the interaction between local systems, a combined system is set up for each link (Fig. 8.3a for a reaction and Fig. 8.3b for diffusion). The energy eigenlevels of the combined system is the combination of energy eigenlevels of the two linked local systems, and the state space is the sum of the Hilbert spaces of the two linked local systems. If the distribution in each linked local system is canonical, the non-equilibrium state of the combined system is in a 2nd-order hypo-equilibrium state even when far-from-equilibrium. Using the equation of motion, Eq. (8.8), of the combined system, the non-equilibrium evolution of the combined system can be calculated so that the non-equilibrium interactions between the two linked local systems can be modeled. The set-up of combined systems for chemical and electrochemical reactions (*Section* 8.2.3.3) and diffusion (*Section* 8.2.3.4) and the calculation of mass and energy flows (*Sections* 8.2.3.5 and 8.2.3.6) are presented below.

8.2.3.3 SEAQT chemical and electrochemical reaction model

The state space of the reactive system is spanned by the eigenstates of the reactants and those of the products. Intermediate states between reactants and products are represented by a mixture of reactant states and product states. This state space can be represented by the Hilbert space H as follows:

$$\mathcal{H} = \mathcal{H}_1 \oplus \mathcal{H}_2 \tag{8.14}$$

where $\mathcal{H}_1$ is the subspace of reactants and $\mathcal{H}_2$ is the subspace of products. Each subspace of the state is generated from single molecular state spaces by the cross product. For example, the reaction

$$A + BC \leftrightarrow AC + B \tag{8.15}$$

is modeled so that each subspace is given by

$$\mathcal{H}_1 = \mathcal{H}_{BC} \otimes \mathcal{H}_A \tag{8.16}$$

$$\mathcal{H}_2 = \mathcal{H}_{AC} \otimes \mathcal{H}_B \tag{8.17}$$

The eigenstate of each particle is generated from the one-particle eigenstates available to each molecule. For example, the state space of BC is expanded to include degrees of freedom for

translation, rotation, and vibration such that

$$\mathcal{H}_{BC} = \text{span}\{|t_x t_y t_z\rangle_{bc} \otimes |lm\rangle_{bc} \otimes |\nu\rangle_{bc}\} \tag{8.18}$$

where $|t_x t_y t_z\rangle$ represents the translational eigenstates, $|lm\rangle$ the rotational ones, and $|\nu\rangle$ the vibrational ones. Inside each ket, are the quantum numbers for the one-particle eigenstate. Starting from these one-particle eigenstates, one can then form the system-level eigenstate of the reactants and products, which spans the system state space. The thermodynamic state of the system at any given instant of time is then represented by a probability distribution among the system eigenstates. More detailed descriptions of this novel approach to describing the chemical and electrochemical kinetics of reacting quantum systems can be found in [15, 46, 67].

Given the energy eigenlevels of the system and each non-equilibrium state represented by a probability distribution $\{p_i, i = 1, 2, \cdots\}$, the SEAQT equation of motion can be used to model the chemical and electrochemical reaction pathways. In the SEAQT SOFC model, the reactant subspace and the product subspace are formed by two local systems linked by chemical a reaction (see Fig. 8.3b).

8.2.3.4 SEAQT diffusion model

The state space of the diffusion system is spanned by the eigenstates of the particle at position x and position x+dx. Strictly speaking, dx needs to be much larger than the De Broglie wave length of the particle, which is about 10^{-11} m for the problem studied here comparing with $dx = 1$ μm. This state space can be represented by the Hilbert space H as follows:

$$\mathcal{H} = \mathcal{H}_1 \oplus \mathcal{H}_2 \tag{8.19}$$

where $\mathcal{H}_1$ is the subspace of the particle at position x and $\mathcal{H}_2$ is the subspace of the particle at position $x + dx$. The eigenstate of the particle at x and $x + dx$ can be generated in the same way as is done for the reactants and products described in the previous section. The set of system eigenstates is composed of the eigenstates of the particle at x and $x + dx$ and is represented by a probability distribution among the system eigenstates. Given the energy eigenstates of the system and each non-equilibrium state represented by a probability distribution $\{p_i, i = 1, 2, \cdots\}$, the

SEAQT equation of motion can be used to model the interaction between two neighboring particle systems via the diffusion process. In the SEAQT SOFC model, subspace 1 and subspace 2 are formed by two local systems linked by diffusion (see Fig. 8.3b).

8.2.3.5 Mass flow rate calculation

The equation of motion in *Section* 8.2.3.1 uses probability distributions to represent system state, and this can be generalized to systems with more than one particle. Consider the interaction (either mass diffusion or reaction) between two linked local systems. Local system 1 has m_1 particles and has the distribution among its energy eigenstates of $\{p_{i,1}, i = 1, 2, \cdots, n_1\}$ where n_1 stands for the number of eigenstates. Local system 2 has m_2 particles and has the distribution among its energy eigenstates of $\{p_{i,2}, i = 1, 2, \cdots, n_2\}$ where n_2 stands for the number of eigenstates. The combined system has $m_1 + m_2$ particles with a new distribution $\{p_{i,1}^{new}, i = 1, 2, \cdots, n_1, p_{i,2}^{new}, i = 1, 2, \cdots, n_2\}$ where

$$p_{i,1}^{new} = m_1 p_{i,1}/(m_1 + m_2), \quad i = 1, 2, \cdots, n_1 \tag{8.20}$$

$$p_{i,2}^{new} = m_2 p_{i,2}/(m_1 + m_2), \quad i = 1, 2, \cdots, n_2 \tag{8.21}$$

Using these new distributions as input to the equation of motion (Eq. (8.8)) leads to a prediction of their time rate of change, i.e.,

$$\{\frac{dp_{i,1}^{new}}{dt}, i = 1, 2, \cdots, n_1\} \text{ and } \{\frac{dp_{i,2}^{new}}{dt}, i = 1, 2, \cdots, n_2\} \tag{8.22}$$

The mass flow for one energy eigenlevel of the system then is

$$\{m_{i,1}^{new} = (m_1 + m_2)\frac{dp_{i,1}^{new}}{dt}, \quad i = 1, 2, \cdots, n_1\} \tag{8.23}$$

$$\{m_{i,2}^{new} = (m_1 + m_2)\frac{dp_{i,2}^{new}}{dt}, \quad i = 1, 2, \cdots, n_2\} \tag{8.24}$$

The mass flow rate for one local system from the interaction is then given by

$$\frac{dm_1}{dt} = (m_1 + m_2)\sum \frac{dp_{i,1}^{new}}{dt} \tag{8.25}$$

$$\frac{dm_1}{dt} = (m_1 + m_2)\sum \frac{dp_{i,2}^{new}}{dt} \tag{8.26}$$

Thus, one can calculate the mass flow along a given link. If a local system has multiple links (e.g., as in Fig. 8.3c), the total flow into one energy eigenlevel of the local system is the sum of the flows through all the links. Recall that each link maintains the local system's distribution canonical. Thus, the total effect from multiple links is to as well keep the local system's distribution canonical [51] so that the temperature is well defined for local systems although it is undergoes a non-equilibrium interaction.

8.2.3.6 Heat flow rate calculation

A local system can also interact with a temperature reservoir with the result that only energy and not mass is transferred. The effect of the energy flow is a redistribution of particle number among the available energy eigenlevels. This heat diffusion between the reservoir and local system is modeled by forming a composite system of a given local system (local system 1) and its duplicate (local system 2) so that the systems have the same mass and energy eigenstructure but different temperatures. At every time step, the duplicate local system is reset to its initial temperature. Also, unlike for the case of mass diffusion and that of reaction, which each yield to one probability conservation law and one energy conservation law, the equation of motion for the case of heat diffusion yields to three conservation laws, i.e., two probability conservation laws (one for each subspace) and one energy conservation law. Thus, the equation of motion for a single energy eigenlevel in local system 1 changes from that for the cases of mass diffusion and reaction, Eq. (8.8), to the following:

$$\frac{dp_{j,1}^{new}}{dt} = -\frac{1}{\tau}\frac{\begin{vmatrix} p_{j,1}^{new}\ln p_{j,1}^{new} & p_{j,1}^{new} & 0 & e_{j,1}^{new}p_{j,1}^{new} \\ \sum p_{j,1}^{new}\ln p_{j,1}^{new} & \sum p_{j,1}^{new} & 0 & \sum e_{j,1}^{new}p_{j,1}^{new} \\ \sum p_{j,2}^{new}\ln p_{j,2}^{new} & 0 & \sum p_{j,2}^{new} & \sum e_{j,2}^{new}p_{j,2}^{new} \\ \sum p_{j,1}^{new}\ln p_{j,1}^{new} + \sum p_{j,2}^{new}\ln p_{j,2}^{new} & \sum e_{j,1}^{new}p_{j,1}^{new} & \sum e_{j,2}^{new}p_{j,2}^{new} & \sum (e_{j,1}^{new})^2 p_{j,1}^{new} + \sum (e_{j,2}^{new})^2 p_{j,2}^{new} \end{vmatrix}}{\begin{vmatrix} \sum p_{j,1}^{new}\ln p_{j,1}^{new} & 0 & \sum p_{j,1}^{new}\ln p_{j,1}^{new} \\ 0 & \sum p_{j,2}^{new} & \sum e_{j,2}^{new}p_{j,2}^{new} \\ \sum p_{j,1}^{new}\ln p_{j,1}^{new} & \sum e_{j,2}^{new}p_{j,2}^{new} & \sum (e_{j,1}^{new})^2 p_{j,1}^{new} + \sum (e_{j,2}^{new})^2 p_{j,2}^{new} \end{vmatrix}} \tag{8.27}$$

where the $p_{j,1}^{new}$ and $p_{j,2}^{new}$ are calculated in the way presented in the previous section, and $e_{j,1}^{new}$ and $e_{j,2}^{new}$ are the energy eigenlevels in local systems 1 and 2. The redistribution of the particle number

in local system 1 ($m_{j,1}$) is then found via

$$\frac{dm_{j,1}}{dt} = (m_1 + m_2)\frac{dp_{j,1}^{new}}{dt} \tag{8.28}$$

For more detailed discussions, the reader is referred to [16].

8.2.4 Numerical method

8.2.4.1 Density of state method for the equation of motion

Since the description of system state uses a probability distribution among energy eigenlevels in the SEAQT framework, the equation of motion consists of a group of first-order ordinary differential equations (ODEs) for each level. Under the condition that quantum effects are significant, the number of energy eigenlevels is relatively small, and only a limited number of ODEs need be solved. However, when the system is at a high temperature, as many as 10^{130} or more energy eigenlevels and, thus, ODEs are required. Li and von Spakovsky [14, 15] have developed a numerical density of state method to deal with systems with large numbers of energy eigenlevels. For a detailed mathematical discussion, the reader is referred to [14]. The key idea here is that if the energy spectrum is divided into intervals with energy differences much smaller than k_bT, the n_j energy levels in the i^{th} interval can be combined into one energy level with average energy E_i and degeneracy n_i. The state of the system is represented by the probability P_i in each energy interval instead of that for each energy eigenlevel. The result is that the equation of motion is rewritten as

$$\frac{dP_j}{dt} = -\frac{1}{\tau}D = -\frac{1}{\tau}\frac{\begin{vmatrix} P_j \ln P_j/n_j & P_j & E_jP_j \\ \sum P_i \ln P_j/n_j & 1 & \sum E_iP_i \\ \sum E_iP_i \ln P_j/n_j & \sum E_iP_i & \sum E_i^2P_i \end{vmatrix}}{\begin{vmatrix} 1 & \sum E_iP_i \\ \sum E_iP_i & \sum E_i^2P_i \end{vmatrix}} \tag{8.29}$$

where P_i is the probability in the i^{th} interval and $E_i = (\sum e_i)/n_i$. It can be proven that if the interval is small enough, this process does not change the macroscopic properties of the system (such as entropy, energy, temperature, etc.) and their evolution. In the SEAQT SOFC model, 750 energy intervals are used to approximate about 10^{130} energy levels in each local system with

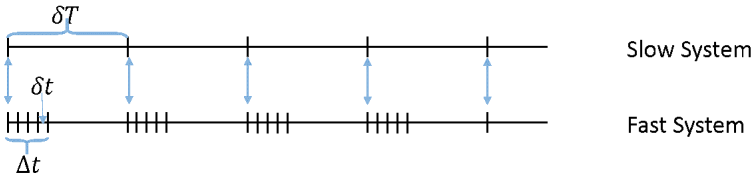

Figure 8.4. Heterogeneous multiscale methods.

excellent accuracy.

8.2.4.2 Heterogeneous multiscale methods

The SEAQT oxygen reduction pathway model includes interactions at different time scales from those for reactions (relaxation times of 10^{-9} s) to those for diffusion in the bulk (relaxation times of 10^{-2} s). Both mesoscopic information (local system separation) and microscopic information (energy eigenstructure) are included in the model. Heterogeneous multiscale methods (HMM) [12, 13, 147] are, thus, needed to solve the coupling between the microscopic and mesoscopic models.

The fast system, which is primarily microscopic, has a time step of δt and comes to equilibrium after a time Δt. In contrast, the slow system, which is mostly mesoscopic/macroscopic, has a time step of δT and comes to equilibrium after a time ΔT. The four times (see Fig. 8.4) have the relation that $\delta t \ll \Delta t \ll \delta T \ll \Delta T$. For each step of the slow system, the information provided by the microscopic (fast) system is assumed constant. In this time period of one step for the slow system, the fast system is solved to an equilibrium (or a steady) state using the information provided by the mesoscopic/macroscopic (slow) system, which is also assumed constant. The two systems then exchange information after ΔT and update the information from both the fast and slow systems. Thus, a multiscale system can be solved coupled, taking into account mesoscopic/macroscopic and microscopic evolutions. In all other methods or frameworks, the mesoscopic/macroscopic (slow) system and microscopic (fast) system have different models, governing equations, and state parameters. These differences make the communication between the two systems difficult, and the communication requires a major part of the computational resources. This is not the case in the SEQT framework since slow and fast systems use the same framework. Thus, for example, for the case of the oxygen reduction pathway, the slow system is the local system network that includes diffusion interactions in the pore, on the surface, and in the bulk and whose relaxation time is on the order of 10^{-2} s. The fast system is the local system network that has the remaining

interactions including reactions and diffusion in the pore and whose relaxation time varies between 10^{-9} s to 10^{-7} s. Slow and fast systems are solved coupled using HMM. Using SEAQT, the model, governing equations, and state parameters of the slow and the fast models are self-consistent, which makes the application of HMM very efficient.

8.2.5 Parameter estimation

8.2.5.1 System parameters

System parameters include the mean-free paths in three regions (pore, surface, and bulk), the distance between local systems, and the total length from the interconnect-cathode interface to the cathode-electrolyte interface. According to experimental observation, the thickness of the LSCF cathode is about 20 μm, the width of the pore is about 0.9 μm and the grain size is about 1 μm. In our model, the mean free path of the particle in the pore is assumed to be 1 μm in each of the three directions, which is approximately the size of a grain in the bulk and the width of the pore. For a particle on the surface, the mean free path is chosen to be 0.1 μm in the direction perpendicular to the surface, which is one order of magnitude smaller than that for the free particle. The mean free paths in the other two directions are the same as for the free particle. For the particle inside the bulk, the mean free path is set to be 1 μm in the direction the particle travels, while those in the other two perpendicular directions are chosen to be 0.1 μm.

The length from the interconnect to the TPB is set at 20 μm. The system is separated into 20 local systems for each region, and the distance between the center point of two local systems is chosen to be 1 μm, which just happens to be equal to the mean free path in the direction a particle travels towards the electrolyte boundary. The choice of mean free path length and that for the distance between two local systems are, however, independent of each other. Results of a parametric study on the effects of these lengths and distances is presented in *Sections* 8.4.2 and 8.4.3 below in which the influence of pore size and grain size change on cathode performance is examined. The particular parameter values chosen are those, which allow comparison with experimental results and are somewhat different (by less than an order of magnitude) from the ones used in the transient process study results presented in *Section* 8.4.1.

8.2.5.2 Parameters for eigenstate calculations

The translational energy eigenstates of O_2, O^-, O_{ad}, and O^X are calculated from the 3D infinite well. The three dimensions of the well are assumed to be the mean-free path in 3 directions. The rotational eigenenergies of O_2, CrO_3, and Cr_2O_3 are calculated from the rigid motor model, while the eigenstate of the electron is set to be the one-level Fermi energy E_f with a density of states of D_f. The potential energy of O_2 is set to its dissociation energy D_{O_2}. The potential energy of O_{ad} is assumed to be $0.5D_{O_2}$, and that of O^- to be $0.5D_{O_2} + 2E_f$. The potential energies of CrO_3 and Cr_2O_3 are set to their dissociation energies. The order of magnitude of the density of state D_f for the electron is estimated based on the electrochemical reaction equilibrium concentration.

Obviously, more experimental or theoretical information about the energy eigenstates and potential energy of a particle could improve the model. However, the estimates used above are reasonable and provide accuracies within the correct order of magnitude for the energy, entropy, and chemical reaction equilibrium concentration.

8.2.5.3 Relaxation time

For a reaction, the relaxation time is chosen so that it coincides with the reaction rate found from experiment, while for diffusion, Fick's law provides the flow rate such that

$$J = -D_{diff}\frac{dc}{dx} \tag{8.30}$$

$$\frac{dm}{dt} = -D_{diff}A\frac{dc}{dx} \tag{8.31}$$

where J is the flux (particle^{1}s^{-1}m^{-2}), D_{diff} the diffusion coefficient (s^{-1}m^2), c the concentration (particle^{1}m^{-3}), m the particle number in the finite volume, and A the cross-sectional area perpendicular to the flux direction. This last expression can in turn be written as

$$\frac{dm}{dt} = -D_{diff}\frac{A}{V}\frac{dm}{dx} \tag{8.32}$$

The discrete form of Eq. (8.32) gives the mass flow between two local systems, namely,

$$\frac{dm_1}{dt} = -D_{diff}\frac{m_1 - m_2}{(\delta x)^2} \tag{8.33}$$

where m_1 and m_2 are the mass of two neighboring local systems and δx the distance between the local systems. Using experimental values for D_{diff} in Eq. (8.33) and comparing with, for example, Eq. (8.25), the relaxation time for diffusion can be determined. The relaxation times of the oxygen reduction pathway are summarized in Table 8.5.

For the chromium oxide poisoning pathway (Table 8.4), the relaxation time of diffusion in the pore (D4) uses the relaxation time of diffusion in the pore (D1) for oxygen as an approximation. The relaxation time of reaction R6 for the chromium oxide pathway uses the relaxation time for R3 of the oxygen pathway, since R3 is the slower step in the two-step reduction R2 and R3.

Table 8.5. System parameters used in the SOFC model.

Reaction		Relaxation time (s)	Exchange rate constant (mol^{1}cm^{-2} s^{-1})[132]
R1	$O_2 \leftrightarrow 2O_{ad}$	$6.20E-09$	$1.00E-07$
R2	$O_{ad} + e^- \leftrightarrow O^-_{ad}$	$9.60E-09$	$1.00E-07$
R3	$O^-_{ad} + V_{\ddot{O},MIEC} + e^- \leftrightarrow O^X_{O,MIEC}$	$9.60E-08$	$1.00E-07$
R4	$O^-_{TPB} + V_{\ddot{O},YSZ} + e^- \leftrightarrow O^X_{O,YSZ}$	$9.60E-08$	$1.00E-07$
R5	$O^X_{MIEC} \leftrightarrow O^X_{YSZ}$ or $V_{\ddot{O},MIEC} \leftrightarrow V_{\ddot{O},YSZ}$	$8.90E-09$	$1.00E-06$
Diffusion		Relaxation time(s)	Diffusion coefficient(cm^2 s^{-1})[132]
D1	$O_2(x) \leftrightarrow O_2(x+\delta x)$	$1.05E-07$	$1.76E-01$
D2	$O^-_{ad}(x) \leftrightarrow O^-_{ad}(x+\delta x)$	$5.70E-02$	$1.00E-06$
D3	$O^X_{MIEC}(x) \leftrightarrow O^X_{MIEC}(x+\delta x)$	$5.30E-02$	$1.00E-06$

8.3 Experimental procedures

8.3.1 Chemicals

$La(NO_3)_3 \cdot 6H_2O$, $Sr(NO_3)_2$, $Co(NO_3)_2 \cdot 6H_2O$, $Fe(NO_3)_3 \cdot 9H_2O$, ethylenediaminetetraacetic acid, citric acid, NH4NO3, sucrose and $NH_3 \cdot H_2O$ were purchased from Alfa Aesar. Microcrystalline cellulose as a pore forming agent was obtained from Gardena, while ethyl cellulose as a binder was bought from Acros Organics. YSZ was purchased from Nextech Materials and AISI 441 was produced by ATI Allegheny Ludlum Corporation. All other chemicals were obtained from Alfa Aesar as-received.

8.3.2 Synthesis of LSCF powder

Perovskite LSCF powder is synthesized by a combustion method. The molar ratio of $La(NO_3)_3 \cdot 6H_2O$, $Sr(NO_3)_2$, $Co(NO_3)_2 \cdot 6H_2O$, and $Fe(NO_3)_3 \cdot 9H_2O$ is $6 : 4 : 2 : 8$ and the molar ratio of metal ions to ethylenediaminetetraacetic acid (EDTA) to citric acid to ammonium nitrate to sucrose is $2 : 1 : 2 : 10 : 0.75$. In the first step, the metal nitrates are dissolved in distilled water in a beaker; EDTA, citric acid, ammonium nitrate, and sucrose are then added. The pH value is subsequently adjusted with ammonium hydroxide to 6 to completely dissolve the EDTA. With the usage of a mesh on top of the beaker, the solution is placed in a pre-heated furnace at $450°C$. After 10 minutes, the combustion process is completed and the beaker is taken out to cool down. The combusted powder is then calcined at $900°C$ for 2 hr and milled before use.

8.3.3 Assembly of AISI 441/LSCF/YSZ tri-layers

The cathode material (56.8 wt%) is mixed and ball-milled with microcrystalline cellulose, ethyl cellulose, and α-terpineol for 1 hr to make pastes for screen printing. The prepared pastes are then screen printed on 8 mol% YSZ substrates, using a $\#330$ mesh. The screen printed pastes are square-like with an area of 0.5 cm^2. The LSCF/YSZ is kept at $200°C$ for 3 hr and at $400°C$ for 1 hr to partially remove the binder and solvent and is then kept at $950°C$ for 2 hr to complete binder removal and bond with YSZ with a heating and cooling rate of $1°C/$min.

AISI 441 ferritic stainless steel pieces are used as the interconnect material and are cut into rectangular substrates (area: 10×10 mm^2). In order to remove the oxidized layer and obtain a scratch free flat surface, the steel pieces are polished to optical finish, and ultrasonically cleaned with water and ethanol. The polished AISI 441 alloy piece is placed on the cathode side of the LSCF/YSZ bi-layer and the configuration of the tri-layer is shown in our previous paper [148].

8.3.4 Thermal treatment under current load

In order to investigate the electrochemical behaviors of the cathodes, AISI 441/cathode/YSZ are heated to $800°C$, using a tube furnace (1730-20 HT Furnace, CM Furnace Inc. Bloomfield, NJ) in a dry air environment. Afterwards, the tri-layers are cathodically polarized using a potentiostat (VersaSTAT 3, Princeton Applied Research, Oak Ridge, TN). A platinum mesh is placed in-between the cathode porous layer and the AISI 441 interconnect to optimize the current distribution, and

the electrodes are connected by Pt wires along with Pd paste. The EIS testing program used is a multi-loop process. In each loop, EIS is run from 100 kHz to 0.025 Hz with an amplitude of 10 mV. After this, a current density of 200 mA/cm^2 is applied to mimic the working condition of an actual fuel cell. EIS data is recorded every 2 hr during the thermal treatment.

8.3.4.1 Characterization and performance testing

The microstructures of the cathodes after the different hours of thermal treatment are examined by a scanning electron microscope (SEM, LEO (Zeiss) 1550) with a palladium layer coating applied before imaging.

8.4 Results and discussion

8.4.1 Transient to steady state process

Among the many strengths of the SEAQT framework is the fact that it is thermodynamically rigorous in the non-equilibrium region, which permits study of the transient process of fuel cell start-up. The following section presents results for the transient behavior of the cathode system considered here. This is followed in *Sections* 8.4.2 and 8.4.3 by results from parametric studies of the influence on cathode performance of distances to the TPB and of mean-free-path lengths, respectively. The time axis for all the figures is on the log scale.

For the transient evolution of particle number distribution in the pore, Fig. 8.5a, shows that i) the local system particle numbers remain almost the same from 10^{-10} s to 10^{-7} s and that ii) significant mass diffusion only occurs in the timescale range from 10^{-7} s to 10^{-4} s. For the evolution of temperature, Fig. 8.5b shows that i) similar local system temperature changes at positions 2 to 20 occur from 10^{-10} s to 10^{-7} s but that ii) from 10^{-7} s to $10^{-3.5}$ s, the temperatures of the different local systems experience different temperature evolutions. Thus, there are two timescales in the pore region: the first is from 10^{-10} s to 10^{-7} s and the second from 10^{-7} s to $10^{-3.5}$ s. In the first timescale, the local systems at positions 2 to 20 have almost the same concentration with little influence from diffusion and follow a similar chemical reaction path to that of the local systems on the cathode surface, which is confirmed by the similar evolutions in temperature across local systems. In contrast, during the second timescale, diffusion couples with

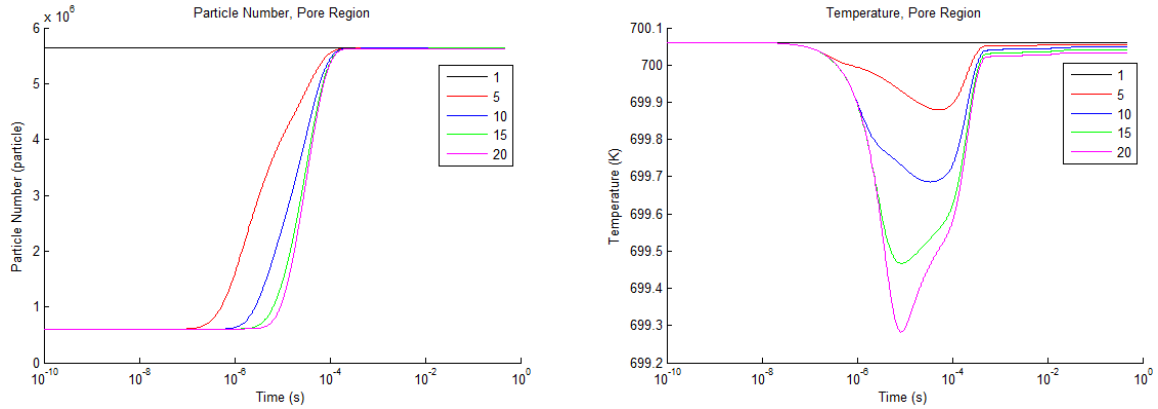

Figure 8.5. Particle number and temperature evolutions in the pore pathway. (a:left) The particle number evolutions at positions 1, 5, 10, 15, 20; and (b:right) the temperature evolutions at positions 1, 5, 10, 15, 20.

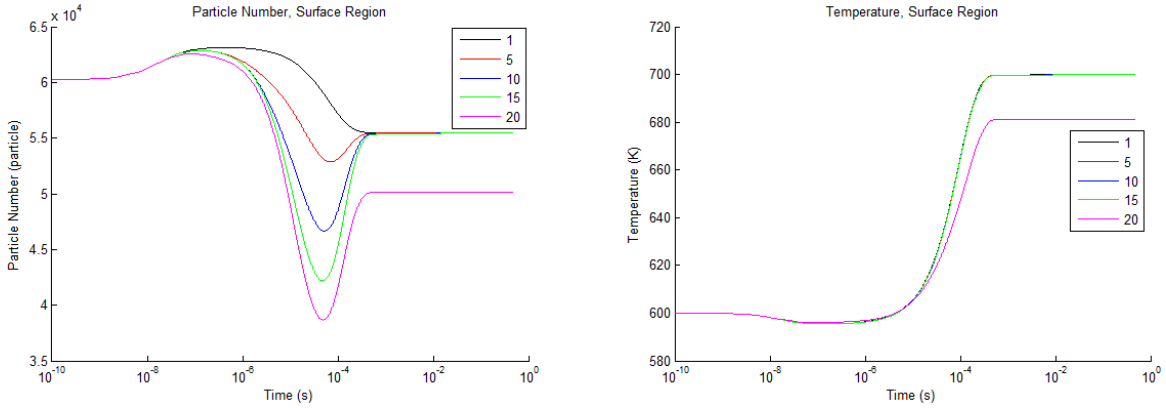

Figure 8.6. Particle number and temperature evolutions in the surface pathway. (a:left) The particle number evolutions at positions 1, 5, 10, 15, 20; and (b:right) the temperature evolutions at positions 1, 5, 10, 15, 20.

the chemical reaction. One can observe that the closer a local system is to the inlet, the earlier the temperature evolution of the system departs from that of the other systems since at this location, the influence of diffusion is greater. Moreover, mass diffusion produces different particle numbers for systems at different times, leading to different chemical reaction equilibriums for local systems at different positions and different more developed temperature profiles. The strong coupling effect comes from the fact that the difference in the characteristic times of diffusion and reaction in the pore is not as large (the reaction speed here is slowed down by the adsorption effectiveness at the surface) as compared to what is happening at the surface and in the bulk. In the end, after the pore pathway reaches steady state, the temperatures in the pore return to about 700 K as seen in Figure 8.5b.

For the transient evolution of particle number distribution on the surface, Fig. 8.6a shows that i)

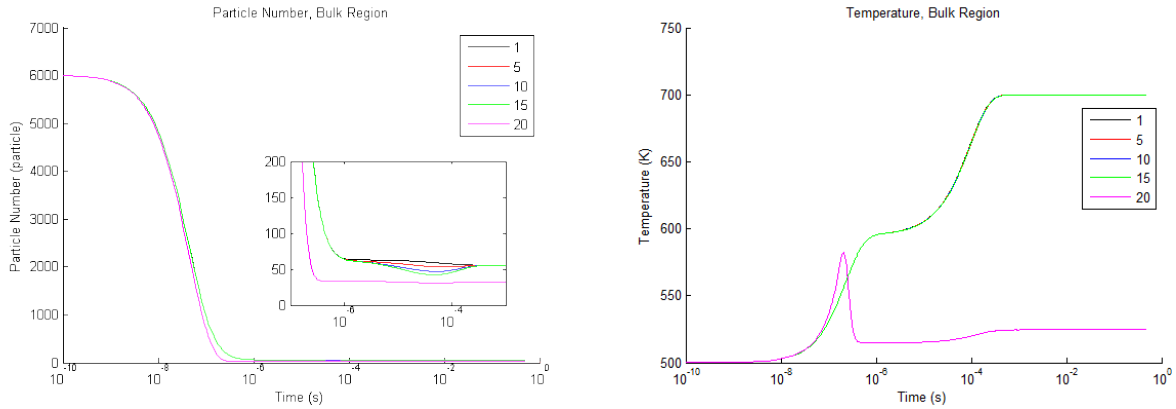

Figure 8.7. Particle number and temperature evolutions in the bulk pathway. (a:left) The particle number evolutions at positions 1, 5, 10, 15, 20; and (b:right) the temperature evolutions at positions 1, 5, 10, 15, 20.

the particle numbers for the local systems at positions 2 to 20 experience almost the same increase from 10^{-10} s to 10^{-7} s, that ii) the mass diffusion process occurs primarily from 10^{-7} s to $10^{-3.5}$ s, and that iii) the equilibrium particle number of the local system at position 20 is significantly different from that of the other local systems. For the temperature evolution, Fig. 8.6b indicates that i) decrease in the temperatures of the local systems at all positions is almost the same from 10^{-10} s to 10^{-7} s, that ii) the temperatures of the local systems at positions 1 to 15 increase to 700 K from 10^{-7} s to $10^{-3.5}$ s, and that iii) the system at position 20 reaches a different temperature of 680 K. The two timescales for the local systems at the surface are the same as those in the pore region. From 10^{-10} s to 10^{-7} s, the surface pathway is influenced primarily by chemical reactions, while mass diffusion significantly influences the chemical reactions occurring on the surface in the timescale from 10^{-7} s to $10^{-3.5}$ s. However, the change in mass at the surface does not occur primarily due to surface diffusion but instead to the chemical reaction balance moving with the pore pathway since the characteristic time of the diffusion process at the surface is about 2 orders of magnitude smaller than that in the pore pathway. Thus, it is diffusion to the surface and not along it that is the driver here, i.e., the preferred path for mass transfer and subsequent reaction is that through the pore followed by adsorption at the surface as opposed to adsorption first and then movement along the surface. In the temperature evolution seen in Fig. 8.6b, the strong influence of the pore pathway on the surface pathway raises the temperature of the surface from 600 K to 700 K via the oxygen reduction reaction. Only the system at position 20 is at a different temperature and particle number at steady state for the reason that it is linked to the outlet, i.e., to the rest of the fuel cell.

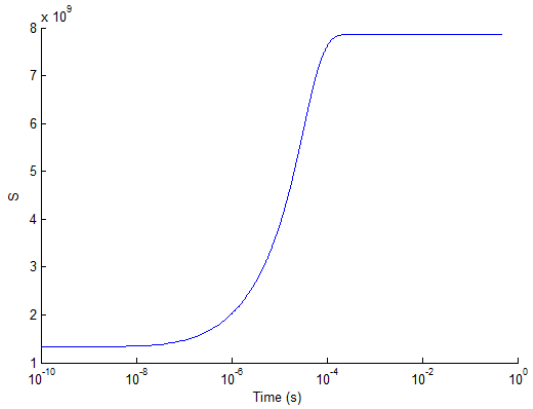

Figure 8.8. Evolution of total system entropy.

For the transient evolution in the bulk, Fig. 8.7, indicates that the reaction process (timescale from 10^{-10} s to 10^{-7} s) and the diffusion process (timescale from 10^{-7} s to $10^{-3.5}$ s) occurs at the same timescales as those for the other two pathways. The difference, however, is that the reaction has a much stronger influence on particle number evolution than the diffusion process, which in Fig. 8.7a can only be detected in the zoomed-in window of the figure. For the chemical reaction process from 10^{-10} s to 10^{-7} s, the large decrease in particle number is somewhat offset by the particle number increase at the surface. From 10^{-7} s to $10^{-3.5}$ s, diffusion in the other two pathways starts to significantly influence the bulk pathway; and as seen in Fig. 8.7, the effect is a large increase in bulk temperature as opposed to bulk particle number since this increase is decided by relative particle numbers, i.e., by the significantly larger number of particles at the surface than in the bulk. This leads to the bulk temperature at steady state being 700 K as well. Furthermore, unlike for temperature, the primary influence on bulk particle number is from the reaction balance moving in the other two pathways since the change in particle number of all three are almost of the same proportion at each position. Moreover, similar to what happens with the surface pathway, the local bulk system at the, i.e., at position 20, reaches a different steady state from that of the other local systems in the bulk. A peak also appears in the temperature evolution at this location resulting in a different temperature history from that of the other local systems. These differences are the result of competition with the pore pathway and the outlet. The other local systems in the bulk also show the effects of this competition from 10^{-7} s to $10^{-3.5}$ s, which is the timescale of pore diffusion, and this results in a flat temperature evolution from 10^{-6} s to 10^{-5} s.

Finally, to understand which interaction is the most important in terms of entropy generation, the evolution in the system entropy is depicted in Fig. 8.8. It is clear that the entropy generation

is strongest in the time range from 10^{-7} s to 10^{-4} s, which is the same range in which the greatest diffusion in the pore occurs (Fig. 8.5a). This is reasonable, since mass transfer in the pore is larger than for the other pathways and the mass in the pore accounts for most of the total mass in the system. The system reaches steady state after $10^{-3.5}$ s, which is much faster than characteristic time of surface and bulk diffusion, and this is a direct result of the dominant role of the pore pathway in mass transfer.

8.4.2 Parametric study on the effects of changes in cathode thickness

The non-equilibrium SEAQT model is used to study the effects of different interconnect-TPB distances ($L = 10$ μm, 20 μm, 40 μm, and 60 μm) on cathode performance. The total charge delivered to the electrolyte is determined, and the time evolution of charge flux calculated. At steady state, the charge flux in the bulk (J_{bulk} equal to about 200 mA/cm^2) and that on the surface ($J_{surface}$ equal to about 20 mA/cm^2) are used to study the influence of the interconnect-TPB distance L. Results shown in Table 8.6 indicate that the greater L is, the smaller the surface as well as bulk flux are. This result is consistent with the idea that longer interconnect-TPB distances cause larger resistances for oxygen ion diffusion. At the same time, as L increases, the ratio of surface flux to bulk flux ($J_{surface}/J_{bulk}$) stays the same because the local systems on the surface and in the bulk are linked by chemical/electrochemical reactions at every position. The ratio of local system surface and local system bulk concentrations at every position satisfies the same chemical equilibrium ratio. The decreasing trend of current flux when distance increases can be regarded as one possible explanation for the degradation in performance due to microstructural changes. However, the model shows that the influence of path length changes on performance is not significant.

8.4.3 Parametric study on the effects of particle mean free path

8.4.3.1 Theoretical explanation and simulation result

Table 8.6. Steady state current comparison for different interconnect-TPB distances resulting from microstructural changes due to grain-size growth.

Distance (μm)		Particle flow (particle/s)	Current flux (mA/cm^2)	Total Current (mA)	Ratio ($J_{surface}/J_{bulk}$)
10	Surface	$6.0059E+07$	$1.9255E+01$		
	Bulk	$5.8959E+07$	$1.8902E+02$		
	Total	$1.1902E+08$		$1.9078E-15$	0.102
20	Surface	$6.0053E+07$	$1.9253E+01$		
	Bulk	$5.8954E+07$	$1.8901E+02$		
	Total	$1.1901E+08$		$1.9077E-15$	0.102
40	Surface	$6.0046E+07$	$1.9251E+01$		
	Bulk	$5.8944E+07$	$1.8897E+02$		
	Total	$1.1899E+08$		$1.9074E-15$	0.102
60	Surface	$5.9995E+07$	$1.9234E+01$		
	Bulk	$5.8892E+07$	$1.8881E+02$		
	Total	$1.1889E+08$		$1.9057E-15$	0.102

The non-equilibrium SEAQT model is also used to study the effects on performance of different mean free paths. The mean free path for all system dimensions is varied by the following factors: 1.1, 1.05, 0.95, and 0.9 relative to the mean free paths defined in *Section* 8.2.5.1. At steady state, the charge flux in the bulk (J_{bulk}) and that on the surface ($J_{surface}$) are used to study the influence of these lengths. The mean free path is related to microscopic structure. A larger pore size (see Fig. 8.9) in the cathode provides a larger mean free path in the pore, and a larger grain size of the material (see Fig. 8.9) provides a larger mean free path on the surface and in the bulk. From an atomistic viewpoint, the mean free path affects the energy eigenstates. The smaller the mean free path, the lower the density of states at a given energy is and the lower the specific entropy for a given temperature. As a consequence, each eigenstate change affects the final cathode system steady state and the speed at which it is approached as well as the rate of entropy generation. In fact, for a given reaction, i.e., a given pair of linked local systems, if the specific entropy of the reactant

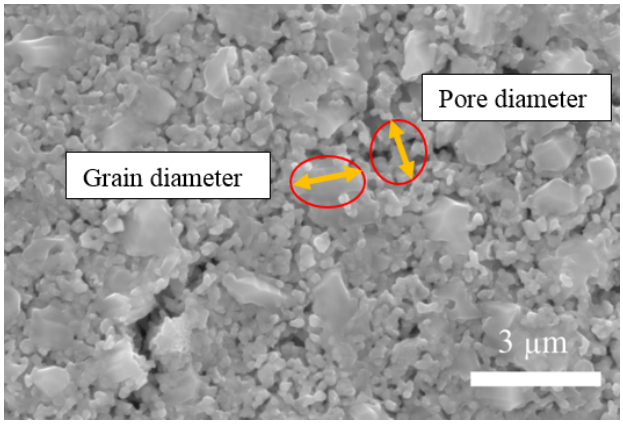

Figure 8.9. SEM image of the microstructure of the cathode material.

increases, the reaction balance moves towards the reactant side, resulting in more reactant as the paired local systems approach chemical stable equilibrium. For diffusion, the larger mean free path results in a larger diffusion coefficient and faster diffusion; but the final stable equilibrium state approached by a given pair of linked local systems remains the same, since the diffusing component has the same energy eigenstructure and specific entropy at different positions. Thus, the dominant factor determining current flux at steady state is the influence of mean free path on the reactions. Neither diffusion in the pore nor the speed at which it occurs are limiting since as seen Fig. 8.5a above, oxygen already has a relatively uniform distribution along the pore after time 10^{-4} s.

Results for different mean free paths in the pore (see Table 8.7) show that the greater the mean free path of the pore is, the smaller the surface as well as bulk current flux are. With increasing mean free path in the pore, the specific entropy in the pore increases and the chemical reaction balance of the adsorption moves towards the oxygen molecule side. When the particle number of the inlet remains the same, there is less oxygen absorbed at the surface and into the bulk so that the current fluxes on the surface and in the bulk both decrease.

Table 8.7. Details of the three pathways for oxygen reduction in the cathode of the SOFC.

Mean free path Scale factor		Particle flow (particle/s)	Current flux (mA/cm^2)	Total Current (mA)	Ratio ($J_{surface}/J_{bulk}$)
1.1	Surface	$2.4624E+07$	$7.8944E+00$		
	Bulk	$2.5470E+07$	$8.1656E+01$		
	Total	$5.0094E+07$		$8.0300E-16$	0.097
1.05	Surface	$4.1537E+07$	$1.3317E+01$		
	Bulk	$4.1166E+07$	$1.3198E+02$		
	Total	$8.2703E+07$		$1.3257E-15$	0.101
1.0	Surface	$6.0053E+07$	$1.9253E+01$		
	Bulk	$5.8954E+07$	$1.8901E+02$		
	Total	$1.1901E+08$		$1.9077E-15$	0.102
0.95	Surface	$8.0387E+07$	$2.5772E+01$		
	Bulk	$7.9227E+07$	$2.5400E+02$		
	Total	$1.5961E+08$		$2.5586E-15$	0.101
0.9	Surface	$1.0275E+08$	$3.2941E+01$		
	Bulk	$1.0248E+08$	$3.2855E+02$		
	Total	$2.0523E+08$		$3.2898E-15$	0.100

Results for different mean free paths on the surface and in the bulk (see Table 8.8) show that the greater the mean free path of the surface and bulk, the larger the surface as well as bulk flux are. The mean free path on the surface and in the bulk increases the specific entropy on the surface and in the bulk, while the chemical reaction balance of the adsorption moves towards the oxygen ion side. When the particle number of the inlet remains the same, there are more oxygen molecules absorbed to the surface and bulk so that the current fluxes on the surface and in the bulk both increase. Another phenomena observed is that the current flux is negative when the mean free path is 0.9. This is because when the mean free path of the surface and bulk are too small, the equilibrium concentration in the bulk and on the surface can be even smaller than the concentration of the outlet, which is decided by other parts of the fuel cell.

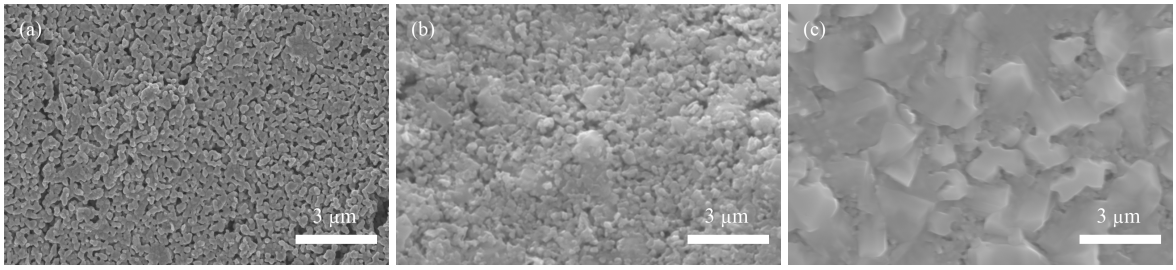

Figure 8.10. SEM images of the microstructure of the cathode after heat processing for (a:left) 0 hr, (b:middle) 20 hr, and (c:right) 40 hr.

Table 8.8. Steady state current comparison for different mean free paths on the surface and in the bulk.

Mean free path Scale factor		Particle flow (particle/s)	Current flux (mA/cm^2)	Total Current (mA)	Ratio ($J_{surface}/J_{bulk}$)
1.1	Surface	$1.3980E+08$	$4.4820E+01$		
	Bulk	$1.4333E+08$	$4.5951E+01$		
	Total	$2.8313E+08$		$4.5385E-15$	0.098
1.05	Surface	$9.9478E+07$	$3.1892E+01$		
	Bulk	$9.9014E+07$	$3.1744E+02$		
	Total	$1.9849E+08$		$3.1818E-15$	0.100
1.0	Surface	$6.0053E+07$	$1.9253E+01$		
	Bulk	$5.8954E+07$	$1.8901E+02$		
	Total	$1.1901E+08$		$1.9077E-15$	0.102
0.95	Surface	$2.2033E+07$	$7.0637E+00$		
	Bulk	$2.3108E+07$	$7.4084E+01$		
	Total	$4.5141E+07$		$7.2361E-16$	0.095
0.9	Surface	$-1.4923E+07$	$-4.7843E+00$		
	Bulk	$-9.2338E+06$	$-2.9603E+01$		
	Total	$-2.4157E+07$		$-3.8723E-16$	0.162

8.4.3.2 Experiment results and discussion

Long-term operation can change the microstructure of the cathode material. This process can be studied by thermal treatment under current load. The resistance of a sample of cathode material is measured for different durations of the thermal treatment, and the results reported in Table 8.9. SEM images of the microstructure of the cathode sample for these different durations are

shown in Fig. 8.10. As is clearly seen, both grain and pore sizes and, thus, mean free path are significantly affected by the duration of the thermal treatment. Pore and grain sizes increase with duration, and as a consequence, the ohmic resistance increases, which, of course, means that the current flux decreases. This is consistent with the non-equilibrium SEAQT model results, which are used here to more deeply analyze the experimental results. A summary of this analysis is provided in Table 8.10. As pore size increases, fewer oxygen molecules are adsorbed leading to a decrease in current flux. In contrast, increasing grain size leads to more oxygen molecules being adsorbed and to increasing current flux. Thus, there are competing effects on current flux from microstructural changes. The experiment shows consistent with our model prediction that the net effect is a decrease in current flux, which means that the influence of pore size is dominant. After microstructural changes, the chemical reaction balance moves towards the oxygen molecule side. Since oxygen in the pore can be regarded as an ideal gas, the change of pore size has a significant influence on the mean free path in the pore. Even though the mean free paths on the surface and in the bulk are also changed by the grain size increase, other factors such as lattice structure and vacancy density limit the effects of these changes. Thus, decreasing pore size is a better way to improve cathode performance since it moves the chemical reaction balance towards the oxygen ion allowing more oxygen molecules to be adsorbed with the result that the current flux is higher. Of course, the caveat is a smaller diffusion speed. However, as discussed above, the limiting step is not the diffusion but rather the effects of mean free path on the reaction. Thus, the decrease in diffusion speed is easily offset by the gain in reactions.

Table 8.9. Ohmic resistance of the cathode sample after the heating process.

Time interval (hr)	0	20	40
R_Ω (Ω cm^2)	0.9	1.0	1.2

Table 8.10. Analysis of the experimental results of the heating process using the non-equilibrium SEAQT model.

Experiment		Model parameter change		Flux predicted by model		Effect strength
Pore size	Increasing	Mean free path in the pore	Increasing	Effect of pore size on flux	Decreasing	Strong
Grain size	Increasing	Mean free path in the bulk and on the surface	Increasing	Effect of grain size on flux	Increasing	Weak
Experiment flux	Decreasing			Net effect on flux	Decreasing	

8.4.4 Chromium oxide accumulation and cathode material poisoning

8.4.4.1 Transient process of the chromium oxide poisoning pathway

The non-equilibrium SEAQT model for the chromium oxide pathway is used to study the kinetics of chromium oxide accumulation and chromium (III) oxide gas distribution in the pore. Results provide insight into the influence on performance of chromium poisoning. The model in this section uses an initial concentration of CrO_3 in the pore of 1×10^{-12} mol/cm^3. Based on Kestell [139], the inlet concentration of CrO_3 is chosen to be 2.33×10^{-10} mol/cm^3, which is more than three orders of magnitude smaller than the concentration of oxygen. Thus, the competition of CrO_3 reduction with that of oxygen is relatively small. In addition, heat diffusion occurs between the chromium oxide and other particles (e.g., O_2) in the pore and on the surface. Because the chromium oxide concentration is low, this diffusion can be modeled by an interaction with a reservoir at 700 K, which is the steady state temperature of the oxygen reduction pathway in the pore. Furthermore, since accumulation on the surface removes the Cr_2O_3 product of the CrO_3 reduction reaction pathway from the pore, the outlet boundary condition for the Cr_2O_3 concentration is set to a very low value. For the results presented in this section, it is assumed that the accumulation does not slow down the reduction process either for the CrO_3 or the oxygen since this is a transient process and the timescale is smaller than the timescale for degradation. In subsequent sections, the degradation effect is taken into account. Fig. 8.11a shows the time evolution of CrO_3 concentration in the pore, while Fig. 8.11b shows the chromium (III) oxide accumulation on the cathode surface. The results indicate that the diffusion process from the inlet concentration into

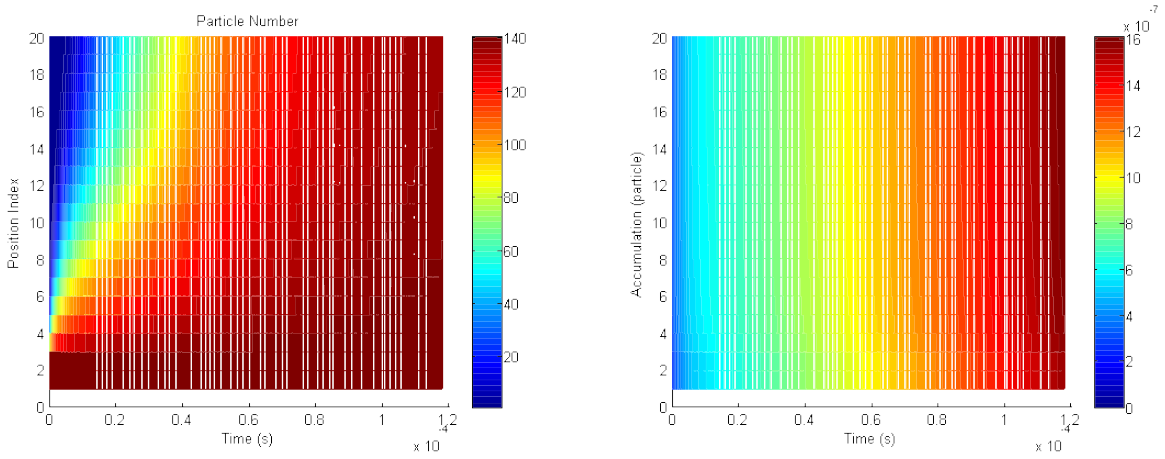

Figure 8.11. Time evolution of (a:left) the concentration distribution of CrO_3 in the pore and (b:right) the Cr_2O_3 accumulation on the surface.

the pore eventually results in a uniform distribution, which leads to a constant accumulation rate of Cr_2O_3 on the surface. During the transient process and after the initial time, the inlet exhibits a lower accumulation rate of Cr_2O_3 as indicated by the slight curvature to the right from top to bottom of the vertical colors in Fig. 8.11b. This is because the diffusion and reduction reaction are in competition with each other, which contrasts with the last local system in the pore where all of the CrO_3 is involved in the reduction reaction.

Finally, the entropy distribution in time in the pore pathway is seen in Fig. 8.12a, while the evolution of total system entropy is given in Fig. 8.12b. Unlike in the results seen in *Section* 8.4.1, the entropy generation is more evenly distributed over the entire timescale range. Furthermore, a uniform steady state and a uniform accumulation rate are reached very quickly (within 10^{-4} s).

8.4.4.2 Chromium oxide accumulation and adsorption site effectiveness

As shown with the results in the previous section, the rate of chromium (III) oxide accumulation is very slow relative to the timescales for reaction and diffusion. Thus, to assess if the chromium reduction process is delayed by the accumulation in the long-term, the mass rate of change of the accumulated chromium oxide expressed with Eqs. (8.3) and (8.4) can be used. These equations are repeated here but with the subscript Cr_2O_3 on m dropped, i.e.,

$$\alpha(m) = 1 - \frac{m}{m_0} \tag{8.34}$$

$$\frac{dm}{dt} = \alpha_0^{Cr_2O_3}\alpha(m)\left(\frac{dm}{dt}\right)_{no\,loss} = \alpha_0^{Cr_2O_3}(1 - \frac{m}{m_0})r_0 \tag{8.35}$$

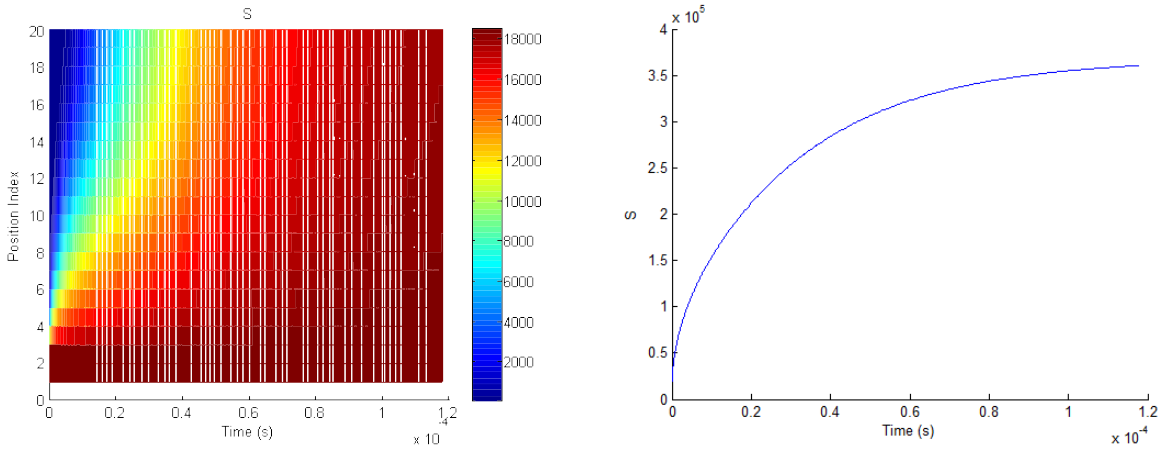

Figure 8.12. Evolution of (a:left) the entropy distribution in the pore pathway and (b:right) the total system entropy.

In this last expression, r_0 is the initial reaction rate of Cr_2O_3 accumulation equal to the steady state rate acquired from the non-equilibrium SEAQT model for the chromium oxide pathway when the accumulating Cr_2O_3 has almost no influence on the reaction rate. The solution of this ODE is

$$m(t) = m_0(1 - e^{-\alpha_0^{Cr_2O_3}\frac{r_0}{m_0}t}) \tag{8.36}$$

or in terms of the accumulation site effectiveness

$$\alpha(t) = \alpha(m(t)) = e^{-\alpha_0^{Cr_2O_3}\frac{r_0}{m_0}t} \tag{8.37}$$

The total adsorption site effectiveness then becomes

$$\alpha_{total}^{O^-}(t) = \alpha_0^{O^-}\alpha(m(t)) = \alpha_0^{O^-}e^{-\alpha_0^{Cr_2O_3}\frac{r_0}{m_0}t} \tag{8.38}$$

$$\alpha_{total}^{Cr_2O_3}(t) = \alpha_0^{Cr_2O_3}\alpha(m(t)) = \alpha_0^{Cr_2O_3}e^{-\alpha_0^{Cr_2O_3}\frac{r_0}{m_0}t} \tag{8.39}$$

where $\alpha_0^{O^-}$ is 0.0003 for oxygen and $\alpha_0^{Cr_2O_3}$ is 1 for chromium oxide.

Based on the results in *Section* 8.4.4.1, the chromium oxide accumulation process is quite uniform on the surface, which means that r_0 can be assumed to be constant across different positions on the cathode surface. Thus, the chromium oxide accumulation effectiveness and total adsorption site effectiveness at different positions yield to the solutions given by Eqs. (8.37) and (8.38).

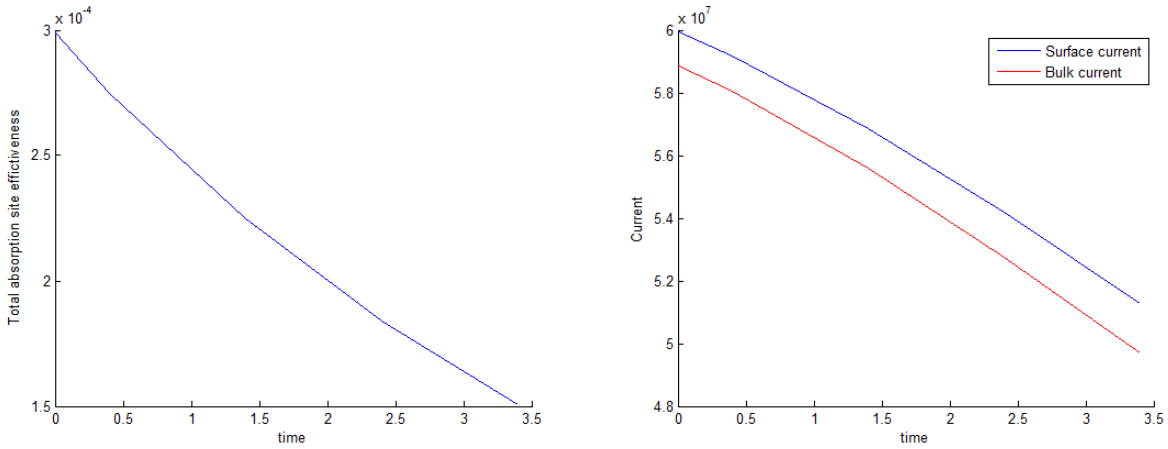

Figure 8.13. Evolution of (a:left) the adsorption site effectiveness and (b:right) the surface and bulk currents for $m_0/r_0 = 5$ s and $\alpha_0^{O^-} = 0.0003$.

8.4.4.3 Influence of chromium oxide on the oxygen reduction pathway and parametric study of total adsorption site effectiveness

Relatively long times are required for chromium poisoning to reduce cathode performance, which as already indicated above is much longer than the timescales of the transient processes for oxygen and chromium oxide reduction. At any instant of time t, the oxygen reduction pathway at steady state exhibits a constant total adsorption site effectiveness $\alpha_{total}^{O^-}(t)$. The steady state surface and bulk currents for the oxygen reduction pathway for different α_{total} are calculated and plotted as a function of time in Fig. 8.13b. Fig. 8.13a provides the total adsorption site effectiveness evolution. Both figures are given for a particular value of the ratio m_0/r_0, which is the ratio between the threshhold value for the accumulated mass when the adsorption site is totally disabled and the value for the steady state reaction rate value for $m_{Cr_2O_3}$ accumulation. In effect, this ratio is a characteristic time for chromium oxide poisoning. For different m_0/r_0, the shape of these curves are the same with only the scaling of the time axis affected. As can be seen from Fig. 8.13b, the performance of the oxygen pathway decreases nonlinearly due to the chromium poisoning process. Of course, the value of 5 s used for m_0/r_0 above in Fig. 8.13 is somewhat arbitrary since a threshold value for m_0 should be determined from experimental data. This is not done here since the purpose is to simply demonstrate how the chromium poisoning process influences the oxygen reduction pathway. A more precise value could nonetheless be determined from, for example, experimental data such as that found in [14] or [13]. However, that is left for a future paper.

Finally, in order to illustrate which process limits the current generation, the focus is placed on

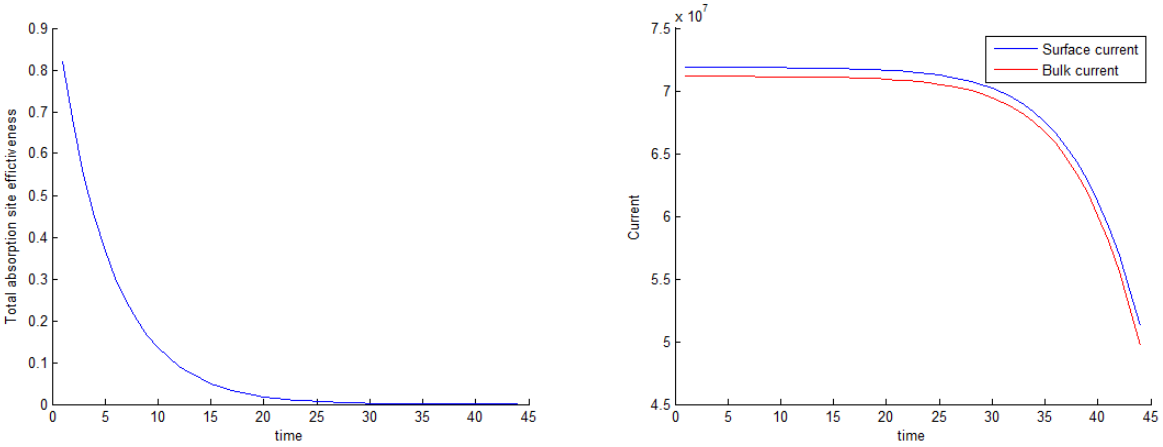

Figure 8.14. Evolution of (a:left) the adsorption site effectiveness and (b:right) the surface and bulk currents for $m_0/r_0 = 5$ s and $\alpha_0^{O^-} = 1$.

the response of current generation to adsorption site degradation. This is done by setting $\alpha_0 = 1$, which implies that there are enough adsorption sites at the initial state to easily accommodate the adsorption of every oxygen molecule. In other words, for the cathode system at steady state, continuity requires that the speed of the adsorption process must be the same as that for the transport as long as there is a sufficient number of adsorption sites for the oxygen molecules and sufficient degradation of the sites has not yet occurred. Hence, to eliminate the first of these as a possible bottleneck or source of performance degradation, the value of $\alpha_0^{O^-} = 1$ is chosen as indicated above for the results reported in Fig. 8.14. Thus, any degradation in performance seen in current in this figure must be due only to the degradation of the sites themselves. For example, in Fig. 8.14b, there is little change in performance before 30 s (i.e., when $\alpha = 10^{-6}$) even though chromium accumulation has led to a significant decrease of total adsorption site effectiveness as seen in Fig. 8.13a. The reason is that before 30 s (i.e., $\alpha > 10^{-6}$,), adsorption is not the limiting step for the mass transfer. On the other hand, after 30 s (i.e., $\alpha < 10^{-6}$), total adsorption site effectiveness has decreased sufficiently due to chromium oxide accumulation to exert a strong influence on performance and, thus, the ability to adsorb becomes the limiting factor.

8.5 Conclusions

Results presented here for the application of the SEAQT framework to a SOFC cathode include those for i) the transient process of oxygen reduction at the cathode, ii) the effects of changes in mean free path and interconnect-TPB distances on cathode performance due to microstructural

changes, and iii) the kinetics of the chromium oxide accumulation and chromium oxide poisoning processes. In the transient study, the multi-timescale features of different non-equilibrium phenomena and how they communicate with each other are illustrated. With the parametric study on changes in mean free path and interconnect-TPB distances, a qualitative explanation of how degradation occurs via microstructural changes is provided so that a clearer understanding of the coupled phenomena underlying the experimental results are obtained. Model predictions and experimental results suggest that pore size reduction as opposed to grain size increases have a more profound effect on improving cathode performance since the former moves the chemical reaction balance towards the oxygen ion allowing more oxygen molecules to be adsorbed at a rate significantly higher than that achieved with the grain size increases. A clearer understanding of the degradation in cathode performance of chromium poisoning is also obtained from the model, underscoring its ability to distinguish between the effects on performance of reaction, transport, and adsorption site effectiveness. This ability makes possible the study in greater detail of the contributions that each of these phenomena individually make to cathode performance.

Finally, the SEAQT framework is able to effectively model coupled non-equilibrium phenomena, including mass diffusion, heat diffusion, and chemical and electrochemical reactions. A major benefit of this framework is that it accounts for both the quantum mechanical and thermodynamic features of the system and the non-equilibrium processes it undergoes. It also allows for a larger range of time and spatial scales to be used in a single model. In addition, it is thermodynamically rigorous even in the far-from-equilibrium realm and provides a consistent description at all scales using entropy and energy as state variables. The result is that particle number and temperature evolutions can be predicted with great efficiency.

Chapter 9

Summary and Conclusions

In this dissertation, a novel methodology based on SEAQT is introduced to model and analyze non-equilibrium relaxation processes. From an entropy generation viewpoint, the relaxation process is explained as the mass and energy redistribution among the system energy eigenlevels, which is mathematically represented by a gradient dynamics in system thermodynamic state space. The methodology is based on identifying and utilizing certain features or patterns of the global thermodynamic-ensemble description of system and state independent of the detailed mechanics of the individual particles, providing a simple, complete and more comprehensive description of each non-equilibrium state and a clear physical picture of non-equilibrium thermodynamic state evolution. This is achieved by the introduction of the concepts of hypo-equilibrium state and non-equilibrium intensive properties. With the categorization of non-equilibrium states by different ordered hypo-equilibrium states, subspace non-equilibrium intensive and extensive properties serve as a good description of the trajectory in system state space (even for very high-dimensional state spaces) determined by the equation of motion or the principle of SEA. This complete description from a thermodynamic-ensemble viewpoint provides access to transient information about the relaxation process, which would otherwise be extremely complex or unavailable in more traditional approaches. In addition, with the use of these two concepts, equilibrium and near-equilibrium thermodynamic relations such as the Gibbs relation, the Clausius inequality, the Onsager relations, the Casimir condition, etc. are generalized into the far-from-equilibrium realm and for quasi-non-equilibrium processes. An Onsager type of investigation can then be applied to the relaxation process of an isolated system via definitions of conjugate forces and conjugate fluxes, which are based on the concepts of hypo-equilibrium state and non-equilibrium intensive properties. By do-

ing so, the non-equilibrium phenomena in one isolated system and between interacting systems can be presented in a single unified form. Furthermore, the variational principle in the spaces spanned by the conjugate forces and fluxes is derived from the variational principle in system state space determined by the principle of steepest entropy ascent.

To be complete, different types of ensembles (i.e., canonical, grand canonical and isothermal-isobaric) are used to study systems with different non-equilibrium intensive properties of interest, leading to fundamental thermodynamic definitions of non-equilibrium temperature, non-equilibrium chemical potential and non-equilibrium pressure. In addition, the modeling of two interacting, non-equilibrium systems enables a fundamental thermodynamic definition of measurements and reservoirs. For the former, the relationship between the non-equilibrium intensive properties of subspaces and their values determined from experimental measurements is established using fluctuations of the subspaces. This implies a potential link between the SEAQT framework and the fluctuation-dissipation theorem that could lead to experimental research into the non-equilibrium relaxation process via the SEAQT framework. As to the fundamental thermodynamic definition of reservoirs, it enables the study of thermodynamic cycles using the SEAQT framework, especially real cycles, which do not undergo a set of quasi-equilibrium processes. In this way, the loss of efficiency of the cycle due to non-quasi-equilibrium effects can be explained from a thermodynamic, first-principle viewpoint using relaxation times. Finally, the study of a single system undergoing multiple interactions with other systems extends the applicability of the concepts of hypo-equilibrium state and non-equilibrium intensive properties to networks of non-equilibrium local systems.

With the development of the density of states method, this SEAQT framework becomes practically applicable across all temporal and spatial scales. Even if the order of the hypo-equilibrium state is very high so that using this concept in such a case may not be practical, the density of state method still permits solution of the equation of motion so that the non-equilibrium thermodynamic trajectory, especially that for the intermediate states of the system, can be determined with the SEAQT equation of motion. In addition, it is shown that hypo-equilibrium state concept is a good approximation for determining the non-equilibrium thermodynamic trajectory when the initial condition or state is not a hypo-equilibrium state but instead one described by a gamma distribution for each of the subspaces. Furthermore, integration of a heterogeneous multiscale method (HMM) with the SEAQT framework permits the modeling of complex multiscale/multi-physics networks

of systems with multiple coupled interactions (e.g., chemical reactions and mass and heat diffusion) such as the oxygen reduction pathways of the SOFC cathode modeled in Chapter 8. This new approach allows the study of the transient process and of coupling and cross-scale effects (such as the influence of microscopic features like the mean free-path and interconnect-TPB distances on overall cathode performance), which may be inaccessible or computationally too expensive using more traditional methods. Thus, the SEAQT framework can strongly support the research and design of devices operating in the non-equilibrium realm with coupling and cross-scale effects and can do so (as shown in Chapters 2 and 8) with very high accuracy and very low computational burdens.

Finally, in addition to the work presented in this dissertation, there are several on-going research topics in our research group, including the use of the SEAQT framework with the Ising model, its use to predict the kinetics of an isothermal chemical reaction, etc. In addition, theoretical studies relative to the application of the concept of hypo-equilibrium state to modeling the coupling of reversible and irreversible relaxations are needed. The study of relaxation time is also of great interest and complementary to the research on thermodynamic trajectories. Based on the methodology developed here, SEAQT can be applied to the study of many unresolved fundamental research topics (e.g., in turbulence, combustion kinetics, quantum entanglement and coherence/decoherence). Applications of multi-scale SEAQT models to biological systems, neutron scattering, and the prediction of transport properties in plasmas are also underway in our group. The modeling and design of spintronic devices and quantum computing with the SEAQT framework are also of interest and part of the possible future directions of our work.

Bibliography

[1] P. Vogl and T. Kubis, "The non-equilibrium Green's function method: an introduction," *Journal of Computational Electronics*, vol. 9, no. 3-4, pp. 237–242, 2010.

[2] C. H. Cheng, Y. W. Chang, and C. W. Hong, "Multiscale parametric studies on the transport phenomenon of a solid oxide fuel cell," *Journal of Fuel Cell Science and Technology*, vol. 2, no. 4, p. 219, 2005.

[3] A. Modak and M. Lusk, "Kinetic monte carlo simulation of a solid-oxide fuel cell: I. Open-circuit voltage and double layer structure," *Solid State Ionics*, vol. 176, no. 29-30, pp. 2181–2191, 2005.

[4] S. Chen and G. D. Doolen, "Lattice Boltzmann method for fluid flows," *Annual Review of Fluid Mechanics*, vol. 30, no. 1, pp. 329–364, 1998.

[5] A. Haghighat, *Monte Carlo Methods for Particle Transport*. CRC Press., 2014.

[6] D. C. Rapaport, *The art of molecular dynamics simulation*. Cambridge university press, 2004.

[7] M. E. J. Newman and G. T. Barkema, *Monte Carlo Methods in Statistical Physics*. Oxford University Press: New York, USA, 1999.

[8] R. M. Dreizler and E. Engel, *Density functional theory*. Springer, 2011.

[9] G. Li and M. R. von Spakovsky, "Study of the transient behavior and microstructure degradation of a SOFC cathode using an oxygen reduction model based on steepest-entropy-ascent quantum thermodynamics," in *ASME 2015 International Mechanical Engineering Congress and Exposition*, American Society of Mechanical Engineers, 2015. No. IMECE2015-53726.

[10] G. Li, M. R. von Spakovsky, F. Shen, and K. Lu, "Multiscale transient and steady state study of the influence of microstructure degradation and chromium oxide poisoning on SOFC cathode performance." (submitted for publication).

[11] E. Weinan, *Principles of multiscale modeling*. Cambridge University Press, 2011.

[12] E. Weinan, B. Engquist, X. Li, W. Ren, and E. Vanden-Eijnden, "Heterogeneous multiscale methods: a review," *Commun. Comput. Phys*, vol. 2, no. 3, pp. 367–450, 2007.

[13] E. Weinan, W. Ren, and E. Vanden-Eijnden, "A general strategy for designing seamless multiscale methods," *Journal of Computational Physics*, vol. 228, no. 15, pp. 5437–5453, 2009.

[14] G. Li and M. R. von Spakovsky, "Steepest-entropy-ascent quantum thermodynamic modeling of the relaxation process of isolated chemically reactive systems using density of states and the concept of hypo-equilibrium state," *Phys. Rev. E*, 2015. (in publication).

[15] G. Li, O. Al-Abbasi, and M. R. von Spakovsky, "Atomistic-level non-equilibrium model for chemically reactive systems based on steepest-entropy-ascent quantum thermodynamics," *Journal of Physics: Conference Series*, vol. 538, no. 1, p. 012013, 2014.

[16] G. Li and M. R. von Spakovsky, "Steepest-entropy-ascent quantum thermodynamic modeling of heat and mass diffusion in a far-from-equilibrium system based on a single particle ensemble." arXiv:1601.01344, 2016.

[17] G. Li and M. R. von Spakovsky, "Steepest-entropy-ascent quantum thermodynamic modeling of the far-from-equilibrium interactions between non-equilibrium systems of indistinguishable particle ensembles." arXiv:1601.02703, 2016.

[18] G. Li and M. R. von Spakovsky, "Application of steepest-entropy-ascent quantum thermodynamics to predicting heat and mass diffusion from the atomistic up to the macroscopic level," in *ASME 2015 International Mechanical Engineering Congress and Exposition*, American Society of Mechanical Engineers, 2015. No. IMECE2015-53581.

[19] G. Li and M. R. von Spakovsky, "Steepest-entropy-ascent model of reservoir and engine cycle in non-equilibrium using hypo-equilibrium state and an isothermal-isobaric ensemble." (unpublished).

[20] M. Grmela and H. C. Öttinger, "Dynamics and thermodynamics of complex fluids. I. Development of a general formalism," *Phys. Rev. E*, vol. 56, pp. 6620–6632, Dec 1997.

[21] H. C. Öttinger and M. Grmela, "Dynamics and thermodynamics of complex fluids. II. Illustrations of a general formalism," *Phys. Rev. E*, vol. 56, pp. 6633–6655, Dec 1997.

[22] K. Mohamed and A. Mohamad, "A review of the development of hybrid atomistic-

continuum methods for dense fluids," *Microfluidics and Nanofluidics*, vol. 8, no. 3, pp. 283–302, 2010.

[23] M. Kalweit and D. Drikakis, "Multiscale simulation strategies and mesoscale modelling of gas and liquid flows," *IMA Journal of Applied Mathematics*, vol. 76, no. 5, pp. 661–671, 2011.

[24] G. P. Beretta, "Steepest entropy ascent model for far-nonequilibrium thermodynamics: Unified implementation of the maximum entropy production principle," *Phys. Rev. E*, vol. 90, p. 042113, Oct 2014.

[25] H. C. Öttinger, *Beyond equilibrium thermodynamics*. John Wiley & Sons, 2005.

[26] G. P. Beretta, E. P. Gyftopoulos, J. L. Park, and G. N. Hatsopoulos, "Quantum thermodynamics. A new equation of motion for a single constituent of matter," *Il Nuovo Cimento B Series 11*, vol. 82, no. 2, pp. 169–191, 1984.

[27] G. P. Beretta, E. P. Gyftopoulos, and J. L. Park, "Quantum thermodynamics. A new equation of motion for a general quantum system," *Il Nuovo Cimento B Series 11*, vol. 87, no. 1, pp. 77–97, 1985.

[28] G. P. Beretta, "Nonlinear model dynamics for closed-system, constrained, maximal-entropy-generation relaxation by energy redistribution," *Phys. Rev. E*, vol. 73, p. 026113, Feb 2006.

[29] G. P. Beretta, "Maximum entropy production rate in quantum thermodynamics," *Journal of Physics: Conference Series*, vol. 237, no. 1, p. 012004, 2010.

[30] G. Beretta, *On the general equation of motion of quantum thermodynamics and the distinction between quantal and nonquantal uncertainties*. PhD thesis, Massachusetts Institute of Technology, Dept. of Mechanical Engineering, 1981. arXiv:quant-ph/0509116.

[31] L. M. Martyushev and V. Seleznev, "Maximum entropy production principle in physics, chemistry and biology," *Physics Reports*, vol. 426, no. 1, pp. 1–45, 2006.

[32] E. P. Gyftopoulos and E. Ç̧ubukçu, "Entropy: Thermodynamic definition and quantum expression," *Phys. Rev. E*, vol. 55, pp. 3851–3858, Apr 1997.

[33] E. Zanchini and G. P. Beretta, "Recent progress in the definition of thermodynamic entropy," *Entropy*, vol. 16, no. 3, p. 1547, 2014.

[34] A. Montefusco, F. Consonni, and G. P. Beretta, "Essential equivalence of the general equation for the nonequilibrium reversible-irreversible coupling (GENERIC) and steepest-

entropy-ascent models of dissipation for nonequilibrium thermodynamics," *Phys. Rev. E*, vol. 91, p. 042138, Apr 2015.

[35] M. Grmela, "Contact geometry of mesoscopic thermodynamics and dynamics," *Entropy*, vol. 16, no. 3, p. 1652, 2014.

[36] S. Cano-Andrade, M. R. von Spakovsky, and G. P. Beretta, "Steepest-entropy-ascent quantum thermodynamic non-equilibrium modeling of decoherence of a composite system of two interacting spin-1/2 systems," in *ASME 2013 International Mechanical Engineering Congress and Exposition*, p. V08BT09A043, American Society of Mechanical Engineers, 2013.

[37] S. Cano-Andrade, G. P. Beretta, and M. R. von Spakovsky, "Non-equilibrium thermodynamic modeling of an atom-field state evolution with comparisons to published experimental data," in *Proceedings of the 12th Joint European Thermodynamics Conference, Brescia, Italy*, pp. 1–5, 2013.

[38] S. Cano-Andrade, G. P. Beretta, and M. R. von Spakovsky, "Steepest-entropy-ascent quantum thermodynamic modeling of decoherence in two different microscopic composite systems," *Phys. Rev. A*, vol. 91, p. 013848, Jan 2015.

[39] M. R. von Spakovsky and J. Gemmer, "Some trends in quantum thermodynamics," *Entropy*, vol. 16, no. 6, p. 3434, 2014.

[40] C. E. Smith and M. R. von Spakovsky, "Comparison of the non-equilibrium predictions of intrinsic quantum thermodynamics at the atomistic level with experimental evidence," *Journal of Physics: Conference Series*, vol. 380, no. 1, p. 012015, 2012.

[41] G. P. Beretta and N. G. Hadjiconstantinou, "Steepest entropy ascent models of the boltzmann equation: Comparisons with hard-sphere dynamics and relaxation-time models for homogeneous relaxation from highly non-equilibrium states," in *ASME 2013 International Mechanical Engineering Congress and Exposition*, p. V08BT09A050, American Society of Mechanical Engineers, 2013.

[42] G. P. Beretta, "Nonlinear quantum evolution equations to model irreversible adiabatic relaxation with maximal entropy production and other nonunitary processes," *Reports on Mathematical Physics*, vol. 64, no. 1-2, pp. 139–168, 2009.

[43] W. K. Wootters, "Statistical distance and Hilbert space," *Phys. Rev. D*, vol. 23, pp. 357–362, Jan 1981.

[44] I. Gyarmati, E. Gyarmati, and W. F. Heinz, *Non-equilibrium thermodynamics*. Springer, 1970.

[45] M. Grmela, V. Klika, and M. Pavelka, "Reductions and extensions in mesoscopic dynamics," *Phys. Rev. E*, vol. 92, p. 032111, Sep 2015.

[46] G. P. Beretta and M. R. von Spakovsky, "Steepest-entropy-ascent quantum thermodynamic framework for describing the non-equilibrium behavior of a chemically reactive system at an atomistic level." e-print arXiv:1504.03994, 04 2015. (submitted for publication).

[47] M. Grmela, "Fluctuations in extended mass-action-law dynamics," *Physica D: Nonlinear Phenomena*, vol. 241, no. 10, pp. 976–986, 2012.

[48] E. P. Gyftopoulos and G. P. Beretta, *Thermodynamics: foundations and applications*. Courier Corporation, 2005.

[49] G. Hatsopoulos and E. Gyftopoulos, "A unified quantum theory of mechanics and thermodynamics. Part I. postulates," *Foundations of Physics*, vol. 6, no. 1, pp. 15–31, 1976.

[50] G. Hatsopoulos and E. Gyftopoulos, "A unified quantum theory of mechanics and thermodynamics. Part IIa. available energy," *Foundations of Physics*, vol. 6, no. 2, pp. 127–141, 1976.

[51] G. Hatsopoulos and E. Gyftopoulos, "A unified quantum theory of mechanics and thermodynamics. Part IIb. stable equilibrium states," *Foundations of Physics*, vol. 6, no. 4, pp. 439–455, 1976.

[52] G. Hatsopoulos and E. Gyftopoulos, "A unified quantum theory of mechanics and thermodynamics. Part III. irreducible quantal dispersions," *Foundations of Physics*, vol. 6, no. 5, pp. 561–570, 1976.

[53] J. L. Park, "Nature of quantum states," *American Journal of Physics*, vol. 36, p. 211, 1968.

[54] R. F. Simmons and J. L. Park, "The essential nonlinearity of N-level quantum thermodynamics," *Foundations of Physics*, vol. 11, no. 3-4, pp. 297–305, 1981.

[55] J. L. Park and R. F. Simmons Jr, "The knots of quantum thermodynamics," in *Old and New Questions in Physics, Cosmology, Philosophy, and Theoretical Biology*, pp. 289–308, Springer, 1983.

[56] G. P. Beretta, "Effect of irreversible atomic relaxation on resonance fluorescence, absorption, and stimulated emission," *International journal of theoretical physics*, vol. 24, no. 12, pp. 1233–1258, 1985.

[57] G. Beretta, "Steepest entropy ascent in quantum thermodynamics," *Lecture Notes in Physics*, vol. 278, no. 441, 1986.

[58] G. P. Beretta, "Quantum thermodynamics of nonequilibrium. Onsager reciprocity and dispersion-dissipation relations," *Foundations of physics*, vol. 17, no. 4, pp. 365–381, 1987.

[59] E. Cubukcu, *Thermodynamics as a non-statistical theory*. PhD thesis, Massachusetts Institute of Technology, Dept. of Nuclear Engineering, 1993.

[60] E. P. Gyftopoulos and M. R. von Spakovsky, "Quantum-theoretic shapes of constituents of systems in various states," *Journal of energy resources technology*, vol. 125, no. 1, pp. 1–8, 2003.

[61] G. P. Beretta and E. P. Gyftopoulos, "Thermodynamic derivations of conditions for chemical equilibrium and of Onsager reciprocal relations for chemical reactors," *The Journal of chemical physics*, vol. 121, no. 6, pp. 2718–2728, 2004.

[62] G. P. Beretta, "Nonlinear extensions of schrödinger–von neumann quantum dynamics: A set of necessary conditions for compatibility with thermodynamics," *Modern Physics Letters A*, vol. 20, no. 13, pp. 977–984, 2005.

[63] G. P. Beretta, "Modeling non-equilibrium dynamics of a discrete probability distribution: General rate equation for maximal entropy generation in a maximum-entropy landscape with time-dependent constraints," *Entropy*, vol. 10, no. 3, pp. 160–182, 2008.

[64] M. R. von Spakovsky, "The second law: A unified approach to thermodynamics applicable to all systems and all states," in *MEETING THE ENTROPY CHALLENGE: An International Thermodynamics Symposium in Honor and Memory of Professor Joseph H. Keenan*, vol. 1033, pp. 302–308, AIP Publishing, 2008.

[65] M. R. Von Spakovsky, "Intrinsic quantum thermodynamic: What it is and what can be done with it," in *Proceedings of the 12th Joint European Thermodynamics Conference, Brescia, Italy*, pp. 1–5, 2013.

[66] O. Al-Abbasi, M. von Spakovsky, and G. Beretta, "Intrinsic quantum thermodynamic prediction of the non-equilibrium atomistic-level behaviour of chemically reactive systems," July 1-5 2013.

[67] O. Al-Abbasi, *Modeling the Non-Equilibrium Behavior of Chemically Reactive Atomistic Level Systems Using Steepest-Entropy-Ascent Quantum Thermodynamics*. PhD thesis, Virginia Tech, Dept. of Mechanical Engineering, 2013.

[68] U. Weiss, *Quantum dissipative systems*, vol. 10. World Scientific, 1999.

[69] K. Blum, *Density matrix theory and applications*, vol. 64. Springer Science & Business Media, 2012.

[70] A. Kossakowski, "On necessary and sufficient conditions for a generator of a quantum dynamical semi-group," *Bull. Acad. Pol. Sci., Ser. Sci. Math. Astr. Phys*, vol. 20, no. 12, pp. 1021–1025, 1972.

[71] A. Kossakowski, "On quantum statistical mechanics of non-hamiltonian systems," *Reports on Mathematical Physics*, vol. 3, no. 4, pp. 247–274, 1972.

[72] R. Ingarden and A. Kossakowski, "On the connection of nonequilibrium information thermodynamics with non-hamiltonian quantum mechanics of open systems," *Annals of Physics*, vol. 89, no. 2, pp. 451–485, 1975.

[73] G. Lindblad, "On the generators of quantum dynamical semigroups," *Communications in Mathematical Physics*, vol. 48, no. 2, pp. 119–130, 1976.

[74] S. Arrhenius, "Über die reaktionsgeschwindigkeit bei der inversion von rohrzucker durch säuren," *Zeitschrift für physikalische Chemie*, vol. 4, pp. 226–248, 1889.

[75] J. H. van't Hoff and E. Cohen, *Studies in chemical dynamics*. F. Muller, 1896.

[76] E. Pollak and P. Talkner, "Reaction rate theory: What it was, where is it today, and where is it going?," *Chaos*, vol. 15, no. 2, p. 26116, 2005.

[77] P. Hänggi and M. Borkovec, "Reaction-rate theory: fifty years after Kramers," *Reviews of Modern Physics*, vol. 62, no. 2, pp. 251–341, 1990.

[78] W. Quapp and D. Heidrich, "Analysis of the concept of minimum energy path on the potential energy surface of chemically reacting systems," *Theoretica chimica acta*, vol. 66, no. 3-4, pp. 245–260, 1984.

[79] F. Aoiz, L. Banares, V. Herrero, K. Stark, and H.-J. Werner, "Reaction cross sections and rate constants for the $\mathrm{F} + \mathrm{H_2(D_2)} \rightarrow \mathrm{HF(DF)} + \mathrm{H(D)}$ reactions from quasiclassical trajectory calculations on a potential energy surface," *Chemical physics letters*, vol. 254, no. 5, pp. 341–348, 1996.

[80] R. L. Wilkins, "Monte Carlo calculations of reaction rates and energy distributions among reaction products. III. $\mathrm{H} + \mathrm{F_2} \rightarrow \mathrm{HF} + \mathrm{F}$ and $\mathrm{D} + \mathrm{F_2} \rightarrow \mathrm{DF} + \mathrm{F}$," *The Journal of Chemical Physics*, vol. 58, no. 6, pp. 2326–2332, 1973.

[81] N. E. Henriksen and F. Y. Hansen, *Theories of molecular reaction dynamics: The microscopic foundation of chemical kinetics*. Oxford University Press, 2008.

[82] M. Karplus, R. Porter, and R. Sharma, "Exchange reactions with activation energy. I. Simple barrier potential for $(\mathrm{H}, \mathrm{H}_2)$," *The Journal of Chemical Physics*, vol. 43, no. 9, pp. 3259–3287, 1965.

[83] K. J. Laidler and M. C. King, "Development of transition-state theory," *The Journal of physical chemistry*, vol. 87, no. 15, pp. 2657–2664, 1983.

[84] D. G. Truhlar, B. C. Garrett, and S. J. Klippenstein, "Current status of transition-state theory," *The Journal of physical chemistry*, vol. 100, no. 31, pp. 12771–12800, 1996.

[85] G. C. Schatz, "Scattering theory and dynamics: time-dependent and time-independent methods," *The Journal of Physical Chemistry*, vol. 100, no. 31, pp. 12839–12847, 1996.

[86] S. C. Althorpe and D. C. Clary, "Quantum scattering calculations on chemical reactions," *Annual review of physical chemistry*, vol. 54, no. 1, pp. 493–529, 2003.

[87] J. Loschmidt, "Sitzungsberichte der akademie der wissenschaften," *Wien, II*, vol. 73, p. 128, 1876.

[88] E. Fehlberg, "Low order classical runge-kutta formulas with stepwise control," tech. rep., NASA TR R-316, 1969.

[89] E. Fehlberg, "Klassische runge-kutta-formeln vierter und niedrigerer ordnung mit schrittweiten-kontrolle und ihre anwendung auf waermeleitungsprobleme," *Computing*, vol. 6, no. 1-2, pp. 61–71, 1970.

[90] E. Hairer and G. Wanner, "Solving ordinary differential equations ii: Stiff and differential-algebraic problems second revised edition with 137 figures," *Springer series in computational mathematics*, vol. 14, 1996.

[91] R. Heidner III, J. Bott, C. Gardner, and J. Melzer, "Absolute rate coefficients for $\mathrm{F} + \mathrm{H}_2$ and $\mathrm{F} + \mathrm{D}_2$ at T= 295–765 K.," *The Journal of Chemical Physics*, vol. 72, no. 9, pp. 4815–4821, 1980.

[92] R. W. Carr, *Modeling of chemical reactions*, vol. 42. Elsevier, 2007.

[93] A. Rossani and G. Kaniadakis, "A generalized quasi-classical Boltzmann equation," *Physica A: Statistical Mechanics and its Applications*, vol. 277, no. 3-4, pp. 349–358, 2000.

[94] A. Garcia and W. Wagner, "Direct simulation Monte Carlo method for the Uehling-Uhlenbeck-Boltzmann equation," *Physical Review E*, vol. 68, no. 5, 2003.

[95] J. M. Torres-Rincon, *Boltzmann-Uehling-Uhlenbeck Equation*, pp. 33–45. Springer, 2014.

[96] S. R. de Groot and P. Mazur, *Non-equilibrium thermodynamics*. North-Holland Publication Co., Amsterdam, 1962.

[97] R. Kubo, M. Toda, and N. Hashitsume, *Statistical physics II: nonequilibrium statistical mechanics*, vol. 31. Springer Science & Business Media, 2012.

[98] U. Seifert, "Stochastic thermodynamics, fluctuation theorems and molecular machines," *Reports on Progress in Physics*, vol. 75, no. 12, p. 126001, 2012.

[99] D. Jou, J. Casas-Vázquez, and G. Lebon, *Extended irreversible thermodynamics*. Springer, 1996.

[100] R. Benzi, S. Succi, and M. Vergassola, "The lattice Boltzmann equation: theory and applications," *Physics Reports*, vol. 222, no. 3, pp. 145–197, 1992.

[101] C. K. Aidun and J. R. Clausen, "Lattice-Boltzmann method for complex flows," *Annual Review of Fluid Mechanics*, vol. 42, pp. 439–472, 2010.

[102] K. H. Hoffmann, "Quantum thermodynamics," *Annalen der Physik*, vol. 10, no. 1-2, pp. 79–88, 2001.

[103] H.-P. Breuer and F. Petruccione, *The Theory of Open Quantum Systems*. Berlin: Oxford Univ. Press, 2002.

[104] V. Gorini, A. Kossakowski, and E. C. G. Sudarshan, "Completely positive dynamical semigroups of N-level systems," *Journal of Mathematical Physics*, vol. 17, no. 5, pp. 821–825, 1976.

[105] J. Gemmer, M. Michel, and G. Mahler, *Quantum Thermodynamics*, vol. 784 of *Lecture Notes in Physics*. Berlin: Springer Verlag, 2009.

[106] G. A. Levin, W. A. Jones, K. Walczak, and K. L. Yerkes, "Energy transport in closed quantum systems," *Physical Review E*, vol. 85, no. 3, 2012.

[107] G. Y. Panasyuk, G. A. Levin, and K. L. Yerkes, "Heat exchange mediated by a quantum system," *Physical Review E*, vol. 86, no. 2, 2012.

[108] L. V. Keldysh, "Diagram technique for nonequilibrium processes," *Sov. Phys. JETP*, vol. 47, pp. 1515–1527, 1965.

[109] L. P. Kadanoff and G. Baym, *Quantum statistical mechanics: Green's function methods in equilibrium and nonequilibrium problems*. Benjamin New York, 1962.

[110] C. Smith, *Intrinsic Quantum Thermodynamics: Application to Hydrogen Storage on a Carbon Nanotube and Theoretical Consideration of Non-Work Interactions*. PhD thesis, Virginia Tech, Dept. of Mechanical Engineering, 2012.

[111] H. Bruus and K. Flensbergy, *Many-Body Quantum Theory in Condensed Matter Physics: An Introduction*. Oxford university press, 2004.

[112] R. Kosloff, "A quantum mechanical open system as a model of a heat engine," *The Journal of Chemical Physics*, vol. 80, no. 4, p. 1625, 1984.

[113] A. Levy, R. Alicki, and R. Kosloff, "Quantum refrigerators and the third law of thermodynamics," *Physical Review E*, vol. 85, no. 6, p. 061126, 2012.

[114] G. P. Beretta, "Quantum thermodynamic carnot and otto-like cycles for a two-level system," *EPL (Europhysics Letters)*, vol. 99, no. 2, p. 20005, 2012.

[115] E. Guggenheim, "Grand partition functions and so-called"thermodynamic probability"," *The Journal of Chemical Physics*, vol. 7, no. 2, pp. 103–107, 1939.

[116] T. L. Hill, *Statistical Mechanics: Principles and Selected Applications*. Courier Corporation, 1956.

[117] A. Münster, "Zur theorie der generalisierten gesamtheiten," *Molecular Physics*, vol. 2, no. 1, pp. 1–7, 1959.

[118] W. B. Brown, "Constant pressure ensembles in statistical mechanics," *Molecular Physics*, vol. 1, no. 1, pp. 68–82, 1958.

[119] R. Sack, "Pressure-dependent partition functions," *Molecular Physics*, vol. 2, no. 1, pp. 8–22, 1959.

[120] D. S. Corti, "Isothermal-isobaric ensemble for small systems," *Physical Review E*, vol. 64, no. 1, p. 016128, 2001. doi: 10.1103/PhysRevE.64.016128.

[121] G. J. Koper and H. Reiss, "Length scale for the constant pressure ensemble: application to small systems and relation to einstein fluctuation theory," *The Journal of Physical Chemistry*, vol. 100, no. 1, pp. 422–432, 1996.

[122] D. S. Corti and G. Soto-Campos, "Deriving the isothermal-isobaric ensemble: The requirement of a "shell" molecule and applicability to small systems," *The Journal of chemical physics*, vol. 108, no. 19, pp. 7959–7966, 1998.

[123] G. Soto-Campos, D. S. Corti, and H. Reiss, "A small system grand ensemble method for the

study of hard-particle systems," *The Journal of chemical physics*, vol. 108, no. 6, pp. 2563–2570, 1998.

[124] P. Attard, "On the density of volume states in the isobaric ensemble," *The Journal of chemical physics*, vol. 103, no. 22, pp. 9884–9885, 1995.

[125] H. Ullmann, N. Trofimenko, F. Tietz, D. Stöver, and A. Ahmad-Khanlou, "Correlation between thermal expansion and oxide ion transport in mixed conducting perovskite-type oxides for sofc cathodes," *Solid state ionics*, vol. 138, no. 1, pp. 79–90, 2000.

[126] A. A. Asadi, A. Behrouzifar, M. Iravaninia, T. Mohammadi, and A. Pak, "Preparation and oxygen permeation of $\mathrm{La_{0.6}Sr_{0.4}Co_{0.2}Fe_{0.8}O_{3-\delta}(LSCF)}$ perovskite-type membranes: Experimental study and mathematical modeling," *Industrial & Engineering Chemistry Research*, vol. 51, no. 7, pp. 3069–3080, 2012.

[127] E. Y. Konysheva, "Effect of current density on poisoning rate of Co-containing fuel cell cathodes by chromium," *Russian Journal of Electrochemistry*, vol. 50, no. 7, pp. 630–637, 2014.

[128] Y. Teraoka, T. Nobunaga, K. Okamoto, N. Miura, and N. Yamazoe, "Influence of constituent metal cations in substituted lacoo3 on mixed conductivity and oxygen permeability," *Solid State Ionics*, vol. 48, no. 3, pp. 207–212, 1991.

[129] M. Mori, T. Yamamoto, H. Itoh, H. Inaba, and H. Tagawa, "Thermal expansion of nickel-zirconia anodes in solid oxide fuel cells during fabrication and operation," *Journal of the Electrochemical Society*, vol. 145, no. 4, pp. 1374–1381, 1998.

[130] M. Ardigò, A. Perron, L. Combemale, O. Heintz, G. Caboche, and S. Chevalier, "Interface reactivity study between $\mathrm{La_{0.6}Sr_{0.4}Co_{0.2}Fe_{0.8}O_{3-\delta}(LSCF)}$ cathode material and metallic interconnect for fuel cell," *Journal of Power Sources*, vol. 196, no. 4, pp. 2037–2045, 2011.

[131] Y. Li, R. Gemmen, and X. Liu, "Oxygen reduction and transportation mechanisms in solid oxide fuel cell cathodes," *Journal of Power Sources*, vol. 195, no. 11, pp. 3345–3358, 2010.

[132] M. Gong, R. S. Gemmen, and X. Liu, "Modeling of oxygen reduction mechanism for 3pb and 2pb pathways at solid oxide fuel cell cathode from multi-step charge transfer," *Journal of Power Sources*, vol. 201, pp. 204–218, 2012.

[133] H. Yokokawa, H. Tu, B. Iwanschitz, and A. Mai, "Fundamental mechanisms limiting solid oxide fuel cell durability," *Journal of Power Sources*, vol. 182, no. 2, pp. 400–412, 2008.

[134] Y. Liu, J. Chen, F. Wang, B. Chi, J. Pu, and L. Jian, "Performance stability of impregnated

$La_{0.6}Sr_{0.4}Co_{0.2}Fe_{0.8}O_{3-\delta}$–$Y_2O_3$ stabilized ZrO_2 cathodes of intermediate temperature solid oxide fuel cells," *International Journal of Hydrogen Energy*, vol. 39, no. 7, pp. 3404–3411, 2014.

[135] K. Lu and F. Shen, "Effect of stoichiometry on $(La_{0.6}Sr_{0.4})_xCo_{0.2}Fe_{0.8}O_3$ cathode evolution in solid oxide fuel cells," *Journal of Power Sources*, vol. 267, pp. 421–429, 2014.

[136] K. Lu and F. Shen, "Long term behaviors of $La_{0.8}Sr_{0.2}MnO_3$ and $La_{0.6}Sr_{0.4}Co_{0.2}Fe_{0.8}O_3$ as cathodes for solid oxide fuel cells," *International Journal of Hydrogen Energy*, vol. 39, no. 15, pp. 7963–7971, 2014.

[137] S. Paulson and V. Birss, "Chromium poisoning of lsm-ysz sofc cathodes i. detailed study of the distribution of chromium species at a porous, single-phase cathode," *Journal of The Electrochemical Society*, vol. 151, no. 11, pp. A1961–A1968, 2004.

[138] J. J. Bentzen, J. V. T. Høgh, R. Barfod, and A. Hagen, "Chromium poisoning of LSM/YSZ and $LSCF/CGO$ composite cathodes," *Fuel Cells*, vol. 9, no. 6, pp. 823–832, 2009.

[139] G. M. Kestell, *Model of chromium poisoning in the cathode of a solid oxide fuel cell using the lattice Boltzmann method*. PhD thesis, Virginia Tech, Dept. of Mechanical Engineering, 2010.

[140] K. Lu and M. R. von Spakovsky, "Material degradation in severe high temperature environments of solid oxide fuel/electrolyzer cells," tech. rep., Annual Report to ONR, Award No. N00014-11-1-0266, MSE and ME Depts., Virginia Tech, 2013.

[141] M. Andersson, J. Yuan, and B. Sundén, "Review on modeling development for multiscale chemical reactions coupled transport phenomena in solid oxide fuel cells," *Applied Energy*, vol. 87, no. 5, pp. 1461–1476, 2010.

[142] A. S. Joshi, K. N. Grew, A. A. Peracchio, and W. K. S. Chiu, "Lattice Boltzmann modeling of 2d gas transport in a solid oxide fuel cell anode," *Journal of Power Sources*, vol. 164, no. 2, pp. 631–638, 2007.

[143] N. Autissier, D. Larrain, J. Van herle, and D. Favrat, "Cfd simulation tool for solid oxide fuel cells," *Journal of Power Sources*, vol. 131, no. 1-2, pp. 313–319, 2004.

[144] S. Harris, *An introduction to the theory of the Boltzmann equation*. Mineola (N.Y.): Dover Publications, 2004.

[145] S. Chapman and T. G. Cowling, *The mathematical theory of non-uniform gases: an account*

of the kinetic theory of viscosity, thermal conduction and diffusion in gases. Cambridge university press, 1970.

[146] C. Cercignani, *Theory and application of the Boltzmann equation*. Scottish Academic Press, 1975.

[147] W. Ren and E. Weinan, "Heterogeneous multiscale method for the modeling of complex fluids and micro-fluidics," *Journal of Computational Physics*, vol. 204, no. 1, pp. 1–26, 2005.

[148] T. Jin and K. Lu, "Chemical compatibility between Sr-doped lanthanum manganite air electrode and aisi 441 interconnect," *International Journal of Hydrogen Energy*, vol. 36, no. 7, pp. 4440–4448, 2011.